AN INVESTIGATION OF THE PHYSICS OF BREAKING / BROKEN WAVES

by

Antonios D. Toumazis
B.Sc.(Eng), M.Sc.(Eng), DIC

September, 1988

A thesis submitted for the degree of
Doctor of Philosophy of the University of London and for
the Diploma of Membership of Imperial College

Hydraulics Section
Department of Civil Engineering
Imperial College of Science and Technology

To Maria and Georgios

ABSTRACT

This fundamental research study investigates the physics of breaking/ broken waves. Transient two-dimensional deep water plunging waves produced in the laboratory are studied in great detail. The answers to fundamental questions raised from the experimental observations have practical applications in engineering problems, like scale effects, modelling of the motion induced by wave plunging, or energy loss during wave breaking.

The experimental facilities available enabled the recording and measurement of some remarkable features of the overturning process of breaking waves, as well as of the kinematics induced by breaking. The segmentation of the tip of the overturning jet of a breaking wave into a number of jets is consistently observed. This process is described by a new, partly analytical and partly computational model. This model presents a theoretical prediction of scale effects in overturning waves. Its results are in agreement with the experimental conclusion that model test results with waves smaller than 0.5m high may not be scaled up.

The segmentation process introduces, both literally and metaphorically, a new dimension into the problem. The induced broken wave motion is no longer two-dimensional. The chaotic, unorganised, three-dimensional broken wave motion may be described as the result of the penetration of the irregular shape of the plunging face. Macroscopically, a shoreward and offshoreward wave disturbance is generated on wave plunging, whilst microscopically, radial dispersive waves are produced by each individual jet of the main overturning mass, the superposition of which results in a complex kinematic field. Such a modelling of the breaking induced secondary wave motion presents a theoretical justification for the use of the bore simulation in the surf zone. Furthermore, it opens new horizons in coastal studies as it shows that breaking waves incident normally on a beach present a source of longshore wave energy, a concept not considered in the past.

A numerical model, based on the above principles, predicts the broken wave motion. Transverse velocity time histories measured experimentally are generally in agreement with the model predictions. Interpretation of the experimental results provides information on the temporal and spacial distribution of the turbulent kinetic energy. The formation of a standing wave across the flume is identified, the generation mechanism of which is attributed to resonant effects.

A semi-empirical model predicting the proportion of wave energy loss associated with air entrainment is presented. This complex problem although

considerably simplified, nevertheless provides results which are in reasonable agreement with the state of the art.

An alternative approach to the problem of the generation of breaking waves in the laboratory was followed. This method makes use of the fundamental law of physics, that the laws of nature have no sense of time: they are time symmetric. By considering wave breaking as an unstable accumulation of energy, a breaker is produced by reversing the motion induced by an accumulation of energy.

Further improvements on experimental techniques include the determination of the proper conditions for the operation of a Fiber Optics Laser Doppler Anemometer in surface wave studies and the use of image processing in breaking waves. Accurate and reliable information is extracted that earlier techiques could not provide.

ACKNOWLEDGEMENTS

The author would like to thank all the laboratory staff for their help, especially Stan Finch, John Audsley and Geoff Thomas.

The author has benefitted from fruitful discussions with Professors P. Holmes, J. Chaplin, D.H. Peregrine and Drs D. Hardwick and Sarma, who all contributed through their invaluable criticism and suggestions in the development of the ideas presented in this thesis.

Many thanks to the author's parents for their continuous support.

But most of all, the author is grateful to his supervisor, Dr Kostas Anastasiou, for the encouragement, help, friendship and all effort he devoted.

Finally, the funding support of the Marine Technology Directorate is acknowledged.

LIST OF CONTENTS

LIST OF TABLES

LIST OF FIGURES

Page

LIST OF PLATES

NOTATION

The most important symbols used in the text are listed below. Symbols used in other authors' works are maintained. Some symbols have therefore, more than one meaning but it is evident from the text which meaning is intended.

a	Amplitude of disturbance
B	Width of flume
c	Air concentration
c_g	Group velocity
C	Phase speed
C_0	Linear theory phase speed
C_c	Air concentration at centre line
C_d	Turbulent constant
D_p	Depth of air penetration
E	Energy per unit width
Fr	Froude number
g	Acceleration of gravity, pixel value
h	Water depth
H	Wave height
H_b	Breaker wave height
k	Turbulent kinetic energy
k_0	Initial turbulent kinetic energy
l	Turbulent length scale
L	Wavelength of gravity surface wave, wavelength of disturbance
L_{pred}	Predominant wavelength
LUT	Look Up Table
m	Beach slope
M_L	Mass of body
p	Pressure
P	Pressure, rate of energy dissipation
q	Rate of growth of a disturbance
r	Radial distance, radius of curvature
R	Radius of curvature
Re	Reynolds number
S	Volume
t	Time
T	Period, surface tension

u	Horizontal longitudinal velocity
U	Horizontal speed
v	Horizontal lateral velocity
V	Volume
w	Vertical velocity
We	Weber number
x	Horizontal distance
z	Depth
α, β	Variables defining a hyperbola
γ	Angle between asymptotes of hyperbola
δ	Angle of rotation of principal axes of hyperbola
η	Elevation of free surface
θ	Angle
λ	U/g
μ	Friction coefficient, kinematic viscosity
ξ	Similarity parameter
ρ	Density of water
σ	Surface area
τ	Shear stress
φ	Potential function
ω	Angular frequency

CHAPTER 1

INTRODUCTION

1.1 PREFACE

The problem of breaking/broken waves is approached from an alternative angle. Techniques and concepts used in other fields of science are employed. Their application to the breaking wave process builds a picture which is in agreement with experimental observations.

Concepts and techniques used in this thesis include, the basic law of physics that nature has no inbuilt sense of time, the tendency of liquid bodies to form shapes of minimum surface area when in a state of free fall, the study of earth tremors from velocity records obtained further away, the digitisation of video pictures and extraction of information.

The chapters of this thesis form complete entities. They start with their own introduction and end with the conclusions drawn. Although they may be read independently, they are nevertheless presented in a logical order.

1.2 DESCRIPTION OF THESIS

The aim of the study is the investigation of the physics of breaking/ broken waves.

The first main task is the preparation of a concise literature review on this topic (chapter 2). A *virgin* area is identified, namely the motion induced by a single deep water breaking wave. This motion is unaffected by secondary effects such as bed friction and return flows. The motion directly related to the overturning water mass is therefore isolated.

The next objective involves the preparation of an experimental set-up such that repeatable conditions can be achieved (chapter 3). The experiment is controlled by a computer, software for which was specifically developed. A deep water breaking wave is generated using a method, developed during the course of the study, and velocity time histories are measured using a Fiber Optics Laser Doppler Anemometer, FOLDA.

The FOLDA is a very good instrument for measurements of turbulence only when the mean velocity is very small. Velocities normal to the main direction of wave propagation are thus measured around the breaker (chapter 4). The characteristics of this motion pose a most interesting challenge. The absence of any similar measurements as well as theory predicting such a motion raise many questions regarding the approach to the interpretation of the results.

A facility that proved very useful in the understanding of the physical process of wave breaking is the photo and video recording and processing system (chapter 5). Breaking takes place so quickly that the human eye cannot distinguish the stages through which the process passes. A neglected phenomenon highlighted by the recorded pictures is the segmentation of the curling face of the wave into a series of jets. This observation initiated the theoretical treatment of the breaking/ broken wave problem.

Surface tension is the predominant agent for the segmentation of the overturning crest of the wave (chapter 6). In a state of free fall, the liquid mass tends to form shapes having minimum surface area for a given volume. In the same fashion as a liquid cylinder splits into spheres, likewise, the smooth horizontal cylindrical edge of a two-dimensional breaking wave segments into jets. The analytical description of this process presents a physical and mathematical explanation of scale effects in breaking waves.

On impact with the forward undisturbed face of the wave, the plunging jets penetrate the receiving water like a solid body. This process generates a new broken wave motion (chapter 7). The description of this motion is approximated to the motion produced by a local disturbance on the water surface, known as the Cauchy-Poisson problem. The broken wave motion is approached from two angles: the macroscopic, or global approach, in which the plunging wave jet is considered as two-dimensional, and the microscopic, or detailed approach, in which the segmentation of the plunging face is considered.

Air is entrained in the penetration process. The potential energy associated with the entrained air is derived from the wave energy. It is then converted into other forms of energy, such as microturbulence, heat, sound and so on. The proportion of the wave energy dissipated due to air-entrainment is proposed, based on the characteristics of plunging liquid jets and the associated air concentration (chapter 8).

Finally, the results from the thesis are discussed (chapter 9) and areas requiring further investigation are highlighted.

The solution to the problem of the motion induced by a local disturbance on the water surface is employed in various parts in this study. A review of the literature on this topic is included (appendix A). The description of the image processing software, developed for this study, is also included (appendix B).

A video cassette containing a considerable amount of information on the breaking/ broken wave problem and the associated processes accompanies this thesis.

CHAPTER 2

LITERATURE REVIEW ON THE KINEMATICS OF BREAKING/BROKEN WAVES

2.1 INTRODUCTION

'The sight and sound of breaking waves and surf are so familiar and enjoyable that one tends to forget how little one really understands and knows about them. The reason lies partly with the difficulty associated with establishing a precise mathematical description of the fluid flow, that is in general non-linear and time-dependent', (Longuet-Higgins, 1976) and partly with the problem of accurately observing and monitoring breaking waves in the field, because breaking occurs rapidly and intermittently (Cokelet, 1977).

Breaking waves are important for a variety of reasons. They impose large hydrodynamic loads on man-made structures, transfer horizontal momentum to surface currents, provide a source of turbulence energy to mix the upper layers of the ocean, move sediment in shallow water and enhance the air-water exchange of gases, heat, particulate matter and salt.

Research work on breaking waves can be divided into three broad categories: those concerning waves **before, during** and **after breaking**.

The aim of this review is to bring together the state of knowledge on these three processes.

2.2 DEFINITIONS

When regular waves approach a uniformly sloping beach, five characteristic regions can be distinguished (fig. 2.1). The **transformation** zone (Hedges and Kirkgoz, 1981) ranges from the transformation point, where the wave begins to lose symmetry about a vertical line through its crest, up to the breaking point, where the front face of the wave becomes vertical. At the plunging point, where the tip of the overturning jet falls on the forward face of the wave, the **outer**, or **transition** zone starts, which extends to several water depths at the breaking point. In this region the motion shows large scale patterns that are repeated with only small variation from wave to wave (Svendsen et al., 1978).

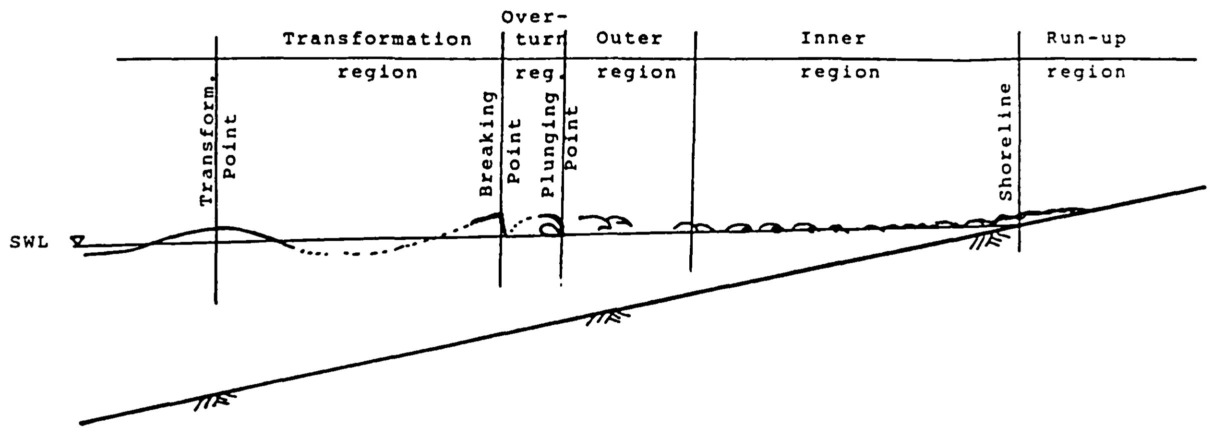

Fig. 2.1 Definition diagram of the breaking zone

Between the breaking and the plunging points, a rapid time-dependent motion takes place which is hereby defined as the **overturning** region. This definition is introduced to bridge the gap between the definition diagrams of different researchers, such as Jansen(1985) and Kirkgoz(1986). As the wave propagates further, the large scale deterministic flow breaks up into small scale details which gradually assume a random turbulent nature. During this process the front of the wave becomes very similar to a moving bore or a hydraulic jump. The **inner** breaking region extends to the shoreline where the **run-up** region starts (Svendsen et al., 1978).

Apart from waves breaking due to shoaling there are many other causes for breaking of water waves such as wind blowing, refraction by depth or current, local concentration of wave energy, random or deterministic superposition of waves and relative motion between water and an obstacle such as a moving ship (Peregrine, 1982). In a research colloquium, namely Euromech 102, some interesting conclusions were reached. An original one is that, whatever the cause of breaking, the details of the initial breaking motion depend only on the neighbourhood of the wave. This can be of considerable value since it indicates that for many applications, the study can concentrate on the actual breaking process rather than its cause.

2.3 WAVE CAHRACTERISTICS BEFORE BREAKING

'For a given wavelength and depth there is a highest wave which is just on the verge of breaking' (Cokelet, 1977). The classical approach to the study of this problem is to start with a small amplitude wave and progressively consider higher waves. These solutions show that the phase speed of the wave increases with the wave height and the particles do not move in closed orbits, but they have a drift,

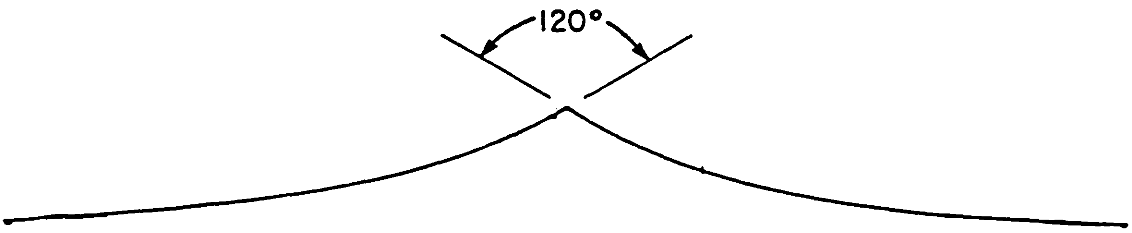

Fig. 2.2 Limiting angle of a symmetric wave

called the Stokes drift. At a wave crest, the particles move with a speed less than the phase speed. As the waves become higher, the particle velocities approach the phase speed. In a limiting wave these two are equal. An early observation was that the limiting angle at the crest of a symmetric wave is 120 degrees (fig 2.2).

A concise review of wave theories describing the particle kinematics of shoaling waves was recently published (Kirkgoz, 1986). The conclusion from this study is that '*no theory is superior to others under all conditions*'. Linear theory, which is the simplest one, is superior to the rest for small amplitude waves. For very steep waves, the stream function theory should be used. Although this conclusion was reached much earlier and a design tool was derived (Shore Protection Manual), the extension of these curves for shoaling waves was not proposed until recently. Water particle velocities, using the Laser Anemometry technique were measured reliably under the crest at the transformation point of breaking waves. The experimental results were compared with computed values using the following wave theories:

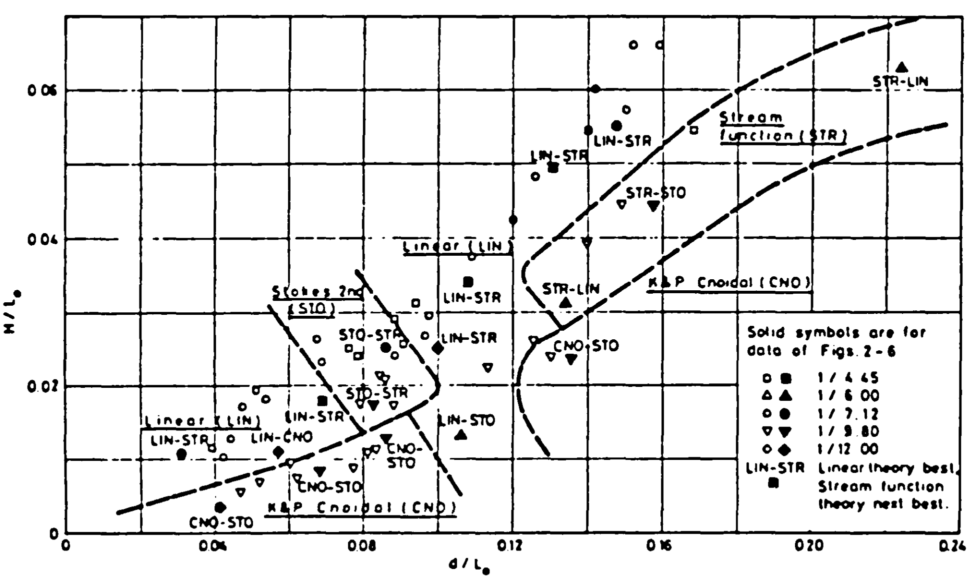

Fig. 2.3 Wave theories giving the best prediction of the horizontal particle velocity distribution under the crest at the transformation point (Kirkgoz, 1986)

1) Linear wave theory
2) Stokes wave theory, second order
3) Cnoidal wave theory

4) Stream function wave theory
5) Solitary wave theory

The regions in which particular theories are better than others in predicting the particle velocities are shown in figure 2.3. The ordinate is the dimensionless wave height, H/L_0 where H and L_0 are the deep water wave height and length respectively and the abscissa is the dimensionless, d/L_0 where d is the depth at the transformation point.

2.4 DURING BREAKING

'A wave will tend to break when the local energy exceeds a critical value' (Cokelet, 1977). This can happen during shoaling when the critical value decreases with depth or in deep water when the energy from different wave components accumulates at a particular point and exceeds the critical value.

2.4.1 SHALLOW WATER

For shoaling waves, the breakers can be classified into four main categories (fig. 2.4, Galvin, 1968).

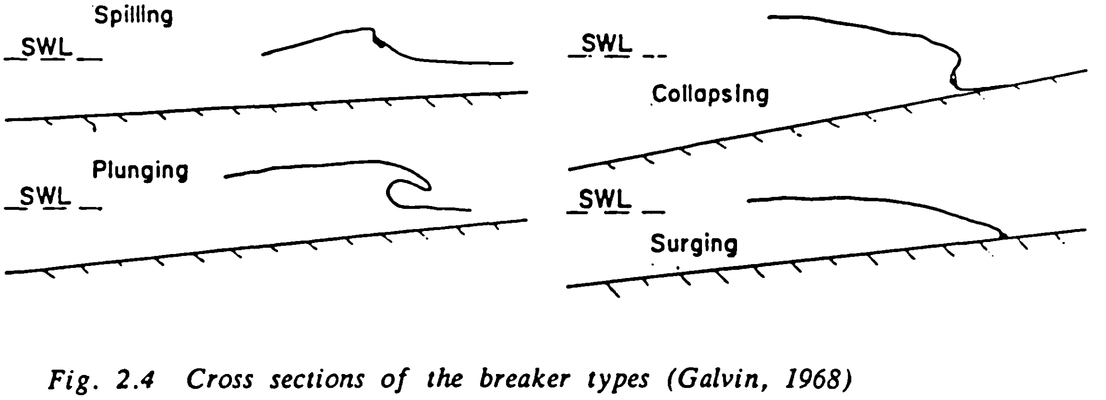

Fig. 2.4 Cross sections of the breaker types (Galvin, 1968)

Spilling breakers are characterised by foam, bubbles and turbulent water generated at the wave crest and eventually covering the front face of the wave.

In a **plunging** breaker, the whole front face of the wave steepens until vertical; the crest curls over the front face and falls into the base of the wave and large sheet-like splash arises from the point where the crest touches down.

In a **collapsing** breaker, the lower part of the front face of the wave steepens until vertical and this front face curls over as an abbreviated plunging wave. The point where the front face begins to curl over is landward of and lower than the point of maximum elevation of the wave.

In a **surging** breaker the front face of the wave remains relatively smooth and the wave slides up the beach with only minor production of foam and bubbles.

The breaker type depends on the beach slope, *m*, the wave period, T, the deep water wavelength, L_0, and the deep water wave height, H_0. It also depends on the type of the beach slope, whether concrete, sand, gravel and so on. For a non-porous, impermeable, solid surface the ranges over which the different types of breakers occur were derived experimentally by a number of researchers. Galvin (1968) defined ranges for the following two parameters which are applicable to each type of breaker: the offshore parameter $H_0/(L_0 m^2)$ and the inshore parameter, $H_b/(gmT^2)$ where H_b is the breaker height and g the acceleration of gravity.

A similarity parameter, ξ, was intoduced by Battjes (1974) for defining the general flow characteristics on slopes.

$$\xi = \tan m/(H/L_0)^{1/2}$$

As this parameter has proved more useful than the offshore/inshore parameters introduced by Galvin, it is convenient to reproduce Galvin's classification using the similarity parameter, ξ.

The offshore parameter can be written as ξ_0^{-2}, where the subscript $_0$ refers to deep water conditions. Figure 2.5 shows the breaker type classification using Galvin's parameters, as well as the deep water similarity parameter.

Spilling	Plunging	Surging/collapsing	Parameter
0.09	4.8		Galvin Offshore
0.003	0.068		Galvin Inshore
0.5	3.3		ξ_0
0.4	2.0		ξ_b

Fig. 2.5 Parametric classification of breaker type

Although the inshore parameter is not equivalent to

$$\xi_b = \tan m/(H_b/L_0)^{1/2}$$

where the subscript b refers to the breaking conditions, re-analysis of Galvin's original data showed that the breaker classification can be performed equally well with ξ_b as with the inshore parameter. This classification is also presented in figure 2.5.

2.4.2 DEEP WATER

In deep water, three distinct types of breaking waves can be observed (Kjeldsen and Myrhaug, 1979); **plunging, deep water bores** and **spilling** breakers. Deep water plunging and spilling breakers have the same physical characteristics as those on a sloping beach. Deep water bores appear as a highly non-linear wave-wave interaction phenomenon where one wave overtakes another. It is characterised by a flow zone covering up to one third of the total wave height over which air-entrainment takes place and it proceeds over the underlying wave in a way very similar to the travel of a tidal bore in a river. A classification of the different types of breakers was made using a set of geometrical parameters. Figure 2.6 shows the definition of the parameters and figure 2.7 the classification of the breakers according to these parameters.

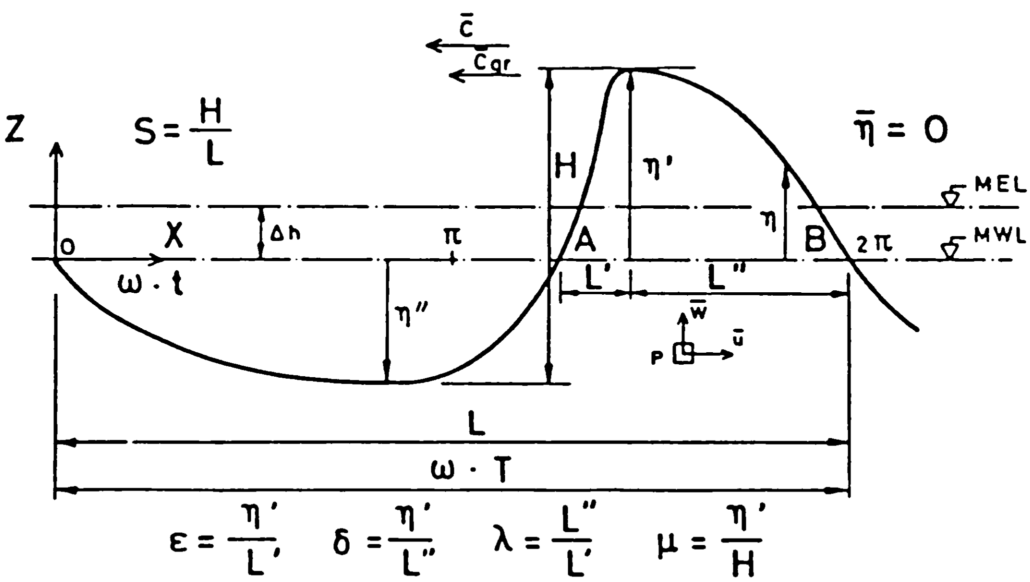

Fig. 2.6 Definition diagram of deep water breaker parameters (Kjeldsen, 1979)

Spilling	Plunging	Bores	Parameter
0.32		0.78	ϵ, crest front steepness
0.26		0.39	δ, crest rear steepness
0.90		2.18	λ, vertical asymmetry
0.84		0.95	μ, horizontal asymmetry

Fig. 2.7 Parametric deep water breaker classification

2.4.3 NUMERICAL MODELS

No analytical theory describes completely the time-dependent process of wave-breaking. However, modern numerical techniques have had some success in describing breaking waves. The most successful formulation is based on the property of irrotational flow that the shape of the fluid boundary and the value of the velocity potential on that boundary uniquely determine the flow field inside. The surface is represented by marked Lagrangian fluid particles, but the solution is neither exclusively Lagrangian nor Eulerian.

Longuet-Higgins and Cokelet (1976) first used this method for waves in deep water, assuming the waves to be periodic in space. The equations of motion were solved after conformal mapping of the physical plane inside a closed contour. The wave form in the physical plane was then found by an inversion of the mapping.

Vinje and Brevig (1980) extended the model by solving the problem in the physical plane and finite depth was introduced. The advantage is that certain other effects can be included without much modification of the program, such as arbitrary boundaries and obstacles.

This method has been used extensively and the motion characteristics were obtained from the results. Noteworthy conclusions reached can be summarised as follows:

a) Velocities at the crest of the wave reach values up to twice the phase velocity of a linear wave (Peregrine,1983).

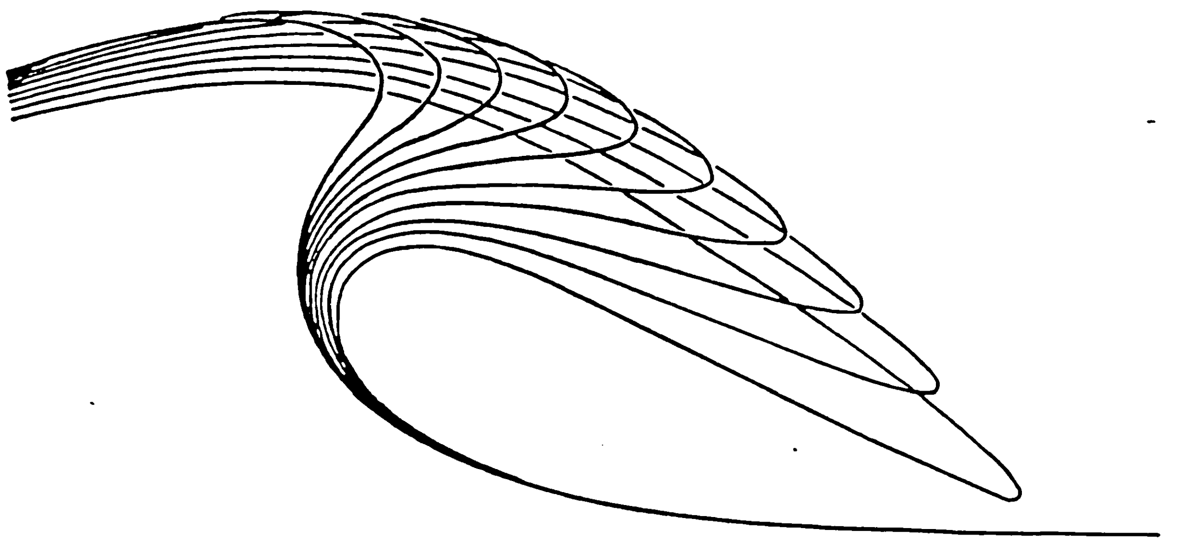

Fig. 2.8 A sequence of computed wave profiles for a periodic wave (Peregrine, 1983)

b) Accelerations at the tip of the wave exceed the acceleration of gravity. These accelerations can reach values higher than 5g in the subsequent development of the overturning.

c) The accelerations on the rear face of the wave are very small.

A graphical illustration of the results produced from such numerical schemes is shown in figure 2.8

New et al. (1985) extended the model of Longuet-Higgins and Cokelet (1976) to account for breaking waves in water of finite depth in a mapped plane. Results obtained from the extended model indicate that a steep beach leads to the development of a large scale jet and a highly asymmetric plunging breaker; whereas a gentle beach results in a near-symmetric spilling breaker with only a small scale jet. This agrees with the observed behaviour of natural breaking waves and it suggests that the two breaker types can be considered as members of a *single family* with continuously changing characteristics.

2.4.4 ANALYTICAL MODEL

Longuet-Higgins (1980) derived a relatively simple analytical model describing the crest of an overturning wave. In this model the pressure field is extended beyond the free surface so that there is a point at which the pressure gradient vanishes, called the *saddle point*. The solution forms the surface on which the pressure, P, and its rate of change, or its material derivative, both vanish so that the dynamic and kinematic conditions on the free surface are satisfied. The particle acceleration at the saddle point is equal to the acceleration of gravity and the saddle point appears to be in a free fall. Assuming that the form of the free surface is hyperbolic, the angle, γ, between the asymptotes and the angle of rotation of the principal axes, δ, are expressed in terms of t/λ where $\lambda=U/g$ and U is the horizontal velocity.

If the equation of the hyperbola is

$$\frac{x^2}{a^2} - \frac{y^2}{b^2} = 1 \tag{2.1}$$

$$\gamma = \cos^{-1}(1+\omega\xi^4)^{-1/2} \tag{2.2}$$

$$\delta = -\int \frac{d\xi}{(1+\omega\xi^4)(1-\xi^2+\omega\xi^4)} \tag{2.3}$$

where

$$\omega = P/\lambda^4 \tag{2.4}$$

$$\frac{t}{\lambda} = \int_0^{1/\xi} f^2 \frac{df}{(\omega-f^2+f^4)} \tag{2.5*}$$

* *Note: The equation corresponding to equation 2.5 presented in Longuet–Higgins paper (1980, eqn. 5.8) does not include the term f^2 in the numerator. This is a misprint.*

The variation of γ and δ with t/λ is shown in figures 2.9 and 2.10 respectively.

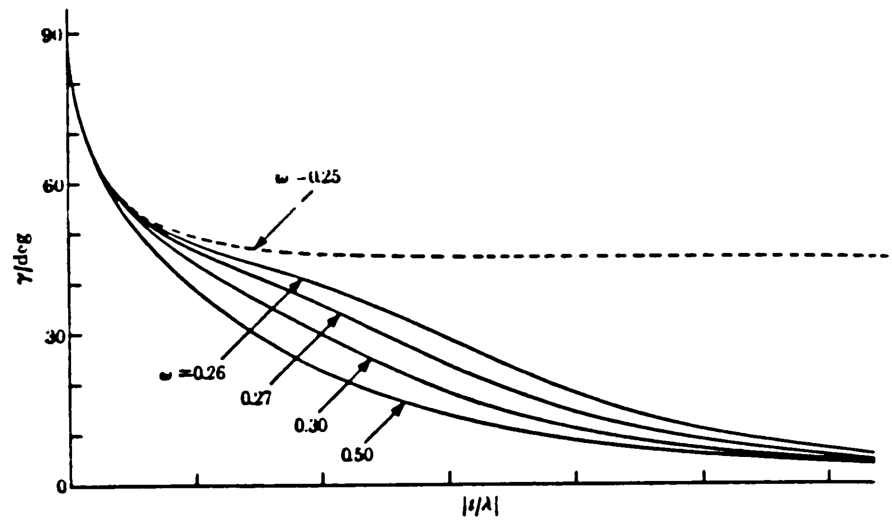

Fig. 2.9 The angle, γ, between the asymptotes as a function of time

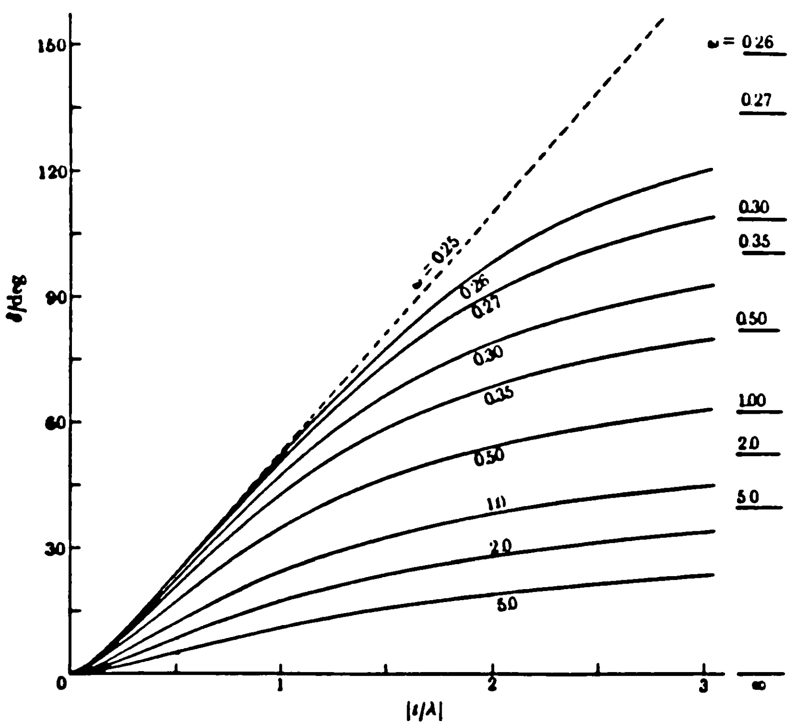

Fig. 2.10 The angle of rotation of the principal axes, δ, as a function of time

2.4.5 EXPERIMENTAL WORK ON BREAKING WAVES

In order to compare the numerically computed breakers with real ones, a number of experiments were performed in different laboratories.

Kjeldsen et al. (1980) carried out a series of experiments on deep water plunging waves and compared the results with their numerical model. The breakers were generated by the interaction of a very steep Stokes wave with a super-harmonic disturbance. The results were obtained from a high speed film with particles of neutral density as tracers. Comparison between the plunging breakers generated in the wave flume and those calculated numerically, showed good agreement with respect to the wave geometry. The measured and computed velocities also agreed well for depths larger than approximately one wave amplitude below the mean water level. In the wave crest, near the plunging jet, the measured velocities were 1.5 times larger than the computed ones. The authors attributed this discrepancy to the method of generating the plunging breakers. The numerical simulation started with a sinusoidal wave; the plunging breaker was then generated because the exact free-surface conditions were not initially satisfied. This wave received no energy before plunging and had no physical counterpart. The measured maximum velocities in the crest corresponded to 2.8 times the first order phase velocity.

In an experimental study of the transformation zone of plunging breakers, Hedges and Kirkgoz (1981) also measured water particle velocities at the crest of plunging breakers. Using a Laser Doppler Anemometer, it was found that the Eulerian horizontal velocities do not attain the speed of the wave crest by the time the breaking point is reached. It was suggested that the two velocities are only equal when breaking takes place on relatively mild slopes and when the deep water steepness is sufficiently great.

By analysing directly the signal from the photodiode of a laser doppler anemometer, velocity measurements were obtained at positions up to 4mm from the crest of deep water breaking waves (Easson and Greated, 1984). Comparison between numerically computed velocities by Cokelet (1979) and measured velocities showed that they agree within 10%, the measured ones being larger (fig. 2.11). The maximum measured velocity, up to the stage when the wave face becomes vertical is 0.94 times the phase velocity, c, which compares favourably with the theoretical prediction of 0.93c. It was concluded that the results of the study must be viewed as confirming the predictions of Longuet-Higgins and Cokelet.

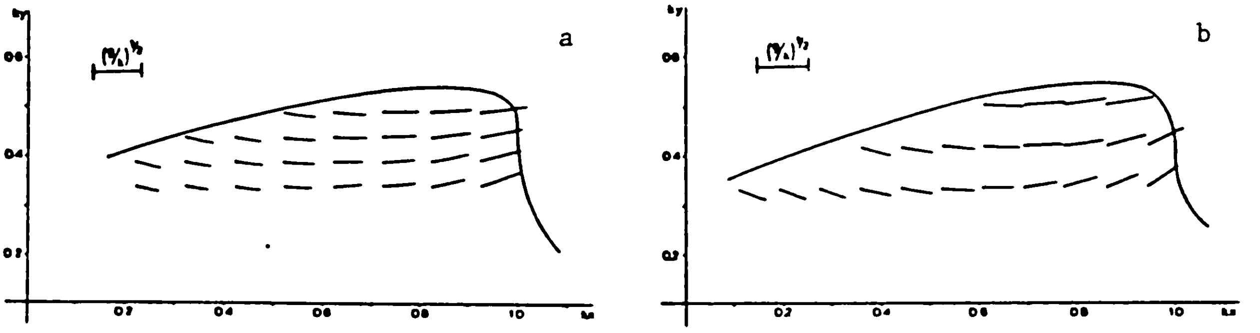

Fig. 2.11 a) Numerical velocity field (Cokelet, 1979)
b) Measured velocity field (Easson et al., 1984)

Kjeldsen (1984) devised an original method for measuring velocities in the crest of a deep water breaking wave. A current meter moved with the phase velocity inside a steep Stokes wave over a long distance until this particular wave phase collapsed as a plunging breaker, due to superposition with other wave components. It was found that the measured velocity increased to a value of 1.36 times the phase velocity in a position of few millimetres below the crest (fig 2.12). Particle

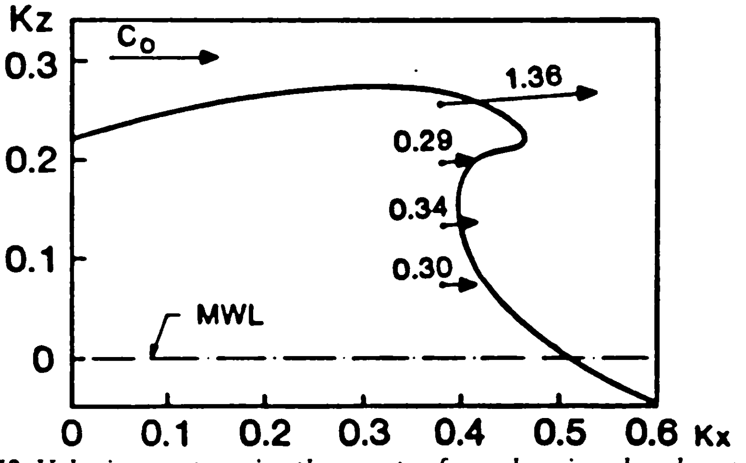

Fig. 2.12 Velocity vectors in the crest of a plunging breaker normalised with respect to the phase velocity (Kjeldsen, 1984)

velocities were measured using frame by frame analysis of a high speed film. These measurements showed that the particle velocity component normal to the boundary of the wave increased to a value that was 2.65 times the phase velocity at the very tip of the plunging jet. These last measurements confirm the high values obtained at this particular position by Longuet-Higgins and Cokelet(1976). Both the velocities measured with the current meter and the ones obtained from analysing the high speed film correspond to neither the Eulerian nor the Lagrangian velocities. These velocities have their own definition and comparison with other studies inevitably involves a discrepancy between the values of the velocities. However, the importance of these results is invaluable as they provide useful information which is very difficult to obtain.

2.5 AFTER BREAKING

From the plunging point onwards, the breaking process appears to degenerate rapidly into a chaotic motion of air and water. This misleading impression is obtained because of the large number of droplets and bubbles which interrupt the lines of sight. Several models have been developed which simplify and formulate this motion.

2.5.1 MODELLING

2.5.1.1 **Longuet–Higgins and Turner**

Longuet–Higgins and Turner (1974) considered a theoretical model of spilling breakers. In this model the breaker is regarded as a **turbulent gravity current riding down the forward slope** of the wave and retaining its identity because it is lighter than the wave below, owing to the trapping of air bubbles. A characteristic property of a spilling breaker is that, as it breaks gently at the crest, it traps air bubbles, resulting in an air–water mixture lighter than the water below it. This air–water mixture, or whitecap, acted upon by gravity, tends to slide down the slope (fig. 2.13). This model implies that air entrainment is both the driving and retarding mechanism. Driving, because it provides an increasing flux of water to accelerate the whitecap down the slope of the wave, and retarding, because the entrained water has momentum in the upslope direction. This model is quite simple and easy to use, but it is only applicable for steady spilling breakers.

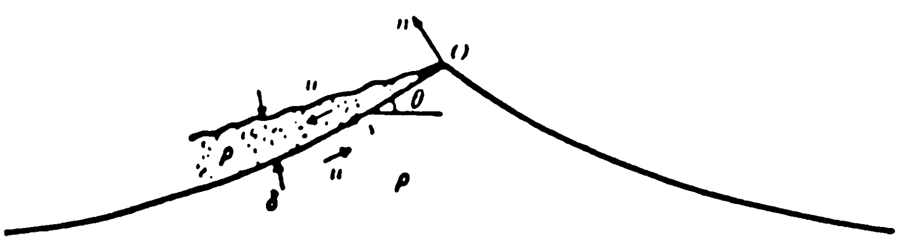

Fig. 2.13 Sketch showing the features of a spilling breaker (Longuet–Higgins and Turner, 1974)

2.5.1.2 **Peregrine, Svendsen, Madsen**

On gently sloping beaches, after the breaking of a number of waves, the breaking motion, or *white water*, becomes fully turbulent and the mean motion becomes quasi–steady, that is, it changes very little during one cycle. This motion can be described as a spilling breaker or a **bore** (Peregrine and Svendsen, 1978). The philosophy behind this reasoning is that, in studying any turbulent flow it is very helpful if it can be shown to be similar to other well known flows.

Using flow visualisation techniques, Peregrine and Svendsen (1978) observed that the strong turbulent motion induced by breaking waves spreads rapidly away from the surface. In shallow depths of water, the turbulent region fills very quickly the whole depth, whereas in deep water, the breaking region is followed by a *wake* just below the free surface which slowly thickens. The turbulent motion is generated by the velocity difference between the undisturbed water and the mass of water tumbling down the wave's face.

The above process is very similar to the mechanism of generation of turbulence when two uniform parallel streams of different velocities, u_1 and u_2, are allowed to meet, for example by passing the end of a partition between them (fig. 2.14). An important property of turbulent mixing layers is that they spread rapidly

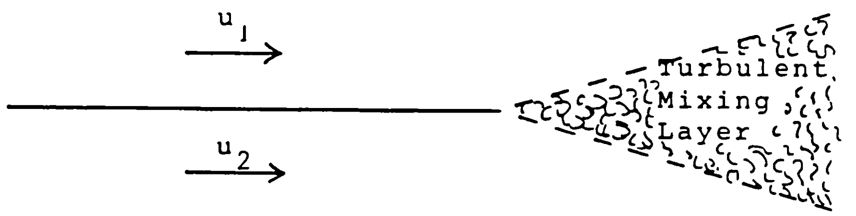

Fig. 2.14 Formation mechanism of a turbulent mixing layer (Peregrine et al., 1978)

with distance in a wedge. The angle of spread depends on the velocity difference between the two layers. In modelling breaking waves one of the velocities is considered very small, or nominally equal to zero, and the other equal to the crest velocity.

This model was extended by Madsen and Svendsen (1983). The turbulence was assumed to be concentrated in a wedge that originates at the toe of the front and spreads towards the bottom (fig. 2.15). The deviations from static pressure were neglected and the longitudinal length scale was assumed to be much longer than

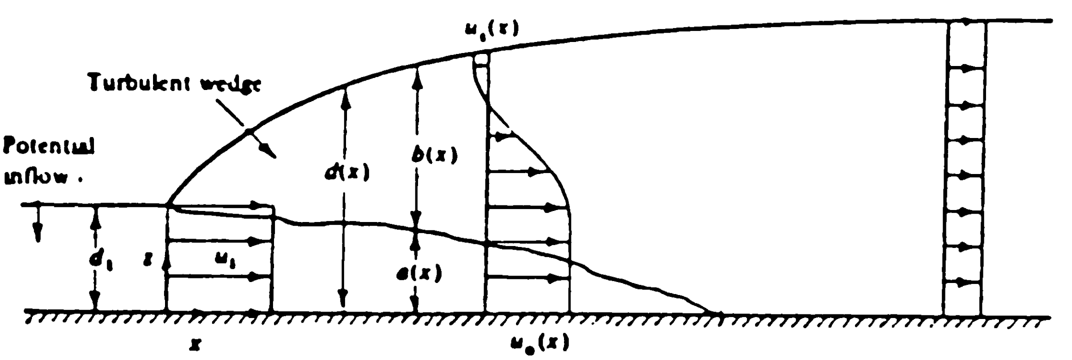

Fig. 2.15 Turbulent wedge model (Madsen et al., 1982)

the vertical one. It was also assumed that the flow has depth-independent velocities which decrease downstream due to increasing pressure. The bottom boundary layer and shear stresses were neglected, which is acceptable for a bore. This model predicted the flow, the shear stresses and the energy dissipation in the flow and comparison with experimental measurements indicated that the vertical variation of the velocities is in good agreement with laboratory measurements.

Svendsen and Madsen (1984) extended the model presented by Madsen and Svendsen (1983) by omitting the assumption of permanent form. Hence, the new model can consider the case of a bore propagating over an arbitrarily varying depth of water.

The above model describes the motion quite well, but it is applicable in the inner region only.

2.5.1.3 **Stive**

Another contribution to the understanding of the surf zone was the development of a theoretical model based on the depth integrated and time averaged conservation equations of mass, momentum and energy (Stive, 1984). The wave heights and set-up in the surf-zone computed from this model show good agreement with experimemtal results. A fundamental breakthrough introduced in the model is that the wave propagating shorewards in the inner region carries along a **volume of water in the form of a surface roller.** The roller is defined as the recirculating part of the flow above the dividing streamline. Since it is resting on the front of the wave, the absolute mean velocity in the roller equals the propagation speed, c, of the wave. A crude simplification of the velocity distribution is shown in figure 2.16. A conclusion from the results obtained from the model is that the decrease of the wave height is primarily (about 60%) due to a redistribution of energy and momentum. Potential energy is converted into forward momentum flux that concentrates in the surface roller.

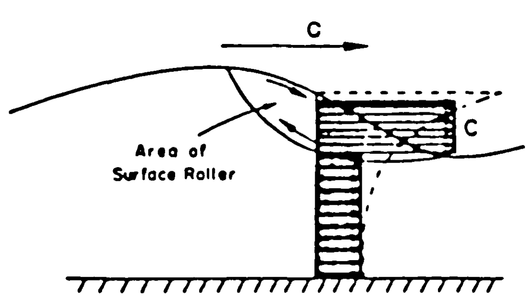

Fig. 2.16 Model of velocity distribution (Stive, 1984)

2.5.1.4 **Battjes and Sakai**

An experimental investigation which looked into the simulation of the turbulent

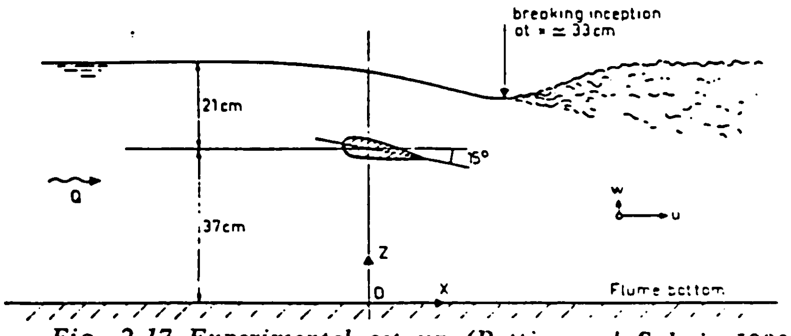

Fig. 2.17 Experimental set-up (Battjes and Sakai, 1980)

flow immediately following a spilling breaker with a turbulent mixing layer was performed using a **submerged hydrofoil in a steady current** (Battjes and Sakai, 1980). The aim of the experiment (fig. 2.17) was to obtain a steady breaker, unaffected by the bottom boundary layer whose geometry should resemble that of a spilling breaker or a post-breaking bore on a beach. Velocity measurements indicated that the region downstream of the initiation of breaking evolves as in a free self-preserving turbulent wake. It was also shown that in this region the velocity field is unaffected by scale effects, if it is scaled according to Froude's law.

2.5.1.5 **Horikawa and Kuo**

An alternative approach to the study of the flow in the surf zone is to simulate the flow with a suitable **wave motion** which is attenuated by the effects of turbulence and bottom friction. In such an approach (Horikawa and Kuo, 1966), the second order approximation of solitary wave theory was adopted to express the features of the broken waves progressing in the surf zone. The bottom shear stress was taken to be proportional to the square of the depth average velocity. The air-entrainment at breaking was assumed to be the cause of a large scale disturbance in the flow, which takes the main role of energy dissipation at the

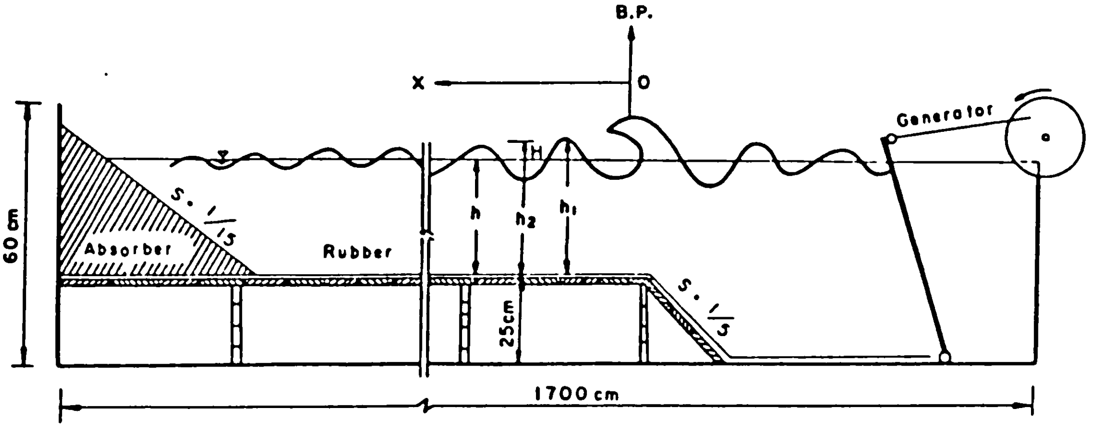

Fig. 2.18 Experimental set-up (Horikawa and Kuo, 1966)

initial stage of wave transformation in the surf zone. The energy dissipation due to turbulence was taken to be proportional to the square of the fluctuating horizontal longitudinal velocity which is inversely proportional to the distance from the breaking point.

Laboratory experiments on the wave transformation on a horizontal bed after breaking over a step (fig. 2.18) provided results consistent with the theoretical ones. However, in the case of wave transformation on a uniformly sloping beach, the analytical treatment was inadequate to explain the actual phenomenon.

2.5.1.6 Sawaragi and Iwata

An experimental and theoretical work on the mechanism of wave deformations after breaking and the factors which contribute to the wave energy dissipation, revealed some interesting results (Sawaragi and Iwata, 1974). In order to isolate the effects of beach slope, return flow, wave set-up and set-down, wave shoaling and wave reflection, the experiments were carried out on a composite slope (fig. 2.19).

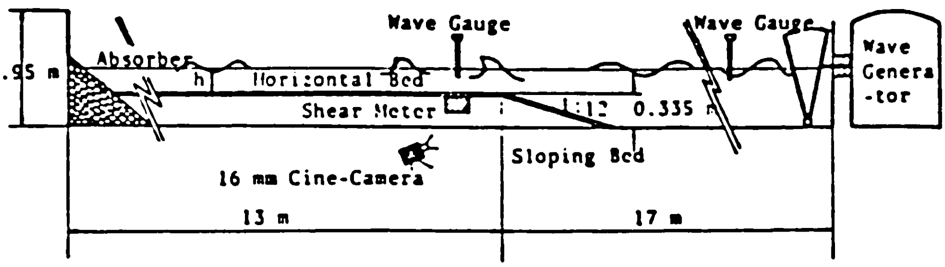

Fig. 2.19 Experimental set-up (Sawaragi and Iwata, 1974)

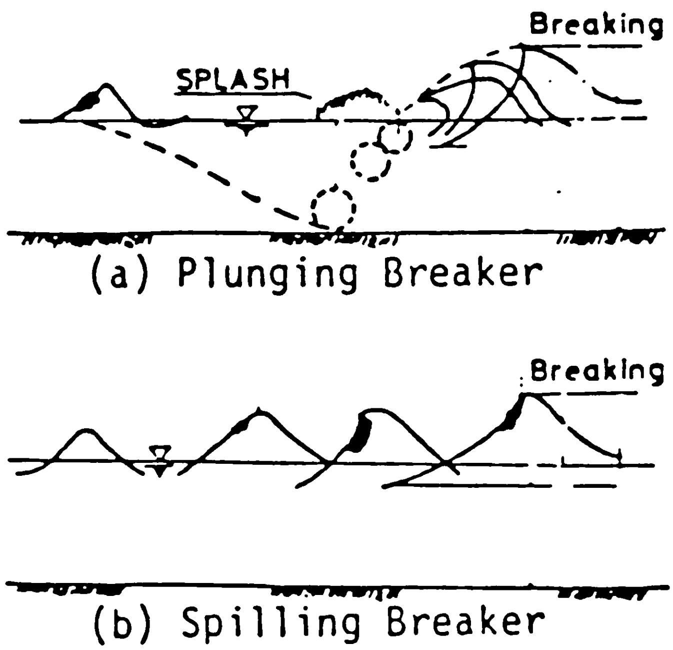

Fig. 2.20 Sketch of the characteristics of the wave breaking patterns (Sawaragi and Iwata, 1974)

The breaking model (fig. 2.20) assumed the formation of a **horizontal roller**. Theoretical results indicated that for plunging 15–30% of the total energy is dissipated by the horizontal roller. Bottom friction effects were found to account for about 9% of the total energy dissipation, leaving turbulence with air-entrainment as the most important factor for the wave decay after breaking. The theoretical results were verified experimentally and it was also established that the stronger the intensity of turbulence, the greater the height attenuation.

2.5.1.7 Fuhrboter

From a simple physical consideration, the sudden reduction of wave height and wave energy after the breaking of a wave can be explained by the air-entrainment into the water (Fuhrboter, 1970). Assuming uniform distribution of air bubbles, the energy required to entrain air in water is proportional to the square of the depth to which bubbles penetrate and to the concentration of the bubbles. Although there are no data available about the size, concentration or depth penetration of bubbles in breaking waves, this approach gives a qualitative understanding of the air-entrainment effects in energy dissipation. The relative significance of air-entrainment in plunging and spilling breakers is directly obtained from this treatment, since the difference in the depth of penetration of bubbles is so obvious between the two types. Another process highlighted from this method is that microturbulence is generated behind the rising bubbles, the predominant frequency of this motion being related to the diameter of the bubbles; the smaller the bubbles the higher the frequency.

2.5.1.8 Miller

The formation and evolution of vortices (Miller, 1976) is another approach from which the fluid motion during the breaking process can be described. When the front face of an overturning wave progressively extends forward and down and

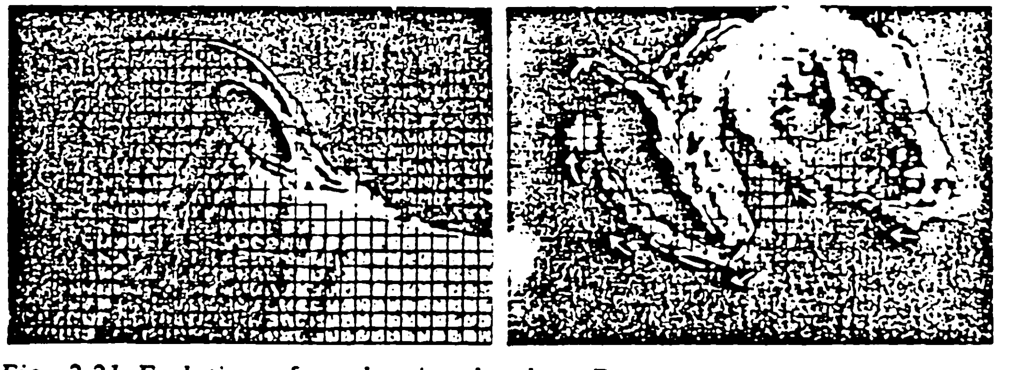

Fig. 2.21 Evolution of a plunging breaker. Formation of second vortex in front of the first one (Miller, 1976)

hits the forward slope of the wave, the first vortex is formed. The splash resulting from plunging forms a second vortex in front of the first one (fig. 2.21) and this process can repeat in as many as five or more successive vortices, with each successive vortex being weaker than the previous one. In this model a series of **large eddies** is introduced from the surface which contributes to the rapid decay of the wave during the breaking phase. As each vortex moves forward and down with enclosed air pockets, a mixing process takes place and the unstable air enclosures disintegrate into stable spherical bubbles. The model is also applicable for spilling breakers; vortices are generated on a much smaller scale and are confined to the near region of the free surface, generally above the mean water level. The rate of energy dissipation reflects the magnitude of penetration of the vortex system.

The internal fluid movements in the breaking wave can be considered to consist of the following components:

a) a shoreward horizontal drift,

b) a superimposed set of vortices whose magnitude and strength are a function of the breaker size and shape, and

c) a bottom boundary layer where the velocity gradient rapidly decreases.

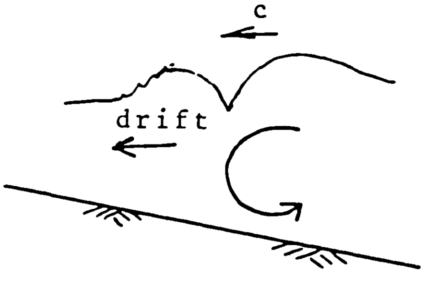

Fig. 2.22 Major velocity components beneath a breaker (Miller, 1976)

The major velocity components beneath a breaker are schematically shown in figure 2.22. It is assumed that the horizontal velocity component due to the progressive wave is essentially constant, surface to bottom, and is equivalent to the phase speed, c. The model was not analytically extended. However, the cornerstone for more detailed investigation was founded and further research on these lines was encouraged.

2.5.1.9 **Peregrine**

'The generation mechanism of the splash-up which follows after plunging is not yet clearly understood. The water must come partly from the jet and partly from previously undisturbed water; the division might be even, or tend towards one extreme' (Peregrine, 1983). On the one extreme, **the jet rebounds** and on the other

Fig. 2.23 Sketches of possible modes of splash-up after the plunging point. Water in and from the falling jet is shaded (Peregrine, 1983)

extreme, **the jet penetrates like a solid surface and pushes up a jet of previously undisturbed water** (fig. 2.23).

2.5.1.10 Basco

One recent hypothesis (Basco, 1985) is that in both spilling and plunging type breakers, which have similar characteristics but at different scales (fig. 2.24), **two**

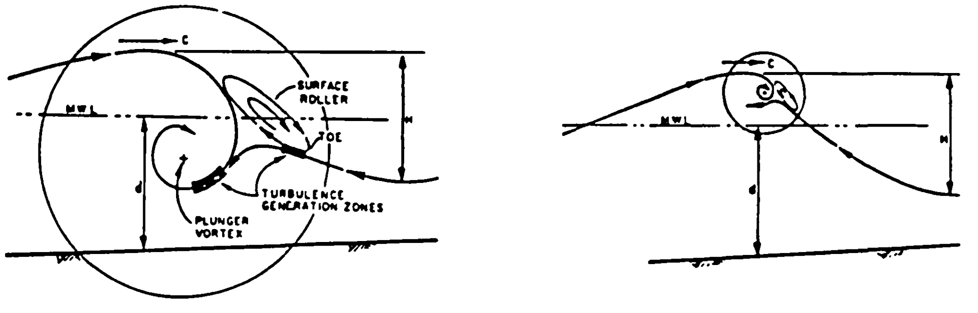

Fig. 2.24 Similarity of fluid motion in spilling and plunging breakers (Basco, 1985)

primary vortex motions are identified. A plunging vortex is initially created by the overturning jet, which in turn causes a splash-up of trough fluid, and the formation of a surface vortex, similar to the roller in a hydraulic jump. The plunger vortex translates horizontally to push up a **new surface wave** with vastly different kinematics that continues propagating into the inner surface zone.

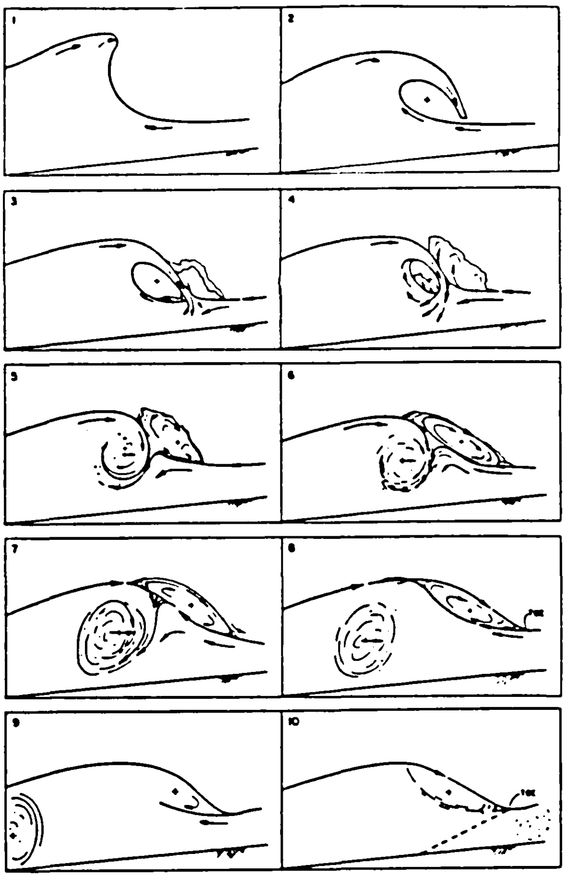

Fig. 2.25 Schematic sequence of breaking wave events (Basco, 1985)

The steps in the wave breaking process are shown diagrammatically in figure 2.25. The generation of the secondary wave disturbance begins in diagram 7 when the plunger vortex translates horizontally and pushes on the oncoming trough. The translation of the plunger vortex slows down and stops as it rotates, enlarges and drifts downwards. However, the secondary wave disturbance it generated continues to propagate forwards (diagram 9). The generation of the secondary disturbance ceases when the horizontal translation of the plunger vortex reaches its stable equilibrium position (diagram 10).

According to this model, the characteristic difference between spilling and plunging breakers is that although the process is similar, the size and role of the vortex and surface rollers is significantly different. In spilling breakers, the initial rollers are proportionately scaled. The small surface roller usually grows in size and it gradually slips down the steep forward face due to its weight component causing an inbalance in local momentum flux. The toe of the surface roller eventually reaches a tentative equilibrium near the lowest trough elevation.

This model also suggests the generation mechanism and scale of turbulence, illustrated in figure 2.24. The two primary zones of turbulence generation are:

a) beneath the surface roller, and

b) the outer radii of the rotating plunger vortex.

In these zones strong interfacial shear is produced due to the difference in velocities between the rollers and the main water mass.

Further to the diagrammatic modelling of the breaking process, a simple analytical model simulating the generation of the secondary wave disturbance was introduced. The forward and downward translation of the plunger vortex is approximated by the motion of a **wedge-type wave generator** (fig. 2.26). The amplitude of the generated wave is dependent on the stroke length, s, and the wedge submerged ratio, w=H/h. In a prototype scale wave, the wedge ratio is equivalent to the breaker index (breaker height/water depth) and the stroke length is equivalent to the horizontal translation distance.

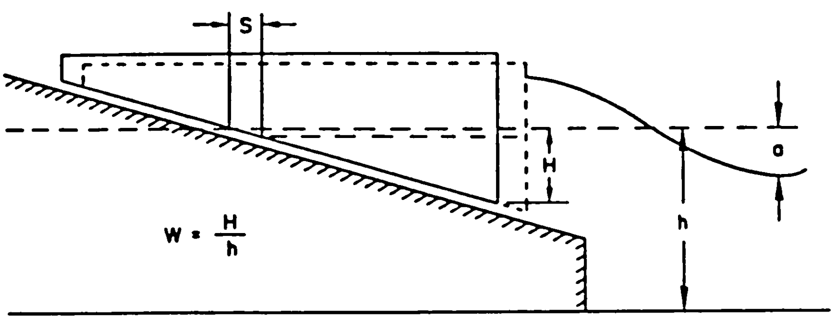

Fig. 2.26 Wedge-type model (Basco, 1985)

Another argument supporting the idea of the generation of a secondary disturbance is the following: since, *'by definition, a wave is simply a disturbance propagating in a fluid medium, it is realistic to believe that, a violently plunging breaker jet can produce another disturbance with far different characteristics.'*

2.5.1.11 Jansen

A new flow visualisation technique was recently developed and used to study

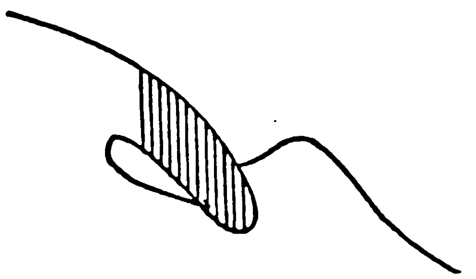

Fig. 2.27 Jet-splash model (Jansen, 1986)

the flow in the aerated upper part of breaking waves in the outer, or transition, region (Jansen, 1986). The **reflection of ultraviolet light from fluorescent particles** in the water mass enabled the tracing of particle motion. Some features of the flow revealed by this method are:

a) A sequence of jet-splash motions takes place for both spilling and plunging breakers. The fluid particles in the splash originate from the forward face of the wave and not from the plunging jet. The jet-splash interactions can thus be described as a **complete plunging mode** (fig. 2.27).

b) The particle trajectories inside the jet-splash motions are smooth, indicating the **absence of significant influence of turbulence**. This observation as well as the reproducibility of the motion suggests that **coherent motions** occur in the flow. Small scale turbulence may be generated by the interaction of these coherent structures with the surrounding wave fluid.

2.5.2 EXPERIMENTAL MEASUREMENTS ON BROKEN WAVES

On the problem of energy dissipation in the surf zone, it can be said that, different non-linear energy transfer mechanisms are dominant according to whether a wave and beach system is reflective or dissipative (Guza and Inman, 1975). In reflective systems, pronounced wave breaking does not occur, and the incident waves are strongly reflected at the shore. Non-linear instabilities exist which favour resonant energy transfer to subharmonic edge waves which then dominate the motion close to the shore (Guza and Davis, 1974; Guza and Bowen, 1976). In contrast to reflective systems, Flick, Guza and Inman (1981) studied experimentally the velocity field in a dissipative system. Velocity measurements with hot-film anemometers on monochromatic waves showed strong energy transfer to higher wave frequencies and that *unorganised* fluctuations under spilling and plunging breakers are of the order of half the wave-induced *organised* fluctuations. Organised fluctuation is the portion of the variation that is repeatable from wave cycle to wave cycle, in contrast to the unorganised fluctuation which represents the component of motion not repeatable from wave to wave.

The deviations of the velocities from the ensemble average were experimentally studied by Sakai et Al (1982). These deviations were called *turbulence* according to Stive's definition (Stive, 1980). Spilling and plunging breakers were generated from monochromatic waves shoaling onto a sloping beach. From the analysis of the experimental data it was concluded that:

a) The turbulence intensity is larger for plunging than spilling breakers,

b) In spilling breakers, significant turbulence does not exist at the breaking point. It begins to grow after the waves propagate some distance shorewards,

c) The turbulent intensity is larger in the upper part of the water column than near the bottom. Its vertical distribution resembles that of the turbulence under a steady breaker, similar to that produced by a submerged hydrofoil in a steady current (Battjes and Sakai, 1980).

Nadaoka and Kondoh (1982) performed a series of laboratory experiments on a sloping beach measuring horizontal longitudinal and vertical velocities around breaking regular waves using a Laser Doppler Velocimeter. The velocities were decomposed into the Eulerian mean velocity, the fluctuating orbital velocity and the turbulent velocity. The mean velocities were obtained by averaging the measured velocities over a period of 70 wave cycles. Due to the fact that the breaking points fluctuated due to long period oscillations in the wave tank, the definition of the turbulent component of velocities under breaking waves (Stive, 1980) was not applicable. Turbulence was thus taken as the velocity signal which passed through an analoque filtering circuit between 10 and 100Hz. The fluctuating orbital velocities were what was left after accounting for the mean and turbulent components.

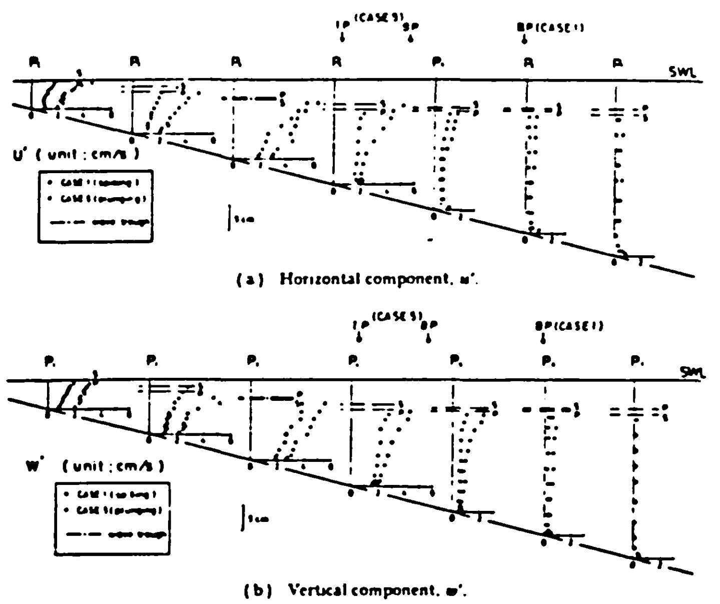

Fig. 2.28 Spatial distribution of turbulent intensity (Nadaoka et al., 1982)

The spatial distribution of the turbulent intensity (fig. 2.28) suggests that the turbulence in the surf zone is dominant in the upper part of the water column and decreases rapidly with depth. A similar pattern was obtained for the distribution of the *drop-out rate* defined as the ratio of the time during which air bubbles cross the measuring volume over the total time, which can be considerd as an index of the bubble concentration (fig. 2.29).

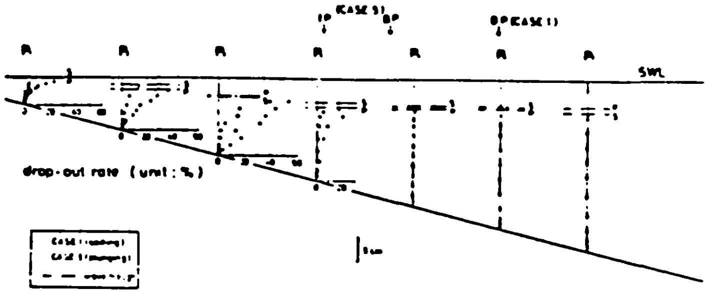

Fig. 2.29 Spatial distribution of drop-out rate (Nadaoka et al., 1982)

A conceptual model of the turbulent flow field based on the measurements is schematically illustrated in figure 2.30. This model can be described as a *two layer*

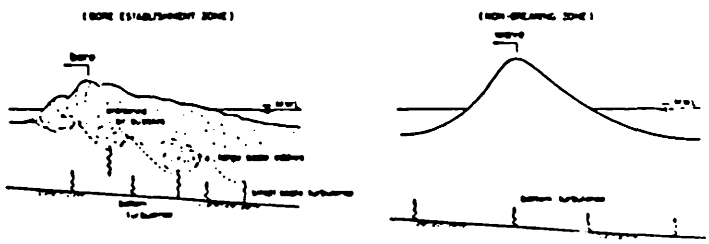

Fig. 2.30 Schematic illustration of the turbulent velocity field (Nadaoka et al.,1982)

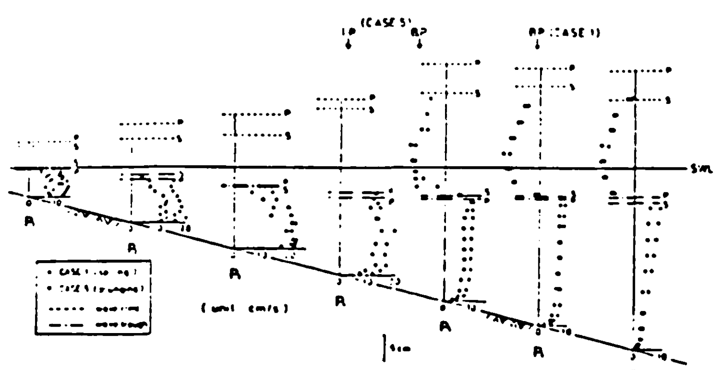

(a) Horizontal component, $\bar{u}$.

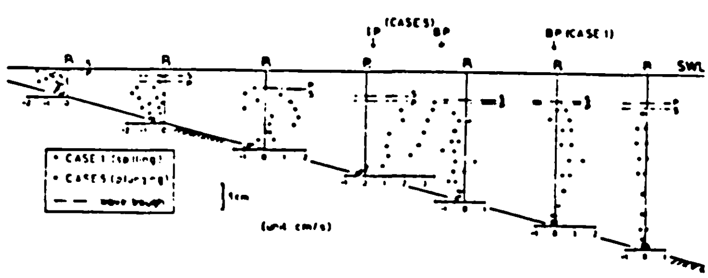

(b) Vertical component, $\bar{w}$.

Fig. 2.31 Spatial distribution of the Eulerian mean velocity (Nadaoka et al., 1982)

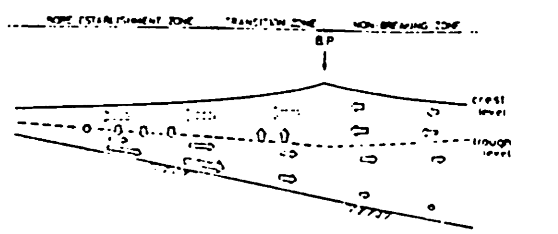

Fig. 2.32 Shematic representation of the Eulerian mean velocity within and near the surf zone (Nadaoka et al., 1982)

model. The upper layer is characterised by the existence of large scale eddies, associated with small scale turbulence and entrained air bubbles. The bottom layer is characterised by the existence of small scale turbulence originated from the upper layer and the bottom originated turbulence. The distribution of the mean horizontal and vertical velocities is shown in figure 2.31 and a schematic representation of these velocities is illustrated in figure 2.32.

The fluctuating orbital velocities were analysed in a different way. The *skewness factor,* $(\sqrt{\beta_1})u$, of the mean profile was computed for different wave conditions. Earlier work by the same authors showed that the mean drift velocity of sand particles in the direction of wave propagation increases with the value of the skewness factor of horizontal velocities. From figure 2.33 it is observed that as the skewness factor is almost always positive the asymmetry of the velocity profile tends to push sand particles shorewards. Since the mean velocities tend to transport sediment offshorewards and the fluctuating orbital velocities shorewards, the relative magnitude of these two factors will determine the net sediment transport.

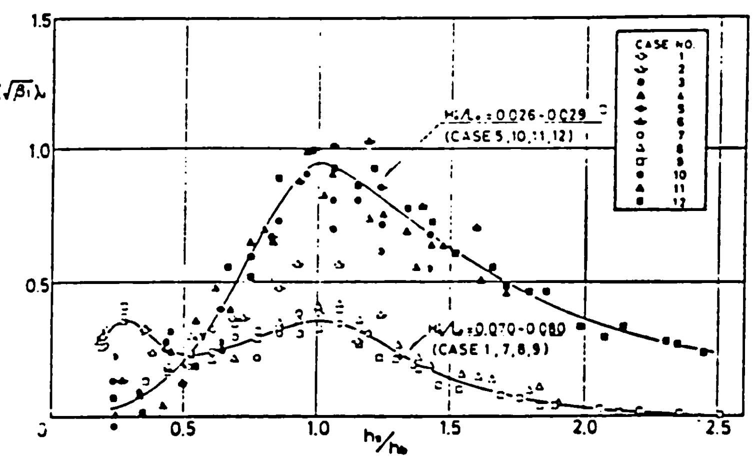

Fig. 2.33 Onshore–offshore distribution of skewness factor (Nadaoka et al., 1982)

Experimental studies of the drift velocity at the breaking point for regular waves shoaling on a sloping beach (Wang et Al, 1982) showed that the drift velocity has onshore direction near the surface and close to the bottom; whereas in the main flow column, the drift velocity is always offshore. A theoretical treatment in a finite length channel with consideration of fluid viscosity in the surface and bottom boundary layers (Longuet-Higgins, 1953) indicates that the drift velocity is in the direction of wave propagation near the surface and the bottom, but in the opposite direction in the middle section. However, Dalrymple (1976) carried out an analytical study on this problem and obtained different results. The main reason for this apparent discrepancy lies in the method of approach to the problem. Longuet-Higgins formulation is based on Lagrangian coordinates whereas Dalrymple's on Eulerian ones. Although these two sets of coordinates are to the first approximation identical, they differ significantly when higher order terms are taken into account.

The first three-dimensional velocity measurements under breaking waves in a laboratory tank (fig. 2.34) were taken by Nakagawa (1983). The velocity measurements were obtained using a flowmeter which measured the flow drag on three *tension threads* 55mm long, each recording a separate flow component. The velocities were decomposed into three components: the steady flow, defined as the mean velocity over a number of wave cycles, the periodic and the turbulent fluctuations. Two methods were used in calculating the periodic flow:

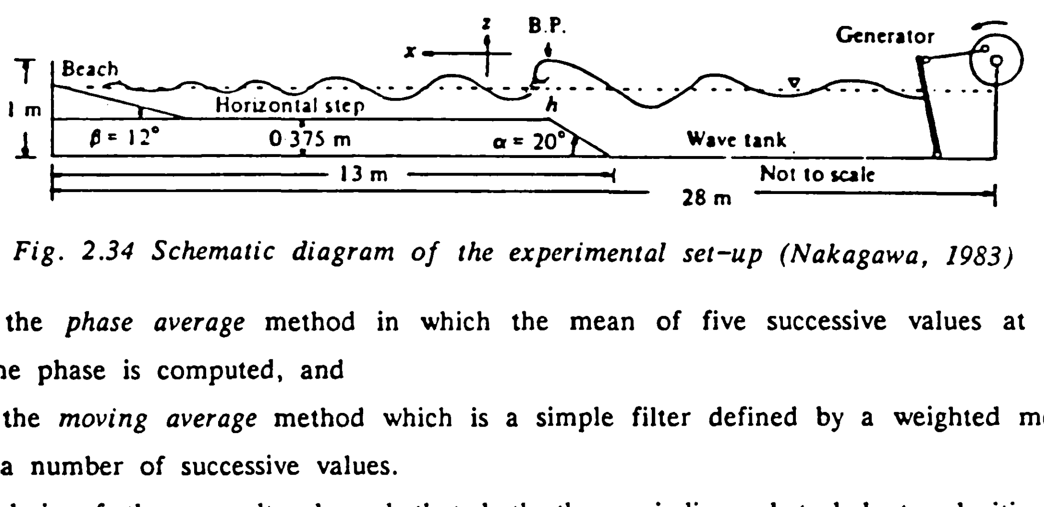

Fig. 2.34 Schematic diagram of the experimental set-up (Nakagawa, 1983)

a) the *phase average* method in which the mean of five successive values at the same phase is computed, and

b) the *moving average* method which is a simple filter defined by a weighted mean of a number of successive values.

Analysis of these results showed that both the periodic and turbulent velocities in the transverse flow component, generated by shoaling and breaking are comparable to those of the longitudinal and vertical velocities. Frequency analysis revealed that the original wave energy is transformed into both higher and lower frequency ranges in all three components.

Although this study did not consider the generation mechanism of the three dimensional nature of the motion, it focused the attention on the fact that transverse motion is produced by two dimensional breaking waves, and this motion can not be ignored.

A new technique for extracting the turbulent component from the velocity field was used in a recent series of experiments on a composite slope (Hattori and Aono, 1985). By assuming that all motion of the water surface is wave motion, turbulence was then defined as, the portion of the velocity not correlated with the wave profile. The separation of the wave induced and turbulent velocity components was made using non-recursive numerical filters having frequency response characteristics determined by the coherence functions between measured water surface elevations and velocities. Analysis of the results showed that regions of large turbulence intensity exist in the outer region near the plunging point and that turbulence motion transfers energy shorewards from the outer region to the inner region.

Assuming the turbulent structure in waves breaking on a beach is similar to that in a **plane wake**, Svendsen (1986) expressed the turbulent kinetic energy, k, as a function of the turbulent velocity fluctuations in *only* the longitudinal, u', and vertical, w', directions. This was achieved by making use of the known relationship between the turbulent velocities in a plane wake,

$$\overline{u'^2} : \overline{w'^2} : \overline{v'^2} = 0.42 : 0.32 : 0.26$$

where v' is the turbulent velocity component in the transverse direction. It was found that the turbulent level shortly after breaking is lower than the level observed further shorewards. There is a tendency for the turbulent energy to decrease slowly in the shoreward direction. Its maximum value occurs around $h_0/h_b \approx 0.7-0.8$ where h_0 and h_b correspond to the depths at maximum turbulence level and breaking location respectively.

As the production of turbulent energy corresponds to the dissipation of wave energy, the proportion of the energy dissipation between successive breakers can be determined from turbulent production considerations. It is estimated that about 20-50% of the energy is dissipated by the time the following breaker passes.

Another point raised by Svendsen is the presence of **random, short waves** on the water surface of broken waves. It is noted that these waves do form part of the turbulent component of the motion.

2.6 SUMMARY

The picture emerging from the review of the theoretical and experimental observations on breaking waves may be described by a number of models depending on the angle from which the problem is approached.

There is a "*consensus*" by almost all researchers that wave breaking is a local phenomenon; whatever the cause of breaking the motion directly involved in the breaking process is very similar. The distinction between the different types of breakers is simply conventional. All types of breakers have similar motions but at different scales.

In the case of breaking waves due to shoaling on a sloping beach, which is the usual process in coastal engineering problems, the wave breaking process can be divided into the transformation, overturning, outer, inner and run-up regions. In the transformation zone, there is no single wave theory which describes exactly the wave motion under all conditions. Different theories describe better than others the motion under different conditions.

Numerical models have been developed based on the Longuet-Higgins and Cokelet (1976) approach for describing the time-dependent motion in the overturning region. These numerical schemes are very powerful in the sense that they can predict the wave profile and hence the internal wave field for different conditions. An important point which must be stressed is that the surface is represented by marked **Lagrangian** fluid particles, but the solution is **neither exclusively Lagrangian nor Eulerian.** It makes use of the powerful properties of potential theory by adopting an **Eulerian** form at each instant of time, and it also makes use of the marked-particle quality of the **Lagrangian** description by following the fluid particles and their **Eulerian** velocity potential through time.

Laboratory measurements of velocities can, however, trace **either the Lagrangian or the Eulerian** time-histories. Comparison between the theoretical and experimental velocities is therefore restricted to instantaneous velocities. Studies on the verification of the numerical models show that the numerical models predict accurately the surface profile evolution and the kinematics in the main water body. Velocities in the plunging jet are usually expressed in terms of the linear phase velocity. Measured values range from 1.3 to 2.8 times the linear phase velocity, in the tip of the plunger, thus broadly confirming the high values obtained by the numerical models. Breaking is a local phenomenon and in deep water conditions the phase velocity is not well defined, since the wave's shape is unsteady and each point has a different time-varying velocity. The conventional linear phase velocity, which is proportional to the zero-downcrossing period at the breaking point is probably the cause of the scatter of the results.

Beyond the plunging point, the problem can be modelled in different ways depending on the conditions considered in each case. When the effect of the bottom is not considered, a spilling breaker can be modelled as a turbulent gravity current riding down the forward slope of the wave. Another special case studied in detail both theoretically and experimentally is that of fluid motion in shallow water in the inner region, where the water motion is uniformly turbulent across the water column, which is successfully modelled to a bore, a hydraulic jump or a turbulent wake.

The motion following the overturning of a plunging wave is very difficult to study experimentally because of the speed and intermittency with which the process takes place and the air entrainment in the surface which prevents measurements of flow characteristics and distorts the visual image of the process. However, recent studies have provided further insight into the initial model suggested by Miller (1976) and Peregrine (1981). The plunging jet penetrates the forward face like a solid surface and pushes up a jet of previously undisturbed water. The splash behaves then like a jet, due to gravity, and a splash-jet system is developed whose strength decays rapidly after the initial plunging. Up to 5 or 6 jet-splash processes can be observed, their number depending on the slope of the forward face and the strength of the initial jet. This motion generates a plunger and a surface roller, or vortex. The shear between the plunging mass of water and the undisturbed water in the forward face, as well as the shear between the surface roller and the undisturbed water are the main sources of turbulence. The plunging jet can produce another disturbance which will then propagate in the water volume with vastly different characteristics from the initial wave. Basco (1985) suggests that the characteristics of the new wave depend on the breaker height, the water depth and the horizontal translation of the plunger roller.

Experimental results are accumulating about the kinematics in the outer region. Most commonly, Eulerian velocities are measured which are then decomposed into organised, unorganised and turbulent flow (Flick et Al), or mean, fluctuating orbital and turbulent (Nadaoka et Al), or steady, periodic and turbulent (Hattori et Al). Apart from this disagreement on the decomposition of the flow, the term *turbulent* motion is not well defined. Table 2.1 shows how turbulence is numerically interpreted from the experimental results.

Having in mind all the experimental data available and the physical characteristics of the wave in the outer region, it may be said that the flow consists of a repeatable motion which depends on the initial wave characteristics, the

Reference	Method
Stive (1980)	Phase average (ensemble average of 20 cycles)
Battjes et Al (1981)	Analogue filtering
Flick et Al (1981)	High frequency component
Nadaoka et Al (1982)	10Hz<frequency<100Hz (analogue filtering)
Sakai et Al (1982)	Moving average (simple weighted filter)
Mizugushi (1982)	10Hz< frequency < 100Hz
Nakagawa (1983)	Phase and moving average
Hattori (1985)	Velocity not correlated with wave profile

TABLE 2.1 : Turbulence interpretation

boundary conditions and the breaker characteristics. There is a turbulent motion, as defined in classical fluid mechanics, which is generated from the interfacial shear on the surface and in the water body due to the formation of a surface and plunger roller. There is also a three-dimensional random wave motion due to the three-dimensional shape of the plunging jet and the inevitable air entrainment. This motion has frequencies both higher and lower than the initial motion.

Note that turbulence in classical fluid mechanics (Bradshaw, 1971) is defined as a three-dimensional time-dependent motion in which vortex stretching causes velocity fluctuations to spread to all wavelengths between a minimum determined by viscous forces and a maximum determined by the boundary conditions of the flow.

2.7 CRITICAL ASSESSMENT AND PHILOSOPHY OF APPROACH

The problem of breaking/broken waves has been, in general, approached from two different angles:

a) the mathematical, and
b) the engineering angle.

Mathematically, the wave motion is fairly well described up to the plunging point, when the overturning face hits the forward face of the wave.

The broken wave motion has been approached from mainly an engineering angle. Unlike the deterministic nature of the overturning wave motion, the broken wave motion is simulated by other physical processes and the probabilistic properties of the motion are predicted. However, the broken wave problem has been examined from a rather macroscopic angle. The bore and hydraulic jump mechanisms are global models, treating the whole process as an entity. The potential for identifying similar physical processes in a microscopic context is investigated in this thesis.

As highlighted in the literature review, the overturning process and the associated effects take place so quickly and are affected by so many factors, such as bottom friction and return flows, that it is difficult to record and study the problem. The effort of this thesis focuses in overcoming these problems, by the fast collection of data in a regime free from bottom friction and return flow effects.

All of the reviewed experimental studies on broken waves deal with regular waves, that is, waves of constant period. Breaking is achieved due to shoaling on a uniform or composite slope. The effects of a **single breaker in deep water conditions** have not been dealt with yet, as far as the broken wave motion is concerned. Such a set-up simplifies the problem, as it isolates the breaker induced motion. In this context, the period of the wave is immediately withdrawn as a parameter affecting directly the broken wave motion. The breaker is now described only by its shape and size. Approaching the problem from this angle introduces a fundamental deviation from the general trend in broken wave studies; the frequency components to which turbulence is decomposed may no longer be associated with the wave period. The local properties of the breaker are the parameters that determine the breaker induced wave motion, not the prevailing overall wave climate.

Experimentally, the problem may be approached from measurements of the kinematics of broken waves in deep water conditions, as well as from visual observations of the whole breaking/broken wave process. The question which then arises is: "given the characteristics of a breaker, what are the kinematics at a given location and a certain time"?

The questions of **why** these processes take place, **how** can they be described and modelled analytically or experimentally, and **what** is their significance, are to be answered. The gap between the broken wave motion and the breaker characteristics needs yet to be bridged. The problem is approached by investigating the physics of both processes and combining them.

In summary,

a) the intention of this thesis is to approach the breaking/broken wave problem from the **physics** angle with a view to forming a coherent mathematical - physical - engineering picture of the complete process, from the stage of wave overturning to the three-dimensional broken wave motion.

b) The study concentrates on not only **macroscopic** processes but focuses attention on the **microscopic** ones, as well.

c) The areas in which very little work had been previously done are tackled, namely:

1. the **transverse** motion induced by two dimensional breaking waves;
2. the **physical** process taking place during wave overturning;
3. the **secondary** wave disturbance induced by the breaker;
4. the **air-entrainment** and associated energy loss;
5. the theoretical prediction of **scale effects** in breaking/broken waves.

CHAPTER 3

EXPERIMENTAL EQUIPMENT AND PROCEDURES

3.1 ABSTRACT

Three main problems are tackled regarding the measurement of velocities under a deep water breaking wave in the laboratory using a Fibre Optics Laser Doppler Anemometer: firstly, the development of special software for the accurate control of the experiment, secondly, the determination of the suitable conditions for the operation of the Anemometer, and thirdly, the determination of a method for the generation of breaking waves in water of finite depth.

3.2 APPROACH

The aim of the project is to measure in the laboratory the kinematics of broken waves. The intention is not to repeat work done in previous studies, but to produce new sets of data and relate them to the current state of knowledge.

The motion in the outer region of breaking waves is decomposed into three parts:

a) mean, or steady;

b) orbital, periodic, or organised; and

c) turbulent, fluctuating or unorganised.

The task of decomposing the velocity field can be avoided by measuring directly one component. In a two- dimensional channel, the mean and orbital components of the velocity in the **transverse** direction are expected to be zero. The velocity field represents therefore, only the turbulent, fluctuating or unorganised motion.

Measurements of kinematics of waves breaking on a beach, or over a step, are affected by not only the plunging of the wave but by other effects as well, such as bottom friction, return flows or wave set-up. The isolation of the plunging induced motion is possible by measuring the velocity field of **deep water** breaking waves.

The purpose of the experiment can then be stated as the measurement of velocities in the transverse direction around deep water breaking waves, with a view to isolating the fluctuating motion induced by breaking waves, and determining its relationship with the breaker characteristics before plunging.

3.3 EXPERIMENTAL FACILITIES

The hydraulics laboratory at Imperial College is equipped with a servo-controlled wave generator installed in a flume 55m long, 2.83m wide and 1.60m deep, a Fibre Optics Laser Doppler Anemometer, FOLDA, a number of BBC microcomputers for data collection and analysis and other equipment (plates 3.1, 3.2).

As the success of an experimental project strongly depends on the reliability and accuracy of the laboratory equipment and the repeatability of the whole process, great emphasis is placed on achieving the optimum conditions for performing the experiments. The main tasks include

a) the development of suitable software for controlling accurately the experiments,
b) the determination of the proper conditions for use with the FOLDA, and
c) the generation of repeatable breaking waves.

The experimental set-up is diagrammatically shown in figure 3.1.

3.4 EXPERIMENTAL CONTROL

The collection of data from transient processes requires accurate control over time, especially when ensemble average values are extracted from the data. In order to achieve such a control, suitable software was developed.

The objective of the main experimental process was the collection of velocity time-histories, around the plunging area of a deep water breaking wave. The driving of the wave generator as well as the collection of data should be controlled accurately by means of a computer. The main parameters input by the user are the duration of the collected time histories and the time difference between the initiation of the wave maker motion and the beginning of the data collection. The development of such a control program was done on a BBC microcomputer in mixed assembly and Basic languages. The flow chart of the software is shown in figure 3.2.

Plate 3.1 Servo controlled wave generator

Plate 3.2 Fibre Optics Laser Doppler Anemometer and data collection instrumentation


DISA
LASER ANEMOMETER
TORCH

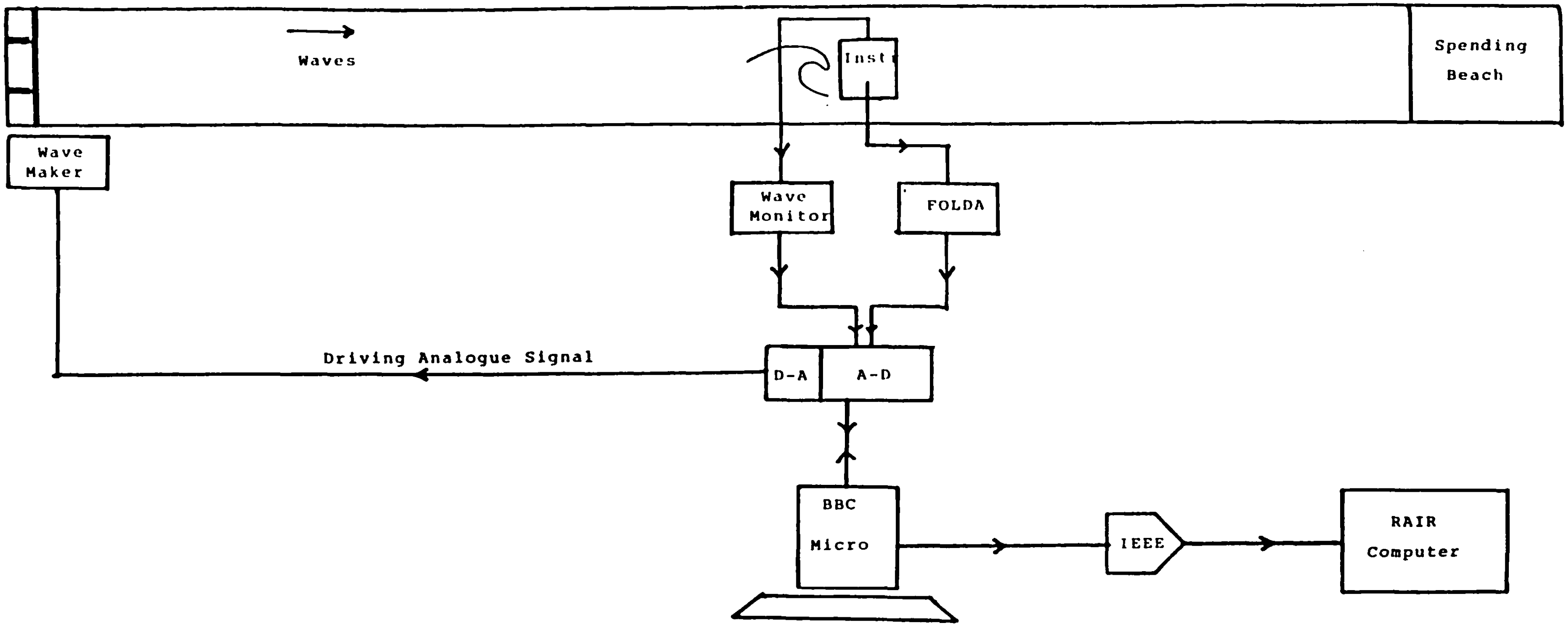

Fig. 3.1 Diagramatic experimental set-up

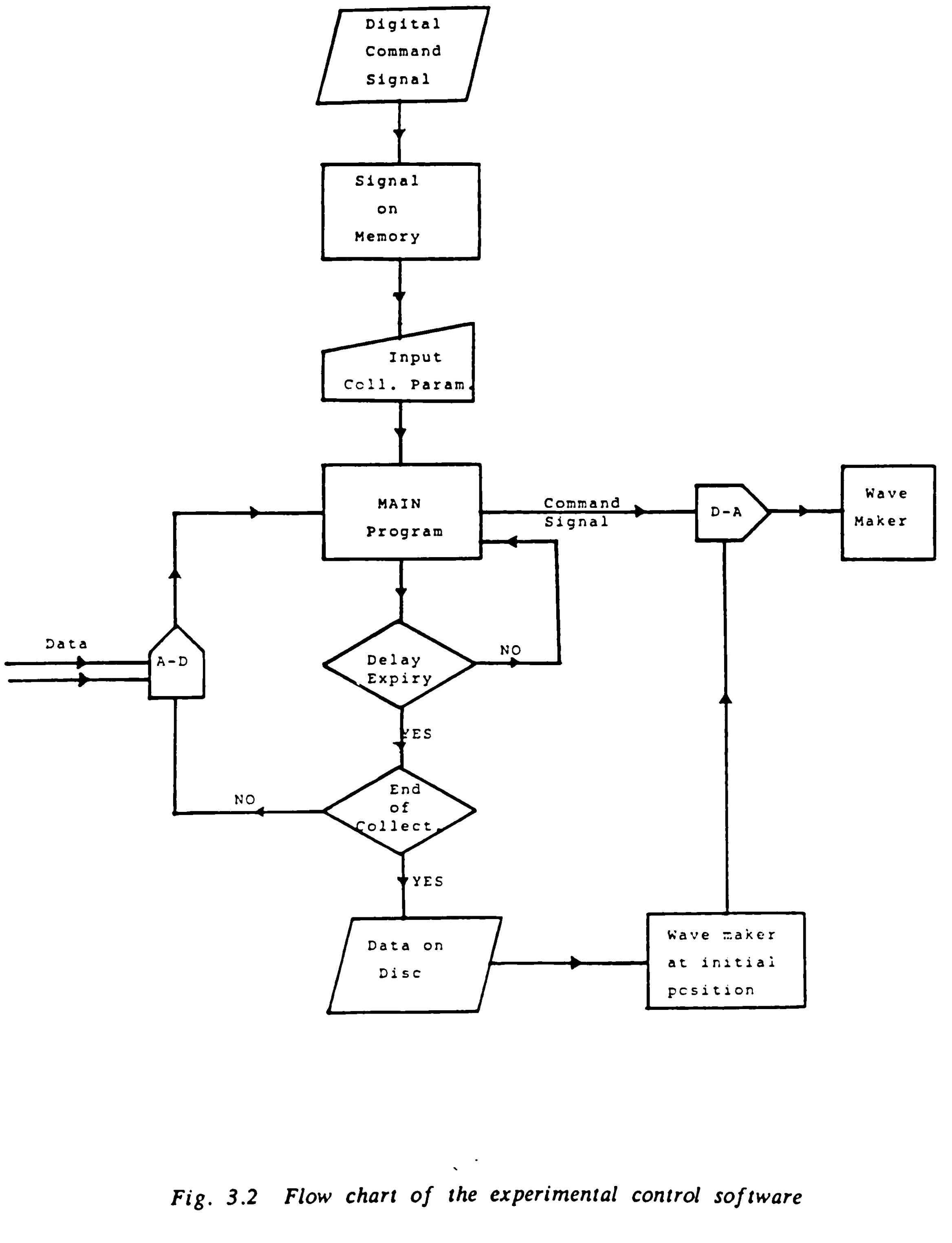

Fig. 3.2 Flow chart of the experimental control software

The command signal is digitised, with 25 values per second and loaded on the memory. However, the smoother the analogue signal, the smoother the operation of the wave generator. The command signal is therefore smoothed by the software to 100 values per second using linear interpolation between successive values stored on the memory. In this way a 100Hz analogue signal is sent to the wave generator whilst only one quarter of the digital values are stored on the memory.

This operation, however, restricts the choice of collection frequency. Since the computer sends a signal to the wave generator, through the analogue to digital converter every one hundredth of a second, the collection frequency must be either a multiple of 100Hz or a whole fraction of 100Hz (i.e. 100, 200, 300, ... or 50, 33.33, 25,...Hz).

The principle on which the software package works is simple. The internal clock of the computer is set to work at a frequency equal to the higher between the collection frequency and the signal frequency, of 100Hz. As soon as the user presses a button, the clock begins and the command signal starts. When the delay time elapses, collection of data begins. At the end of the collection stage, the collected data is stored onto a floppy disc. The package also includes a facility which ensures that the wave generator returns to its mean position.

The collected data are then transferred for analysis to a more powerful computer, namely the RAIR microcomputer, through an IEEE 488.

The development of the programs was not easy. Big parts of the programs were written in assembly language, which has only very basic commands and offers limited error diagnostics. Two existing programs, one for data collection and one for digital to analogue conversion formed the foundations on which the new software was developed.

3.5 FIBRE OPTICS LASER DOPPLER ANEMOMETER

3.5.1 CHARACTERISTICS

The laser anemometer is a non-contact optical instrument measuring fluid velocity in gases and liquids, without disturbing the flow in the measuring field. The only necessary conditions are a transparent medium with a suitable concentration of tracer particles, or seeding, and access to the flow through windows, or via a submerged optical probe.

The laser anemometer has an absolute linear response to fluid velocity. The measurement is based on the stability and linearity of optical electromagnetic waves and is only slightly affected by other physical parameters such as temperature and pressure.

The velocity measured by the instrument is the projection of the velocity vector on the measuring direction defined by the optical system.

The optics of the laser anemometer define a very small measuring volume, allowing local measurements of Eulerian velocities.

3.5.2 PRINCIPLES

The laser Doppler anemometer measures the rate of change of frequency of the light waves after scattering from particles moving with the fluid. The quantity measured is the time-dependent velocity of the scattering elements.

Where two laser beams intersect, interference patterns result (fig. 3.3). These

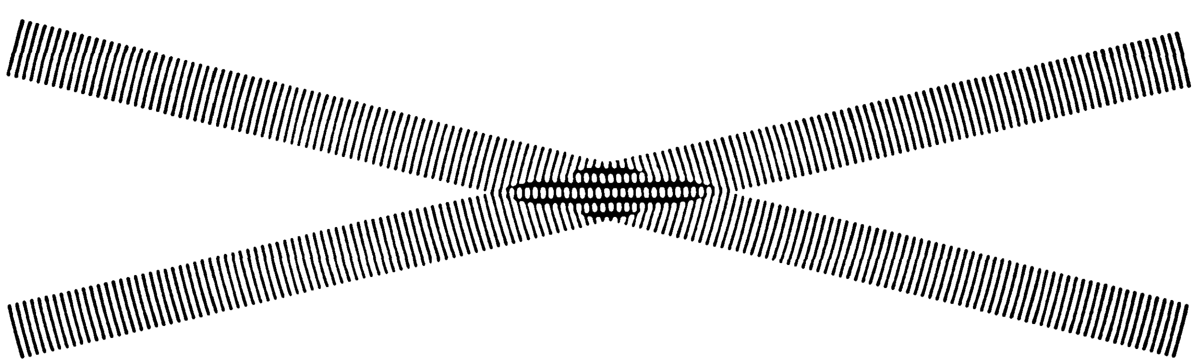

Fig. 3.3 Interference patterns resulting from two intersecting laser beams

regions of intensity maxima and minima are known as line fringes. When the frequencies of the two beams are different, the interference fringes move with a velocity,

$$V_s = f_s \, d_f$$

where f_s is the difference between the two frequencies and d_f is the fringe spacing. A flow moving against the fringe pattern will increase the frequency of the light scattered from a particle moving in the measuring volume by the Doppler frequency shift. The scattered signal is received by the photodetector and processed electrically by the Frequency Tracker and Frequency Shifter. An analogue presentation of the detected Doppler frequency is produced in the range 1 to 10 volts. The velocity is directly related to the analogue voltage.

3.5.3 SEEDING

The seeding particles can be considered to be the actual velocity probes. The particles must be small enough to track the flow accurately, yet large enough to scatter/ reflect sufficient light for the proper operation of the photodetector. Smaller particles scatter more evenly and larger particles are more unpredictable.

In deciding what seeding to be used some practical problems must be considered. The seeding concentration must be uniform in the vicinity of the measuring point and if the experiment lasts for a long time, the seeding must have a density very close to that of the fluid in which the measurements are taken. A further consideration might be the cost of the seeding, especially in large scale experiments where a big volume must have uniform seeding concentration.

All particles reflect the frequencies of light present in their colour spectrum and absorb the rest. The monochromatic laser beam (wavelenght, λ=632.8nm) is reflected by shining particles or particles whose colour spectrum contains the frequency of the laser light.

It was found that jeweller's rouge is a very good seeding powder. It has a density of 1.05 g/cm^3 which allows suspension in the water for a long time. 3.5% of the particles are greater than 45μm. Although jeweller's rouge is not shiny, its colour is dark red which reflects the red laser light quite well.

3.5.4 SIGNALS

Apart from the frequency information related to the velocity to be measured, the photodetector also contains noise. The primary source of noise is the photodetector shot noise, which is a fundamental property of the detection process. In addition there is a mean photocurrent and shot noise from undesired light reaching the photodetector. Further noise sources are secondary electron noise from the photomultiplier dynode chain and preamplifier noise in the signal processor.

Noise can be minimised by selecting only the minimum bandwidth needed for measuring the desired velocity range by setting low-pass and high-pass filters in the signal processor input. It is also helpful to work in as dark an environment as is practical to reduce undesired sources of light.

Noise is also induced at the signal processing stage. Since the seeding particles are located randomly in space, the individual current contributions are added with random phases and generate a noise signal in the tracker output. This phase noise does not influence the mean velocity results, but adds a certain amount to the r.m.s. value. The noise contribution depends on the optical configuration but is typically of the order 1-10% of the mean value.

In order to keep the noise level to a minimum, the instrument is operated in *ranges*. A physical equivalent of the *ranges* is the gear operation of a car. The higher the gear, the less the ability of the driver to change the speed of the car by small amounts. Similarly, the Doppler anemometer tracker system is not very well suited for high resolution, fine-scale turbulence measurements in flows with a relatively large mean velocity.

3.5.5 CRITICAL ASSESSMENT OF THE FOLDA

The main problem of operating a FOLDA of 35mW power, is that its power is weak and the intensity of the signal received by the photodetector is very low. In order to improve the signal,

a) the concentration of the seeding must be high,
b) the backscattering, or reflection, from the seeding must be improved, and
c) the noise level must be minimised.

Although the smaller the seeding particles the better the scattering, reflection is higher the bigger the particles. Jeweller's rouge was found to reflect light satisfactorily and the concentration was acceptable as the seeding is light and particles remain suspended for a sufficiently long time.

The noise level is minimised by covering the area around the measurement position with black curtains and polysterine sheets. In this way safety regulations are also satisfied.

As the FOLDA is not very well suited for turbulence measurements in flows with large mean velocities, the instrument is operated in different ranges. The higher the range of velocities, the higher the noise level and the less reliable the turbulent component. Before collecting data from the FOLDA the optimum range is found so that the instrument is not saturated and the noise level is low.

3.6 AN APPLICATION OF THE TIME SYMMETRIC PROPERTIES OF SURFACE WAVES: GENERATION OF BREAKING WAVES

3.6.1 ABSTRACT

The dispersive properties of deep water waves permit the generation of breaking waves at a predetermined location in a laboratory flume equiped with a servo-controlled wave maker. The semi-empirical expressions normally used up to now to drive the wave maker cannot provide a satisfactory degree of control over the profile of the wave transient. An alternative approach to this problem is based on the principle that the equations governing the motion of small amplitude water waves are independent of the origin and direction of the time and space axes. Wave breaking is achieved by the focussing of energy at a given location. The motion at the wave generator's position required to produce an accumulation of energy at a particular location is therefore the reverse of the motion induced by the release of the same amount of energy at that location. The analytical solutions to this problem are thus directly employed to drive the wave maker. This method incorporates the principles on which earlier methods were based in controlling the breaking location, and in addition it allows control over the breaker shape, in terms of the shape of the initial elevation considered in the solution.

3.6.2 INTRODUCTION

Longuet-Higgins (1976) suggested two methods for the generation of breaking waves in a laboratory channel. One is by decelerating the wave maker, and the other using the Fresnel envelope of an advancing wave front.

The first method is based on the dispersive properties of deep water waves; that is, longer waves travel faster than shorter ones. According to linear theory, the wave energy propagates with the group velocity, c_g, which is one half of the phase velocity, c. Suppose that at time t, a wave train is generated with angular frequency, ω, and at time $t+\delta t$ it is followed by a second train of longer waves with angular frequency $\omega+\delta\omega$. The energies of the two wave trains will meet at time t' at distance x from the generation point (Fig. 3.4), such that

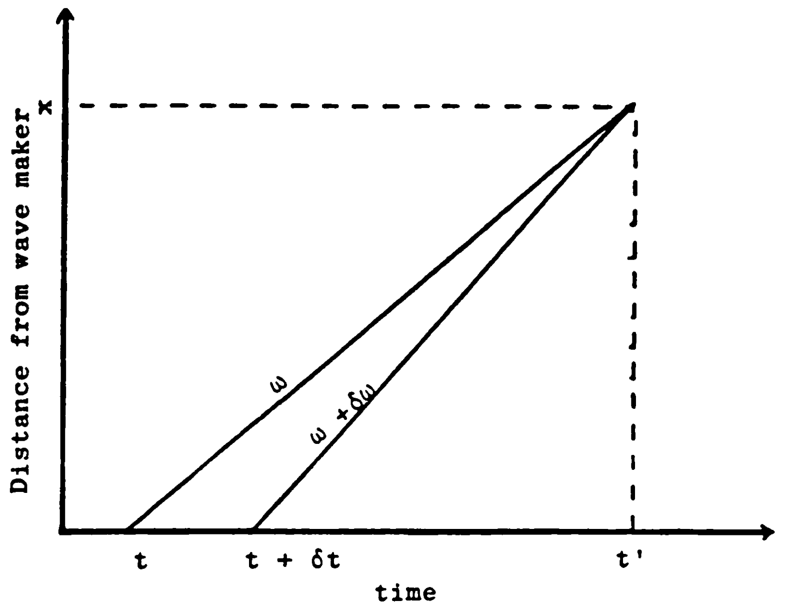

Fig. 3.4 Energy propagation diagram for two wave trains of different frequencies.

$$\frac{x}{t'-t} = \frac{g}{2\omega} \quad \text{and} \quad \frac{x}{t'-(t+\delta t)} = \frac{g}{2(\omega+\delta\omega)} \qquad 3.1$$

eliminating t',

$$2x\delta\omega = -g\ \delta t \quad \text{or} \quad \frac{\delta\omega}{\delta t} = -\frac{g}{2x} \qquad 3.2$$

If the angular frequency of a wave generator is changed continuously at a rate $d\omega/dt=-g/2x$, the wave energy will tend to converge to a position at distance x from the wave generator. If the accumulation of energy is large enough to cause instability, a deep water breaking wave will be produced.

The second method depends on the finite bandwidth of frequencies associated with the sudden starting or stopping of the wavemaker. If the wavemaker is switched on suddenly with constant amplitude, a, and frequency, ω, a wave train is propagated down the tank with group velocity $g/2\omega$ and the elevation of the free surface at position x and time t is

$$\eta(x,t) \sim i\ B\ F(\tau)\ e^{i(\omega t-\omega^2 x/g)} \qquad 3.3$$

where B is a constant depending on the form of the wave maker, and

$$F(\tau) = \frac{1}{2} + \frac{1}{(2i)^{1/2}} \int_0^{\tau} e^{i\pi\lambda^2/2}\, d\lambda \tag{3.4}$$

The waves tend to break when the crest passes the position of a maximum in the wave envelope.

Kjeldsen (1982), using the properties of non-linear solitons derived an expression for the command signal to the wave generator required to produce deep water breaking waves. The obtained expression is:

$$\eta(x,t) = \sqrt{2}\left[\frac{kg}{2\pi x}\right]^{1/2} f(t)\cos\left[\frac{g}{4kx}t^2 - \frac{\pi}{4}\right] \tag{3.5}$$

where k is a non-linear dispersion factor depending on the wave steepness, which is taken as constant ($k \approx 1 \sim 1.2$) and f(t) is an increasing function of time. This method has the advantage that it takes into consideration the wave steepness, thus allowing better control over the breaker location, but it provides no information about the relationship between the wave profile ($\propto$ f(t)) and the breaker characteristics.

Mansard and Funke (1982) used the linear dispersion theory to produce breaking waves. The sweep frequency method, as it is called, has proved that control over the wave breaker location is possible, but this method does not permit any control over the profile of the wave. In the absence of an analytical description of such a wave as a function of time, a mathematical function was composed which describes the water surface elevation $\eta(t)$. This formula is:

$$\eta(i\,\Delta t) = \sum_{n=1}^{n_{max}} \frac{H\,T\,e^{-(\gamma t)^2}\sin(n\pi\rho/T)}{\pi^2\, n^2\, \rho\,(1-\rho/T)} \sin\left[\frac{2\pi n i\,\Delta t}{T}\right] \tag{3.6}$$

where
- n_{max} = max number of participating components
- H = wave height of an unmodulated saw tooth wave form
- T = period of the saw tooth
- γ = $\sqrt{3}/(\beta T)$
- β = half amplitude width of the Gaussian envelope function
- ρ = a steepness parameter

This expression contains parameters which do not reflect the physical characteristics of the breaking wave.

The above expressions (eqns. 3.2, 3.3, 3.5 and 3.6) used for the generation of breaking waves in the laboratory consist of two parts :

a) the fast varying, oscillatory motion, and
b) the slow varying envelope, or profile of the motion.

Generally, the rate of change of the angular frequency, of the oscillatory motion, is constant and related to the distance of the target breaking area from the wave maker (eqn. 3.2). The form of the slow varying envelope is not provided analytically by any method. Kjeldsen (1982) partly describes this shape, whilst including a broadly defined function of time, f(t), with the only characteristic of being an increasing function of time. Mansard and Funke (1982) composed a mathematical function which includes a number of variables which are not directly related with the shape or size of the target breaking wave.

It can, therefore, be said that the methods used up to now for the generation of breaking waves in the laboratory although succeed in controling the location of the breaker, they are nevertheless restricted by their inadequacy in providing control over the profile of the wave transient and hence the characteristics of the target breaking wave. This limitation is overcome by approaching the problem from a new angle.

The equations governing the motion of small amplitude water waves are time symmetric; they are independent of the origin and direction of the space and time axes. By considering wave breaking as an accumulation of energy derived from small amplitude water waves, the motion at the wave generator's position required to produce an accumulation of energy at a particular location must therefore be the **reverse** of the motion induced by the release of the same amount of energy at that location.

3.6.3 THEORETICAL BASIS OF THE PROPOSED METHOD

The solution to the problem of the motion generated by an initial disturbance on a water surface is not a simple one. A literature review on this subject is presented in appendix A.

The works by Burnside (1888) and Kranzer and Keller (1959) are the most appropriate ones, as they provide mathematical expressions describing the motion in the physical space and time domains. For the sake of completeness, these two remarkable contributions are briefly described.

Burnside (1888) approached the problem for deep water conditions by employing Fourier's theorem; any shape can be expressed as the summation of a series of trigonometric functions. Consequently, the waves generated by a local elevation, constitute the summation of the waves produced by the individual components of the local elevation.

If the water surface is initially displaced and motionless, the surface profile being of the form

$$\eta_0 = A \cos(mx) \tag{3.7}$$

then the surface elevation as a function of time and space is

$$\eta = A \cos(mx) \cos(\sqrt{mg}\ t) \tag{3.8}$$

For an initial elevation of the form

$$\eta_0 = c \frac{a^2}{a^2 + x^2} \tag{3.9}$$

$$\eta = \sqrt{\pi}\, \frac{ca}{x} \left[\frac{gt^2}{4x} \right]^{1/2} \exp\left[- \frac{gt^2 a}{4x^2} \right] \sin\left[\frac{gt^2}{4x} + \frac{\pi}{4} \right] \tag{3.10}$$

Similar expressions can be derived for different forms of initial disturbances.

Kranzer and Keller (1959) derived explicit formulae for the waves produced by an arbitrary symmetric 2-dimensional initial disturbance in water of finite depth. The solution was derived according to the linear theory of surface waves. By application of the Hankel transform to the Laplace equation describing the flow and using Kelvin's stationary phase method, the surface elevation is given by,

$$\eta(x,t) \sim \frac{\eta_0 X^{1/2}}{x^{1/2}} B \sin 2\pi \left[\frac{t}{T} - \frac{x}{\lambda} + \frac{1}{8} \right] \quad \text{for } x < (gh)^{1/2} t \tag{3.11}$$

where η_0 = initial elevation at the origin

X = effective width of initial displacement

h = water depth

$$\lambda = \frac{2\pi h}{\sigma} \tag{3.12}$$

$$T = 2\pi / \left((g\sigma/h) \tanh\sigma \right)^{1/2} \tag{3.13}$$

$$X = \left| \eta_0 \right|^{-1} \int_0^{\infty} \left| E(x) \right| dx \tag{3.14}$$

where $E(x)$ = initial elevation

σ = auxiliary variable = $2\pi h/\lambda$

$$B = \frac{1}{\eta_0 (hX)^{1/2}} E(\sigma/h) \left[\frac{\sigma \Phi(\sigma)}{-\Phi'(\sigma)} \right]^{1/2} \sigma^{-1/2} \tag{3.15}$$

$$E(\sigma/h) = (2/\pi)^{1/2} \int_0^{\infty} E(x) \cos\frac{x\sigma}{h}\, dx \tag{3.16}$$

and $$\Phi(\sigma) = \frac{1}{2} \left[\frac{\tanh\sigma}{\sigma} \right]^{1/2} + \frac{1}{2(\cosh\sigma)^{3/2}} \left[\frac{\sigma}{\sinh\sigma} \right]^{1/2} - \frac{x}{\sqrt{gh}\; t} \tag{3.17}$$

A characteristic property of the waves produced by a local disturbance, in deep water conditions, is that any particular phase of the motion (e.g. a crest or trough) travels over the surface with a constant acceleration (Lamb, 1932). The fast varying oscillatory motion is described in both equations 3.10 and 3.11 by

$$\sin \left[\frac{gt^2}{4x} + \frac{\pi}{4} \right] \tag{3.18}$$

The time interval, Δt, between the arrival of two consecutive phases, at a given location, x, corresponds to the period of oscillation, T, hence,

$$\Delta \left[\frac{gt^2}{4x} + \frac{\pi}{4} \right] = 2\pi \tag{3.19}$$

or $$\frac{gtT}{2x} = 2\pi \tag{3.20}$$

Substituting for $\omega = 2\pi/T$ and differentiating with respect to t,

$$\frac{d\omega}{dt} = \frac{g}{2x} \qquad 3.21$$

Equation 3.21 is identical with equation 3.2 when the time axis is reversed.

3.6.4 DESCRIPTION AND DISCUSSION OF THE PROPOSED METHOD

According to the properties of surface water waves, if two wave makers, positioned at the two ends of a wave flume, generate wave motion described by the reverse of the motion produced by a hypothetical local elevation in the middle of the flume, that local elevation will be formed. With only one wave maker however, the asymmetry of the motion implies that the concentrated energy cannot be stored only as potential energy. The forward momentum and kinetic energy are preserved and an overturning wave is produced. The shape of the breaking wave is reflected by the shape of the initial elevation used in computing the driving signal.

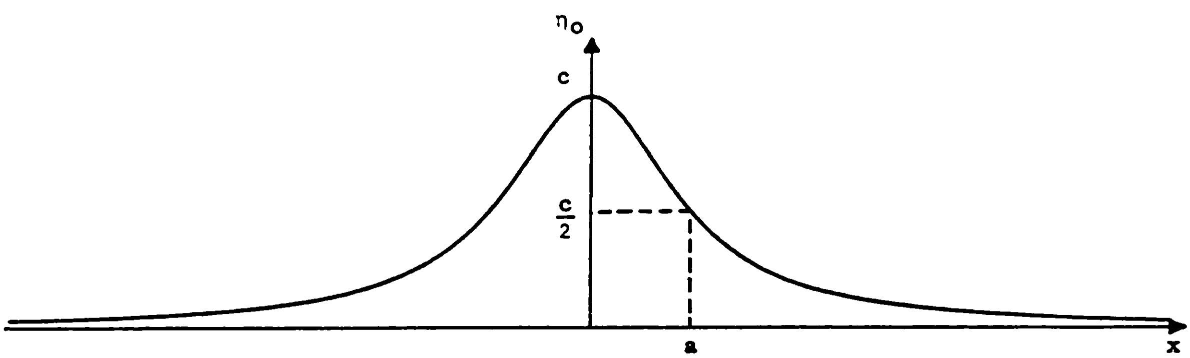

Fig. 3.5 Initial surface elevation (eqn 3.9)

A simple shape, similar to breakers observed in the sea, is the parabolic one described by equation 3.9 and shown in figure 3.5. This shape has the advantage of having only two parameters, c and a; c reflects the breaker height and c/a the breaker steepness or breaker type (spilling for small c/a and plunging for large c/a). These two parameters as well as the distance of the target breaker from the wave maker, are the only variables required in generating the driving signal. They both represent physical characteristics, a property that makes this method quite easy to implement.

The choice of the method of computing the driving signal depends on the computational facilities available. Undoubtly, equation 11 (Kranzer and Keller method) provides the most complete solution. It imposes however, a heavy computational penalty, whilst equation 10 (Burnside) is very simple and straightforward to use, imposing a limitation on the range of wavelengths of wave trains, as the solution assumes deep water wave conditions.

3.6.4.1 **Solution 1**

The distance, x, between the wave maker and the desired breaking location is first specified. The elevation time history, at distance x, from a local elevation is then computed using equation 3.10 (Fig. 3.6a). As the time history is an open ended one, a cut-off point is selected, t_1, beyond which the wave oscillation is considered as negligible. The elevation time history may now be reversed about this point (t_1).

The solution used is valid only for deep water conditions. A second cut-off point is therefore introduced, t_2, beyond which the deep water condition is no longer valid (Fig. 3.6b). The driving signal of the wave maker is then obtained by applying its transfer function on the derived elevation time history.

3.6.4.2 **Solution 2**

A complete solution for the waves generated by a local elevation in water of finite depth is the one by Kranzer and Keller, expressed by equation 3.11. In deep water conditions and using linear theory, the group velocity of the waves, c_g, is related to the period, T, by

$$c_g = \frac{gT}{4\pi} \qquad 3.19$$

The effect of limited depth is to reduce the group velocity of the waves. The physical mechanism behind the method of generating breaking waves is that the individual phases of the wave trains catch up all at the desired location and thus induce breaking. If the solution given by equation 3.11 is reversed intact, the phases which were already decelerated by the bottom effects would not be able to catch up with the rest of the phases which do not *feel* the bottom. In order to overcome this problem, the phases which were decelerated by the bottom effects have to be accelerated by the same amount. When they are then generated by the wave

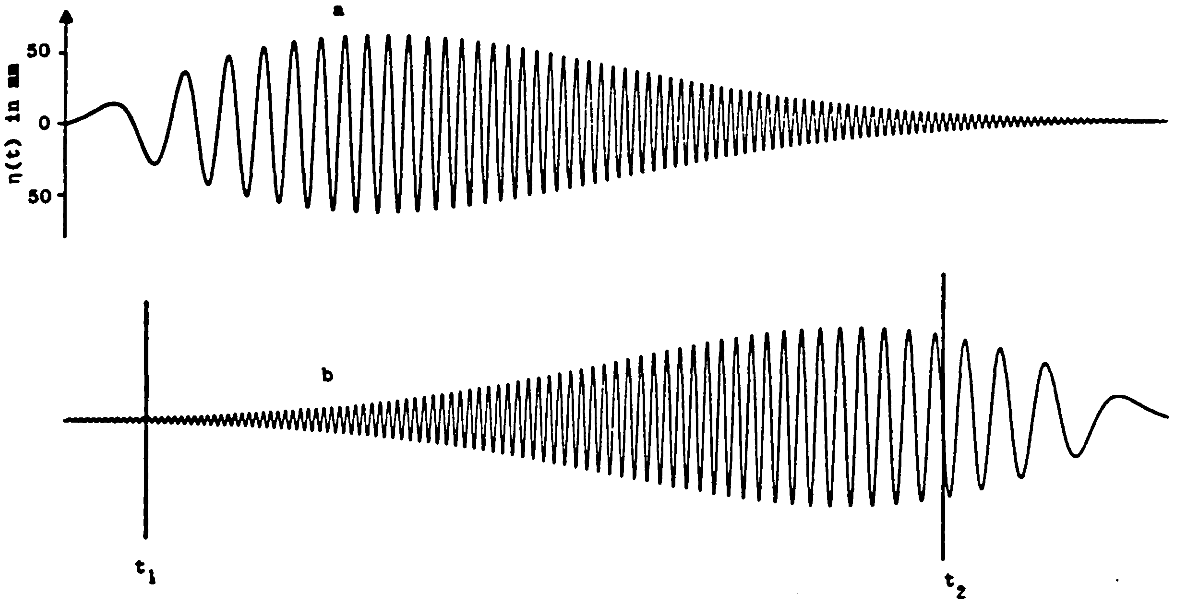

Fig. 3.6 a) Elevation time history, 90sec long, 34 m from a local elevation (a=0.35, c=0.8m)

b) The elevation time history is reversed and the cut-off points, t_1 and t_2, are specified.

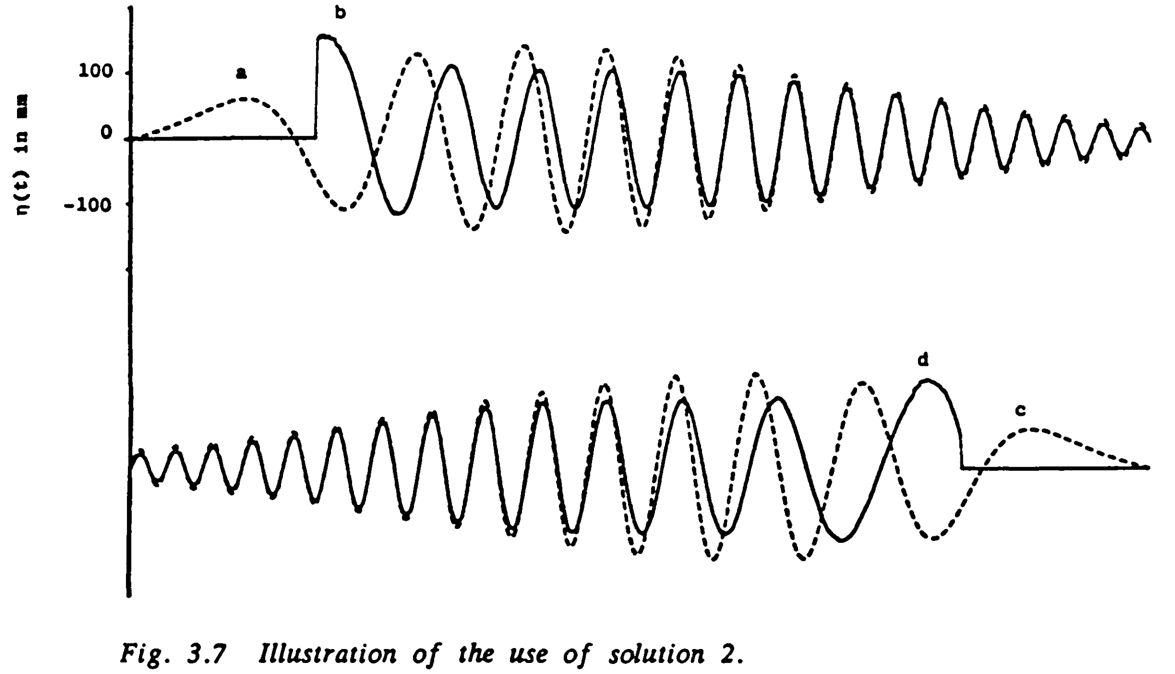

Fig. 3.7 Illustration of the use of solution 2.

(Elevation time history, 19.2 sec long, a=0.35 m, c=1.0 m, x=10 m, h=1 m)

a) Deep water solution

b) Shallow water solution – bed affects the long waves

c) Reversal of a)

d) Reversal of b) – effects of bed also reversed.

maker, these modified phases will be decelerated by the bottom and will catch up with the *deep water phases* at the required location.

An illustration of the use of this method is shown in Figure 3.7. The solution obtained from the expressions derived by Kranzer and Keller is first computed (Fig. 3.7a). The period of the waves affected by the bed are then modified, whilst the slow varying envelope remains the same (Fig. 3.7b). The driving signal is obtained by following the same procedure as in solution 1.

3.6.5 CONCLUSIONS

A new method for the generation of breaking waves in the laboratory has been presented. The principle behind this method is the well known property of small amplitude waves that the equations governing their motion may be reversed in the time domain and shifted in the space domain. The time history of the required elevation at the wave paddle's location is determined by reversing the elevation time history induced by a hypothetical local concentration of energy at the target breaking point.

This method has overcome the limitations faced by previously used methods, by considering the case of waves in finite water depth and by providing an analytical expression for the profile of the wave transient, which is directly derived from the shape of the initial elevation used in obtaining the solution. The parameters required for deriving the control signal for the generation of the breaking wave all have a physical meaning, that is water depth, distance between wave maker and target breaking location, size and shape of initial elevation reflecting the breaker height and type. The presented examples highlight these attributes of the technique and it is hoped that it will find its way into applications other than generation of breaking waves in the laboratory.

3.7 SUMMARY

The original contibutions with regard to the experimental procedure may be summarised as follows:

a) The development of suitable software for the achievement of accurate and repeatable control of the experiment. This software has been already successfully used in a number of occasions by other researchers. It is flexible and portable and very easy to use.

b) The determination of the suitable conditions for the operation of the FOLDA.

c) The development of a new method for the generation of breaking waves in the laboratory. This method has attracted the interest of a number of researchers studying the effects of breaking waves. It is hoped that the property that, the equations that describe the motion of surface gravity waves are **time symmetric** will find applications in other wave processes as well.

CHAPTER 4

EXPERIMENTAL RESULTS

4.1 ABSTRACT

Transverse velocity time histories at a number of locations around a deep water breaking wave were measured using a Fibre Optics Laser Doppler Anemometer. As such measurements were performed for the first time, the obtained records are examined from a number of angles. The turbulent and mean motions are extracted and then studied both independently and in conjuction with each other. A striking result from these tests is the identification of a transverse motion not associated with the high frequencies of turbulence. Furthermore, a standing surface wave motion, corresponding to the 5^{th} harmonic mode of transverse oscillations in the flume, is identified. The spacial and temporal variation of the turbulent kinetic energy and the associated eddy viscosity are also examined and estimates of the rate of energy dissipation are obtained. The mechanisms associated with the generation of the turbulent motion are examined and conclusions are drawn regarding the modelling of the motion.

4.2 INTRODUCTION

Turbulence generated by breaking waves plays an important role in most processes in the surf zone. Such processes include:

a) dissipation of wave energy
b) wave transformation
c) nearshore circulation
d) sediment transport
e) dispersion of pollutants.

Although accurate models of the turbulence structure are required for modelling coastal processes, lack of adequate knowledge of the characteristics of turbulence under breaking waves is still hindering understanding and proper treatment of such processes.

The chaotic, unorganised, three-dimensional motion following the breaking of a wave does have some repeatable and characteristic features (see chapter 2). The aim of this study is to assemble as much information as possible about the features of this motion, by approaching the problem from a number of angles. Apart from standard methods of analysis, such as spectral analysis, alternative techniques are used. A common technique used in Seismology for determining ground motions is the plot of the accumulation of the energy released by the source of the disturbance, with time. This data analysis method reveals so much information to seismologists, that it is thought worth testing in hydraulics. Not surprisingly, this technique proved very useful and it is extensively employed.

4.3 DATA COLLECTION

The acquisition of reliable and accurate data is most important in experimental studies. Owing to the originality of the experimental set-up and the consequent lack of any comparable data, extreme care was taken in order that the information from the experiments was as accurate and reliable as possible. The most important consideration was the achievement of repeatability of the experiment.

Elevation and transverse velocity time histories were collected at about 10 positions around two deep water breaking waves, at a sampling rate of 100 values per second. The locations of these points are shown in figure 4.1. At each location 20-25 records were obtained. For the first collected data, many more records were collected, so that confidence on the validity of the results was established before continuing the work.

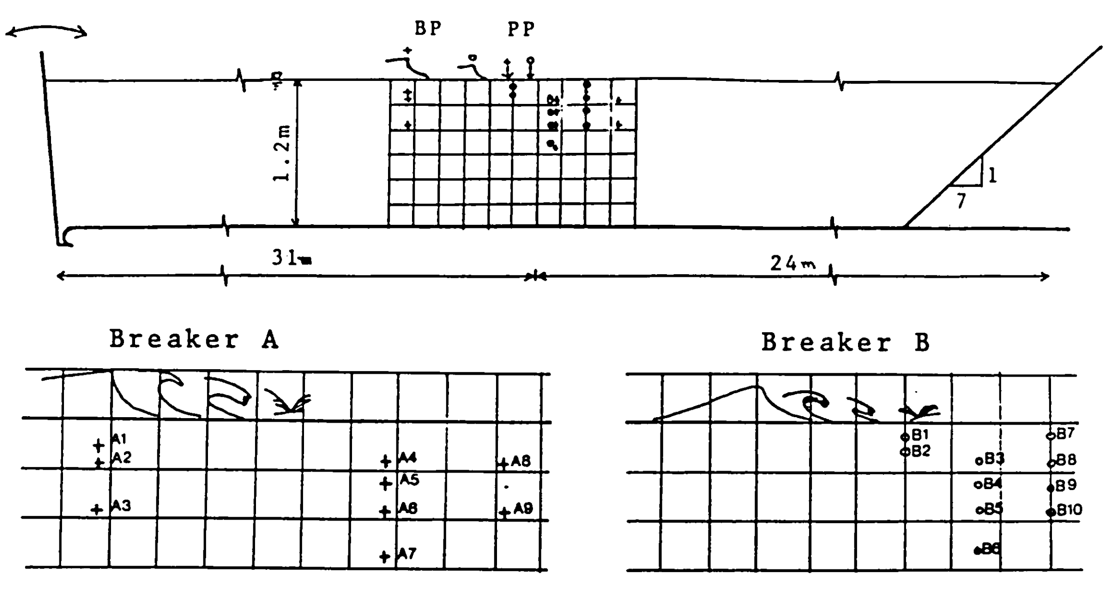

Fig. 4.1 Cross-section of the flume, indicating the locations where data were collected.

The time interval between successive experiments was long enough for the water surface to calm down and be reasonably still. Too long intervals between runs, although desirable for repetitiveness of the breaking process, had an adverse effect on the velocity measurements. The seeding material tended to gradually settle down when the water was calm, whereas breaking enhances its suspension and uniform distribution in space. Allowing 10-12 minutes between runs was considered as a reasonable compromise between the two requirements.

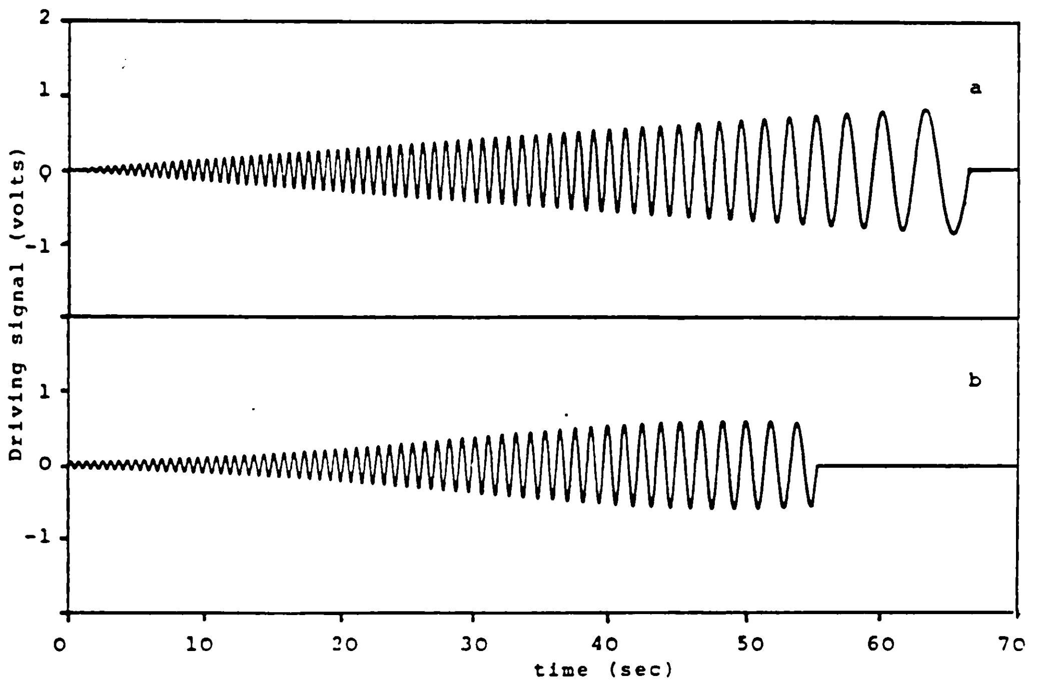

Fig. 4.2 Driving signals. a) SIGN1 (breaker A), b) B4 (breaker B).

The driving signals generating the two breaking waves are shown in figure 4.2. The first signal, *SIGN1*, employs Longuet-Higgins (1974) method with an empirical function for the profile of the wave transient. The second signal, *B4*, was developed at a later stage. It employs the presented method, (chapter 3, solution 1) with a=0.35m, c=0.80m and x=34m. Both signals produce plunging breakers, 20cm high, as illustrated in figure 4.1. A reasonable degree of repeatability was achieved, with the plunging point deviating by less than 15cm from the mean position, or less than 0.5% of the distance from the wave maker. The repeatability of the experiment may also be observed in the accompanying video cassette.

4.4 TURBULENCE DEFINITION

In this study, **turbulence** is defined as the deviation from the mean motion. The mean motion is the **ensemble average** of all the recorded time histories. This definition of turbulence can include the motion associated with random surface waves. It also includes motion with frequencies less than 10Hz, the cut-off frequency used in many studies.

It is reasonable to assume that velocity records, in the transverse direction, at the same location, for identical breakers, and with the same collection parameters (delay, frequency, number of channels and number of points) measure the same properties of the motion generated in the transverse direction by a two-dimensional breaking wave.

4.5 EARLY IDEAS AND PRESENTATION OF MEASUREMENTS

Wave breaking generates turbulence. Turbulence is a three dimensional motion. In the transverse direction of a two dimensional breaking wave, motion is initiated at the instant the plunging jet hits the forward face of the wave. The turbulence intensity decays with time, the high frequency components having a faster rate of decay. Based on the above simple arguments, the form of the velocity time history in the transverse direction is predicted as shown in figure 4.3. The duration of the turbulent motion remains to be determined.

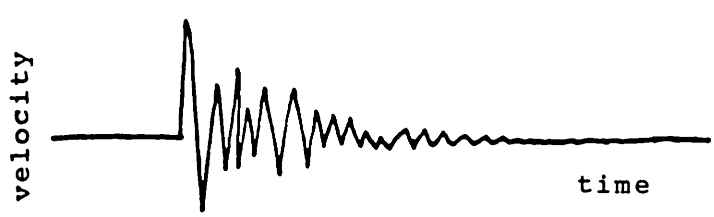

Fig. 4.3 Heuristic prediction of the breaker induced turbulent velocity time history.

The shape of this curve looks very similar to the seismogram records (fig. 4.4), that is, the displacement produced by an earthquake as measured at a distant location. The sudden increase of activity is associated with the initiation of the release of energy at the focus of the event. This is followed by the arrival of the different forms of waves that are also generated during the earthquake. The velocity record, which is the derivative with respect to time of the displacement record has a similar form. The square of this record provides information on the energy

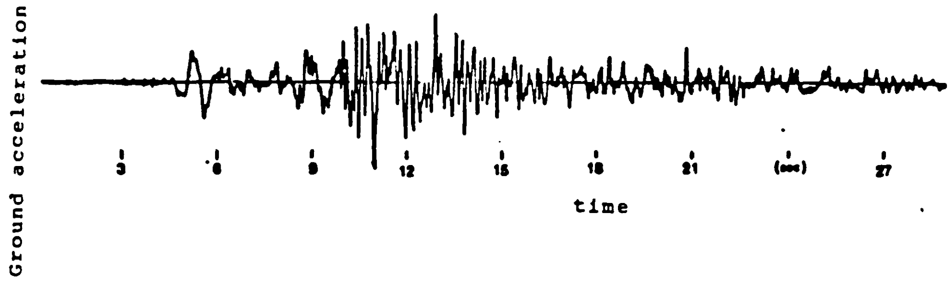

Fig. 4.4 Typical seismogram record, produced by an earthquake.

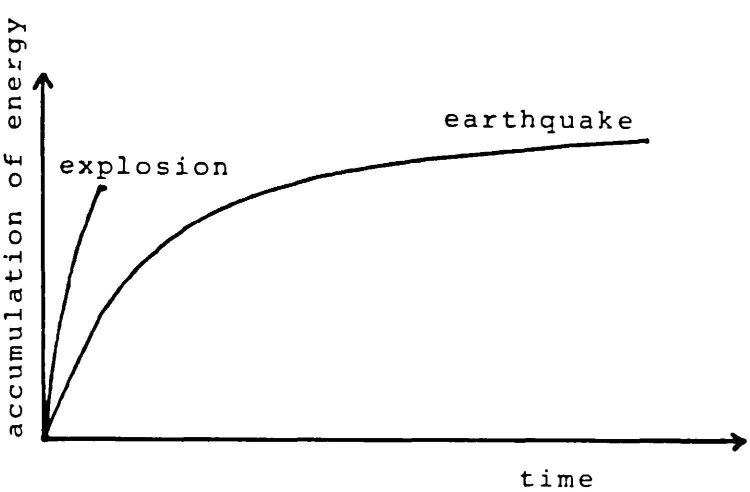

Fig. 4.5 Interpretation of seismograms reveals the cause of the ground motion.

released. The integral of this curve with respect to time, indicates the rate of release of energy. This is a very informative curve, as the characteristics of the disturbance are directly related to the shape of this curve. A nuclear explosion, for example, is associated with an abrupt release of energy, whereas an earthquake is associated with a release of energy during a finite length of time (fig. 4.5).

Both an earthquake and a breaking wave are associated with a release of energy, although from the coastal engineering point of view, it is the dissipation of energy at breaking which is usually dealt with. It is predicted that the shape and size of the breaker will be reflected in the transverse velocity records, in a fashion similar to the earthquake process. The amplitude of the velocity oscillation is expected to be related to the size of the breaker and the curve of the accumulation of energy related to the shape of the breaker; plunging breakers associated with an abrupt increase of activity, whilst spillers associated with a gradual rise.

Based on the above arguments, the first collected transverse velocities were plotted in the following ways:

a) superposition of the time histories corresponding to the same conditions,
b) superposition of the square of the velocities, representing the kinetic energy in the transverse direction,
c) superposition of the accumulation of energy with time, and
d) superposition of the normalised accumulation of energy with time, indicating the rate of energy input. (at time=0, energy=0; time=record length, energy=100%)

The initial results proved very encouraging as they revealed a constistent pattern in the motion. A typical result from such analysis is shown in figure 4.6. Further data were collected and analysed. The ensemble average values were derived from each set of data and the turbulent component for each individual record was extracted. The following plots were then obtained:

a) Mean transverse velocity (ensemble average) time histories
b) Mean turbulent kinetic energy (ensemble average of the square of the turbulent component) time histories
c) Accumulation of the mean turbulent energy with time
d) Normalised accumulation of the mean turbulent energy with time
e) Mean energy spectrum of the turbulent component

A typical result from such analysis is shown in figure 4.7. Figures 4.8 and table 4.1 present the results from all the conditions tested. The interpretation of these results is discussed in the following sections.

4.6 INTERPRETATION OF DATA

4.6.1 TRANSVERSE VELOCITY TIME HISTORY

In line with the early predictions, the general form of the velocity record presents an abrupt rise of activity at the plunging point (fig. 4.6). This unorganised motion decays with time and eventually returns to its initial stage. The random nature of this record does not allow the derivation of any conclusions from a single time history. The collection of many more measurements under identical conditions is necessary and the results should be based on the average of these records.

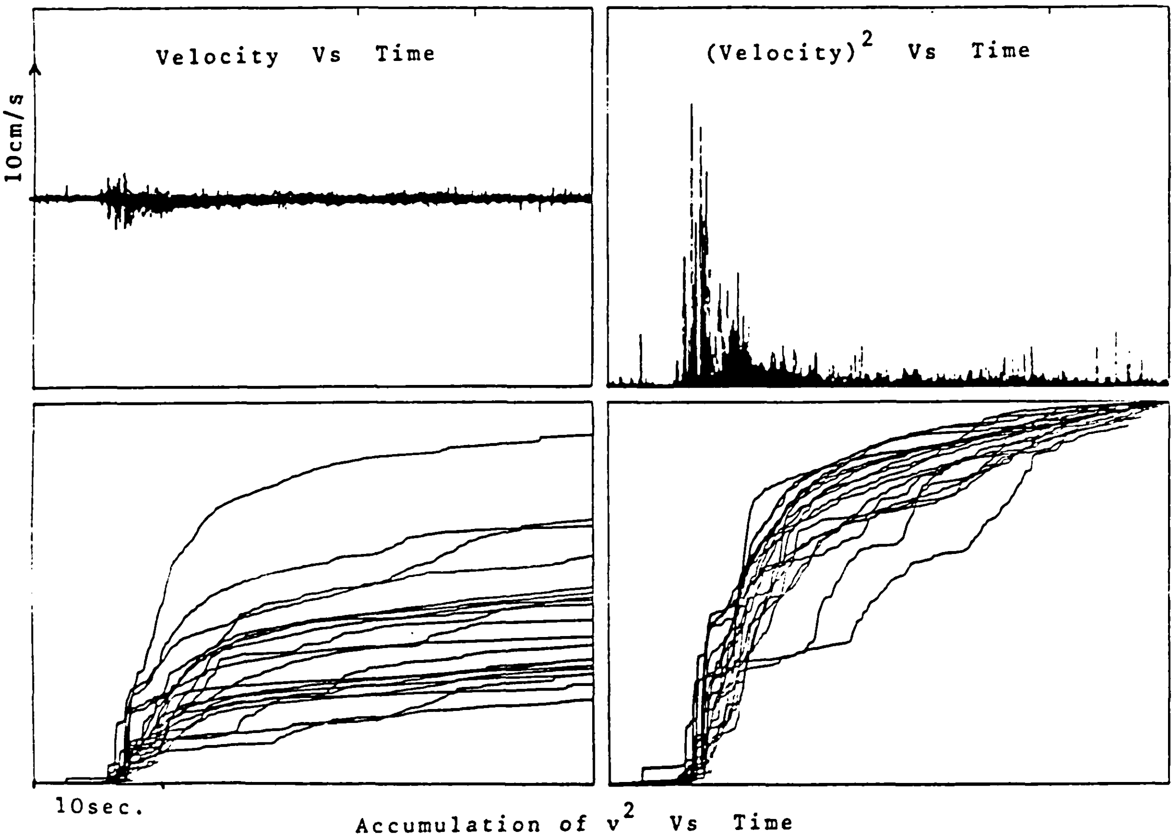

Fig. 4.6 Superposition of plots of velocity, v, v^2 , Σv^2 and normalised Σv^2 against time, for Breaker A, at position A4.

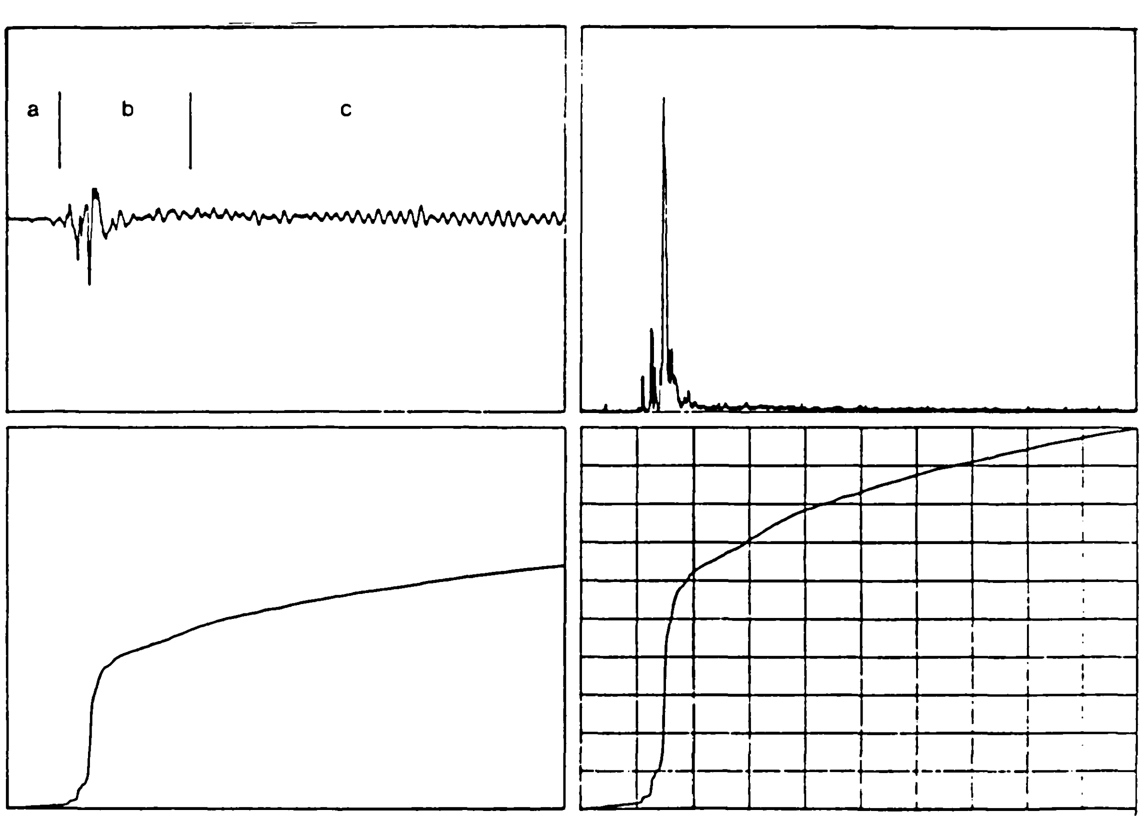

Fig. 4.7 Typical result. Breaker A, at position A1

Pos.	Range cm/s	$\Sigma v'^2 \Delta t$ cm^2/s	% of energy dissipation in 1	2	3	4	5	7	10	15	Standing wave Per. sec	Vel. mm/s	Ampl. mm
A1	9.8	17.4	10	52	65	69	72	77	83	92	0.844	3.19	0.78
A2	10.7	15.0	65	78	80	84	84	89	92	100	0.846	2.87	0.98
A3	4.8	4.8	50	74	80	83	83	100	100	100			
A4	8.5	19.5	10	30	47	56	70	81	91	100	0.85	1.9	0.6
A5	6.5	11.2	15	40	50	58	64	75	85	97	0.841	1.49	0.83
A6	6.8	9.4	42	51	56	61	65	68	77	93			
A7													
A8	15.0	112.9	10	17	28	45	53	72	92	99	0.844	3.4	1.21
A9	8.2	12.8	48	54	57	59	60	64	74	94			
B1	7.6	25.9	25	27	30	34	40	67	78		0.848	4.0	0.7
B2	6.3	10.7									0.848	3.6	0.85
B3	7.3		20	35	65	72	85	95			0.849	2.3	0.73
B4	7.6	11.2	37	58	67	73	77	84	92		0.84	2.0	1.1
B5	5.7	4.9	45	55	65	70	72	79	85				
B6	5.3	4.1											
B7	8.6	24.0	34	39	45	57	70	90	100		0.844	5.	0.89
B8	8.7	28.6	5	17	32	49	58	80	89		0.844	2.65	0.83
B9	5.4	6.4	12	34	42	50	54	63	76				
B10	5.3	5.6	29	55	62	69	73	79	88				

Table 4.1 Summary of experimental results

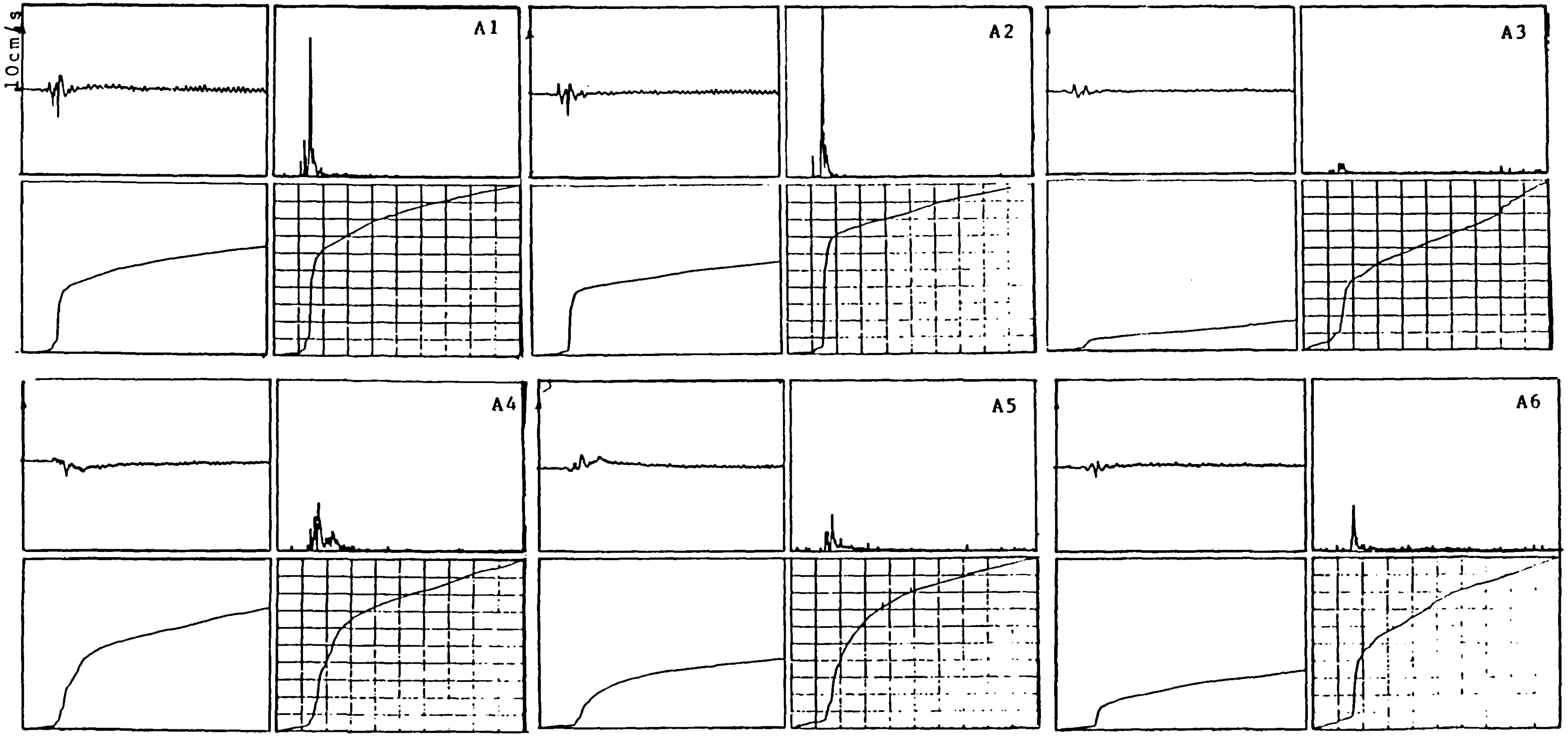

Fig. 4.8   Results for all conditions

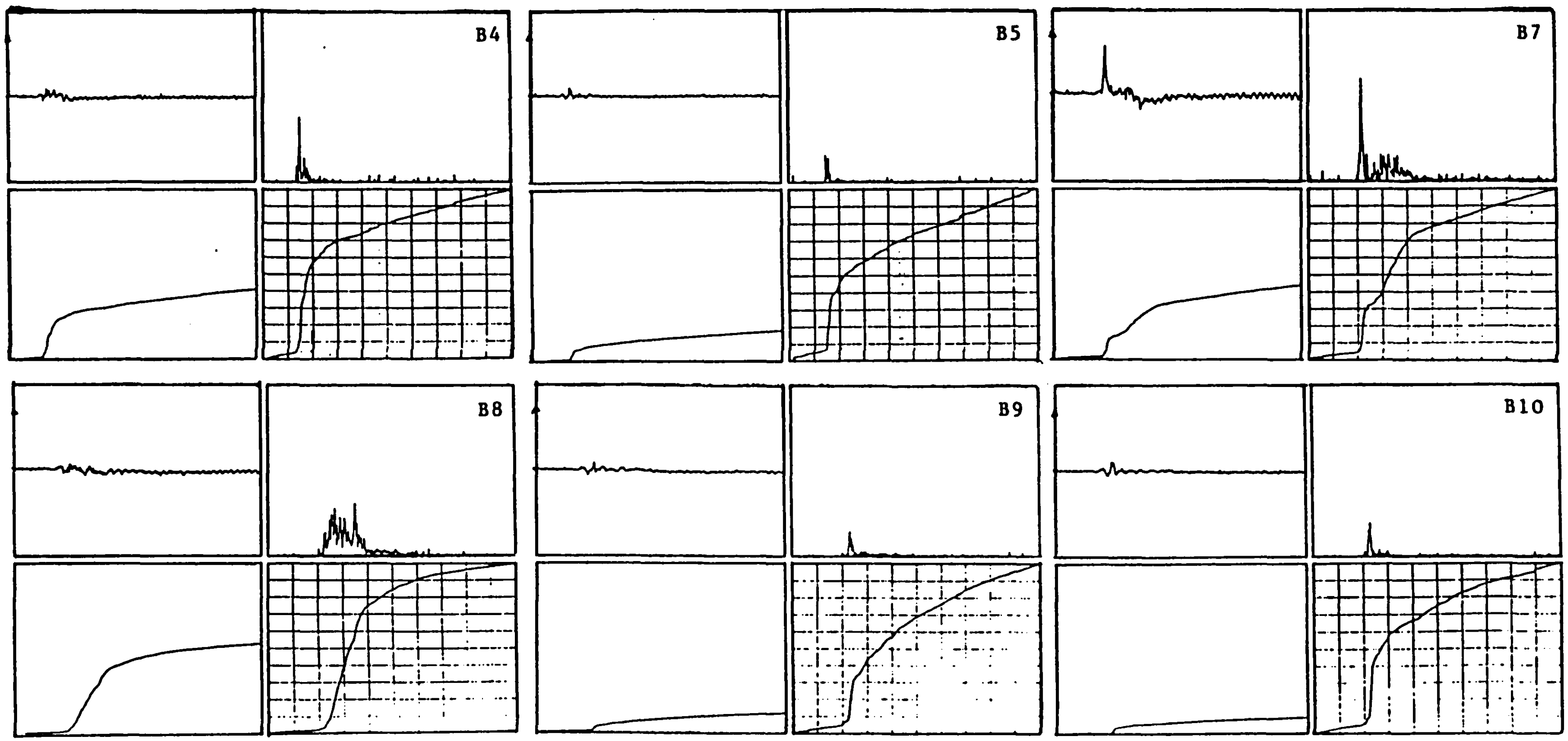

Fig. 4.8 Experimental results (continued)

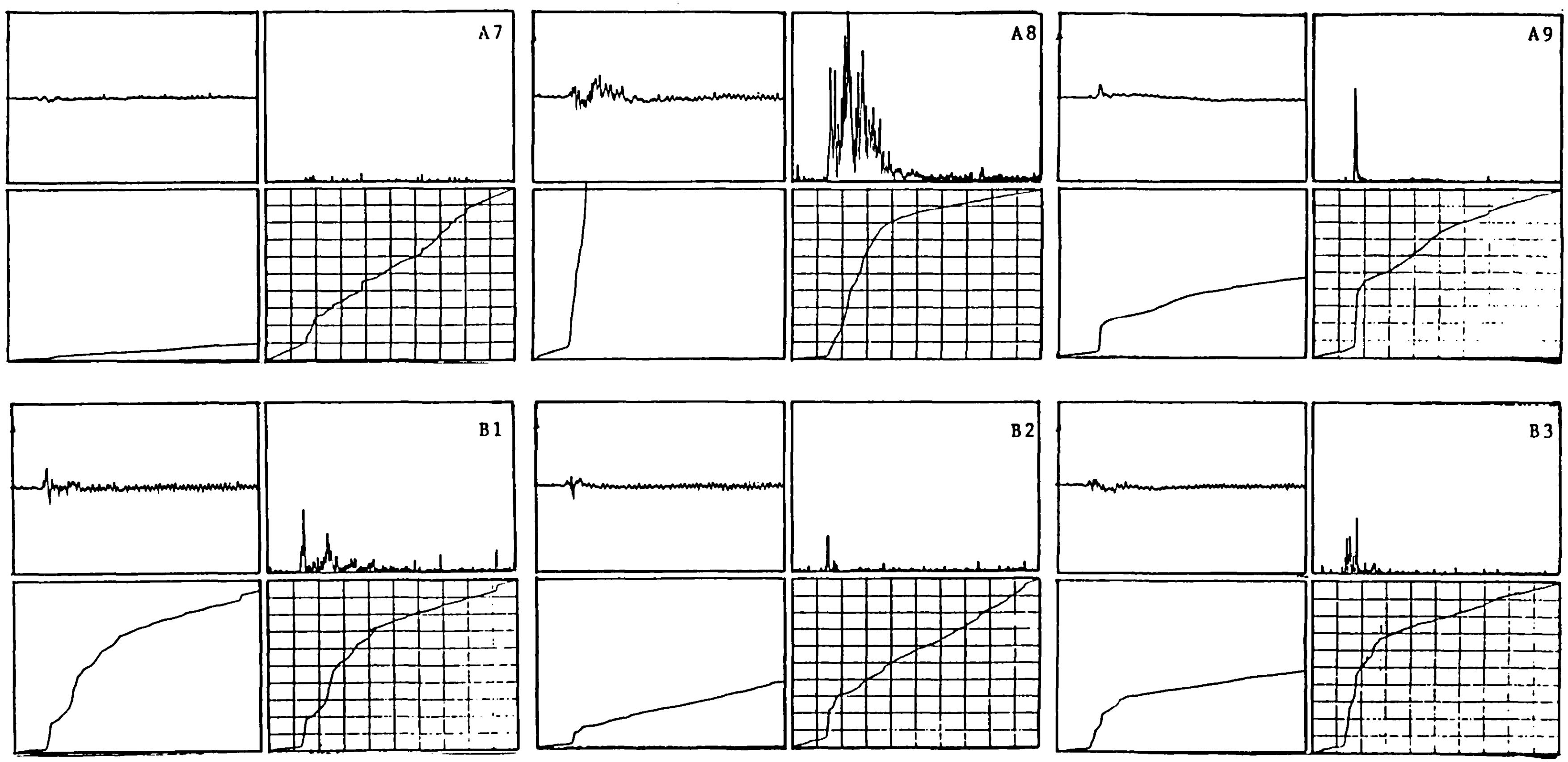

Fig. 4.8 Experimental results (continued)

4.6.2 MEAN TRANSVERSE VELOCITY TIME HISTORY

The plot of the ensemble average velocity against time can be divided into three parts (fig. 4.7):

a) No velocity (no breaking) part
b) Disorganised, random motion (soon after breaking)
c) Regular, organised motion (some time after breaking).

In the first part, no motion is measured. This is compatible with the assumption that the waves generated by the wave paddle are two-dimensional. It is also in agreement with the definition of turbulence, as used by Bradshaw (1971), as no fluctuating velocity in any one direction implies that there is no turbulence.

In the second part of the plot, the motion is highly disorganised. Owing to the rigid boundaries of the wave flume one would expect this motion to be ideally zero, or to show a slow varying circulation. The reason for this highly fluctuating mean motion, could probably be found in the plots which show the original data records superimposed on each other. From these plots, it seems that the motion is random with no preferred mode. However, the limited amount of data, produce a mathematical *mean* which is not necessarily the same as the physical mean motion.

The third part of the plot is the most unexpected and interesting result. Unexpected, because the formation of a regular lateral motion after the plunging of a breaker had not been predicted. Interesting, because it poses many questions as to its generation mechanism, the factors affecting its characteristics and the importance of this motion.

In this regular motion, the time between successive maxima is in all records the same (0.844±0.005 sec). As the amplitude remains more or less the same for a considerable length of time (10–20 sec), a standing wave is probably formed across the flume. The period of the mean oscillation coincides remarkably well with the fifth harmonic period of oscillation of the flume, as computed from linear theory,

$$T_i = \sqrt{\frac{4\pi B}{ig} \Big/ \tanh\left(\pi i h/B\right)} \qquad 4.1$$

where T_i is the i^{th} harmonic period, B is the width of the flume and h the depth of the water.

By considering the position of the velocimeter in the flume and using again linear theory the amplitude of the standing wave is found to be of the order of 0.7 to 1.2 mm.

The formation of the 5^{th} harmonic mode in the transverse oscillation is a natural phenomenon taking place in all fields of science, known as **resonance**.

When the period of a monochromatic exciting disturbance coincides with one of the natural periods of oscillation of the system, a standing wave is formed. Disturbances corresponding to other periods attenuate with time. According to Fourier's theorem, whatever the form of a disturbance is, it can be expressed by a series of monochromatic waves. The effect of an arbitrary disturbance therefore, is to induce a motion whose frequency components other than the ones corresponding to the natural frequencies of the system decay with time. The prevailing motion thus, corresponds to the natural modes of oscillation of the system. The predominant mode is governed by:

a) the energy required to drive each mode of oscillation, and
b) the energy available for driving each mode.

In an area of width B, the natural periods of transverse oscillations are given from equation 4.1. The exciting energy is determined by the breaking process. The predominant motion is therefore defined from the energy spectrum of the exciting disturbance (broken wave motion) and the width of the wave flume.

The principle of the described mechanism is diagramatically presented in figure 4.9.

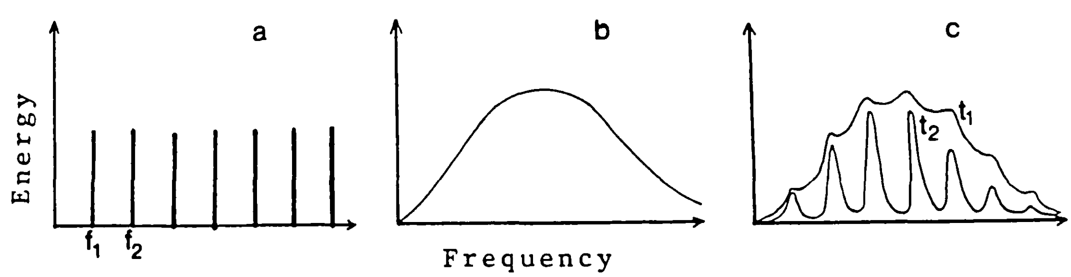

Fig. 4.9 Mechanism of formation of harmonic oscillations in a system subjected to a disturbance with a continuous energy spectrum.

a) Energy required to excite the natural harmonic oscillations

b) Energy input from the disturbance

c) Energy content at two different times. The energy corresponding to the natural frequencies decays slowly and the attenuation is faster the higher the frequency

4.6.3 TEMPORAL DISTRIBUTION OF MEAN TURBULENT KINETIC ENERGY

All mean turbulent energy time-history plots show some distinct features.

a) They start with a ***plateau***, which means no turbulence is present.
b) A sharp increase of turbulence appears, called ***spike*** hereafter, which is the energy fed into the system from the energy initially stored in the breaker. A ***hump*** is shown in some records. This is probably the energy input from a secondary plunger, much weaker than the original one. The presence of this hump in records taken shorewards of the breaker only, gives more support to this explanation, as the secondary plungers are hardly noticed offshorewards from the plunging area.
c) The turbulent energy decays rapidly with time and a ***plateau***, similar to the one before breaking, follows the hump.

4.6.4 ACCUMULATION OF ENERGY WITH TIME

The integral of the turbulent energy with respect to time represents the accumulation of energy in the transverse direction. Since this energy comes from the other two components, this plot can also be termed as *dissipation of energy with time*. Large input of energy into the transverse direction implies large dissipation of energy from the longitudinal and vertical directions.

The striking similarity of the plots of the accumulation of turbulent energy with time encouraged further investigation of the results. Although the superposition of the individual curves for the same location and breaker does not show the curves coinciding with each other, the plots of the *normalised* energy time history reveal that they follow a repeatable pattern.

The normalised curve, in the same way as the velocity time histories, can be divided into three parts:

a) The almost horizontal part (before plunging). The slope of this curve is an indication of the noise level present in the signal. The milder the slope of the curve the less the noise level present in the record.
b) The steep, almost vertical part (primary plunger). This corresponds to the *spike* of the velocity record.
c) The mild slope (broken wave motion). Random motion results after the initial plunging and any subsequent secondary plungers. The steeper the slope

of this part, the more unorganised the motion, the higher the intensity of turbulence.

Since wave breaking is a local phenomenon and turbulent motion is induced by plunging, the proportion of the energy dissipated at arbitrary times can be derived. It is found that offshorewards, up to 75% of the energy is dissipated within the first two seconds, whereas onshorewards it takes about 4 seconds for half the energy to be dissipated. This is accounted for by the system of splash-jets which forms shorewards of the plunging area. Energy continues to be input into the system and the net dissipation rate is thus smaller and longer time is required to dissipate the turbulent energy. A complete list of the dissipation rates is presented in table 4.1.

4.6.5 SPACIAL DISTRIBUTION OF TURBULENT KINETIC ENERGY

A measure of the intensity of the turbulent kinetic energy is the magnitude of the *spike* appearing on the transverse velocity time history, called ***range*** of the turbulent motion, hereafter. The range of the turbulent motion is defined as the difference between the maximum and minimum turbulent velocities in each time-history. As the maximum and minimum velocities in the lateral direction occur in the second part of the time-history, when the mathematical mean motion does not have a regular pattern and it probably depends on the number of records available, a more representative value might be the range of the raw data

$$\text{Range} = v_{max} - v_{min} \qquad 4.2$$

These values are presented in table 4.1 and illustrated in figure 4.10. Contour lines

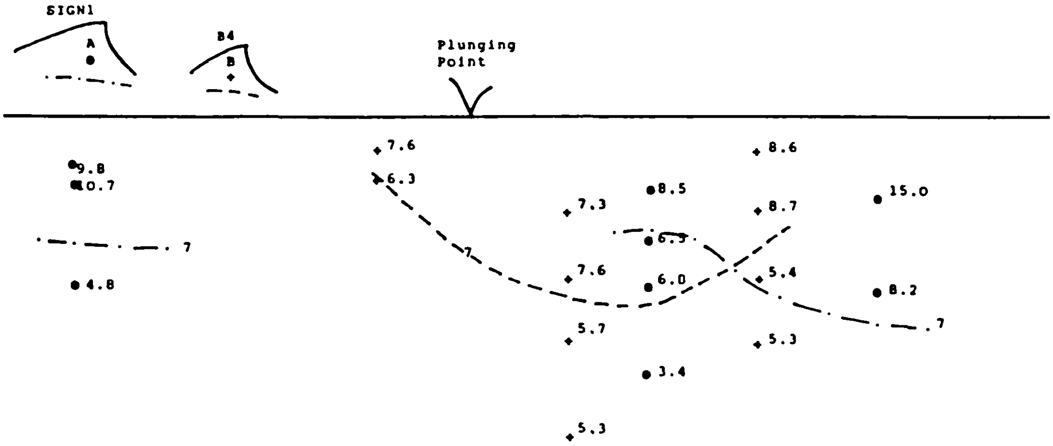

Fig. 4.10 Spacial distribution of intensity of turbulent kinetic energy (cm/s)

showing the spacial distribution of the intensity of the turbulent kinetic energy are sketched. Although the number of points is limited, certain characteristics are quite evident:

a) The vertical decay of the turbulent kinetic energy intensity is much more rapid than the longitudinal one.

b) The breaker *B4*, although being slightly smaller in height than *SIGN1*, it induces turbulent motion in greater depths. This may be explained by considering the steepness of the two breakers. Breaker *B4* hits the receiving water surface at a steeper angle; its effects spread over a shorter longitudinal span but penetrate in deeper water depths.

These results may be interpreted so as to assess the different effects of spilling and plunging breakers. The turbulence induced by spillers although extends over a wide longitudinal distance it is bounded close to the surface only. In the case of plungers however, turbulence is concentrated over a short longitudinal distance but penetrates quite deep in the water, at least 3 times the breaker height. In shallow water conditions, this intense turbulent activity reaches the bed. In the case of a loose boundary, sediment will be suspended, whilst a spiller of greater height might not have such an effect.

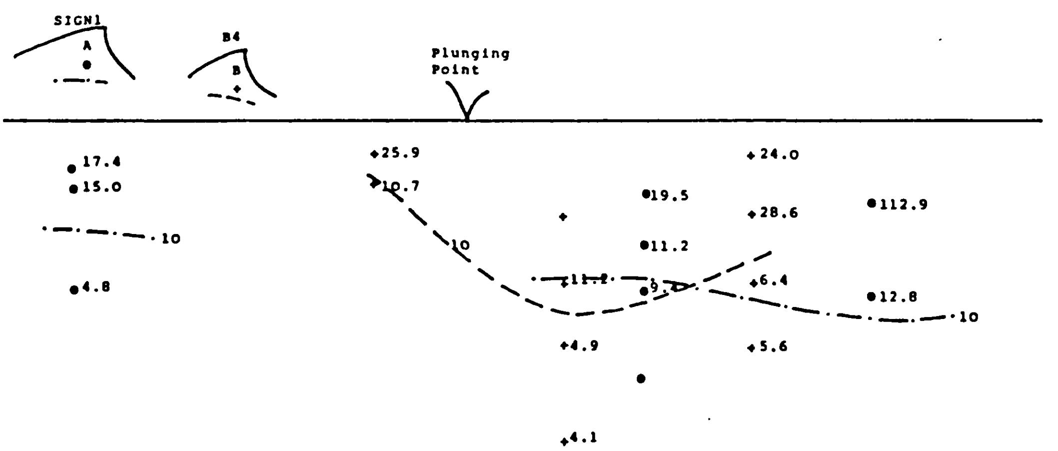

Fig. 4.11 Spacial distribution of total amount of turbulent kinetic energy (cm^2/s)

The total amount of the turbulent kinetic energy production, or the dissipation of wave energy, at each point is presented in table 4.1 and illustrated in figure 4.11. It may be deduced that more energy is dissipated shorewards of the plunging point rather than offshorewards. This difference probably arises from the fact that the axis of the overturning jet when it hits the forward face of the wave is inclined away from the vertical, pointing shorewards. This inclination introduces a horizontal momentum which produces splash-jet systems in the shoreward direction. These qualitative results are in agreement with Miller's (1976) work regarding the identification of secondary plungers following wave breaking.

4.6.6 SPECTRAL ANALYSIS

The frequency spectra of the turbulent component of the transverse velocity component (deviation from the ensemble average), are firstly obtained. The ensemble average of these spectra is then derived, a representative plot shown in figure 4.12.

It is evident that a **wide range of frequency components are present**. This observation contradicts the early propositions predicting a motion with high frequency content - higher that 10 Hz. It is however in agreement with the interpretation of the velocity records suggesting indirectly the presence of random surface wave motion.

This remarkable observation opens new horizons in the understanding of the broken wave motion. Apart from the turbulent motion arising from the shear between the plunging jet and the receiving water mass, a further mechanism exists that generates three-dimensional random surface waves, even when the breaking wave is a two-dimensional one. The form of this mechanism is not directly revealed from these measurements. Alternative experimental observations are required for investigating this mechanism.

4.7 DISCUSSION AND COMPARISON WITH PREVIOUS STUDIES

In this study the turbulent velocity component is defined as the deviation from the ensemble average. This definition is in agreement with a recent study by Svendsen (1986). It was characteristically pointed out, in that study, that "*ensemble averaging is the most (or only) suitable*" method for extracting the turbulent fluctuations. This method takes into account "*random, short waves on the water surface, and the corresponding particle velocities*". Surface wave induced velocity fluctuations as well as shear induced motions are therefore treated in the same way. Experimentally there is no method for distinguishing the two types of motion. The significance of each of the two sources of fluctuating motion may be assessed by treating their effects separately; firstly, as shear induced motion, and secondly, as surface wave induced motion.

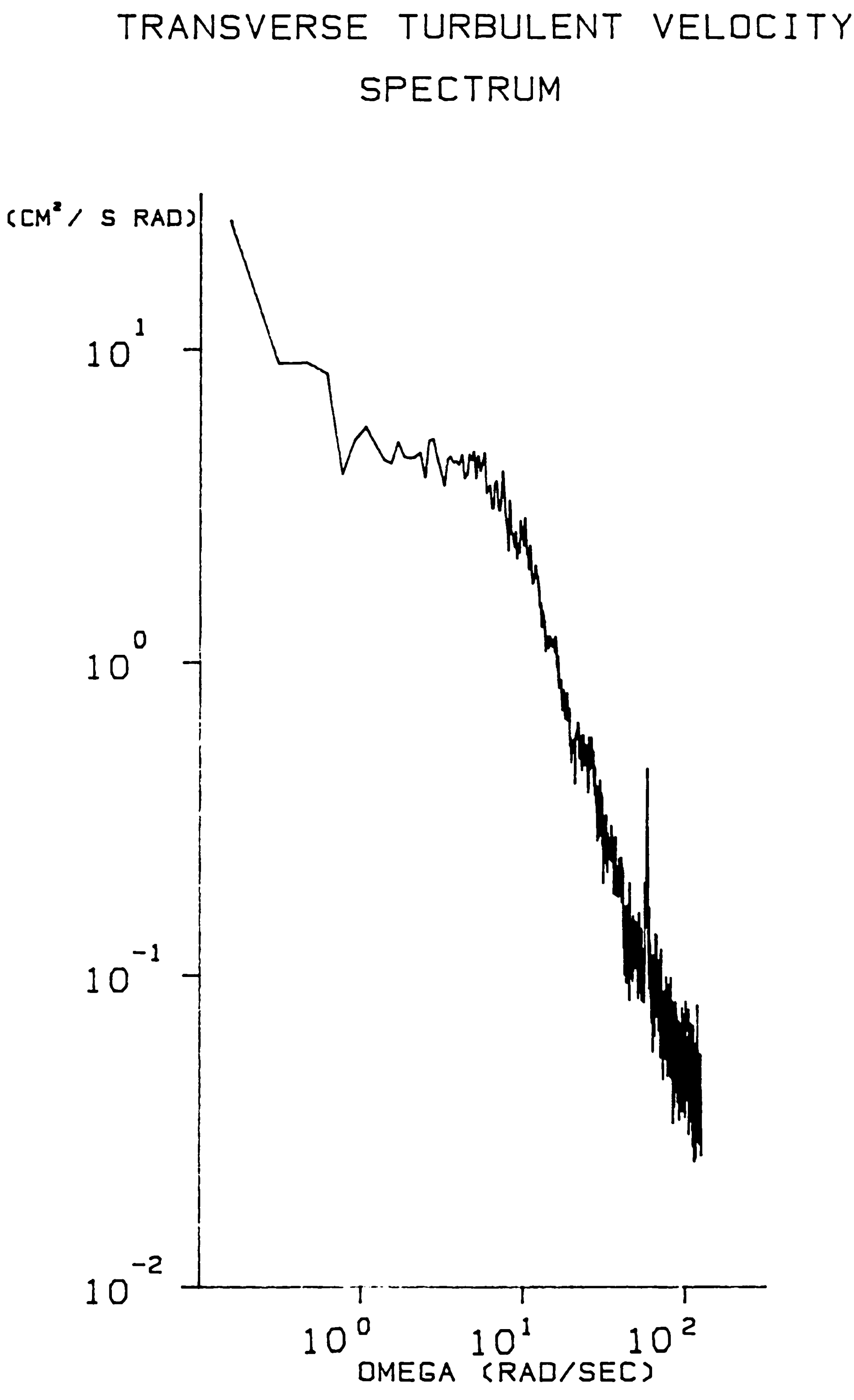

Fig. 4.12 Ensemble average of velocity spectra of test A2.

4.7.1 TURBULENCE TREATED AS SHEAR INDUCED MOTION

The concept of eddy viscosity is frequently used in turbulence modelling in spilling breaking waves. In the light of the success of such models in the surf zone, the collected data may be interpreted from the eddy viscosity point of view.

4.7.1.1 Eddy viscosity definition

In analogy to the viscous stresses in laminar flows, where

$$\tau = \mu \frac{du}{dy} \qquad 4.3$$

where τ is the shear stress,
μ the kinematic viscosity and
du/dy the velocity gradient,

the turbulent stresses are assumed to be proportional to the mean velocity gradients

$$-\overline{u_i u_j} = \nu_t \left(\frac{\partial u_i}{\partial x_j} + \frac{\partial u_j}{\partial x_i}\right) - \frac{2}{3} k \, \delta_{ij} \qquad 4.4$$

where ν_t is the turbulent, or eddy viscosity,
k is the turbulent kinetic energy,
$\delta_{ij}=0$ for $i \neq j$, $\delta_{ij}=1$ for $i=j$.

Contrary to the kinematic viscosity, which is a fluid characteristic, eddy viscosity depends strongly on the state of turbulence.

The eddy viscosity concept has often been found to work well in practice, because ν_t, as defined above, can be determined to a good approximation in many flow situations. Eddy viscosity is proportional to a velocity scale, v, and a length scale, l, characterising the turbulent motion.

$$\nu_t \propto v \, l \qquad 4.5$$

The distribution of v and l can be approximated reasonably well in many flows. It is the relationship between ν_t, v and l that makes the eddy viscosity concept a successful one in many turbulent models used at present.

4.7.1.2 Eddy viscosity in breaking waves

In spilling breaking waves, the turbulent length scale, l, is usually prescribed. In the surf zone, close to the bed, l has the variation normally used for boundary layer modelling, whilst it is constant away from the bed (~0.2–0.3 x local water depth), as in free turbulence conditions. Assuming that a similar turbulence structure occurs in plunging breakers, the significant parameter in determining the eddy viscosity is the turbulent velocity, $\sqrt{k}$.

The ensemble average of the square of the turbulent velocity time history, v'^2, may be related to the turbulent kinetic energy, k,

$$k = \frac{1}{2} \left(\overline{u'^2} + \overline{v'^2} + \overline{w'^2} \right) \tag{4.6}$$

If the turbulence structure under a breaking wave is assumed to be the same as that in the outer region of a boundary layer, (Svendsen, 1986) the relationship between the turbulent components, u', v' and w' is,

$$\overline{u'^2} : \overline{v'^2} : \overline{w'^2} = 0.45 : 0.32 : 0.23 \tag{4.7}$$

and
$$\frac{\overline{v'^2}}{2k} = 0.32 \tag{4.8}$$

$$k = 1.56\, \overline{v'^2} \tag{4.9}$$

The turbulent kinetic energy is therefore directly proportional to the ensemble average of the square of the turbulent transverse velocity component. The temporal variation of the turbulent kinetic energy may thus be derived directly from the plots of v'^2 against time.

$$\nu_t \propto \sqrt{k} \propto \sqrt{\overline{v'^2}} \tag{4.10}$$

The eddy viscosity, is therefore proportional to the fluctuating component of the transverse velocity, v'. The spacial and temporal distribution of eddy viscosity is therefore directly related to that for v'^2, and k, as obtained in sections 4.6.3 and 4.6.5.

4.7.1.3 Rate of dissipation of turbulent kinetic energy

The turbulence characteristics of the surf zone were investigated for a quasi-steady state (that is, the conditions are the same between wave cycles) (Svendsen, 1986). The temporal and spacial variation of the turbulent kinetic energy, k, were described analytically and compared with experimental results.
The local dissipation of k is expressed by

$$\frac{\partial k}{\partial t} = -\frac{C_d}{l} k^{3/2} \qquad 4.11$$

where C_d is a turbulent constant (~ 0.09)
l is a turbulent length scale

The solution to the above equation is

$$k = k_0 \frac{1}{(At + 1)^2} \;; \qquad A = \frac{C_d\, k_0^{1/2}}{2\, l} \qquad 4.12$$

where k_0 is the initial turbulent kinetic energy, k(t=0). This condition corresponds to the idealised assumption that at time t=0 the turbulence level is abruptly raised to k_0 from which it decays with time.

Svendsen's (1986) work is hereby extended to consider the accumulation of the turbulent kinetic energy with time. The variation of Σk with time, t, is then

$$\Sigma k(t) = \int_0^t \frac{k_0}{(At+1)^2} dt \qquad 4.13$$

$$\Sigma k(t) = k_0 \frac{t}{At+1} \qquad 4.14$$

Equation 4.14 represents the summation of the turbulent kinetic energy with respect to time. For large values of t, Σk tends to k_0/A.

$$\frac{\Sigma k(t)}{k_0/A} = A \frac{t}{At+1} \qquad 4.15$$

The graphical illustration of the above equation, (fig. 4.13) represents the **normalised** accumulation of the turbulent kinetic energy with respect to time. The higher the value of A, that is the higher the initial kinetic energy, the faster the attenuation of the energy. The rate of energy dissipation may be easily derived by substituting different values into equation 4.15. For a dissipation rate of 75% say,

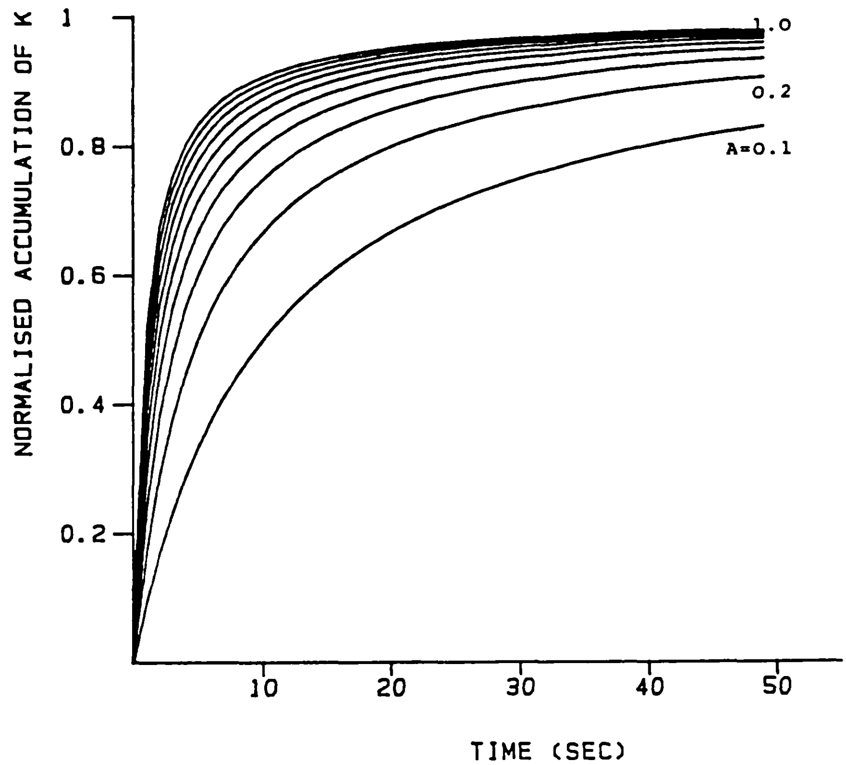

Fig. 4.13 Normalised accumulation of turbulent kinetic energy with respect to time.

$$At = 0.75\ (At+1) \tag{4.16}$$

$$At = 3 \tag{4.17}$$

Equation 4.17 implies that it takes 4 sec, say to dissipate 75% of the turbulent kinetic energy for A=0.75 sec^{-1}. Similar values may be obtained for other dissipation rates.

The results presented in this thesis may be compared with Svendsen's (1986) work. Qualitatively, the shapes of the curves of the normalised accumulation of turbulent kinetic energy have similar shapes in both the experimental results and the theoretical predictions. As seen on table 4.1 the rate of energy dissipation is generally in agreement with the theoretical prediction that, the higher the initial turbulent energy the faster the rate of dissipation. The reason that not all the experimental results indicate the same trend might be due to the random nature of the process and the limited number of data records.

Quantitatively, useful information may be derived from the experimental results.

Taking t=5 seconds as a reasonable time for the approximation – this time corresponds to the time at which the initial data indicate reasonably little scatter of the results – the rate of energy dissipation, P(t=5), is deduced and the value of A is:

$$A = \frac{P}{t(1-P)} \qquad 4.18$$

Taking the initial turbulent kinetic energy, k_0, as expressed by equation 4.9,

$$k_0 = 1.56\ \overline{v_0'^2} \qquad 4.19$$

and v_0' as equal to 1/2x(range), where the range is defined by equation 4.6 and listed in table 4.1, then the length scale remains as the only variable,

$$l = \frac{C_d\ k_0^{1/2}}{2\ A} \qquad 4.20$$

Assuming the value of C_d=0.09 (Svendsen, 1986) a table is prepared (table 4.2) listing the values of A and l.

The length scale, l, is commonly expressed as a function of a geometrical length related to the boundary conditions. In the case of jets in stagnant surroundings the width of 1/2 jet, δ, is used as the geometric physical length scale; δ is the distance between the symmetry axis and the point where the velocity is 1% of the maximum velocity. The ratio, l/δ, under these conditions, varies between 0.075 and 0.125 (Launder and Spalding, 1972). Battjes and Sakai (1980) simulated the fluctuating motion to that of a wake flow in which case the length scale is approximately proportional to the square root of the distance from the breaking inception point. Svendsen (1986) assumed that l is proportional to the local water depth, h (~0.2–0.3 h).

In the plunging breaker in deep water conditions the jet simulation is appropriate in the immediate vicinity of the plunging point. Measurements in this area have not been recorded due to the presence of air. Shorewards of the plunging area (points *A4–A6* and *B3–B5*) the experimental results suggest a constant value for the length scale (5mm and 3mm respectively). Further shorewards (*A8, A9* and *B7–B10*) the experimental results do not show any consistent values. These observations indicate that:

a) The fluctuating motion is induced by not only fluid shearing, but by surface wave motion, as well.

Position	Range cm/s	% of energy dissipation P, in 5 sec	A sec	l mm
A1	9.8	72	0.51	5.3
A2	10.7	84	1.05	2.0
A3	4.8	83	0.98	1.4
A4	8.5	70	0.46	5.1
A5	6.5	64	0.35	5.1
A6	6.8	65	0.37	5.1
A7				
A8	15.0	53	0.22	18.6
A9	8.2	60	0.30	7.6
B1	7.6	40	0.13	1.6
B2	6.3			
B3	7.3	85	1.13	1.8
B4	7.6	77	0.67	3.2
B5	5.7	72	0.51	3.1
B6	5.3			
B7	8.6	70	0.46	5.2
B8	8.7	58	0.27	8.8
B9	5.4	54	0.23	6.4
B10	5.3	73	0.54	2.7

Table 4.2 Experimental results and derived values of A and l.

b) Shear induced fluctuating motions are concentrated in the "immediate" vicinity of the plunging point(s). The size of this area depends on the type and size of the breaker as well as on the water depth. In the surf zone, Svendsen's model is appropriate. In deeper water Battjes' model, turbulent wake, is suitable for spilling breakers. The jet simulation is appropriate for the case of strong plunging breakers. Such breakers are followed by a series of jet-splash processes which become weaker with time. These weak jets are more like spilling breakers, since spilling and plunging breakers have the same features but at diferrent scales, in which case Battje's model is appropriate. The limited information presented in this thesis indicates that Battjes' model may be used shorewards of the plunging area.

c) Offshorewards of the plunging area, in both shallow and deep water conditions, the fluctuating motion does not follow the characteristics of shear induced motion. This is also the case for deep water breaking waves at locations beyond a certain depth and shoreward length, determined by the characteristics of the breaker. This motion is predominantly associated with surface wave motion.

d) Qualitatively, the rate of accumulation of the turbulent kinetic energy associated with both types of fluctuating motion is very similar. This similarity together with that of the fluctuating velocity records makes the distinction between the two motions a most difficult task.

4.7.2 TURBULENCE TREATED AS SURFACE WAVE INDUCED MOTION

The deviation from the ensemble average velocity records, or turbulent component as it is called, may be also viewed as the result of three dimensional surface wave motion. Although this mechanism was mentioned by Svendsen (1986), no further consideration was given to this case. The reason might be the absence of a physical mechanism initiating such a three dimensional surface wave disturbance after the breaking of an otherwise two dimensional wave.

The characteristics of the surface wave induced turbulence motion are presented later in the thesis, after the identification and description of the mechanism of generation of this motion.

4.8 SUMMARY - CONCLUSIONS

Measurements of the transverse velocity component around two deep water breaking waves were recorded using Laser Doppler Anemometry. The results were analysed in a number of novel ways and interpreted accordingly.

The velocity time history at any point is characterised by

a) quiescent part, no transverse velocity,
b) disorganised, fluctuating, turbulent motion, and
c) regular, organised motion.

Using Fourier's theorem, the disorganised part is decomposed into a wide range of frequency components, covering both the turbulent range, >10Hz, and the surface wave motion range, of lower frequencies. The generation of a fluctuating, random, three-dimensional surface wave at the plunging stage of the breaking wave process although mentioned in previous studies (Svendsen, 1986) it is nevertheless not treated in the literature.

The following regular, organised motion is the consequence of the presence of a surface wave disturbance in a domain with discreet natural modes of oscillation. A standing wave is formed whose period corresponds to one of the natural harmonic periods of transverse oscillations in the flume. The formation of this standing wave reinforces the conclusion that wave breaking also generates three- dimensional surface wave motion.

The distinction between the surface wave induced motion and the shear induced one is not possible on the experimental records. As a result the data were analysed as a whole. The turbulent kinetic energy in the transverse direction was looked at in great depth and the spacial and temporal variation of its rate of accumulation was derived. When the data were viewed from the shear induced angle, the total turbulent kinetic energy, k, was related to the transverse velocity fluctuations as well as to eddy viscosity. Measurements of turbulent velocities in the transverse direction have the advantage that they are not only accurate, owing to the small magnitude of the slow varying component, but they can be directly related to the total turbulent kinetic energy and eddy viscosity, as well.

Some of the results derived from the analysis of the data may be listed as follows:

a) Breaking may be viewed as a **source of energy** at the plunging point. Secondary plungers that follow, act as weaker sources of energy. The energy input into the system, or lost by the breaker, is reflected in the velocity measurements. These measurements are also directly related to the eddy viscosity, a concept widely used in engineering models.

b) The maximum intensity of turbulence occurs shorewards of the plunging point, verifying thus the generation of a series of jet–splash system.

c) The accumulation of energy in the transverse direction, or loss of energy from the plane of the breaking wave is not an instantaneous process. The rate of energy accumulation is directly derived from the plots of the normalised summation of the square of the turbulent transverse velocity component with time. The results show that if wave breaking under the tested conditions had occured at intervals of say T=5sec, about 30% of the energy input from the previous wave would still be present on plunging of the following breaker.

d) The breaking induced turbulence spreads over a wide longitudinal distance and a shorter vertical depth. The extend of the water volume affected by breaking depends on the steepness of the breaker; the steeper the breaker, the bigger the penetration of turbulence. Mild spillers therefore, induce surface turbulence, whilst steep plungers, like the tested ones, generate intense motion in depths exceeding three times the breaker heigth.

4.9 CRITICAL ASSESSMENT OF EXPERIMENTAL RESULTS

The collected data indicate that the turbulent motion produced by breaking waves is associated with both **shear** and **surface wave** induced motion. The relative importance of each mechanism is a function of the breaker characteristics, the water depth and the location of the point under consideration with respect to the plunging point. Close to the plunging area, the motion is in general dominated by shear induced turbulent motion. The extent of this area is very important as the physical processes taking place within and outside this domain are quite different. Regarding energy considerations, the shear induced fluctuating motion is dissipative whilst the surface induced motion is not. The kinematics associated with the two types of motion, although they cannot be distinguished, are nevertheless governed by different principles. The shear induced kinematics are, in general, governed by viscous effects whilst the surface waves by gravity.

The mechanism of generation of the surface wave induced fluctuating, or turbulent motion is a problem to be addressed. The challenge posed in identifying, describing and assessing the effects of this mechanism is taken up in the chapters that follow.

CHAPTER 5

VISUAL OBSERVATIONS ON BREAKING/BROKEN WAVES

5.1 ABSTRACT

A property of breaking waves, neglected by scientists, but extensively recognised in the arts, is the segmentation of the overturning crest of the wave into a number of jets. The physics behind this phenomenon suggests that this is a surface tension effect. In the free fall of an overturning wave, surface tension is a predominant force, a force which tends to minimise the free surface area for a given volume of liquid. The process of segmentation takes place over such a short period of time that the human eye cannot individually distinguish between the stages through which the shape of the wave passes. Pictures of breaking waves in deep and shallow water, produced in the laboratory and captured using a number of techniques, throw some *light* on the segmentation process and the associated effects. A video cassette accompanying the thesis illustrates clearly the stages of the breaking process: the segmentation of the curling face, the splash following plunging, the penetration of the plunging jet and the induced wave disturbance.

5.2 INTRODUCTION

The human eye provides information about the size, shape, distance, colour and beauty of the objects around us. It can analyse movement when this takes place at a reasonable speed. The cut-off point of the speed, beyond which individual movements blur into a continuous flow, is about 10 pictures per second. This limitation is imposed by the way human vision works. The *retina*, the sensitive surface at the back of the eye ball, cannot receive and transmit impressions to the brain any more quickly. Furthermore, the brain needs at least 1/4 of a second to interpret a simple action.

The limitations of the human eye were realised when man started questioning his environment - how birds fly, horses gallop and so on. With the advent of fast moving machinery and other technological developments, the actions of wheels, explosions and projectiles were almost invisible. Various techniques have been developed over a number of years that now enable the study of fast changing processes, such as breaking waves.

Four different ways of capturing the overturning process have been used:

a) conventional video recording with ordinary light (25 frames per second),
b) conventional video with stroboscopic light,
c) high speed video recording (1000 frames per second), and
d) high speed camera (200 frames per second).

The first observation of the segmentation process was made using a conventional video camera. The purpose of the recordings was the monitoring of the waves in the flume, as the area was enclosed with black curtains owing to the presence of the Laser Doppler Anemometer. The consistent formation of transverse patterns across the crest of the plunging wave led to the adoption of more sophisticated methods of recording the phenomenon.

Studies of splashes, a phenomenon which takes place quite rapidly as well, have been conducted using stroboscopic flashing. The stroboscopic light was developed by Edgerton in the early 1930s. Unable to see how electric motors behaved when rotated at various speeds, he designed a light that could flash so quickly and brightly that motion seemed to stop. When used with a camera *"a whole new age of high speed photography was born"* (Secker et Al, 1980). Pictures taken with continuous light display the image during the period the shutter of the camera is open, whilst those taken with stroboscopic light display the image during the flashing of the light, which is of the order of millionths of a second. Stroboscopic light of $5\mu s$ flash duration was used with a video camera recorder.

A high speed cine camera was also used. This camera provided better quality pictures with a much higher number of pictures per second. It was not used with stroboscopic light because the two instruments cannot be tuned together.

A high speed video camera was used at a later stage of the work. This facility enabled the collection of images of up to 1000 frames per second, a speed which almost freezes the motion.

Extracts from the recordings made are presented in the video tape accompanying the thesis. There is no sound in the tape. Single frames briefly describe the contents of the different scenes. Selected frames were processed using various image processing operations. The principles of imaging processing and a brief description of the routines, developed by the author, and used in this work are presented in appendix B.

5.3 DESCRIPTION OF VIDEO CASSETTE

A series of continuous scenes recorded with the conventional video system are first presented. Single frames follow, highlighting some features of the scenes. These are followed by a sample of recordings made using both high speed video and photo techniques. Finally, some pictures relevant to the overturning process of breaking waves conclude the story of the cassette.

Printed images from the video cassette are presented at the end of the chapter (plates 5.1–5.41).

5.3.1 CONTINUOUS SCENES

5.3.1.1 **Deep water breaking waves, observed from the side and above the crest**

A sequence of breaking events is presented. All breakers were produced under the same conditions (water depth = 1.2m, same driving signal, named *sign1*). The repeatability and consistency of the breaking process is evident. When the cassette is played at real time, the overturning process takes place over such a short time, that a blurred picture is seen. When however, it is played at slow motion, or *paused* successively, some distinct features are clearly visible on the tip of the overturning crest of the wave. The tip of the wave breaks up into jets (dark and bright lines perpendicular to the crest), whilst the back of the wave shows cusp-like shapes, spaced at wider intervals than the jets. This **segmentation** of the wave crest, as it is called hereafter, is observed in all the breakers presented. (See also plates 5.27–31).

5.3.1.2 **Deep water breaking waves, as seen from the front**

A few scenes, shot from a position shorewards of the plunging point, with the camera pointing towards the wave maker, show the segmentation process *en face*. The pictures are rather dark, owing to the limited lighting and the presence of undesirable reflections. Nevertheless, in slow motion the stages in the overturning process are distinguishable. These scenes provide a challenge for the application of image processing techniques, as shown later on.

5.3.1.3 **Deep water breaking waves, as seen from behind**

The unique set up of the experimental procedure offered the oportunity to observe a process that takes place during the wave breaking process. The image of the edge of the flume, reflected on the water surface, revealed the presence of a *new* wave disturbance generated at the plunging area and travelling in the *opposite* direction to the breaking wave. The actual amplitude of this wave, seen at the line of intersection between the water surface and the wall, is very small; hardly any motion is seen. Measurements with the wave gauges also failed in identifying this motion. The low angle of view and the reflection of a distant line provided a suitable combination for amplification of the amplitude of this motion. It is evident that

a) a series of waves are generated at the plunging area,
b) at a given point, the time history of the surface elevation indicates that, the period of the motion decreases with time,
c) at a given time, the profile of the wave indicates that the wavelength of the motion is longer the further away from the plunging area.

(See also plates 5.39–40)

5.3.1.4 **Deep water breaking wave – induced oscillations**

Apart from longitudinal wave motion, wave plunging induces transverse disturbance, as well. The amplitude of this motion is also very small. Its observation is possible through the reflection of the horizontal platform spanning across the flume (the white strip shown in the middle, above the centre of the picture). The shape of this strip indicates the presence of a transverse standing wave, the two ends being *antinodes*, having maximum amplitude of oscillation. The existence of standing transverse waves was also suggested from the velocity records, presented in chapter 4. The frequency of the oscillation decreases with time, the high frequency components decaying faster. Towards the end of the scene, two complete cycles may be seen, suggesting the presence of the 4^{th} harmonic mode of a standing wave. (See also plate 5.41).

5.3.1.5 **Shallow water breaking waves, seen approaching the camera**

A number of scenes were shot from behind a slope, 1:7. They illustrate that the physical mechanism of wave overturning is the same as for deep water breakers. Long and short, big and small waves, all show the overturning tip of the wave segmenting into jets. The presence of these jets is more evident in the splash that follows plunging. In regular periodic waves, unlike freak deep water breaking waves, the overturning wave is affected by the motion induced by the previous breakers. The shape of the crest at breaking point, that is when the forward face becomes vertical, is no longer smooth and straight. Short wave disturbances are evident, which become increasingly bigger with time, due to the disturbance generated by the previous breakers. (See also plates 5.9, 31–35).

5.3.1.6 Shallow water breaking waves, seen from the side

The formation of transverse channels at the back of the wave is seen in these shots. **Three-dimensional, short, irregular waves** are generated during the breaking process. The presence of these waves is emphasised by the reflections reaching the camera. Their presence was predicted from the interpretation of the velocity measurements obtained with the FOLDA. (Plates 5.36–38).

5.3.1.7 Deep water breaking waves, recorded under stroboscopic lighting

Inspired by the successful use of stroboscopic lighting in studying the fast changing process of liquid splashing, an attempt was made to *freeze* the individual stages of the overturning process using a similar technique. The rate of flashing was adjusted until a steady picture was obtained by the camera. At this rate, the camera was capturing the motion taking place over the short period of $5\mu s$. Owing to the large space illuminated and the limited power of the stroboscope, the pictures are quite dark. Image processing was used, as discussed later on, to enhance the quality of the picture.

5.3.1.8 Free fall of a mass of water – segmentation

The duration of wave overturning is so short that the segmentation process is not fully developed. An alternative process, physically similar to the segmentation of the plunging jet of breaking waves, is the free fall of a sheet of water. A series of scenes is presented showing a tray filled with water which is suddenly tilted. The tip of the falling mass of water segments into jets, similar in form with those formed in breaking waves. The consistency of the segmentation process is evident in all shots, although the initial conditions vary significantly, due to the nature of the experimental procedure. The purpose of this experiment was restricted to qualitative observations, in the understanding of the physical process. (Plates 5.10–11).

5.3.1.9 Free fall of a mass of water – penetration – secondary disturbance

The previous experiment was repeated with dyed water falling on a still water surface. The plunging coloured jet penetrates the receiving water mass like a solid body. A splash is formed, whose mass originates from the initially undisturbed water. The surface elevation at the plunging point oscillates and a surface wave disturbance is generated propagating in both directions away from the plunging area. The characteristics of this motion are described by the properties of the waves produced by a local disturbance on the water surface (appendix A). These observations are in line with Jansen's (1986) results on the **solid body penetration** and the **secondary disturbance generation** observed in plunging breakers. (See also plates 5.5–8, 12–15).

5.3.1.10 **Free fall of a mass of water – penetration depth**

In deep water conditions, the penetrating mass of water retains its shape during the initial stages, with very little mixing with the receiving water. The penetration is slowed down due to the drag force acting on the jet, and the coloured water gradually diffuses in the rest of the water mass. It is observed that the shape of the transverse jets changes as the jets penetrate the receiving water body. The "wavelength", as well as the "amplitude" of the jets increase. The use of the terms "wavelength" and "amplitude" is explained in chapter 6. (Plates 5.16–19).

5.3.2 SINGLE FRAMES

Selected frames from the continuous scenes are presented. They highlight the points discussed above. The theme of each frame, how it was recorded and what image processing techniques (if any) were applied are reasonably clear. Appendix B describes the principles of image processing and the routines employed in producing the presented pictures.

One set of pictures which deserves particular attention is the subtraction of successive frames. Two successive frames from a motionless subject have theoretically identical pixel values in the 512x512 array. It should be stressed that in practice, there is a slight discrepancy between the two frames, arising from a number of sources of noise. However, within certain limits, it may be said that the two frames are the same. Subtraction of these frames results in a frame whose pixel values are all zero; hence a black picture is displayed.

A movement of the subject implies that the values in certain pixels are changed. Subtraction of the two images gives black everywhere apart from the pixels which experienced the movement. When this resulting frame is contrast-enhanced, the motion that took place within the time interval between the two original frames comes out white on a black backround.

This techique is applied on breaking waves. The velocities at different points along the free water surface are directly derived from the subtraction of successive frames. Some conclusions drawn from just looking at these pictures are:

a) the maximum horizontal velocity occurs at the tip of the wave,

b) the maximum velocity does not occur at the breaking point, but slightly later on,

c) the backward face moves downwards and forwards, the curling face mainly forwards and the forward face of the wave moves backwards, and

d) the segmentation process starts soon after breaking point and grows rapidly.

Qualitatively the first three observations are in agreement with the state of the art on breaking waves (fig. 5.1). The last observation is treated by a new model proposed and discussed in chapter 6.

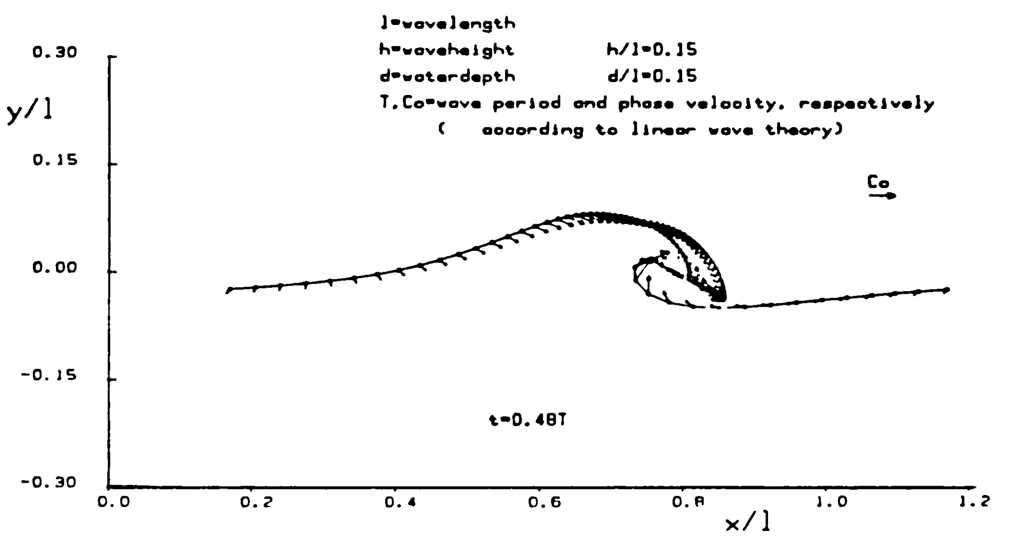

Fig. 5.1 Velocities along the free surface (W.K. Shih)

An estimate of the crest velocity in an overturning wave may be calculated from the presented pictures (plate 5.1). The grid lines are spaced at 200mm intervals. The distance covered by the wave crest over a period of 0.08 seconds is about 91mm; the velocity at the crest is therefore 1.14m/s. The wavelength of the wave, L, is taken approximately as 163mm; this is the horizontal distance between the plunging point and the trough of the backward face of the wave. The celerity of a linear wave, in deep water conditions, is

$$c_0 = \sqrt{\frac{L\,g}{2\pi}} = 0.5 \text{ m/s} \qquad 5.1$$

The crest velocity is therefore **2.28** times the celerity calculated using linear theory. This value compares favourably with other experimental values (1.3 ~ 2.8) obtained by elaborate and complex methods (chapter 2). The attractive feature of this method is that it is very simple to use and the velocity is visualised. For best results, the camera must be pointing perpendicularly on to the wall.

Image subtraction also provides a simple form of high pass filtering, in the time domain. The differences between successive frames are highlighted, whereas the slow changing characteristics are suppressed. The transverse formations on the surface of the overturning wave are enhanced more efficiently with image subtraction rather than spacial high pass filtering.

5.3.3 HIGH SPEED VIDEO PICTURES

A unique facility offered by the SERC is the high speed video recording system. This system allows recording of up to 1000 frames per second. The information displayed on each frame is the following: the time of day and elapsed time of recording are displayed on the top left hand corner. The frame number, date, rate of recording and session number are shown on the top right hand side. The rest of the displayed information describes the general status of the system.

The high speed video pictures show deep water breaking waves. The characteristic features observed on the conventional video pictures are shown more clearly. Especially the pictures in *sesn 44* show the plunging **jets** of the overturning face hitting the forward face of the wave at a rate of 1000 frames per second. The segmentation process is so fast that even at this high speed there is a distinct change between successive frames. (See also plates 5.20–25).

5.3.4 HIGH SPEED CAMERA PICTURES

A high speed cine camera was also used. The cine film was projected at a slow and variable speed onto a screen and then recorded by a video camera onto the video cassette. Although the quality of the pictures was significantly reduced, nevertheless the characteristic features of the breaking wave process are clearly seen. The segmentation process, which is the main theme of these shots is shown at a considerably slowed down speed, highlighting thus the fast nature of the process. An interesting observation is the appearance of the splash as clear, trasparent, thin sheets of water and not as white foam, as seen by the naked eye.

5.4 RELEVANT PICTURES IN THE ARTS

A series of pictures on surface tension effects, as seen from the arts point of view, are presented. These high quality pictures show clearly the influence of the forces arising from surface tension on a drop of liquid falling both on a liquid and a solid plate. The segmentation of the splash, or *crown*, as well as the central water column offer an ideal theme for photography.

A most interesting drawing on the *artistic modelling* of overturning waves is the picture used in the promotion of a washing powder product. It illustrates the presence of jets across the overturning face of the wave, in a fashion similar to the segmentation process as observed in the laboratory. The author was "inspired" by this picture in developing a model of the segmentation process.

Finally, an extract from a film shown on television in April 1988 on *the making of a splash* is presented. This film is presented because it was felt that it helps in the understanding of the physics of breaking waves, especially the solid body penetration of a falling mass, the formation of a splash and the associated wave motion. Although the main theme of the television film was the music, *water opera*, the presented pictures provide an interesting study on splashes.

5.5 SUMMARY

The process of wave overturning has been approached from a new angle. Although this process has received a lot of attention, attracting the interest of artists and mathematicians, some new features on the physics of the process have surfaced from this study. These are:

(a) Segmentation.

It has been shown that it occurs in both deep and shallow water conditions, in small and large waves as well as short and long ones. Little jets are seen at the external surface of the overturning wave, followed by ridges spaced at wider intervals. The penetration of the main plunging jet in the receiving mass of water suggests the presence of a series of jets. Although macroscopically the plunging face of the wave appears the same in a series of experiments, microscopically, it is observed that the transverse jet-like formations do not have repetitive characteristics, that is the "amplitude", "wavelength", "plunging point" and "plunging time" vary not only between breakers, but across the wave crest of a single breaker, as well.

(b) Secondary wave disturbance

Wave plunging generates a secondary wave disturbance. The main plunging jet (macroscopic angle) produces a wave disturbance travelling opposite to the direction of propagation of the breaking wave. A much stronger secondary disturbance is expected to be generated in the breaking wave direction, whose characteristics are suppressed by the main wave motion. In addition to this two-dimensional disturbance, the three-dimensional nature of the segmented plunging jet produces a series of radial waves, whose summation results in an irregular, three dimensional, surface wave field. The restriction of this motion by finite boundaries has the effect that wave components are attenuated in different proportions, the ones corresponding to the natural modes of oscillation of the system having the less attenuation. A standing transverse wave therefore results.

(c) Image processing potential

The control of the generation of overturning waves provides a new challenge for photography and image processing. With relative simplicity, remarkable results are obtained, as illustrated in the determination of the velocities of the free surface boundary.

PLATE 5 1.

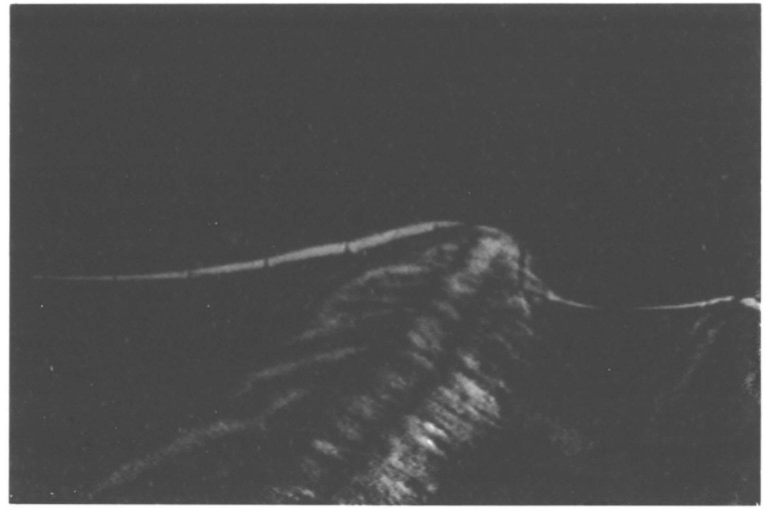

PLATE 5 2.

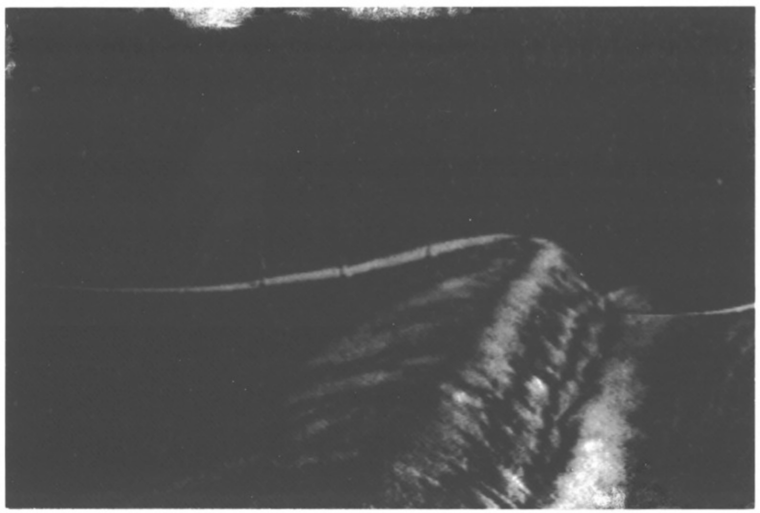

PLATE 5 3

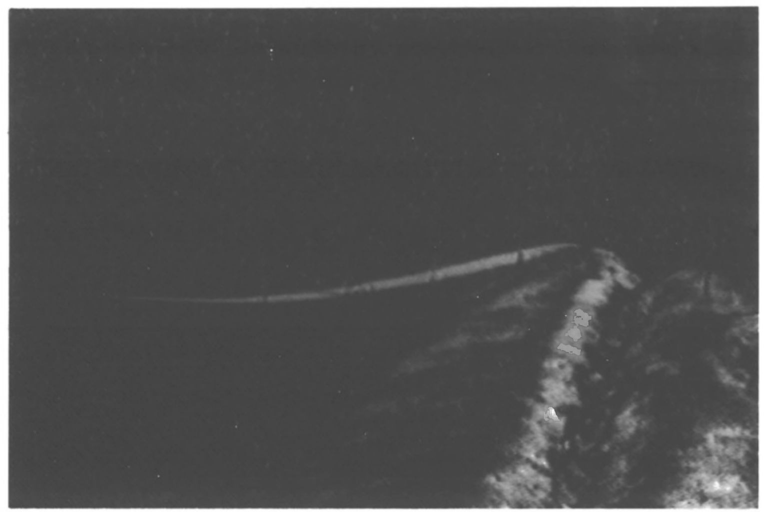

PLATE 5 4.

IMAGE SUBTRACTION - VISUALISATION OF VELOCITIES - TRANSVERSE JET FORMATIONS PROMINENT.

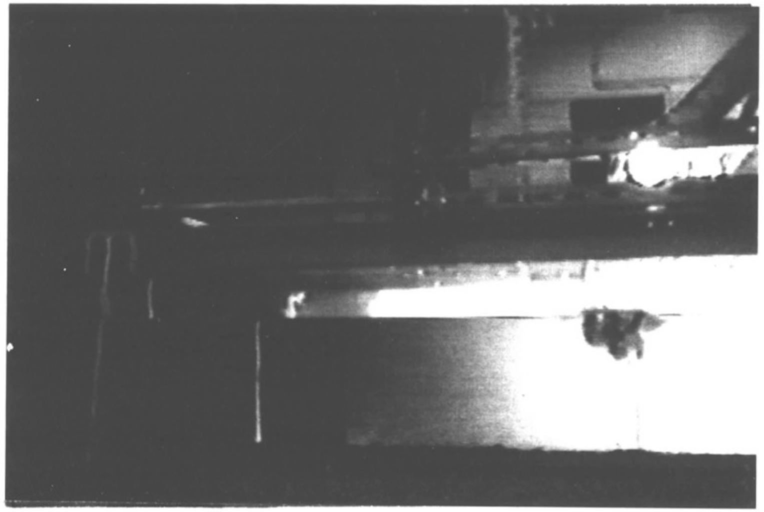

PLATE 5 5.

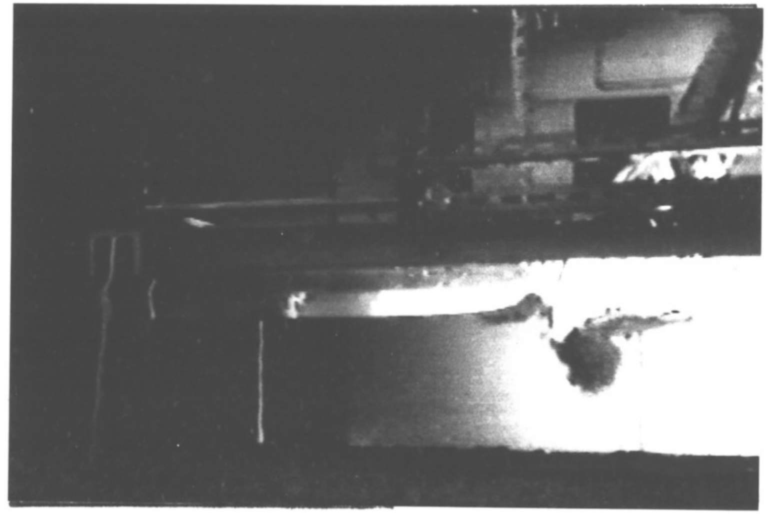

PLATE 5 6.

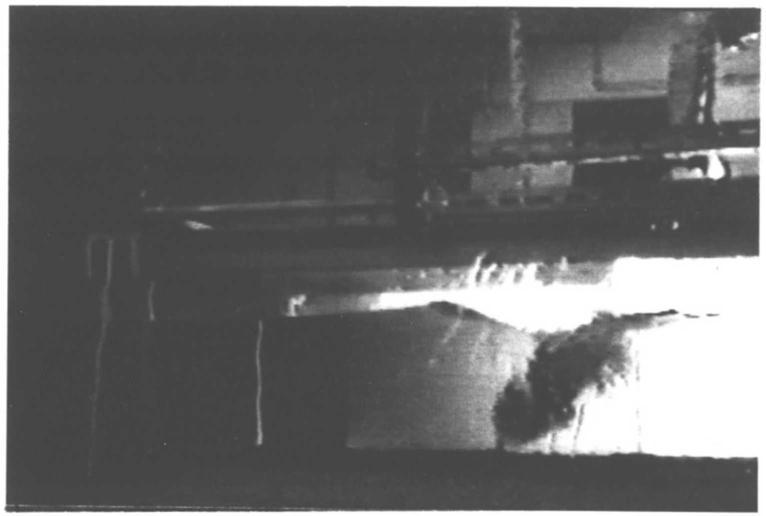

PLATE 5 7

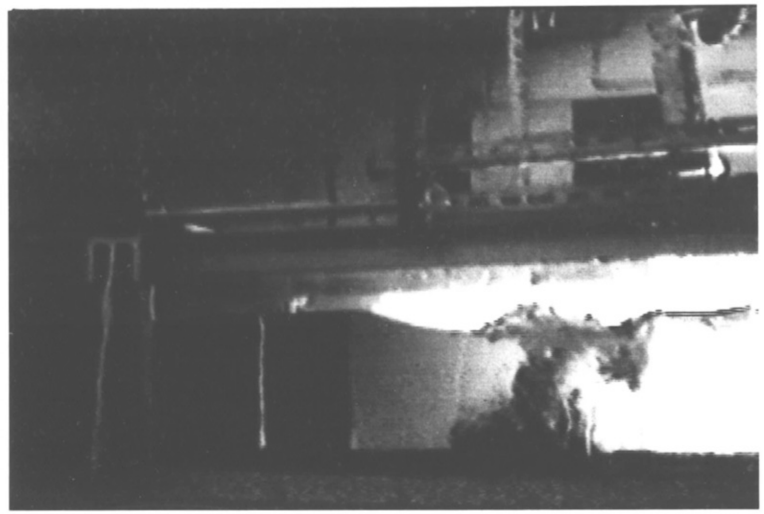

PLATE 5 8.

GENERATION OF WAVE DISTURBANCE DUE TO PLUNGING OF A FALLING WATER MASS.

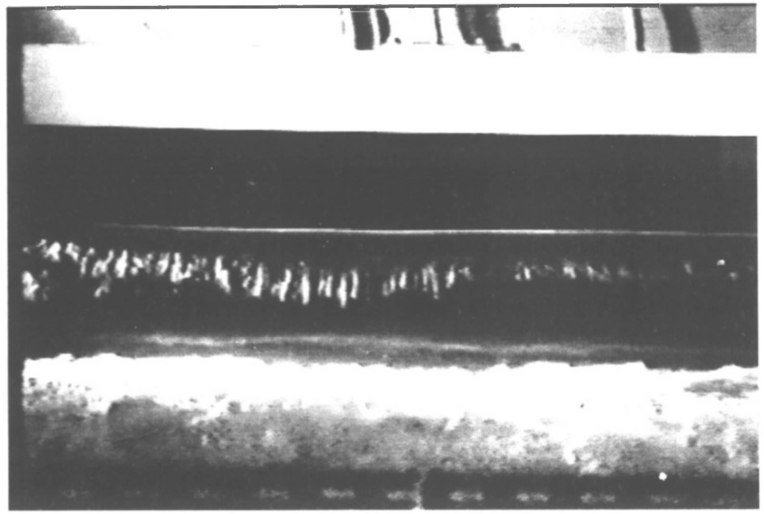

PLATE 5 9.

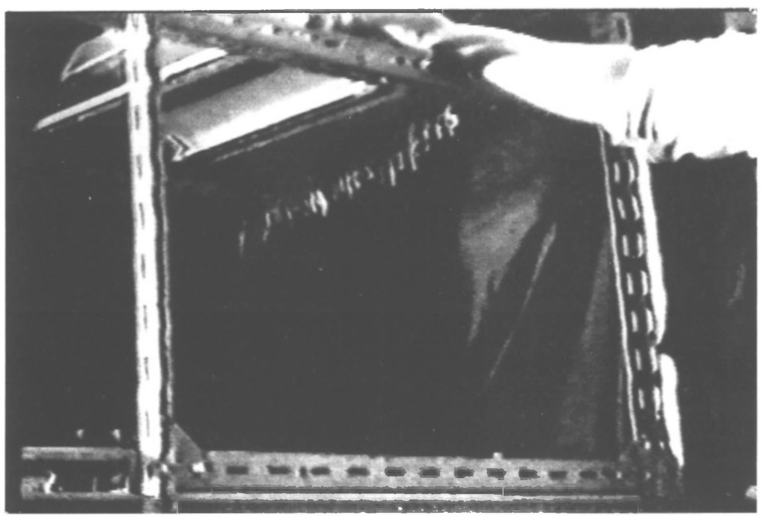

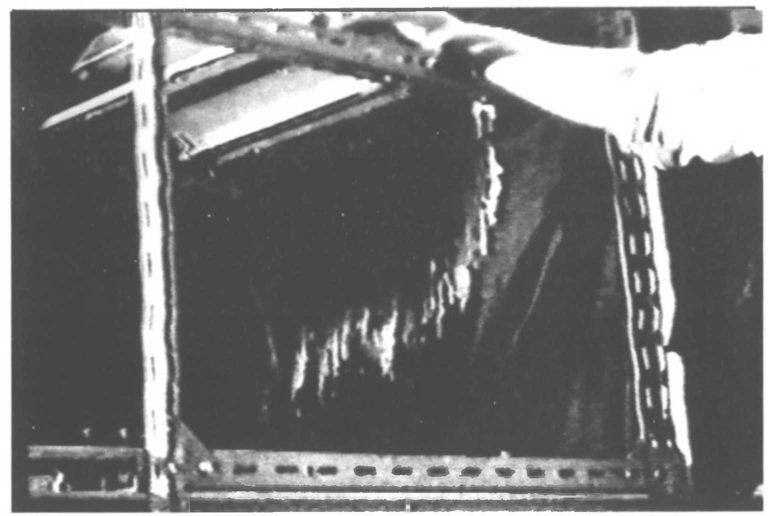

PLATE 5 10

SIMILARITY BETWEEN OVERTURNING WAVES AND FALL OF A SHEET OF WATER.

PLATE 5 11.

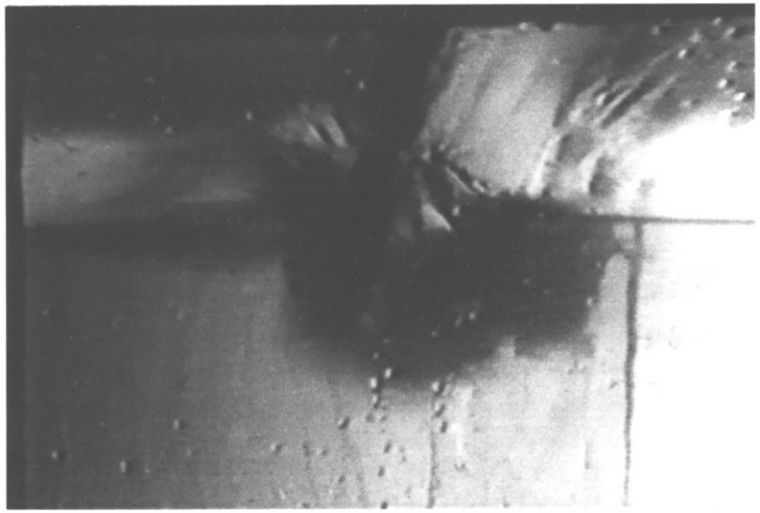

PLATE 5 12.

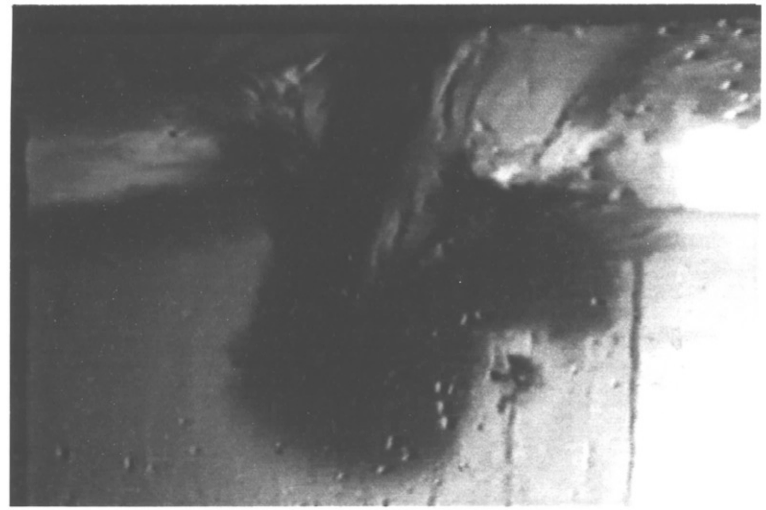

PLATE 5 13.

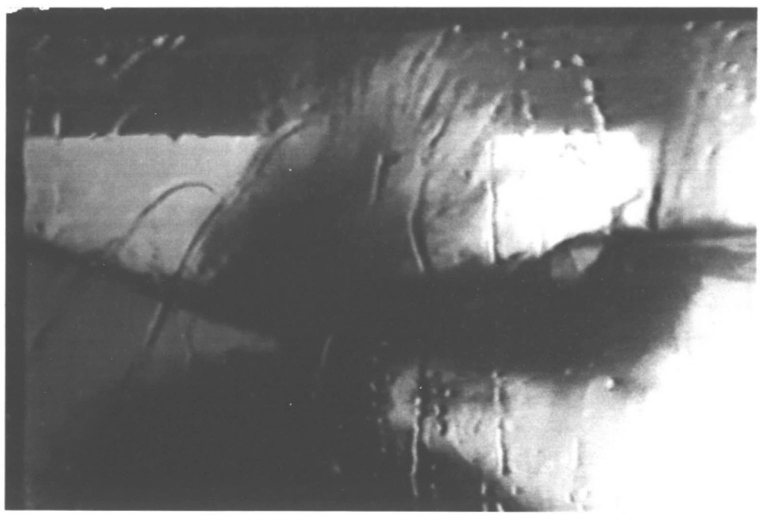

PLATE 5 14

PLUNGING JET PENETRATES THE RECEIVING WATER SURFACE LIKE A SOLID BODY.

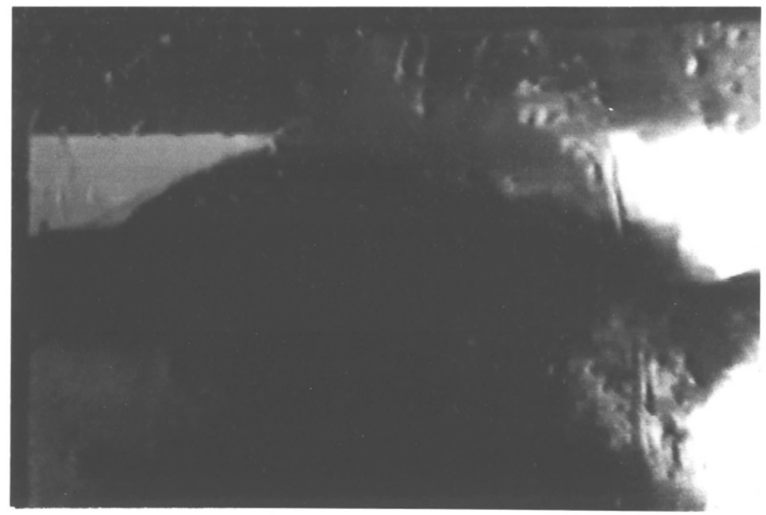

PLATE 5 15.

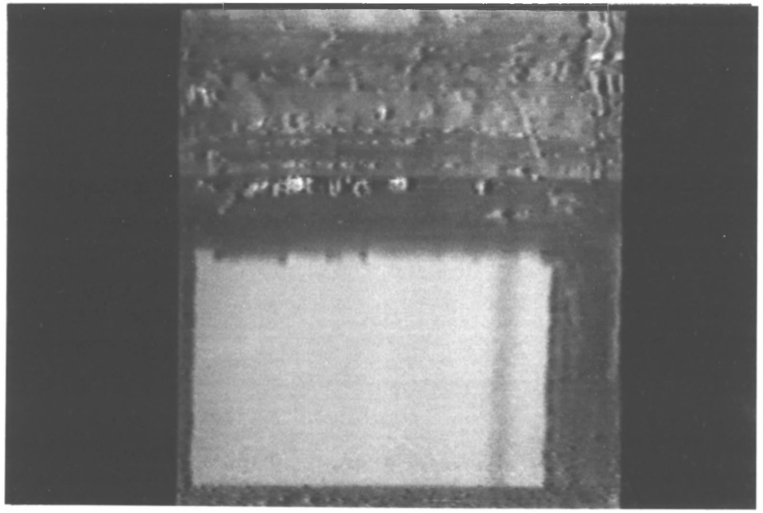

PLATE 5 16.

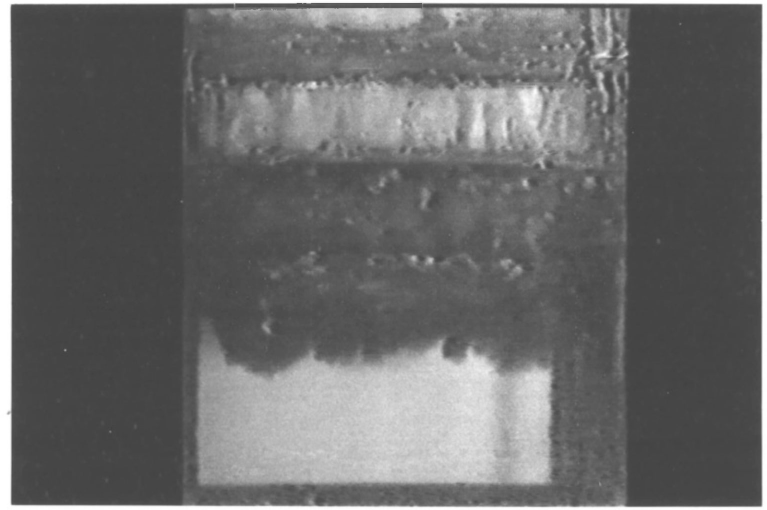

PLATE 5 17.

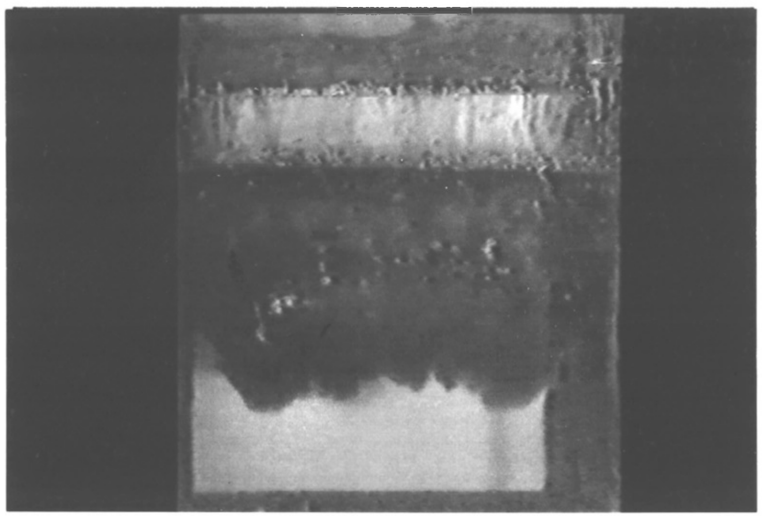

PLATE 5 18

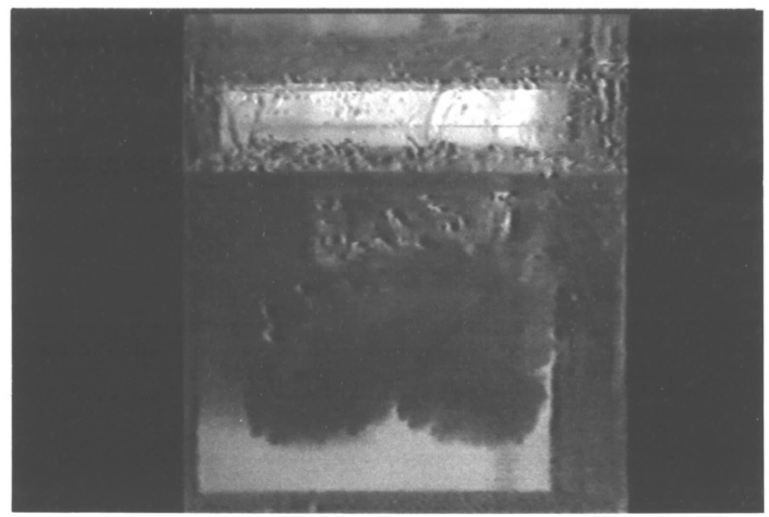

PLATE 5 19.

PENETRATION OF PLUNGING LIQUID JET - NOTE DIFFERENCE IN SHAPE AND SIZE OF TRANSVERSE JETS.

PLATE 5 20.

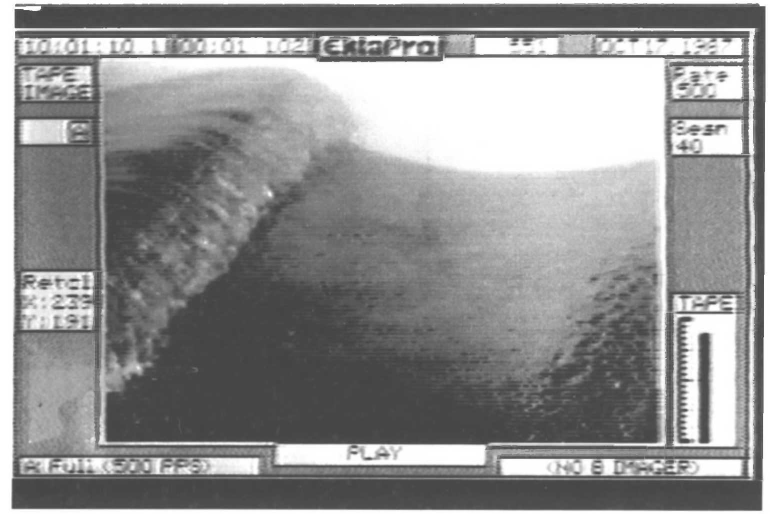

PLATE 5 21.

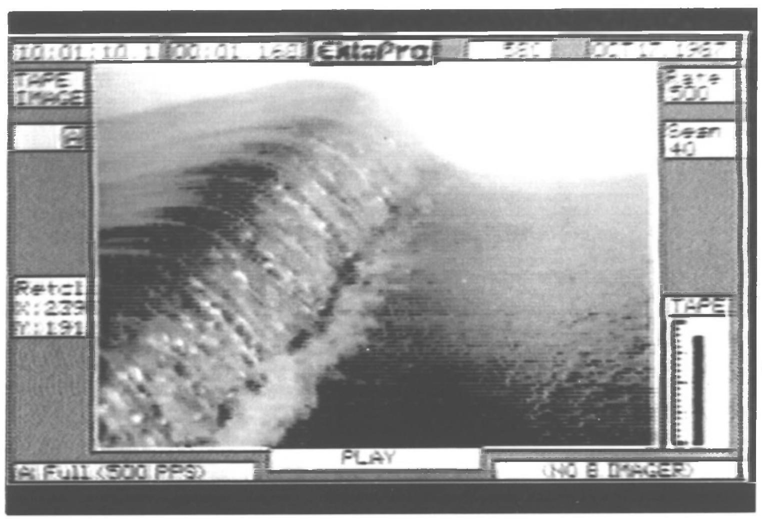

PLATE 5 22

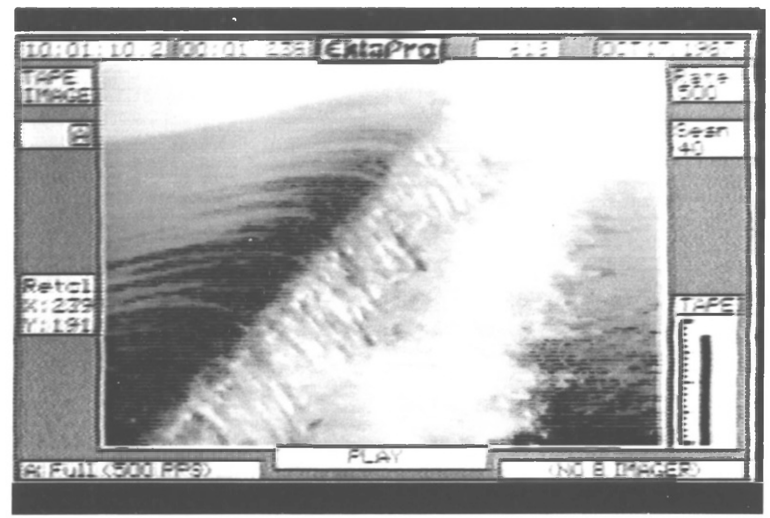

HIGH SPEED VIDEO PICTURES - WAVE OVERTURNING PROCESS - DEEP WATER.

PLATE 5 23.

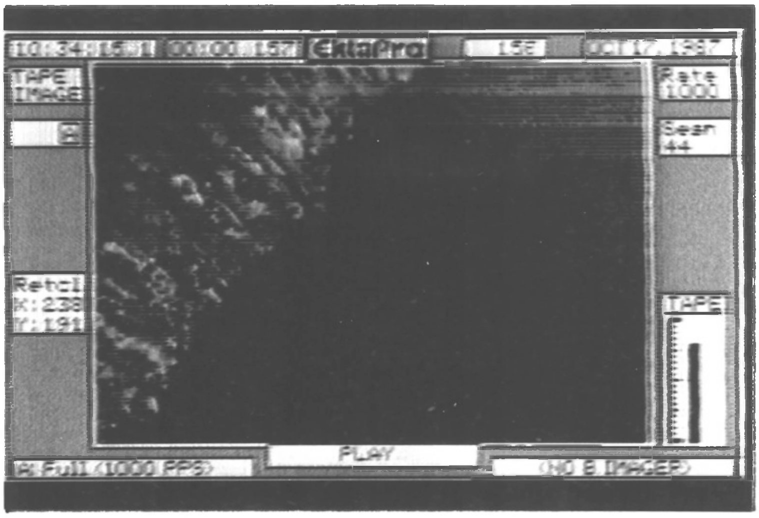

PLATE 5 24   CLOSE-UP OF PLUNGING JET OF OVERTURNING WAVE.

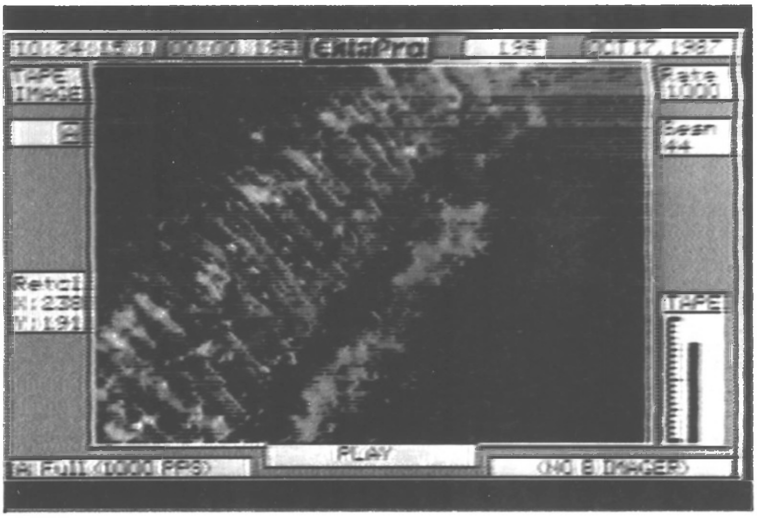

PLATE 5 25   CLOSE-UP OF PLUNGING AND SPLASH FORMATION.

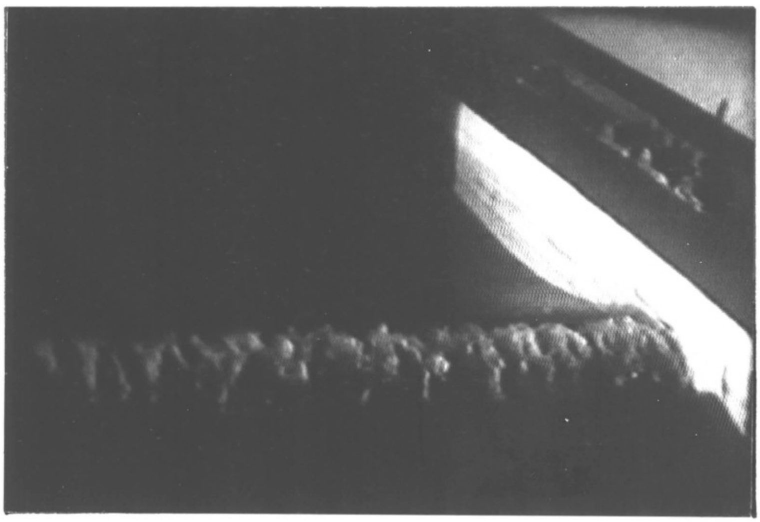

PLATE 5 26   HIGH SPEED CINE PICTURE - TRANSVERSE FORMATIONS.
SPLASH PRODUCED BY 2-D DEEP WATER BREAKING WAVE.

Evolution of a breaking wave in deep water.

Top left : Plate 5.27

Top right : Plate 5.28

Bottom left : Plate 5.29

Bottom right : Plate 5.30

Grid spacing : 20cm

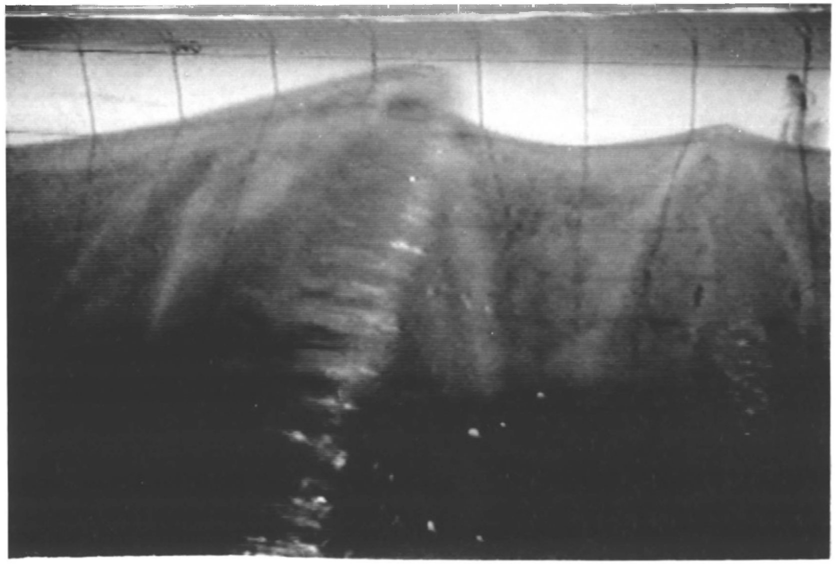
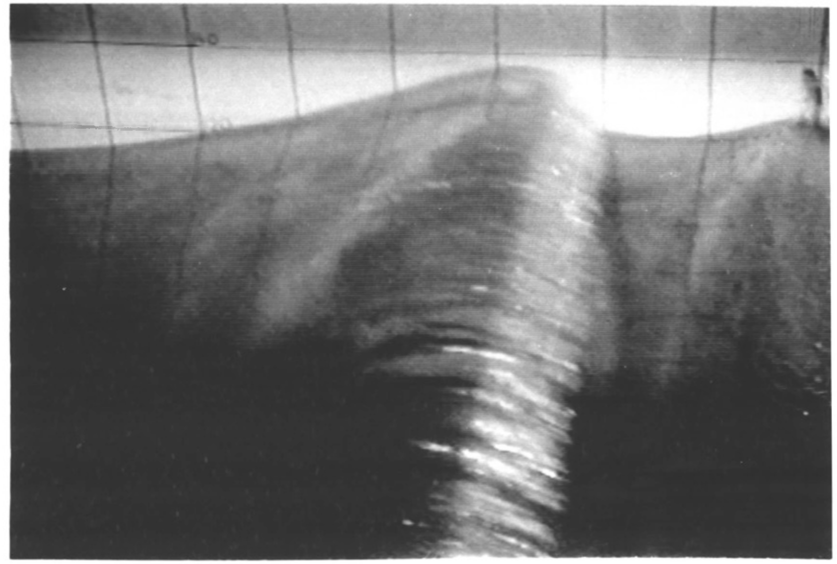
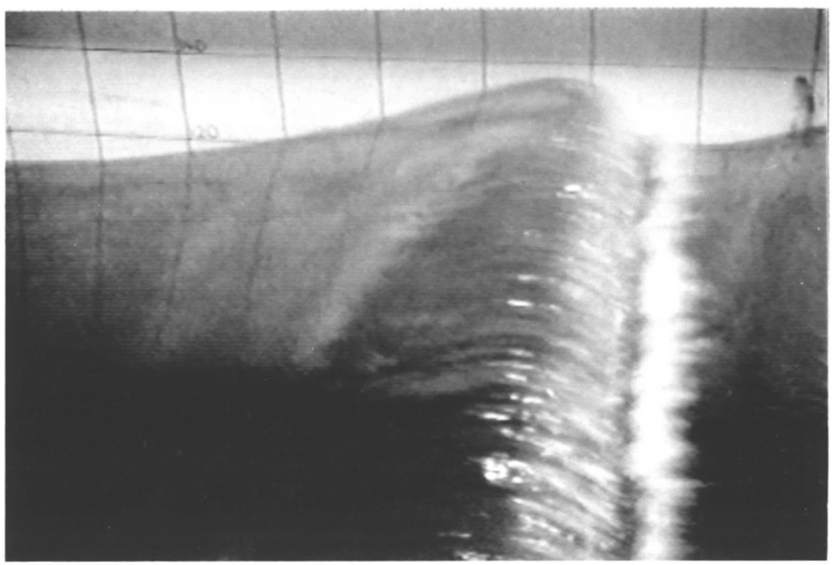
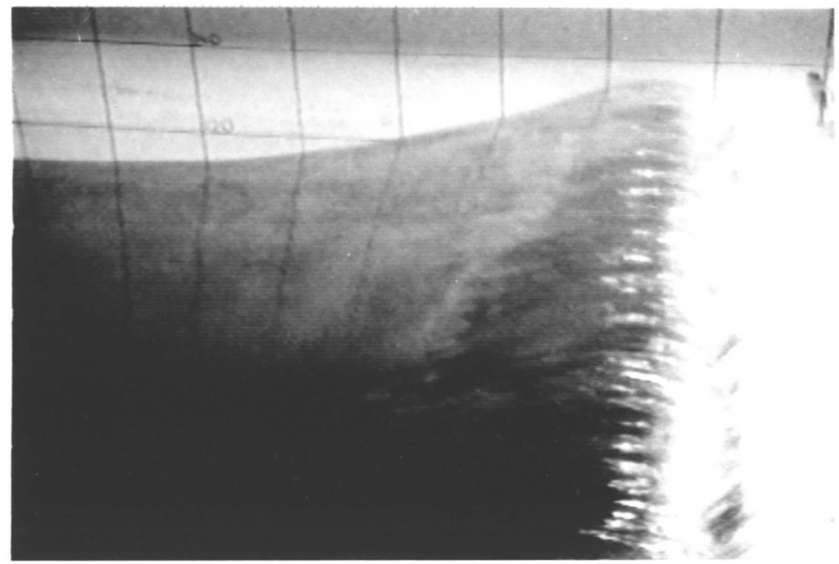

Process of wave breaking on a slope

Top left : Plate 5.31

Top right : Plate 5.32

Bottom : Plate 5.33

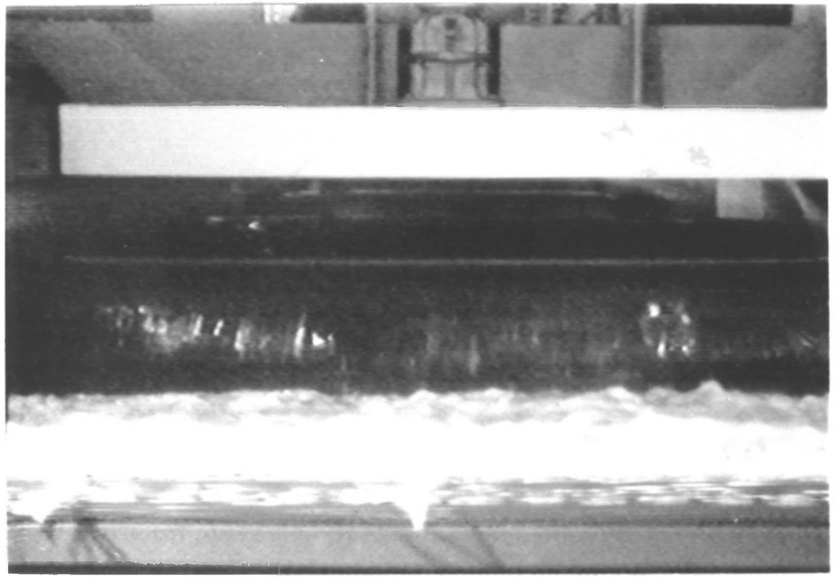

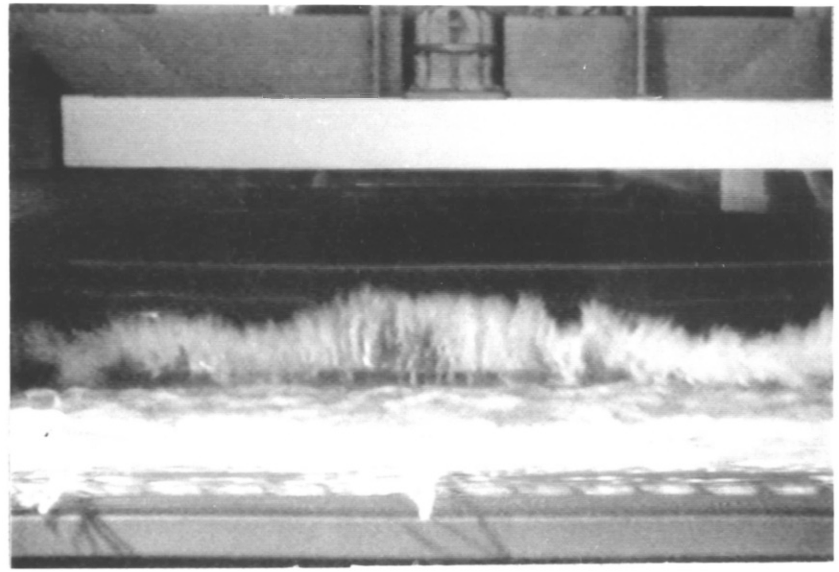

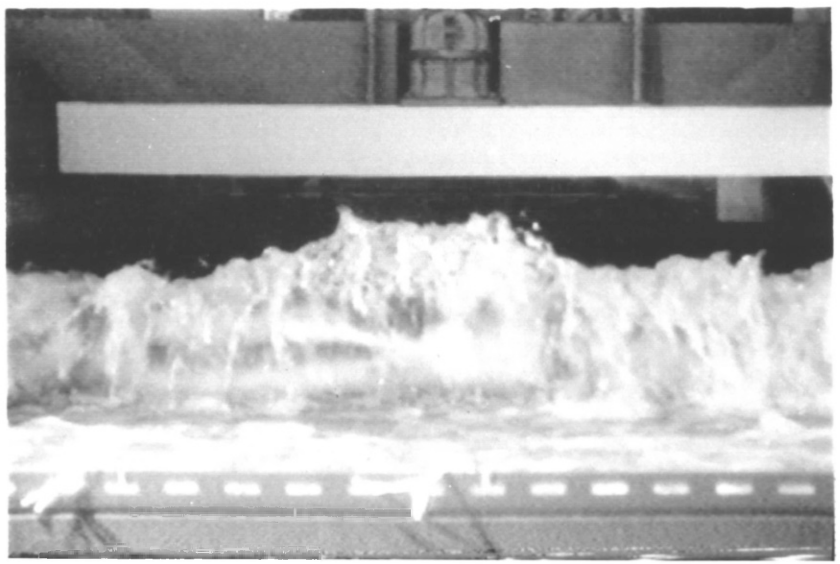

Segmentation of the overturning face

Top : Plate 5.34

Bottom : Plate 5.35

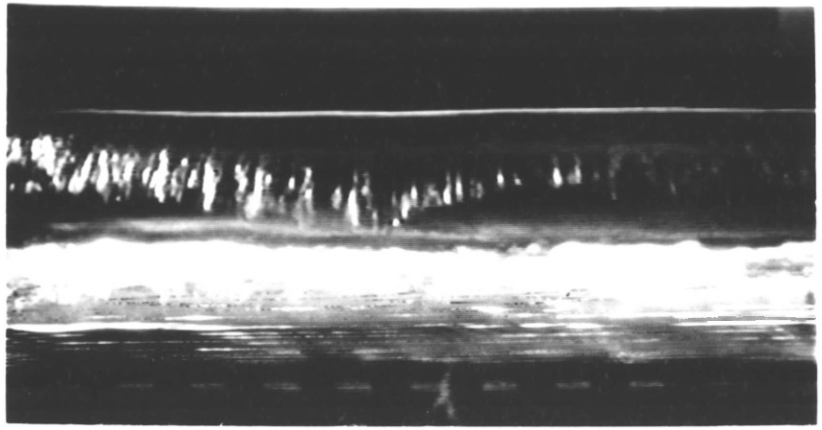

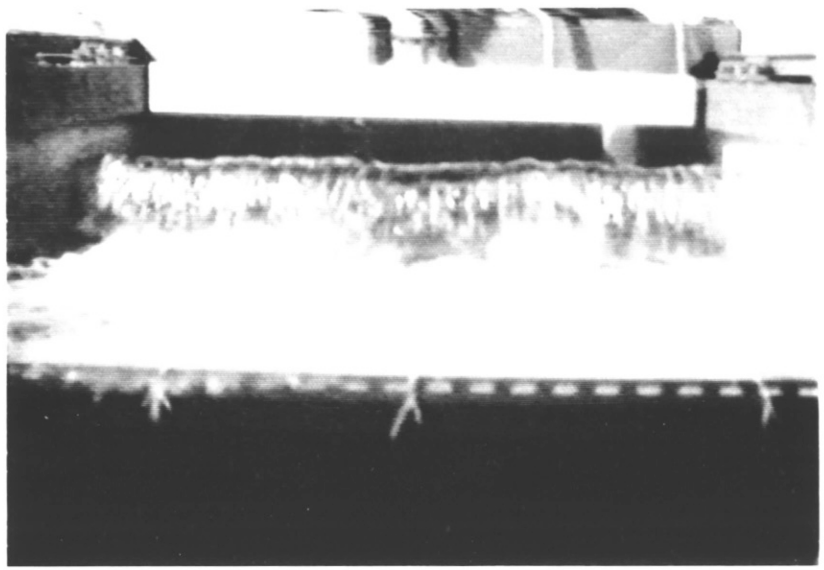

Motion after wave plunging on a slope

Top left : Plate 5.36

Top right : Plate 5.37

Bottom : Plate 5.38

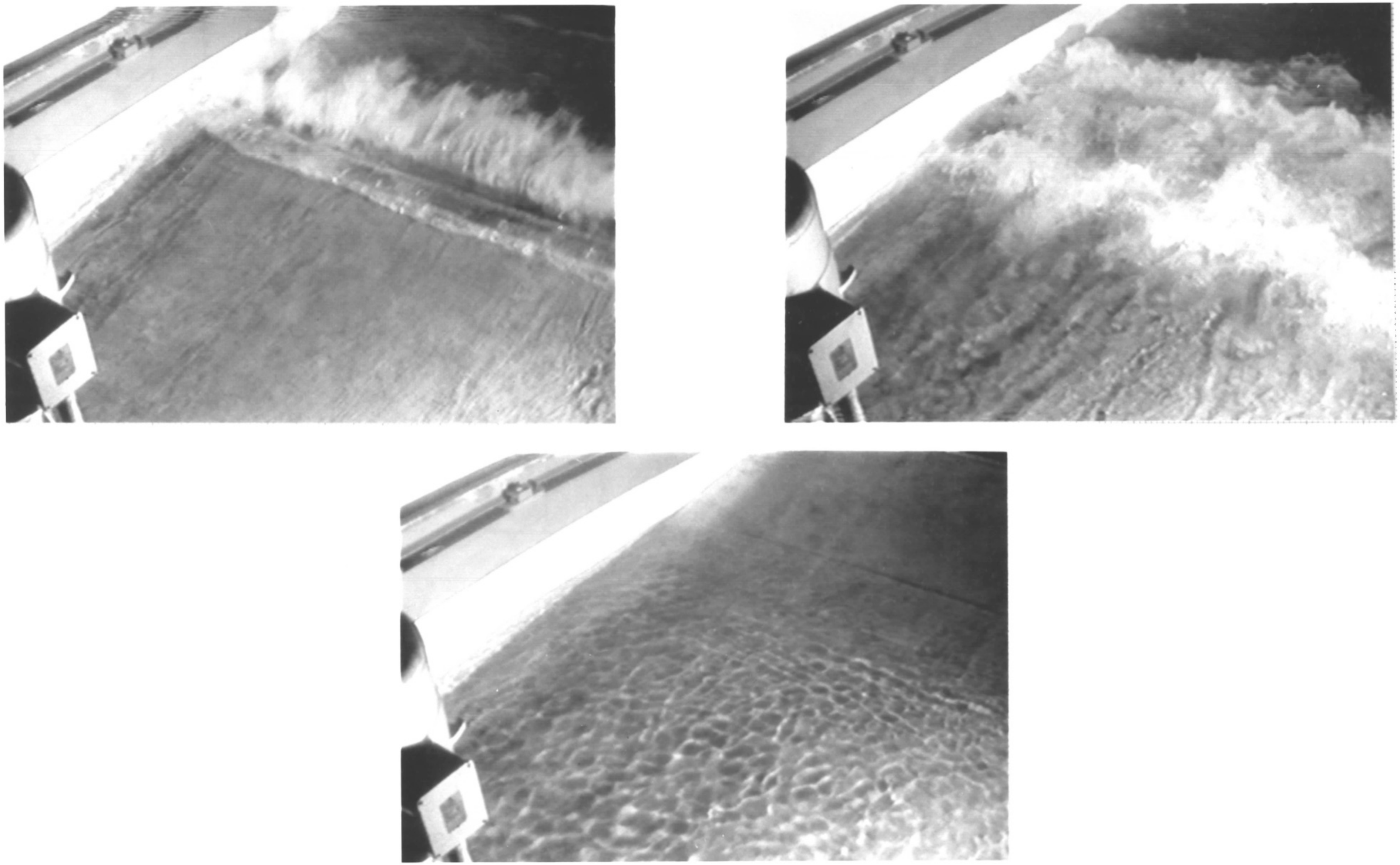

Reflections from the surface of waves emitted from the plunging area

Standing wave across the flume

Top left : Plate 5.39

Top right : Plate 5.40

Bottom : Plate 5.41

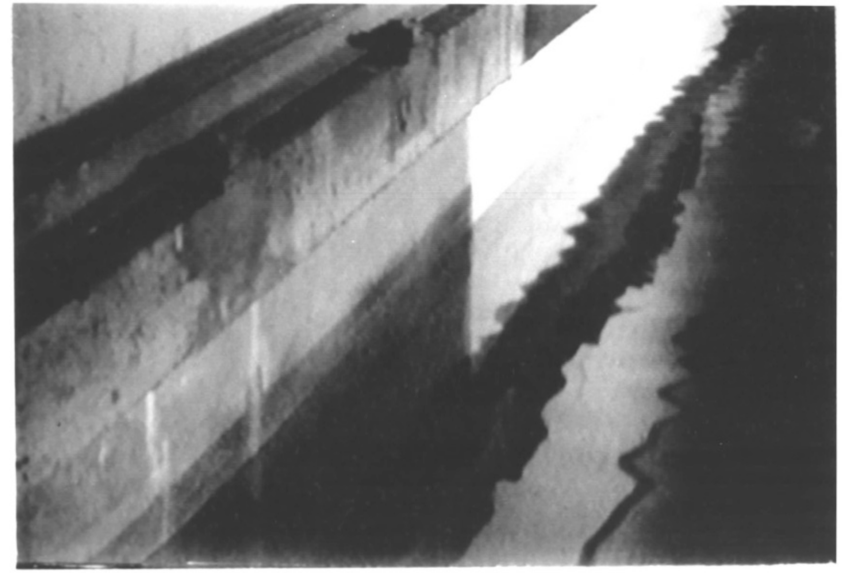

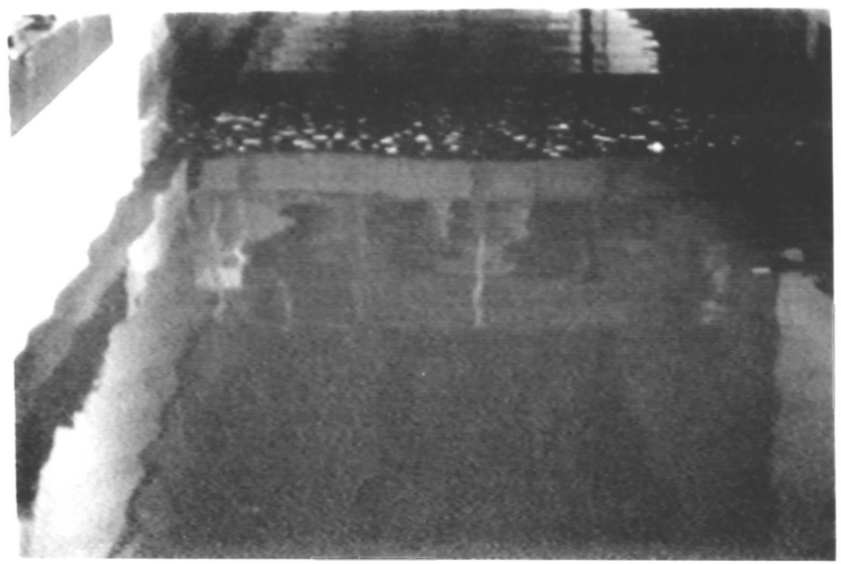

CHAPTER 6

SEGMENTATION OF THE OVERTURNING FACE OF A BREAKING WAVE

6.1 ABSTRACT

A relatively simple model, partly physical and partly analytical, is proposed. This breaking wave model is based on Worthinghton's (1908) observations and suggestion that up to a certain moment the wave presents a long, smooth, horizontal, cylindrical edge, which then segments due to **surface tension** effects. A disturbance on a cylindrical surface, withdrawn from the influence of gravity, becomes unstable when its wavelength exceeds the circumference of the cylinder (Plateau, 1863). The rate of growth of the instability, is a function of the radius of the cylinder and the wavelength of the disturbance (Lord Rayleigh, 1878). Using Longuet-Higgins (1980) theory describing the evolution of the assumed hyperbolic shape of the tip of a breaking wave, the radius of the cylindrical edge is approximated to the radius of curvature of the hyperbola. The model combines the formulations by Longuet-Higgins and Lord Rayleigh to describe the three-dimensional evolution of the curling wave crest. Scale effects are then derived which show good agreement with experimental results.

6.2 INTRODUCTION

In the absence of gravitational effects, forces arising from surface tension are very significant. A liquid in a state of free fall is considered to be static in a reference frame moving with the acceleration of gravity.

During the overturning process of a breaking wave, the plunging jet is in a state of free fall. In a frame of reference moving in the horizontal direction with velocity, U, the crest velocity, and in the vertical direction with constant acceleration, g, the gravitational acceleration, **surface tension** is the predominant force acting on the fluid particles, assuming that the wave is two-dimensional with no transverse inertial forces and air friction is negligible.

A description of the principles governing motion under capillary, or surface tension, forces is presented in section 6.3 and the mathematical modelling of surface tension effects on a liquid cylinder is described in section 6.4. The effects of inertial and gravity forces on the shape of the tip of the overturning wave crest are presented in section 6.5 and the combination of the two models is proposed in section 6.6. The results of the combined model are presented in sections 6.7, 6.8 and 6.9. The proposed model is discussed in section 6.10 and the conclusions are described in section 6.11.

6.3 PRINCIPLES GOVERNING MOTION UNDER SURFACE TENSION

6.3.1 SURFACE TENSION DEFINITION

Surface tension arises from the forces between the molecules of a liquid and the forces between the liquid molecules and those of any adjacent substance. There is, in consequence, a resulting force which opposes any increase in the area of a liquid surface. The magnitude of surface tension is defined as that of the tensile force acting across and perpendicular to a short, straight element of the line, divided by the length of that line element. Water in contact with air has a surface tension of about 0.073N/m at 20^{o}C (Massey, 1980).

A physical equivalent of surface tension can be visualised by stretching a tape upon a flat table. Whatever the tension of the tape, there is no pressure acting upon the table below. If the tape however, is stretched over a curved surface, a cylinder for instance, a downward pressure is exercised upon the cylinder. The more curved the surface, the greater is the pressure (Thompson, 1942). Mathematically, the pressure, P, varies directly as the surface tension, T, and inversely as the radius of curvature, R.

$$P = \frac{T}{R} \qquad 6.1$$

If instead of a cylinder, whose curvature lies only in one direction, a shape with curvature in two directions is considered, then the effects of these two curvatures must be added together to give the resulting pressure, P,

$$P = \frac{T}{R} + \frac{T}{R'} \qquad 6.2$$

where R and R' are the radii of curvature in any two normal directions.

6.3.2 SHAPES OF EQUILIBRIUM

Equation 6.2 is an equation of equilibrium. The resistance to compression of the fluid mass is a constant quantity, P. The pressure inwards, T(1/R+1/R'), is also constant and if the surface of the fluid is homogeneous, so that T is everywhere the same, it follows that the mean curvature, 1/R+1/R', is a constant throughout the whole surface.

Any system tends to move towards a condition of stable equilibrium, in which its potential energy is a minimum. Therefore, a quantity of a liquid will adjust its shape until its surface area is a minimum (Lamb, 1932, art.265). A surface which has the same mean curvature at all points is equivalent to a surface of minimal area for the volume enclosed. The plane and the sphere are two obvious examples for such surfaces and they are the **only** shapes of stable equilibrium.

Plateau (1863) studied the possible shapes which are symmetrical about an axis and found that there are only six such shapes which have constant mean curvature. These are the plane, the sphere, the cylinder, the catenoid, the unduloid and the nodoid (fig. 6.1). In the plane, the sphere and the cylinder the two principal

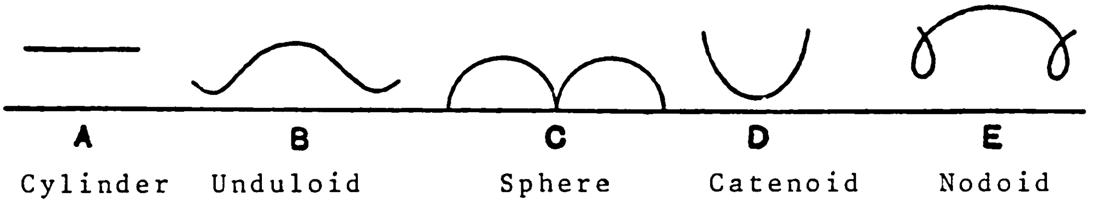

Fig. 6.1 Shapes of surfaces of revolution

curvatures are constant. In the unduloid the curvatures change from one point to another. The catenoid has its curvature in one direction equal and opposite to the curvature in the other direction. The catenoid, like the plane itself, has no curvature and exerts no pressure.

There are certain limits on the dimensions of the shapes, within which equilibrium is stable, and beyond which it breaks down. Only the plane and the sphere, or any portion of a sphere, are perfectly stable, because they are perfectly symmetrical figures. *"Perhaps it is better to say that their symmetry is such that any small disturbance will probably readjust itself and leave the plane or spherical surface as it was before, while in other configurations the chances are that a disturbance once set up will travel in one direction or another, increasing as it* *goes. For equilibrium and probability are nearly allied: so nearly that the state of a system which is most likely to occur, or more likely to endure, is precisely that which we call the state of equilibrium.*" (Thompson, 1942)

6.3.3 PHYSICAL MODELLING

Plateau (1863) devised a method by which a liquid may be withdrawn from the influence of gravity and left free to assume the figure which is produced by the interaction of its own molecules. The method used was essentially the introduction of a mass of oil into a mixture of water and alcohol, the density of which is exactly equal to that of the oil. The mass then remains suspended in the surrounding liquid and behaves as if withdrawn from gravity.

The case of the cylinder is the simplest. If a liquid cylinder is constructed and liquid is drawn out gradually, the diameter of the cylinder decreases until the length of the cylinder becomes just about three times as great as its diameter. Soon afterwards instability begins, and the cylinder alters its form; it narrows at the waist, so passing into an unduloid and the deformation progresses quickly until the cylinder breaks in two, and its halves become portions of spheres. Plateau established experimentally that the distance between the spheres is proportional to the diameter of the cylinder. In the case of a very long cylinder, when many spheres are formed, the parts between consecutive dilations or constrictions undergo identically and simultaneously the same modifications as described above (fig. 6.2).

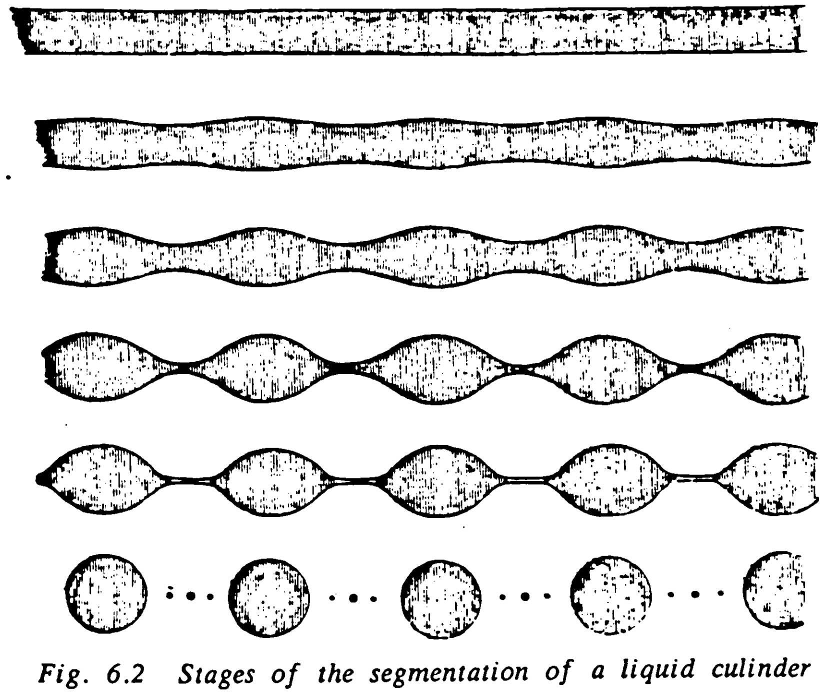

Fig. 6.2 Stages of the segmentation of a liquid culinder

"The phenomenon of the formation of lines and their resolution into spherules is not confined to the case of the rupture of the equilibrium of liquid cylinders; it is always manifested when one of the liquid masses, whatever may be its figure, is divided into partial masses. The phenomenon is also produced when liquids are submitted to the free action of gravity, although it is then less easily shown." (Plateau, 1863)

Worthington (1879) made some experiments on the spontaneous segmentation of a liquid annulus lying on a plate in order to ascertain whether the principles governing the instability of the annulus are the same as those for the cylinder. The experiments verified Plateau's hypothesis that other figures of unstable equilibrium are divided into partial equally spaced masses.

In a study on splashes (Worthington, 1908) it was found that the fall of a round pebble into water from a height first forms a dip or hollow in the surface and then causes a filmy *cup* water to rise up all round. The edge of the cup is practically like a liquid annulus and it topples into a more or less regular set of *protuberances*, the liquid being driven from the parts between the protuberances. While the cup or *crater* rises, the liquid is flowing up from below towards the rim, and the spontaneous segmentation of the rim means that channels of easier flow are created.

According to Worthington (1908), this explanation of the formation of the jets applies also to a similar phenomenon on a much larger scale. *"On a still day, on a straight, slightly shelving sandy shore, a wave that has just impetus enough to curl over and break, up to a certain moment it presents a long, smooth, horizontal, cylindrical edge, from which, at a given instant, are shot out an immense array of little jets which speedily break into foam, and at the same moment the back of the wave, hitherto smooth, is seen to be furrowed and combed. The jets are due to the segmentation of the cylindrical rim according to Plateau's law, and the ridges between the furrows mark the lines of easier flow determined by the jets."* (Worthington, 1908), (fig. 6.3)

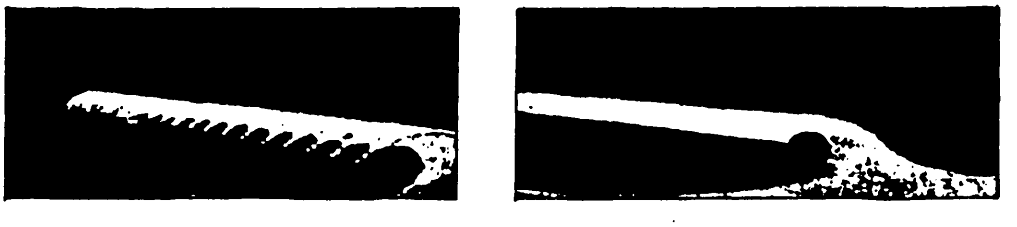

Fig. 6.3 Diagrams of a breaking wave (Worthington, 1908)

6.3.4 VISUALISATION OF SURFACE TENSION EFFECTS

High speed photography is the technique used in studies of surface tension effects. In a book called "Split second. The world of high-speed photography" (S. Dalton, 1983), a number of good quality pictures are presented, showing some interesting shapes formed due to surface tension effects.

6.3.4.1 **Raindrop in a pond**

Five pictures illustrating the physical process taking place during the impact of a single raindrop on a still water surface are shown in plates 6.1–5. The stable spherical raindrop creates an unstable thin *cup* of water which breaks up into tiny jets. From the centre of the cup, a cylindrical unstable column rises up, which breaks up into spherical drops. Small circular waves are generated due to the local disturbance on the water surface (see appendix A). The point of impact seems like a source of wave energy, emitting a succession of circular wave trains.

6.3.4.2 **Milk drop**

Some classical examples of surface tension effects are derived from the impact of milk drops on an empty saucer (plates 6.6–10). The liquid of the first milk drop spreads out radially forming cusp like shapes, in the same fashion that a drop of ink splashes on paper. The second drop however, instead of spreading radially in contact with the saucer, is forced up vertically due to inertial forces arising from the liquid of the first drop. As the hollow column rises, surface tension causes the top of the ring to disintegrate into the classical *crown* shape. As the walls collapse, thin jets of milk are formed which in turn break up into small spherical drops.

6.3.4.3 **Surface tension effects in the field**

The elegant symmetric shapes formed due to surface tension effects are usually distorted by other effects, such as air friction, gravity or collision with other objects. An illustration of such distortions is presented in plates 6.11–12. The shapes of the raindrops and the resultant formations after hitting an object, all tend towards shapes of stable equilibrium. The thin layers of liquid on the leaves tend towards forming cylindrical shapes which then break up into spherical ones. The stable spheres, under the effects of gravity and air friction change their form to flattened, elongated or other distorted spherical shapes.

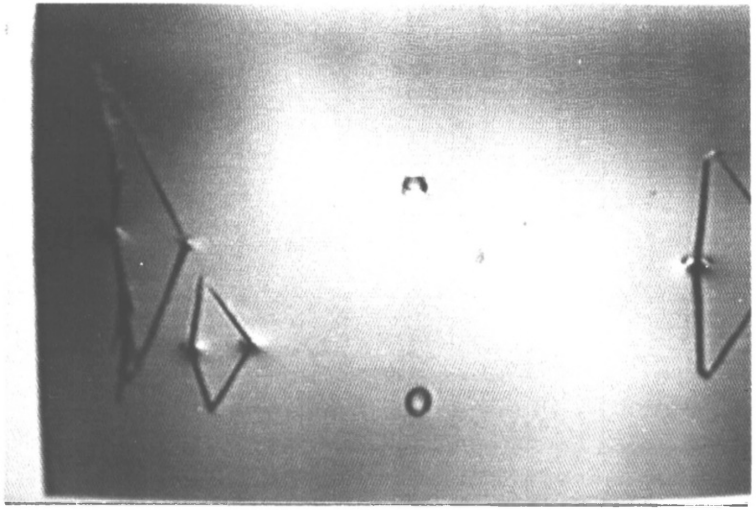

PLATE 6 1.

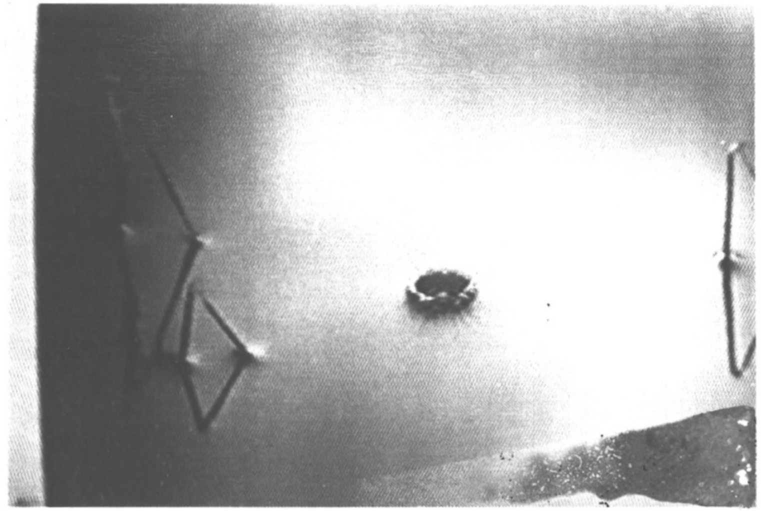

PLATE 6 2.

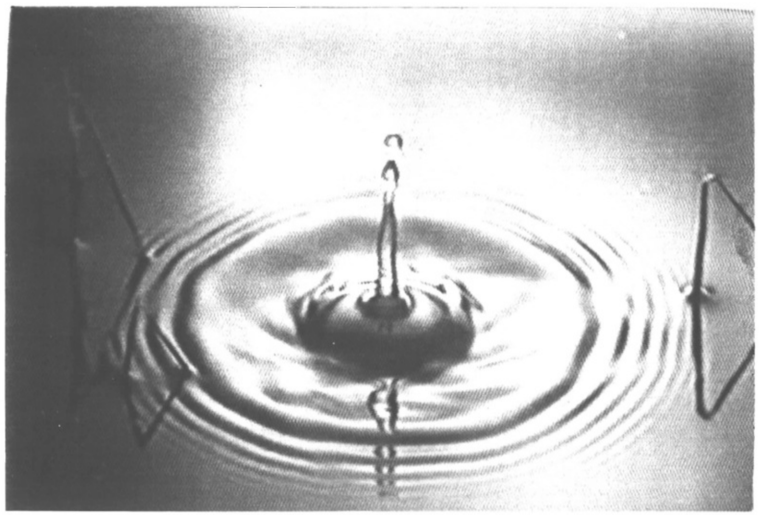

PLATE 6 3

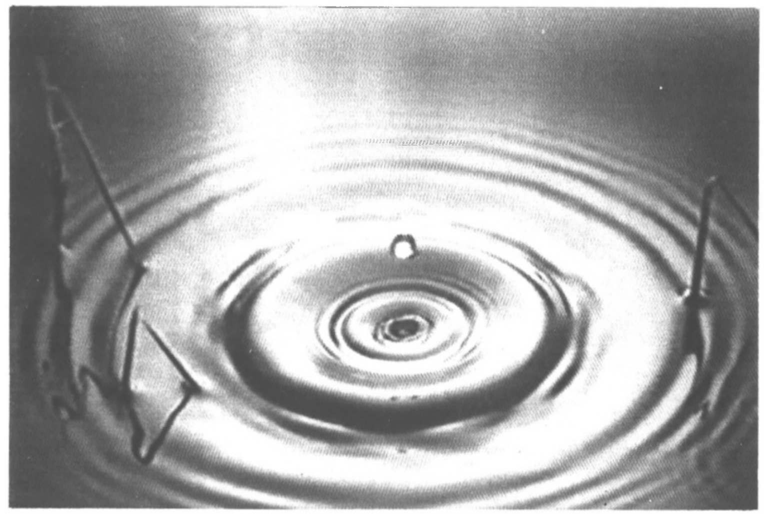

PLATE 6 4.

RAINDROP FALLING IN A POND - SURFACE TENSION EFFECTS AND FORMATION OF CIRCULAR WAVES.

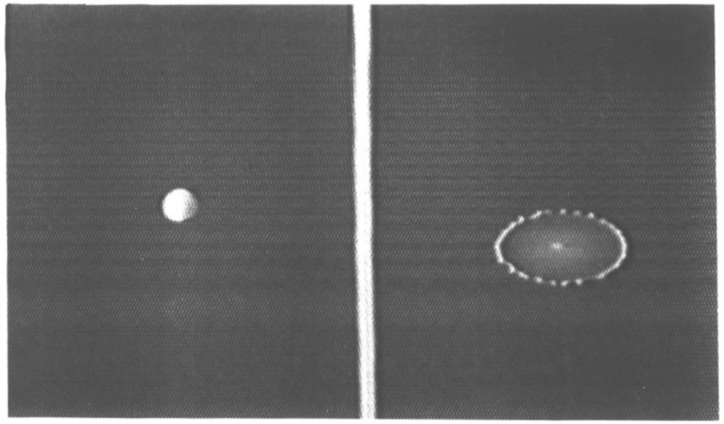

PLATE 6 5 MILK DROP HITTING AN EMPTY SAUCER.

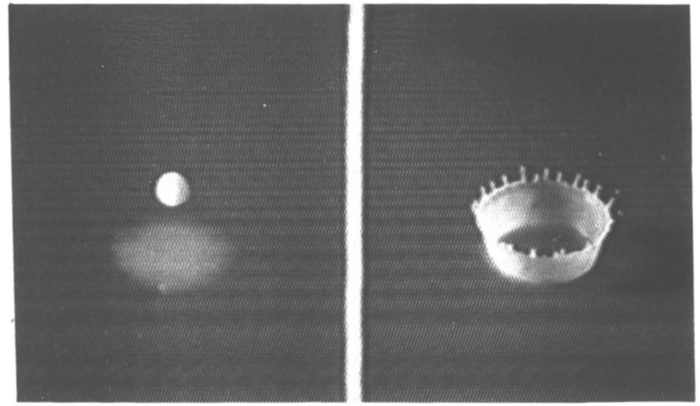

PLATE 6 6 MILK DROP FALLING ON TOP OF PREVIOUS MILK DROP.

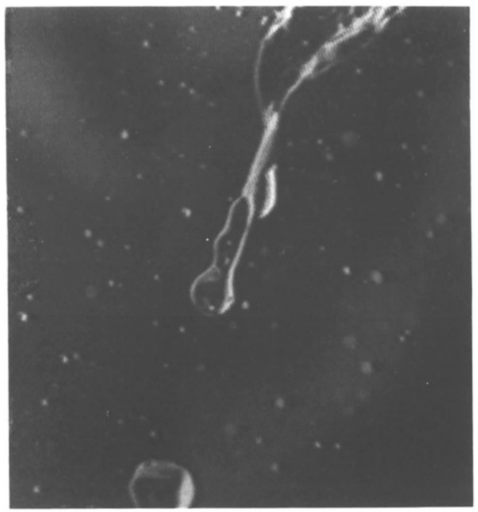

PLATE 6 7

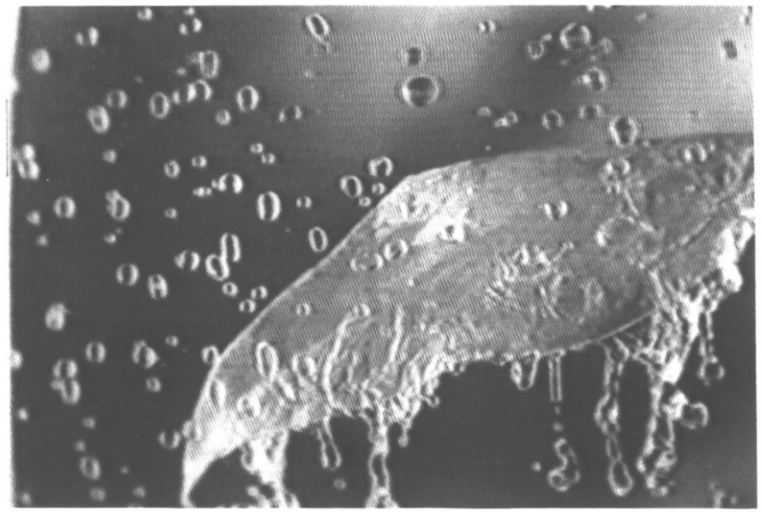

PLATE 6 8.

DISTORTION OF SURFACE TENSION EFFECTS.

6.4 MATHEMATICAL MODELLING

Any small disturbance on a liquid cylinder may be considered, according to Fourier's theorem, as the summation of a series of sinusoidal wave disturbances. The surface area of the cylinder will change whereas the volume of the liquid remains the same. As surface tension results in contracting the volume to the minimum possible surface area, an **increase** of the surface area due to the disturbance will be **opposed** by surface tension, whereas a **contraction** of the surface will be **enhanced**. The criterion for stability is therefore the change of surface area for a given volume after the appearance of a small disturbance.

If a cylinder with radius r is slightly deformed so that

$$y = r + a \cos \frac{2\pi}{L} x \qquad 6.3$$

where x is measured parallel to the axis,
y is the distance normal to the axis,
a is the amplitude of the deformation, and
L is the wavelength of the deformation,

Plateau showed that the cylinder is stable if

$$L < 2 \pi r \qquad 6.4$$

The theory is hereby extended to consider a **sector** of a liquid cylinder with a slight sinusoidal deformation.

$$y = r + a \cos(kx) \quad , \text{ where } k=2\pi/L \qquad 6.5$$

The mean surface area between two consecutive crests, σ, is then

$$\sigma = r\,\theta + \frac{1}{2} r\,\theta\, a^2\, k^2 \qquad 6.6$$

where θ is the angle between the radii of the sector.

Assuming the volume of water in the cylindrical sector remains the same, the mean volume S is

$$S = \frac{1}{2}\,\theta\, r^2 + \frac{1}{4}\,\theta\, a^2 \qquad 6.7$$

Combining the two expressions for σ and S together,

$$\sigma = \sqrt{2\ \theta\ S} + \frac{\theta}{4}\frac{a^2}{r}(\ k^2\ r^2\ -\ 1\ ) \qquad 6.8$$

The surface area of the undisturbed liquid (a=0) is,

$$\sigma_0 = \sqrt{2\ \theta\ S} \qquad 6.9$$

Therefore, the change in the surface area is,

$$\sigma - \sigma_0 = \frac{\theta\ a^2}{4\ r}(\ k^2\ r^2\ -\ 1) \qquad 6.10$$

If k.r > 1 the surface area increases and hence the liquid is stable. Since $k=2\pi/L$,

$$L < 2\ \pi\ r \quad \rightarrow \quad \text{Stability} \qquad 6.11$$

$$L > 2\ \pi\ r \quad \rightarrow \quad \text{Instability} \qquad 6.12$$

The obtained result is independent of the angle θ. The cylinder is a special case of the considered case, with $\theta=2\pi$. Plateau (1864) and Rayleigh (1878) reached the same result by considering the cylindrical shape as the initial condition.

The mode of falling away from unstable equilibrium necessarily depends on the small deformations to which the system is subjected. In an ideal situation of no deformations, even if $L>2\pi r$ the cylinder would still be in equilibrium. In practice however, some kinds of disturbances are always present. Although all disturbances corresponding to $L>2\pi r$ are unstable, the rate of change of the shape due to each wavelength, L is different.

Assuming that the amplitude of the disturbance, a, once unstable, grows exponentially with time,

$$a = a_0\ e^{qt} \qquad 6.13$$

where a_0 is the initial amplitude. Lord Rayleigh (1878) showed that for a cylindrical surface,

$$q^2 \approx \frac{T}{\rho r^3}\left[\ x^2 - \frac{9}{8}\ x^4 + \frac{7}{2^4 \cdot 3}\ x^6 - \frac{25}{2^{10}}\ x^8 + \frac{91}{2^{11} \cdot 3 \cdot 5}\ x^{10}\ \right] \qquad 6.14$$

where $x=kr=2\pi r/L$.

Figure 6.4 shows the variation of $q\ r^{3/2}$ against $2\pi r/L$. For given r, all

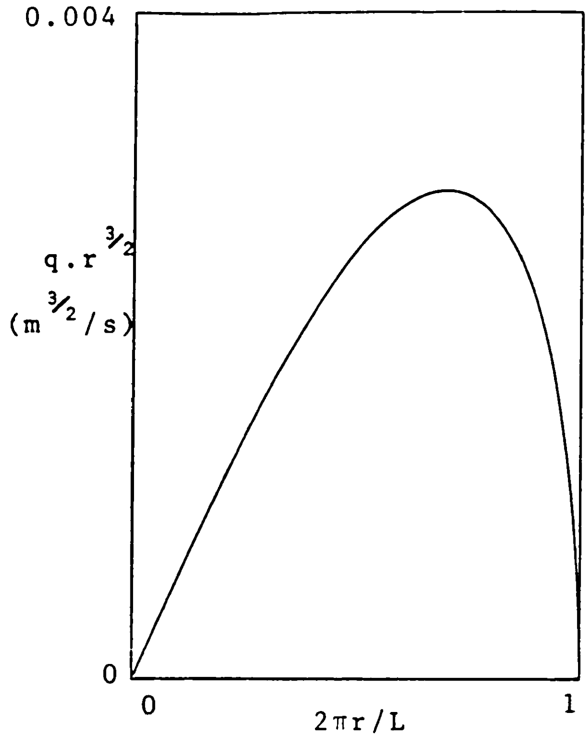

Fig. 6.4 Plot of $q^2\ r^{3/2}$ against $2\pi r/L$.

disturbances with wavelength, L, less than $2\pi r$ ($2\pi r/L>1$) are stable. For L greater than $2\pi r$ the disturbances grow with time, the fastest growing one having $L\approx 9r$.

6.5 GRAVITY AND INERTIAL EFFECTS ON THE TIP OF THE BREAKER

The mathematical description of the free surface area of a two-dimensional overturning wave, as governed by inertial and gravitational forces, is presented by Longuet-Higgins (1980). A frame of reference is used in which the x-axis is longitudinal horizontal, in the same direction as the propagation of the wave, the y-axis is transverse horizontal and the z-axis is vertical. The saddle-point, the point where the pressure gradient vanishes (see section 2.4.4), follows a free fall trajectory. Its motion therefore satisfies

$$x = x_1 + U\ (t-t_1) \qquad 6.15$$

and

$$z = z_1 - 1/2\ g\ (t-t_1)^2 \qquad 6.16$$

where x_1, z_1, t_1 and U define the initial coordinates, time and horizontal velocity respectively.

The tip of the wave is approximated by the hyperbola, (fig. 6.5)

$$\frac{x^2}{\alpha^2} - \frac{y^2}{\beta^2} = 1 \qquad 6.17$$

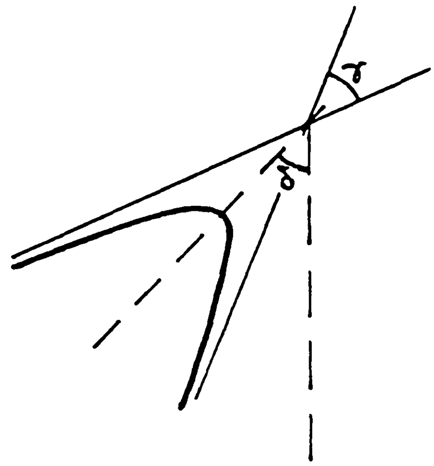

Fig. 6.5 Hyperbola approximatig the tip of the wave.

which has the following properties,

$$\tan\frac{\gamma}{2} = \frac{\beta}{\alpha} \qquad 6.18$$

$$r = \left|-\frac{\beta^2}{\alpha}\right| \qquad 6.19$$

where γ is the angle between the asymptotes of the hyperbola and
r is the radius of curvature at the tip of the breaker.

Since $\alpha\beta$=constant,c (Longuet-Higgins, 1980, eqn. 9.1) the initial radius of curvature, r_0, when $\gamma=90^{\circ}$ is

$$r_0 = \beta_0 = \alpha_0 \qquad 6.20$$

Therefore,

$$\text{constant},c = r_0^{\,2} \qquad 6.21$$

and

$$\alpha = \frac{r_0}{(\tan\gamma/2)^{1/2}} \quad \text{and} \quad \beta = r_0\,(\tan\gamma/2)^{1/2} \qquad 6.22$$

Given the initial conditions, the two-dimensional evolution of the crest of the wave is completely described, using figures 2.9 and 2.10.

6.6 DESCRIPTION OF THE PROPOSED MODEL

Worthinghton's proposition (1908) is adopted as the fundamental assumption on which the presented model is based. That is, the crest of the overturning wave presents a long, smooth, horizontal, cylindrical edge.

The horizontal cylindrical edge, in the state of free fall, is modified in a manner governed by surface tension principles. The radius of the cylindrical edge is assumed to be independent of the these modifications and only governed by inertial and gravitational forces. The formulations derived by Longuet-Higgins (1980) are therefore applicable in this problem. The radius of the cylindrical edge (Worthinghton) is equated to the radius of curvature of the hyperbolic edge of the wave (Longuet-Higgins). The proposed model is therefore a combination of two distinct analytical descriptions, namely of inertial/ gravitational and surface tension effects.

However perfectly smooth the crest of a wave might look, some imperfections are always inevitable. These irregularities on the wave crest may be described mathematically by employing Fourier's theorem. That is, the profile of the surface may be obtained by the summation of a number of sinusoidal profiles with different wavelengths, amplitudes and phases. The effect of the irregularities is then the summation of the effects of the individual sinusoidal disturbances that constitute the original disturbance.

By adopting the above procedure, the problem is studied by considering the evolution of only monochromatic sinusoidal disturbances on the tip of an overturning wave.

Consider a small sinusoidal disturbance of amplitude a_0, and wavelength L, on a liquid cylindrical edge. Surface tension considerations suggest that the amplitude of the disturbance will start growing when the wavelength, L, exceeds $2\pi r$, with an exponential rate of growth, $a_t=a_0 \exp(qt)$ (as equation 6.13). The value of q is obtained from equation 6.14. For a cylindrical edge with a continuously varying radius, r, it is more appropriate to rearrange equation 6.13 so that,

$$a_{t+\delta t} = a_t \exp(q\ \delta t) \qquad 6.23$$

The radius of the cylindrical edge, which is assumed as being equal to the radius of curvature of the hyperbola used in Longuet-Higgins's derivations, may be estimated at any time using equation 6.19. Given the initial conditions of the

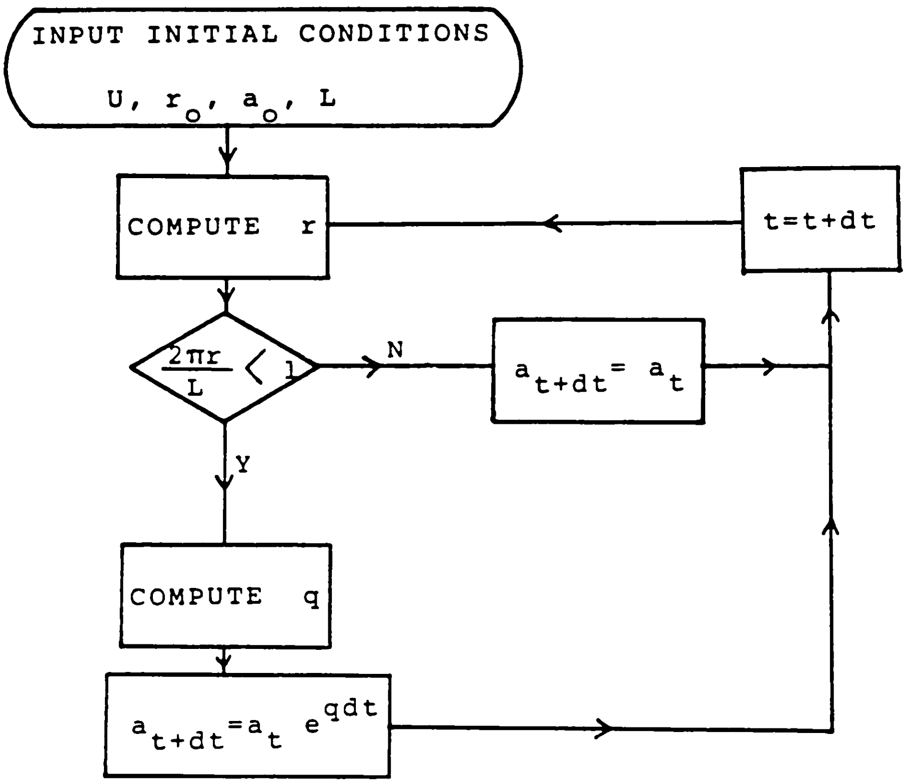

Fig. 6.6 Flow chart of computational model.

overturning wave, that is the conditions at breaking point, the evolution of the breaker shape is computed. The above procedure is followed in a numerical model, the flow chart of which is shown in figure 6.6. Some further points regarding the development of the model are clarified in the following paragraph.

At time t=0, the angle $\delta=45^0$ and $\gamma=90^0$. At t=infinity, the angle would be 180^0, or $\delta_\infty-\delta_0=135^0$. This total angle of rotation of the axis of the hyperbola corresponds to $\omega\approx0.27$. Given the horizontal velocity of the crest U, which is assumed constant throughout the overturning stage, the value of $\lambda=U/g$ is obtained. Longuet-Higgins (1980) formulations describe the variation of the angles δ and γ in terms of t/λ. For any time t, the values of δ and γ are thus obtained. These values together with the coordinates of the point of intersection of the axes of the hyperbola, which are determined from equations 6.15 and 6.16 describe completely the evolution of the tip of the breaker in the two- dimensional plane of the wave. The radius of curvature of the tip of the breaker is equal to

$$r = \left| -\frac{\beta^2}{\alpha} \right| = r_0 \tan^{3/2}(\gamma/2) \qquad 6.24$$

Assuming that the rate of increase of the amplitude of a disturbance on the tip of the breaker is the same as that for a cylinder, as derived by Rayleigh (1878), the amplitude of a disturbance of wavelength L is then obtained using equations 6.23 and 6.14.

6.7 RESULTS FROM THE PROPOSED MODEL

Figure 6.7 shows the time dependent characteristics of six distinct sinusoids with the same initial amplitude. From this figure it can be seen that, as the radius of curvature of the curling wave crest decreases with time, the long disturbances start growing first. The rate of growth of the amplitude decreases with increasing wavelength of the disturbance (eqn. 6.14). A long wavelength starts growing early and slowly, whereas a short wavelength starts growing late and rapidly. There is consequently a particular wavelength which attains the maximum amplitude at the instant of hitting the water surface. This **predominant wavelength** is therefore a function of the type and size of the breaker (initial radius of curvature, breaker height and horizontal velocity) and the form of the initial disturbance.

Quantitative results regarding the predominant wavelength as well as scale effects on the segmentation process may be derived for given initial conditions.

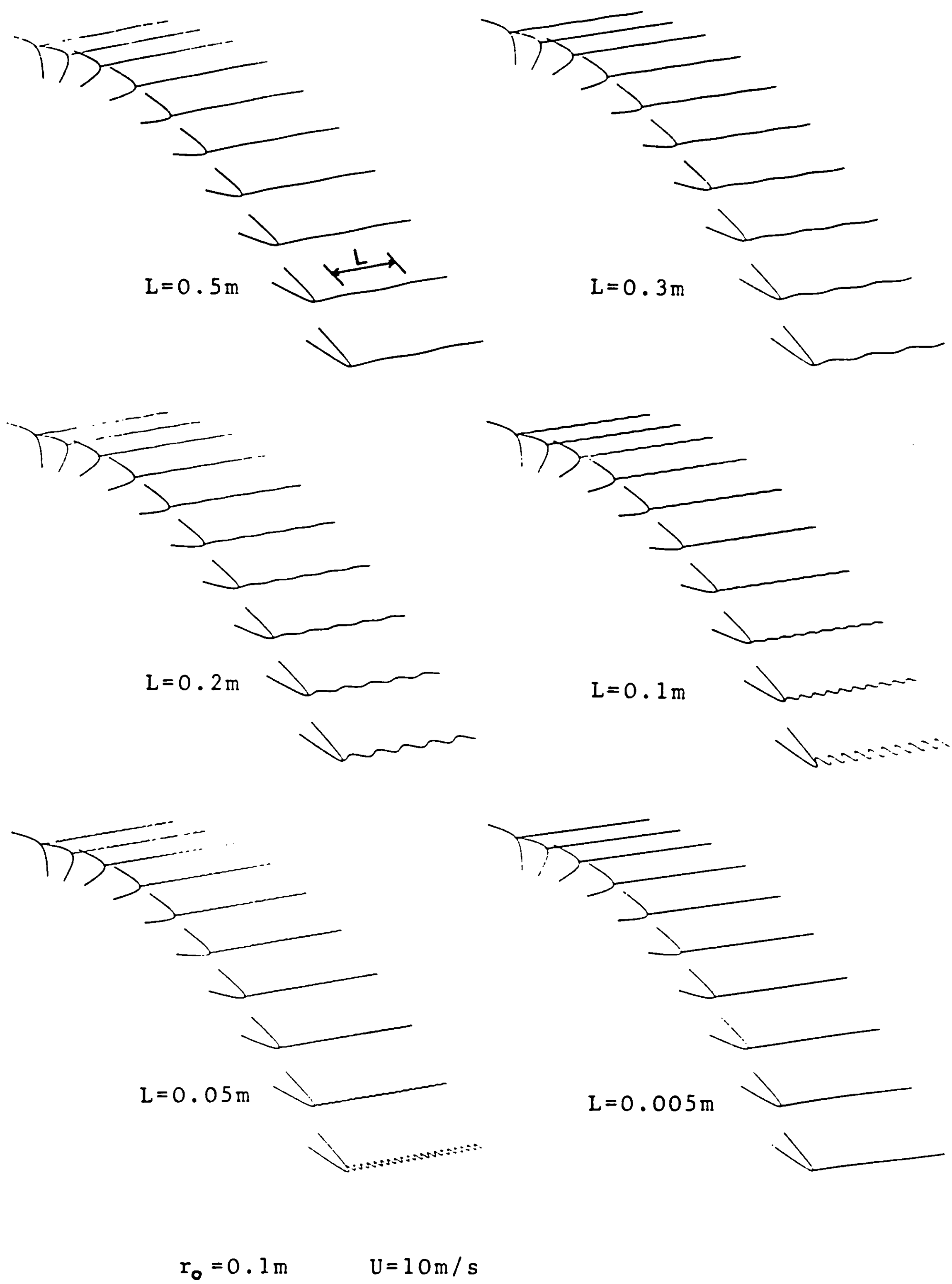

Fig. 6.7 Evolution of six sinusoids, of different wavelength, on the tip of an overturning wave

6.7.1 APPROACH TO THE PROBLEM

Consider a wave breaking in shallow water (fig. 6.8). The wavelength, according to linear theory is

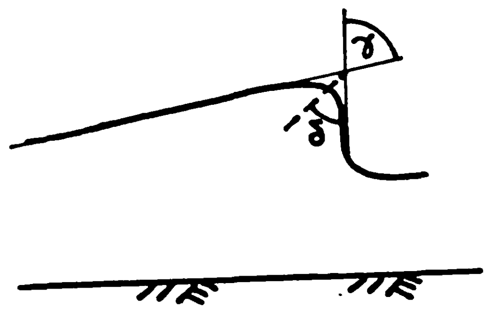

Fig. 6.8 Breaking wave in shallow water depth.

$$L \sim T\sqrt{gh}$$

and $H_b \sim h$

where

$\sim$ means order of,

T is the wave period,

h is the water depth at breaking point

H_b is the breaker height.

In order to determine the angle γ when the forward face of the wave becomes vertical, the assumption is made that the backward face of the wave is straight such that,

$$\tan\gamma \approx \frac{L_b}{H_b} = \frac{T\sqrt{gH_b}}{H_b} = T\sqrt{\frac{g}{H_b}}$$

The initial conditions are therefore

$$\gamma_0 \approx \tan^{-1}\left(T\sqrt{g/H_b}\right)$$
$$\delta_0 \approx 1/2\ \gamma_0$$

The duration of overturning is equal to the time required for a free fall from height H_b

$$t_b \approx \sqrt{2H_b/g}$$

In the absence of a description -theoretical or experimental- of the nature of the disturbances on the wave crest, it is assumed that all wavelengths are present and they all have the same amplitude, the equivalent of *white noise*.

In summary the following assumptions are made in order to derive quantitaitve results from the proposed model:

a) At breaking point, t=0 and forward face is vertical, $\tan\gamma_0 = T\sqrt{g/H_b}$

b) The angle $\delta_0 = 1/2\ \gamma_0$

c) The duration of overturning, $t_b = \sqrt{2H_b/g}$

d) The disturbance has white noise characteristics

6.7.2 NUMERICAL SCHEME

For a given breaking wave height, H_b, and wave period, T, the evolution of a transverse sinusoidal disturbance on the wave crest, with wavelength L, and amplitude a_0, is traced up to plunging point. The ratio of the amplitude of the disturbance at plunging point, a_p, to the initial amplitude, a_0, i.e. a_p/a_0, is a measure of the surface tension effect on the wave breaking process for the assumed wavelength of initial disturbance.

When the above procedure is followed for a range of wavelengths, L, the maximum value of a_p/a_0, corresponding to the predominant wavelength, is deduced. Any given breaker is therefore associated with a predominant wavelength, L_{pred}, of disturbance whose amplitude at plunging point is amplified by the factor a_p/a_0. A numerical scheme was developed which produces these results for any given breaker characteristics. That is, given H_b and T, it computes the predominant wavelength and the corresponding a_p/a_0.

Field and laboratory data were used as input data in the proposed model. These data were taken from a study by Takeda and Sunamura (1983). In addition to these data, four more pairs of data were input in order to consider small values of H_b. These extra data have the same period, 1sec, with breaker height 0.02, 0.03, 0.04 and 0.05m The variations of L_{pred} and a_p/a_0, as derived from the model, with breaker height, H_b, are shown in figures 6.9 and 6.10 respectively. The interpretation of these plots is discussed in the following sections.

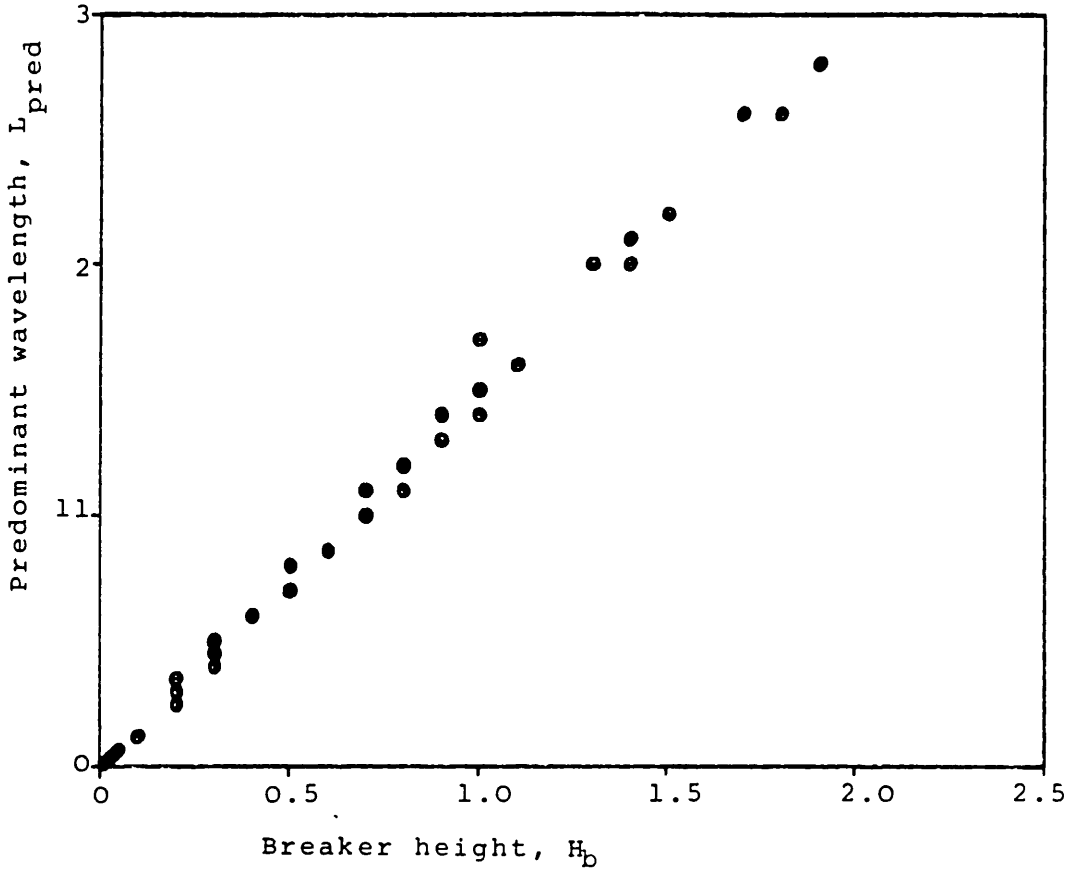

Fig. 6.9 Model results. Wavelength of predominant disturbance, against breaker height.

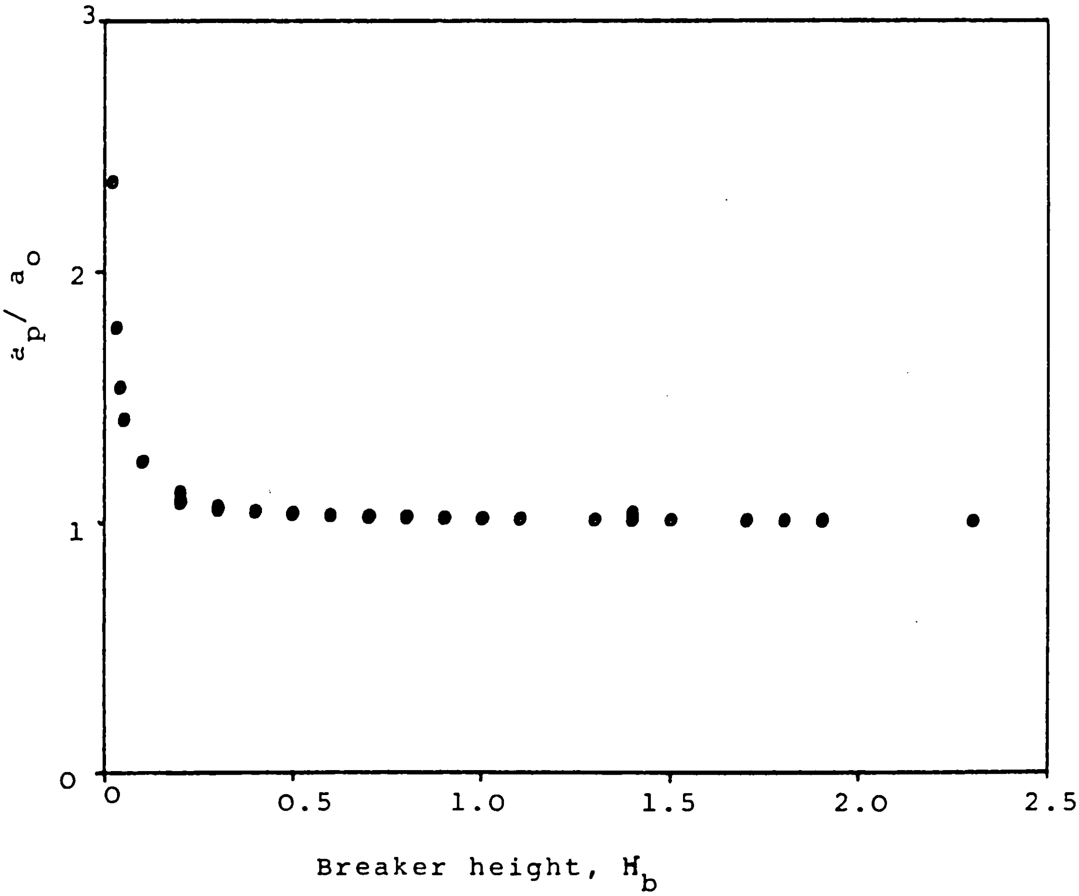

Fig. 6.10 Model results. Relative growth of predominant disturbance, against breaker height.

6.7.3 PREDOMINANT WAVELENGTH

Short wavelengths are in general associated with small breaker heights and small radii of curvature at the tip of the breaker. The duration of overturning is short. Sinusoidal disturbances of long wavelengths although unstable, grow very slowly and the short duration of overturning does not allow them to become dominant. The smaller the breaker, the shorter the predominant wavelength.

On the other hand, big breakers have large radii of curvature even at plunging point. Disturbances of short wavelengths do not become unstable. As a result, the bigger the breaker, the longer the predominant disturbance.

The variation of breaker height with the wavelength of the predominant disturbance, fig. 6.9, shows that $L_{pred} \approx 1.3H_b$.

6.8 DERIVATION OF SCALE EFFECTS FROM THE PROPOSED MODEL

6.8.1 INTRODUCTION

In modelling surface non breaking water waves, the predominant forces which are scaled are the gravitational ones. This scaling is performed using Froude scaling criteria, according to which, the ratio of the inertial to the gravitational forces is the same under both prototype and model conditions. In other words, the Froude number,

$$F_r = \frac{u}{\sqrt{lg}} \qquad 6.24$$

is the same in both conditions, where u is a velocity scale, l is a length scale and g the gravitational acceleration.

In breaking waves, apart from the gravitational and inertial effects, surface tension plays a significant role as well. In scaling surface tension effects the ratio of the inertial to the surface tension forces must be the same. The Weber number

$$W_e = u \sqrt{(l\rho/T)} \qquad 6.25$$

must be the same in both prototype and model conditions, where ρ and T are the density and surface tension of the fluid, u and l are velocity and length scales respectively.

It is evident that the Froude and Weber criteria cannot be satisfied simultaneously. In model tests involving breaking waves, Froude scaling is the adopted criterion, as it models satisfactorily the overall conditions, such as wave reflection, although the breaking wave process is not fully modelled. It is of vital importance, in the interpretation of the model test results, to know how the non–scaling of surface tension effects affects the prototype conditions.

6.8.2 NUMERICAL MODEL PREDICTIONS

The proposed physical/computational model can be used in assessing the scale effects in breaking waves, as this model takes into consideration both gravitational and surface tension effects. The non–dimensional ratio, a_p/a_0, reflects the effects of scaling. A constant value for this ratio implies that the shape of the breaker does not change between large and small scale cases. This variation is plotted in figure 6.10.

It is evident from this plot that, surface tension effects are the same for breaking waves bigger than about 0.5m in height, whilst they become increasingly important for smaller waves. This observation suggests that, assuming the curling face of the wave retains a hyperbolic shape, big waves, which have small curvatures, do not *feel* the surface tension forces. This is in agreement with the broad characteristics of surface tension; surface tension is a molecular effect which becomes important for high curvatures.

As a conclusion from the numerical scheme, it may be said that, **waves bigger than about 0.5m high are not sensitive to surface tension,** provided the shape of their crest remains hyperbolic. **No scale effects,** due to surface tension, are therefore expected for such waves.

6.8.3 STATE OF THE ART ON SCALE EFFECTS IN OVERTURNING WAVES

Scale effects in breaking waves have been reported in the literature. Fuhrboter (1986) studied impact loading by breaking waves on slopes and found that scale effects do exist.

Skladnev and Popov (1969) measured impact pressures induced by waves breaking on a slope in a more systematic way. Waves of the same steepness but of wave height ranging between 3 and 120 cm were tested. Prototype conditions were

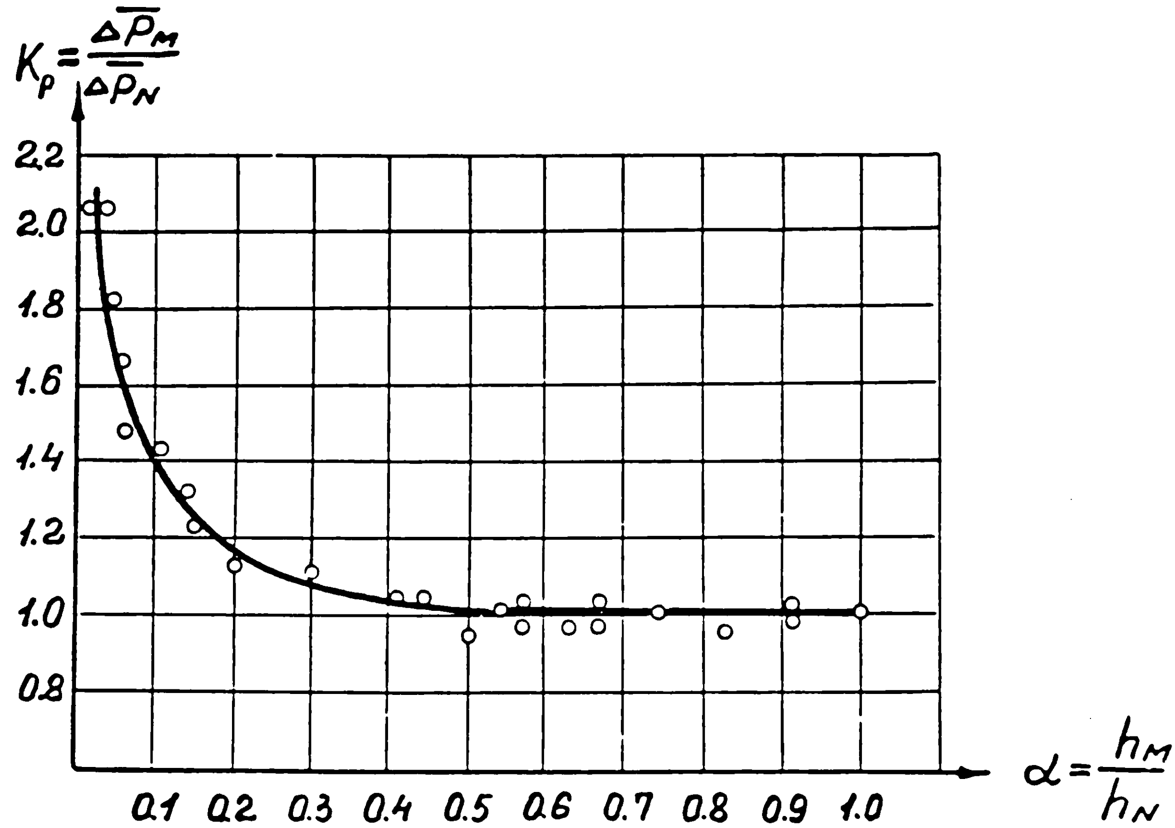

Fig. 6.11 Effects of wave height on the relative wave pressure value in the wave impact zone. (Skladnev and Popov, 1969)

considered the ones with the 120 cm wave height. The results were presented in graphical form (fig. 6.11). The abscissa is the ratio of the model to the prototype (120cm) wave heights and the ordinate is the ratio of the model to the prototype impact pressure factor K_p, defined as the ratio of the measured pressure to the static pressure ρgh, where h is the wave height. From these results it is evident that, it is not permissible to use Froude criteria to scale up experimental results on breaking waves with model breaker height less than about 0.5m.

Stive (1984) reached the same conclusion, stating that "*in order to avoid disturbing influence of the surface tension on the amount of air absorption in the broken wave, the incident wave height in the model must exceed approximately 0.5m*".

In summary, it may be said that, experimental results suggest that scale effects are significant for breaking waves with wave height less than about 0.5m.

6.8.4 COMPARISON BETWEEN THEORETICAL AND EXPERIMENTAL RESULTS

The presented model is in agreement with the experimental results, in that, scale effects do exist for breaking waves smaller than 0.5m high. The two sets of results, however, appear to disagree on the sense of the difference in scaling; the proposed model predicts no segmentation of the tip of the wave for big waves, whilst the experimental results suggest that big waves are highly aerated and sprayed, whilst in small waves aeration is negligible or does not occur at all (Skladnev and Popov, 1969). This apparent contradiction may be justified by looking at the overturning process from two distinct angles: the *macro* and *microscopic* angles.

The description of the tip of the overturning wave as a hyperbolic shape, or as part of a circular one, is a macroscopic approach. When looked in more detail, from a microscopic angle, the tip of the breaker has irregularities in not only the transverse direction but in the longitudinal- vertical, x-z, plane, as well. In small waves these irregularities will tend to smooth out and disappear, as surface tension forces are strong. In bigger waves however, the tip of the wave is not smooth, as shown in figure 6.12 (Fuhrboter, 1986). The overall overturning process is therefore the combined effect of the macroscale process, as proposed above, plus the growth of the micro scale irregularities.

The 0.5m cut-off point may be taken as the point at which the physical process of wave overturning changes. For breaker heights up to 0.5m, the global surface tension effects are more significant than the microscopic ones. For bigger waves, as the results from the proposed model suggest, the global surface tension effects are negligible. *Micro* modelling of the process is hence required.

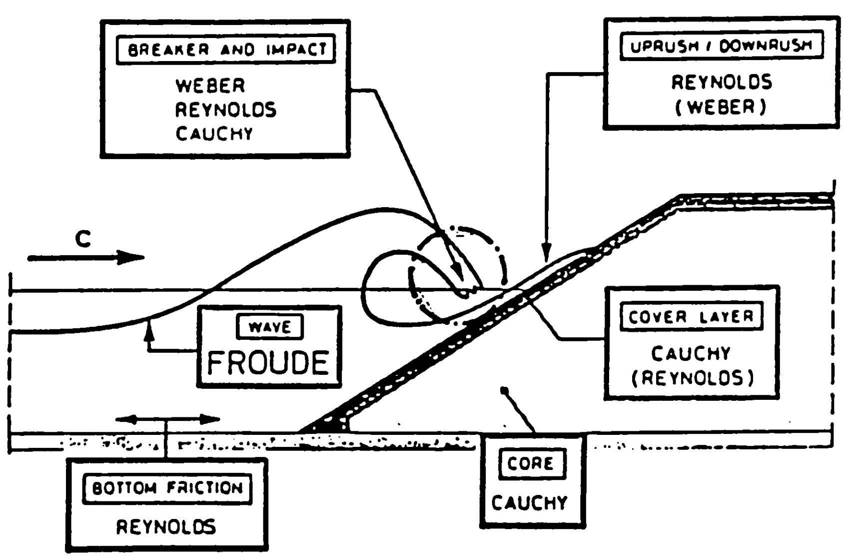

Fig. 3: Similarity laws for breaking waves

Fig. 6.12 Breaking wave - Irregularities on the tip of the breaker (Fuhrboter, 1986)

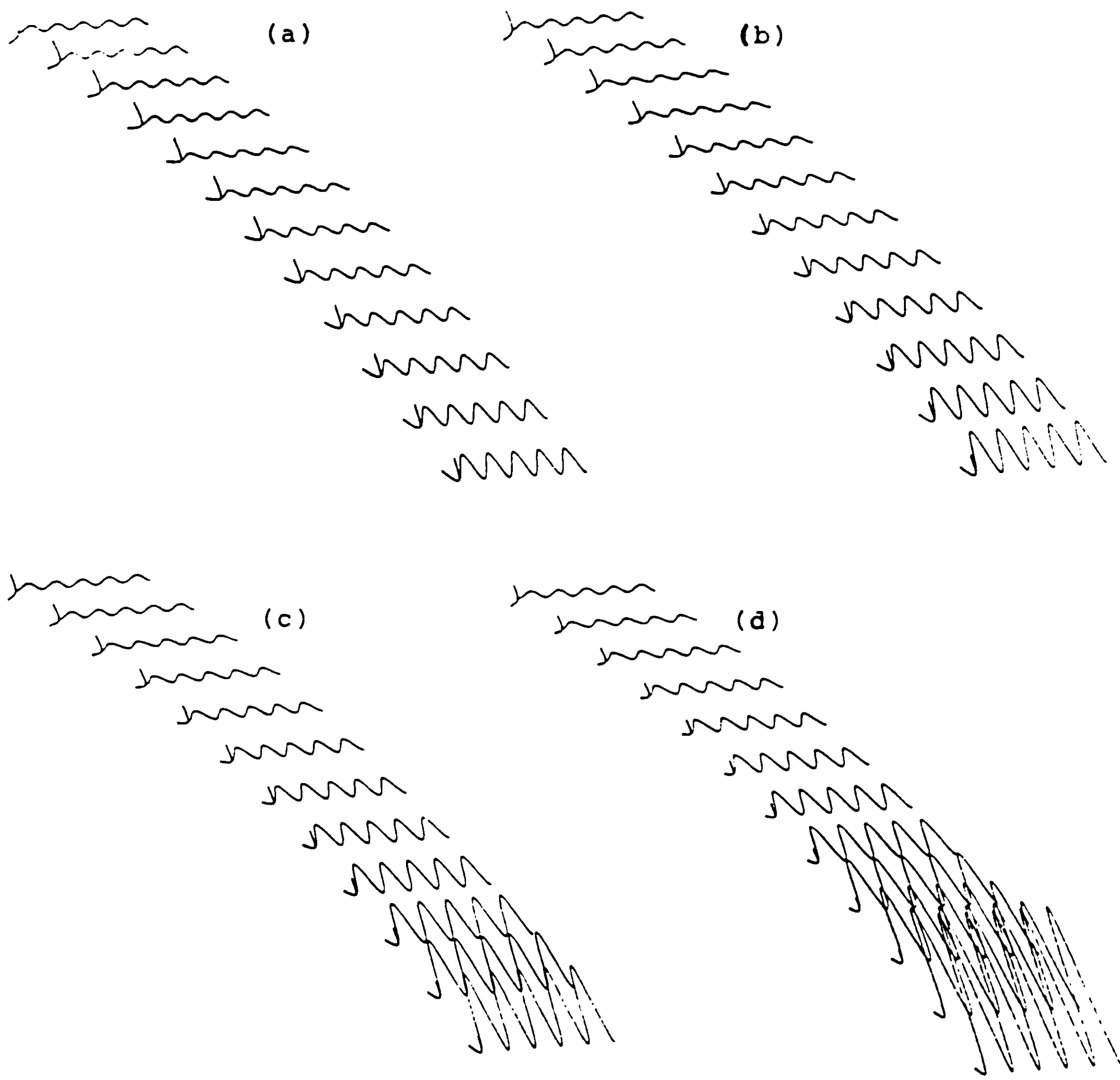

Fig. 6.13 Evolution of a transverse disturbance (L=40mm), on 4 waves of different curvatures: r_0= a) 14mm, b)12mm, c)10mm, d) 8mm. Time interval=0.02sec.

6.9 MICRO-SCALE MODELLING OF THE SEGMENTATION PROCESS

The proposed model may be used for the description of the micro-scale segmentation of the tip of the breaker, as this process is governed by the same laws of gravity, inertia and surface tension. In this case however, the initial characteristics of these irregularities may not be related to the wave characteristics, in the fashion that they were related in the macro-scale case. However, certain initial conditions may be assumed, based on experimental observations, in order to derive some results.

The radius of curvature of an assumed irregularity on the tip of the wave is very small compared to that of the tip of the breaker. The short wavelength disturbances grow much faster than the longer ones, when unstable. These properties imply that, the short sinusoidal transverse disturbances, which are stable from the macroscopic point of view, are now unstable and fast growing. They thus prevail on the tip of the wave. The described process is illustrated in figure 6.13. The evolution of the same monochromatic disturbance is presented, as predicted from the numerical model, for four different radii of curvature. The fast growth of the disturbance associated with the small radii of curvature is evident. Irregularities on the tip of the breaker, therefore tend to produce closely spaced jets. These jets are seen on the curling crest of two- dimensional overturning waves, breaking in both deep and shallow water conditions, as presented in the video cassette and described in chapter 5.

6.10 CRITICAL ASSESSMENT OF THE PROPOSED MODEL

The accuracy of any model depends on the validity of the assumptions inherent in the modelling. In the proposed model two distinct theories are used:

a) segmentation due to **surface tension**, and
b) stretching of the tip of the plunging jet, due to **gravity** and **inertia**.

The formulations on surface tension used in the proposed model are based on linear theory. Non-linear solutions have been developed since the original formulations by Plateau and Rayleigh. Bogy (1979) presented a literature review on the problem of the segmentation of liquid jets. Recent theories take into account finite amplitude disturbances, viscosity and air friction. The approximations inherent in the proposed model are such that the use of linear theory in describing surface tension effects is quite reasonable.

Experiments testing the validity of surface tension formulations indicate that there is a wide scatter of the results. Under controlled experimental conditions, Plateau (1864) observed the segmentation of liquid cylinders. In 10 identical experimental set-ups, the number of drops formed by a 90mm long cylinder varied between 10 and 15. Worthington (1879) performed a series of tests on the segmentation of a liquid annulus. In one set of 14 identical runs, the number of drops ranged between 6 and 12. This scatter of the results arises probably by the form of the initial disturbance on the surface of the liquid, a parameter which cannot be controlled or monitored.

Regarding the formulations derived by Longuet-Higgins (1980) on the change of form of the tip of the curling wave, no experimental work has been done to test the theory. The reason for the absence of such a work becomes apparent when one looks at photographs showing the overturning process. The curling face loses its continuity, as it spreads into jets and the free surface boundary is no longer two-dimensional, making the description of the cross sectional profile a most difficult task. The theory and assumptions however, on which the derivations are based are reasonable and, overall, the results are broadly in agreement with observations.

The assumptions inherent in the proposed model introduce their own limitations. Firstly, it is assumed that the tip of the overturning wave behaves like a horizontal liquid cylinder. The surface tension formulations for liquid cylinders are based on the assumption that there is no flow across the surface of the cylinder, a condition which, in the absence of any evidence supporting or rejecting this proposition, is not necessarily valid in a breaking wave. The effect of this assumption is that the model is strictly applicable to the very tip of the wave crest.

The ridges formed at the back of the wave are not treated by the proposed model. Their formation may be explained by the physics on which the model is built. The back of the wave has its own radius of curvature and any transverse disturbance on its surface will grow or diminish according to surface tension principles. The segmentation of the tip of the wave spreads in the vicinity of the crest. The long wavelengths of the enhanced transverse disturbances are further amplified, as the radius of curvature at the back of the wave is longer than at the tip. These disturbances appear as ridges, or *channels of easier flow* according to Worthington's (1908) terminology, spaced at wider intervals as their distance from the tip of the breaker becomes greater.

A further assumption built in the model is that the two theories used, namely surface tension and gravity, do not affect each other. That is, the radius of the cylinder is not modified by the growth of the disturbance. This assumption affects mostly the short disturbances which rapidly form thin jets, in which case the horizontal cylinder loses its physical meaning.

The model is based on linear theory. This assumption implies that there is no interaction between the individual sinusoidal components that make up the wave crest. Non-linear interactions do take place in wave processes and it is reasonable to expect such effects to be present in the segmentation of the overturning wave crest.

An alternative approach to the modelling of the segmentation of the crest of an overturning wave, that was considered, is the treatment of the overturning jet as a liquid sheet. Extensive literature is available on this field, as it is an important chemical engineering problem. Dombrowski and Johns (1963) presented a mathematical model describing the transition from a liquid sheet into droplets (fig. 6.14). Longitudinal waves grow on the sheet, as a result of *aerodynamic instability*, until they reach a critical amplitude. Tears then occur in the crests and troughs. The *fragments* then contract due to surface tension into unstable cylindrical *ligaments,* which subsequently break down into drops. (note: the authors' terminology is used and highlighted by *italics*).

This modelling considers primarily the growth of waves due to aerodynamic effects on a liquid sheet. Although this approach is appropriate for high velocity thin sheets (thickness in the order of 5mm), in the case of overturning waves there is no evidence that aerodynamic instability occurs. Experimental observations do not indicate the formation of horizontal *ligaments* and then their segmentation due to surface tension into drops. As a result, the negligible effects of aerodynamic instability make the application of this model unsuitable for the overturning wave problem.

6.11 CONCLUSIONS

Surface tension has been shown to play an important role in the overturning stage of a breaking wave. During this stage, any unstable disturbances on the tip of the breaker will grow as the curling face follows a free fall trajectory. The effects of the two main forces, namely gravity and surface tension have been combined together to produce an analytical/ numerical model that describes the evolution of

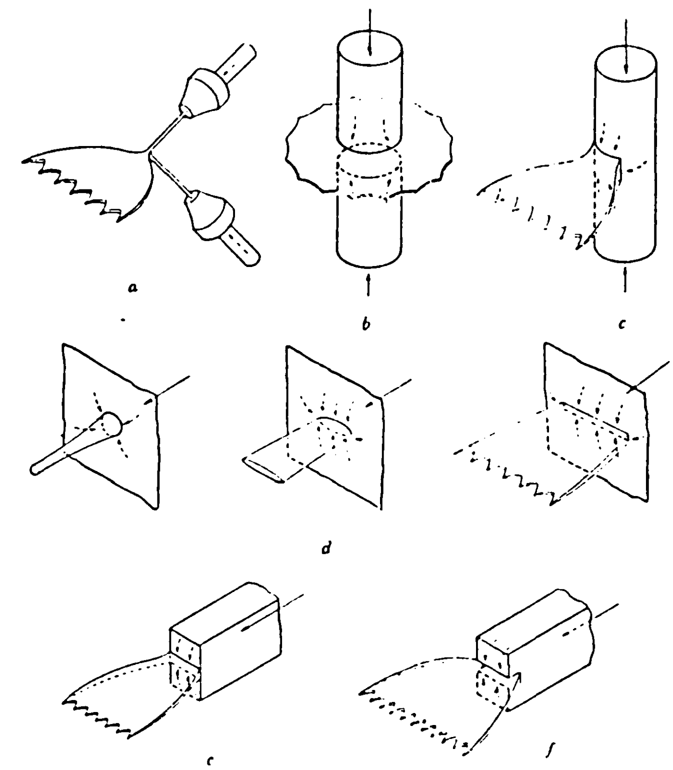

a

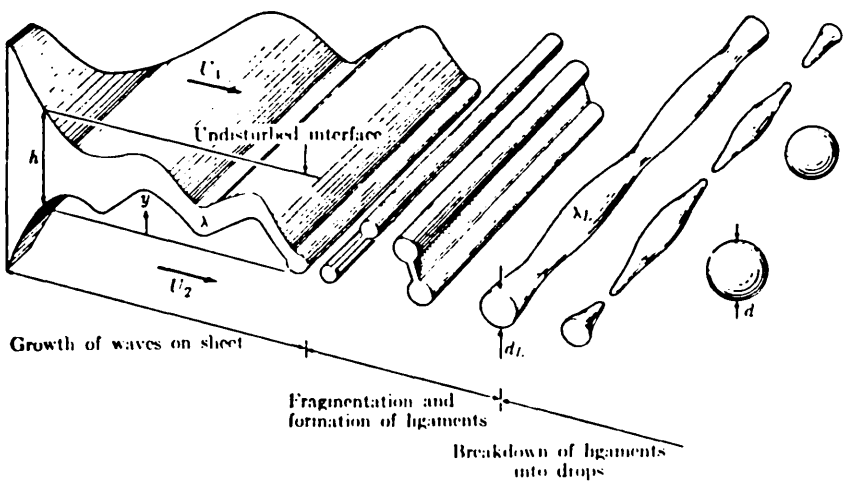

b

Fig. 6.14 a) the formation of flat sheets (Dombrowski & Fraser, 1954)
b) Modelling of breakup process (Dombrowski & Johns, 1963)

the overturning face of a breaking wave. This model has been used to assess both the macroscopic and microscopic characteristics of the segmentation process.

From the macroscopic, or global, point of view the initial conditions of the overturning face were related to the breaker height and period, after making certain approximations. The wavelength of the disturbance, whose amplitude increases the most due to surface tension effects, was found to be directly proportional to the breaker height. A most interesting result derived from the model is that breaking characteristics are independent of surface tension effects, for breakers bigger than 0.5m high, a result which is in agreement with earlier experimental results.

From the microscopic, or detailed, point of view, the irregularities of the tip of the breaker in the longitudinal- vertical, x-z, plane, are the predominant cause of segmentation seen in breaking waves. These tiny little jets are not directly related to the global properties of the incident wave. Their characteristics depend on random local irregularities. It is probably the random nature of these irregularities that makes the effects of surface tension appear the same for big waves (H_b>0.5m), rather that surface tension effects are not significant.

The combination the macro and micro scale models provides an overall picture of the effects of surface tension on the overturning process of breaking waves, which is in agreement with experimental observations.

CHAPTER 7

BROKEN WAVE MODEL

7.1 ABSTRACT

Recent studies have shown that the overturning face of a plunging wave penetrates the forward face like a solid body. The penetration of a solid body on an originally undisturbed water surface produces a surface wave disturbance whose characteristics depend on the shape and size of the penetrating body, as well as on the water depth. The process of wave breaking is approached, in this study, both macro- and micro-scopically. Macro-scopically, the plunging jet of a breaking wave may be considered as 2-dimensional, and the induced motion is therefore 2-dimensional as well (shorewards - offshorewards). The formation of the offshorewards travelling wave disturbance was observed in the laboratory. A model is proposed that describes this motion and also predicts the formation of a bore in shallow water conditions, a similarity widely used in surf zone studies. From a microscopic angle, the plunging jet may be considered as the summation of a series of bell-shaped jets, arising from surface tension effects. The superposition of the motion produced by each individual jet provides a prediction of the three-dimensional surface wave field induced by wave breaking. The predicted kinematics field is in reasonable agreement with the kinematics measured in the laboratory. The proposed model presents a mechanism for the generation of longshore wave motion produced by breaking waves incident normally on a beach.

7.2 INTRODUCTION

The broken wave motion is a problem about which very little is known, especially in the outer zone (see fig. 2.1). A recent concept (Basco, 1985), which was not treated in depth, is that a secondary wave disturbance is generated at the plunging area having very different characteristics from the initial wave. The offshoreward wave disturbance was observed in this study (section 5.3.1.3). The modelling of this motion is based on Peregrine's (1983) proposition and Jansen's (1986) results that the plunging jet penetrates the forward face like a solid body. This approach is a global, or macroscopic one, and it is presented in section 7.3.

The generation of the three-dimensional surface wave motion is modelled by approaching the problem from a closer, or microscopic angle. The basic concept is the same as for the macroscopic approach, but the formulation is more complex. This micromodel is proposed and discussed in section 7.4

7.3 MACROSCOPIC MODELLING

7.3.1 APPROACH

The penetration of the plunging jet into the forward face of the wave is similar to the fall of a solid body onto an originally undisturbed water surface. This problem attracted a lot of interest in the mathematical circles in the begining of the previous century, and in the first few decades after the development of the nuclear bomb. The former interest arose from intellectual curiosity, whilst the latter for military purposes, for assessing the effects of underwater nuclear explosions. The results from these theoretical and experimental studies are applied to the problem of the motion produced by wave plunging.

The problem of the motion produced by a local disturbance on the water surface is reviewed in appendix A.

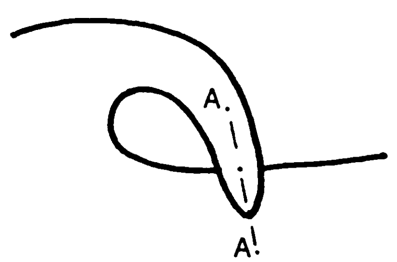

Fig. 7.1 Breaking wave.

Assuming the plunging jet is symmetrical about the central axis A–A (fig. 7.1), which is very close to the vertical, the broken wave motion may be simulated to the motion produced by a **local depression** on the water surface. The shape of this depression, based on experimental results (plates 5.5, 5.12, 5.13), may be described mathematically by equation 7.1 (fig. 7.2).

$$\eta_0 = - c \cos\frac{\pi x}{L} \qquad \text{for} \quad -\frac{L}{2} \leq x \leq \frac{L}{2} \qquad 7.1$$

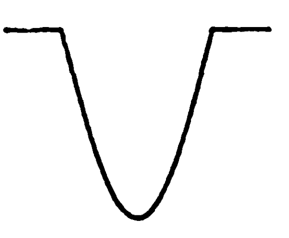

Fig. 7.2 Local depression modelled to a sinusoidal shape (eqn 7.1)

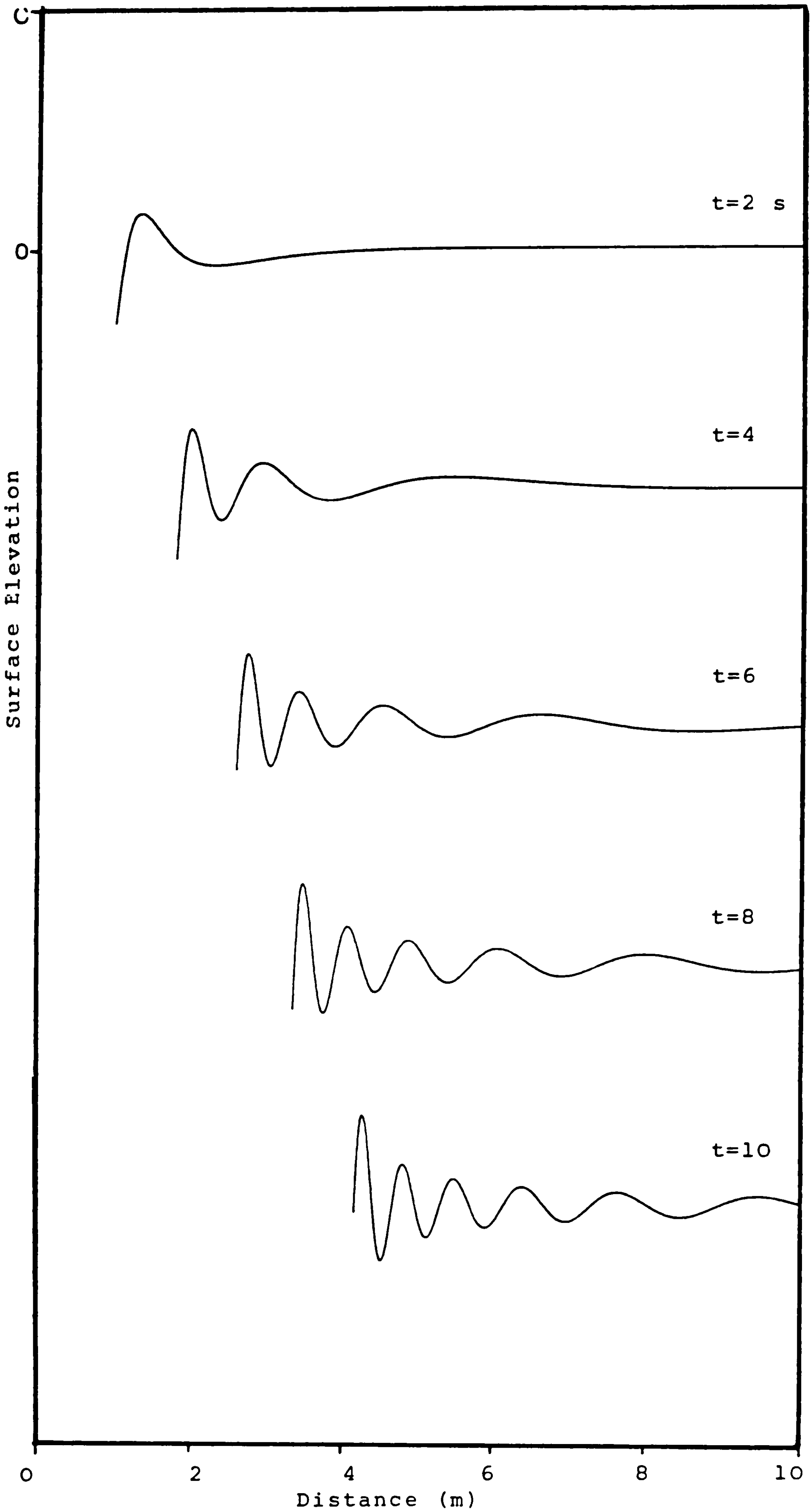

Fig. 7.3 Wave profiles at different times for a=0.2m.

The solution to this problem, for deep water conditions is,

$$y = \frac{2\sqrt{\pi}c}{xL}\left[\frac{gt^2}{4x}\right]^{1/2}\frac{1}{\left[\frac{\pi}{L}\right]^2-\left[\frac{gt^2}{4x^2}\right]^2}\cos\frac{gt^2L}{8x^2}\sin\left[\frac{gt^2}{4x}+\frac{\pi}{4}\right] \qquad 7.2$$

as obtained using the derivations of Kranzer and Keller (1959). The plunging area appears like a source of wave energy, emitting a continuous series of waves with increasing frequency. The waves stretch out as they propagate away from the plunging area, the phases of the waves accelerating at a constant rate. The wave profiles at various times, as obtained from equation 7.2 are shown on figure 7.3.

7.3.2 COMPARISON BETWEEN EXPERIMENTAL AND THEORETICAL RESULTS

The continuous scenes presented in the video cassette show quite clearly the generation of a new wave disturbance at the plunging area (see also plates 5.39–40). This wave motion has similar characteristics with the motion induced by a local disturbance on the water surface, as described above and discussed in detail in appendix A.

The identification of this similarity supports the argument that the plunging jet penetrates the forward face like a solid body and hence introduces a local disturbance on the water surface.

Basco, (1985) suggested that the mechanism of the generation of the secondary wave disturbance is similar to the wedge–type wave maker (fig. 2.26). The amplitude of this new wave motion is related to the angle of plunging, the depth of penetration and the water depth, whilst the period of the wave is the same as the period of the incident wave motion. Curves were presented indicating how the amplitude of the secondary wave motion is derived, given the incident wave conditions. This approach has the disadvantage that, *a priori*, it cannot take into consideration offshoreward travelling wave disturbances. It may be valid when the breaking waves are not very steep, in which case the offshorewards wave disturbance may be neglected.

It may therefore be said, that the secondary wave disturbance arises from the penetration of the overturning face of the breaking wave. In steep plunging breaking waves the local depression of the water surface is an appropriate simulation, as it explains well the formation mechanism and the characteristics of the offshoreward wave disturbance. The wedge–type mechanism may be appropriate in the case of breakers in which the angle at which the overturning jet hits the forward face deviates significantly from the vertical; a case not considered by the author's proposed model.

Attempts to quantify the experimentally produced motion using wave gauge measurements proved fruitless, due to the presence of *noise*. This arises mainly from the measuring device (signal very weak, hence poor signal to noise ratio) and the inability of the system to distinguish the longitudinal and the transverse components in a three-dimensional motion. The visual records are superior from the wave gauge records in that:

a) the reflections amplify the motion,

b) the longitudinal motion is distinguished,

c) the wave direction is immediately identified,

Comparison between the experimental and theoretical results is therefore restricted to wave profiles at particular instances. The theoretical profiles of the surface elevation at various times, as derived from equation 7.2, are shown in figure 7.3. It is evident from these profiles that the waves have dispersive properties, stretching out as they travel away from the plunging area. Qualitatively, the theoretical and experimental results are in reasonable agreement.

It may therefore be said that, the disturbance generated by breaking waves has dispersive properties, the waves elongating as they propagate away from the plunging area, whilst new waves are formed with increasing frequency. The actual plunging process is a combination of both a local depression of the water surface and a forward and downward movement of a solid body. Although neither of the two models accurately represents the plunging process, the local depression model provides an analytical solution to the problem and describes successfully the secondary wave motion characteristics.

7.3.3 DISCUSSION

The presented results suggest that wave plunging generates a new wave disturbance with vastly different characteristics from the original wave. The proposed mechanism responsible for the generation of this motion, namely, the local depression on the forward face of the breaker, describes qualitatively well the new wave motion.

The proposed mechanism has a significant implication on breaking waves in shallow water. The limited depth imposes an upper bound on the speed of propagation of the generated wave disturbance. The first wave trains, which have large wavelenghts and periods, are slowed down, resulting in a mass of water travelling with the depth limited velocity, $\sqrt{gh}$. Mathematically, this motion is represented by a discontinuity, and physically it is known as a **bore** (see also appendix A).

The similarity of the broken wave motion in the surf zone with the motion of a bore has been extensively used (Madsen and Svendsen, 1983). This simulation was based on visual observations. The proposed mechanism on the generation of the broken wave motion not only supports the simulation used, but it provides a physical justification for the **bore** simulation as well.

The dimensionless amplitude and duration of the bore, as derived by Kranzer and Keller (1959) are:

$$B_{bore} = \frac{R'}{2h}\frac{R'}{R} \tag{7.3}$$

$$T_{bore} = 1.4\ h^{1/6}\ r^{1/3}\ /\ g^{1/2} \tag{7.4}$$

where R' is such that

$$\frac{1}{2}\ \left|\ \eta_0\ \right|\ R'^2 = \left|\ \int_0^\infty r\ E(r)\ dr\ \right| \tag{7.5}$$

The other symbols are as defined in appendix A.

As a conclusion, it may be said that, breaking waves produce a new wave disturbance which may be described by the motion induced by a local disturbance on the water surface. In shallow water conditions, a bore results from such a disturbance.

7.4 MICROSCOPIC MODELLING

7.4.1 APPROACH

The overturning face of a plunging wave is segmented due to surface tension. On impact with the forward face of the wave, the penetrating plunging jet presents an irregular shape. Assuming that this shape may be decomposed into a series of sinusoidal bell-shaped jets, the motion induced by breaking is the summation of the disturbances induced by each individual jet.

In the longitudinal and vertical directions, the effects of the individual contributions to the motion are added together, whilst in the transverse direction, some contributions might cancel each other. In a symmetric case, there is no motion in the transverse direction. However, the random nature of the initial disturbance, which is the primary agent for the three-dimensional disintegration of the breaker crest, makes the symmetric condition virtually impossible.

The experimental observations (chapter 5) indicate that the plunging process is random in many ways, as shown on plates 5.3, 5.9, 5.22, 5.25, 5.34 and listed below:

a) in the longitudinal direction
b) in the time domain
c) in the components that constitute the plunging face
d) in the size of the individual jets

The aim of the proposed model is to derive the overall properties of the broken wave motion and statistically predict the transverse velocity time histories in the vicinity of breaking, considering the random nature of the process.

7.4.2 DESCRIPTION OF THE NUMERICAL MODEL

A computational model has been developed by the author which predicts the motion induced by the sudden penetration of a series of sinusoidal bell-shaped solid bodies in an undisturbed water surface. The computational scheme is split into three different parts, so that the results from each individual part may be accessed and studied separately.

The solution to the problem of the motion generated by a local depression on an undisturbed water surface is computed (as described in appendix A) in the first part of the scheme. The 3-dimensional depression is described mathematically by

$$\eta_0 = -\ \frac{c}{2}\left[\ 1 + \cos\frac{2\pi x}{L}\ \right] \qquad \text{for } -\frac{L}{2} \leq x \leq \frac{L}{2} \qquad 7.6$$

where c is the height and L the width of the bell shaped depression.

This solution is stored in the form of a two-dimensional array containing the surface elevation values at discrete intervals of time and space, that is $\eta(x,t)$ is obtained over a range of both space, x, and time, t, at finite intervals δx and δt.

The elevation time history at any distance from the local depression, as well as the elevation profile at any instant of time, may be therefore directly obtained.

The conversion from elevations into velocities is based on linear theory. The transformation is described by,

$$\text{horizontal velocity,} \quad u = \frac{2\pi}{T} \frac{\cosh[2\pi(z+h)/L]}{\sinh(2\pi h/L)} \eta \qquad 7.7$$

$$\text{vertical velocity,} \quad w = \frac{\pi H}{T} \frac{\sinh[2\pi(z+h)/L]}{\sinh(2\pi h/L)} \sin(-2\pi t/T) \qquad 7.8$$

where H is the wave height,

h is the water depth,

z is the depth of the point under consideration, and

η is the water surface elevation.

A two-dimensional array, velocity(x,t), is computed in the second part of the scheme. The result is stored in a file, of the same format as the elevation array, so that the same programs may be used for accessing and studying both types of output files.

In the final part of the numerical scheme, the velocity time history at a particular location is derived by superimposing the effects of the individual local depressions, that simulate the disturbance produced by the plunging of the breaker (fig. 7.4). Mathematically, this procedure is expressed as,

$$u_r(x,t) = \sum_{i=1}^{N} u(r_i,t_i) \cos(\theta_i) \qquad 7.9$$

where,

u_r is the resultant velocity,

r_i is the distance of the considered point from the i^{th} jet,

t_i is the time elapsed between the plunging of the i^{th} jet and the beggining of the time history, i.e. t_i=t + (delay time of impact),

N is the total number of jets considered,

θ_i is the angle between the direction of u_r and the line joining the i^{th} jet with the point under consideration.

The determimation of the way in which the individual contributions to the motion are superimposed poses a difficult task (e.g. what is the delay time, how

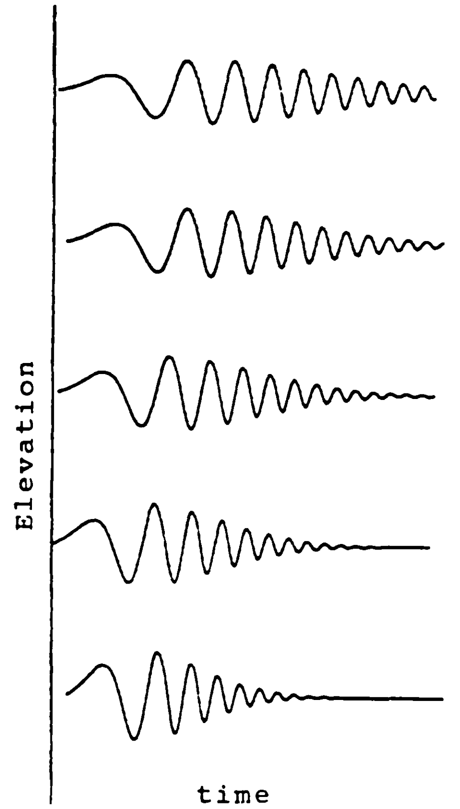

Fig. 7.4 Motions produced by individual depressions are superimposed with different delay times.

much is r_i). In the absence of an established method for tackling this problem, an heuristic approach is adopted. Qualitative experimental observations indicate that even under carefully controlled conditions, the profile of the plunging jet of the breaker varies significantly from wave to wave. This observation is evident in the video cassette.

In order to simplify things and make the derivation of some meaningful results a feasible task, the irregular profile of the plunging jet is simplified significantly. Only one random variable is changed at a time, namely

a) the deviation of impact point from the mean plunging line,
b) the time delay for each individual jet impact, relative to the first impact, (fig. 7.5)
c) the size of each bell-shape jet.

The width, L, of the jets was kept constant in all three cases.

A further requirement for such a simplified approach is the determination of the fashion in which each variable changes. A semi-empirical approach is adopted.

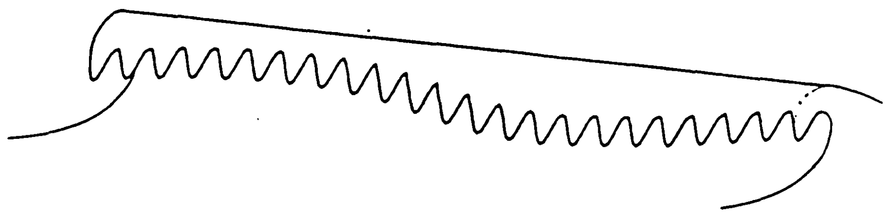

Fig. 7.5 Part of the crest of an overturning breaker with equally spaced jets and same amplitude but different time of plunging

A continuous random oscillatory function is arbitrarily picked, which is then modified in amplitude, so that its range of values corresponds to a physical property (e.g. in the case of the delay function, the range of the delay times does not exceed the duration of overturning). The choice of the form of the random function was based primarily on visual observations, which failed to distinguish a particular pattern in the breaking process. A heuristic approach was followed in which a digital series was obtained from the summation of 60 sinusoidal components of different amplitude, added with random phases, and then arbitrarily stretched or squeezed so that the "randomness" of the function is enhanced. A sample of such random functions is shown in figure 7.6.

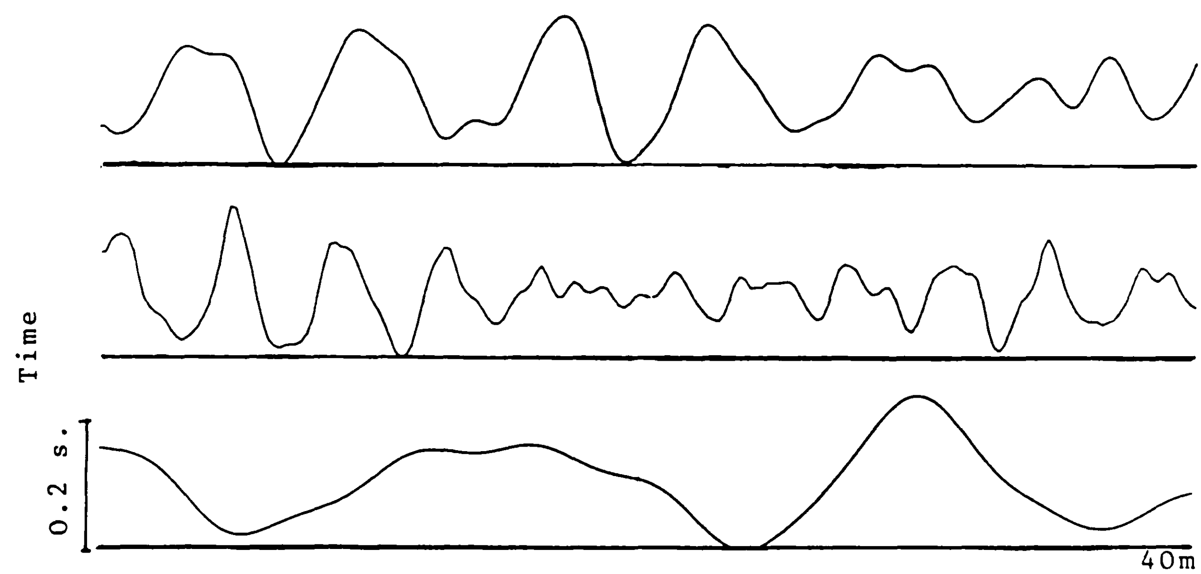

Fig. 7.6 Sample of delay functions used in the model

7.4.3 MICRO-MODEL RESULTS

Velocity time histories were produced using all three heuristic methods of representing the impact process. Although there is a great amount of variation in the results, the overall form of the results nevertheless, appears to be the same. In order to illustrate the characteristics of the derived wave motion, one complete set of results is presented.

Transverse velocity time histories are computed, as described above, for 25 different delay functions, with L=0.2m, c=1.0m in deep water conditions, for a number of points around the origin of the disturbance produced by a 0.2m height breaker. The locations where velocities are predicted are shown in figure 7.7. The results are plotted (fig. 7.8) in the same fashion as the experimental results, namely, superposition of:

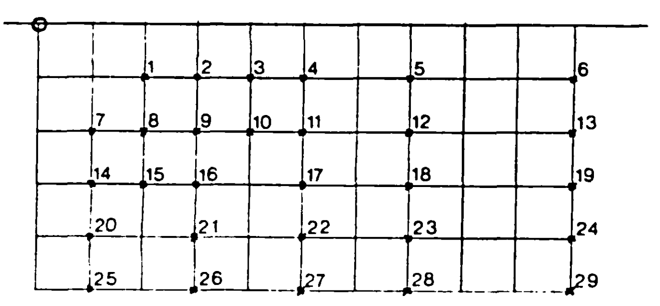

Fig. 7.7 Locations where transverse velocity time histories where computed. Grid spacing=0.1m.

a) velocity, v, time histories,
b) velocity squared, v^2, against time,
c) accumulation of kinetic energy, Σv^2, with time, and
d) normalised accumulation of energy with time.

The ensemble average from the 25 records is obtained and the plots of the mean velocity squared against time and the accumulation of the mean velocity squared against time is hence derived. A sample from such plots is shown in figure 7.9.

7.4.4 INTERPRETATION OF MICRO-MODEL RESULTS

The transverse velocity time histories show a large scatter in the results. Some characteristic features are however quite apparent. Firstly, a ***spike*** is generally

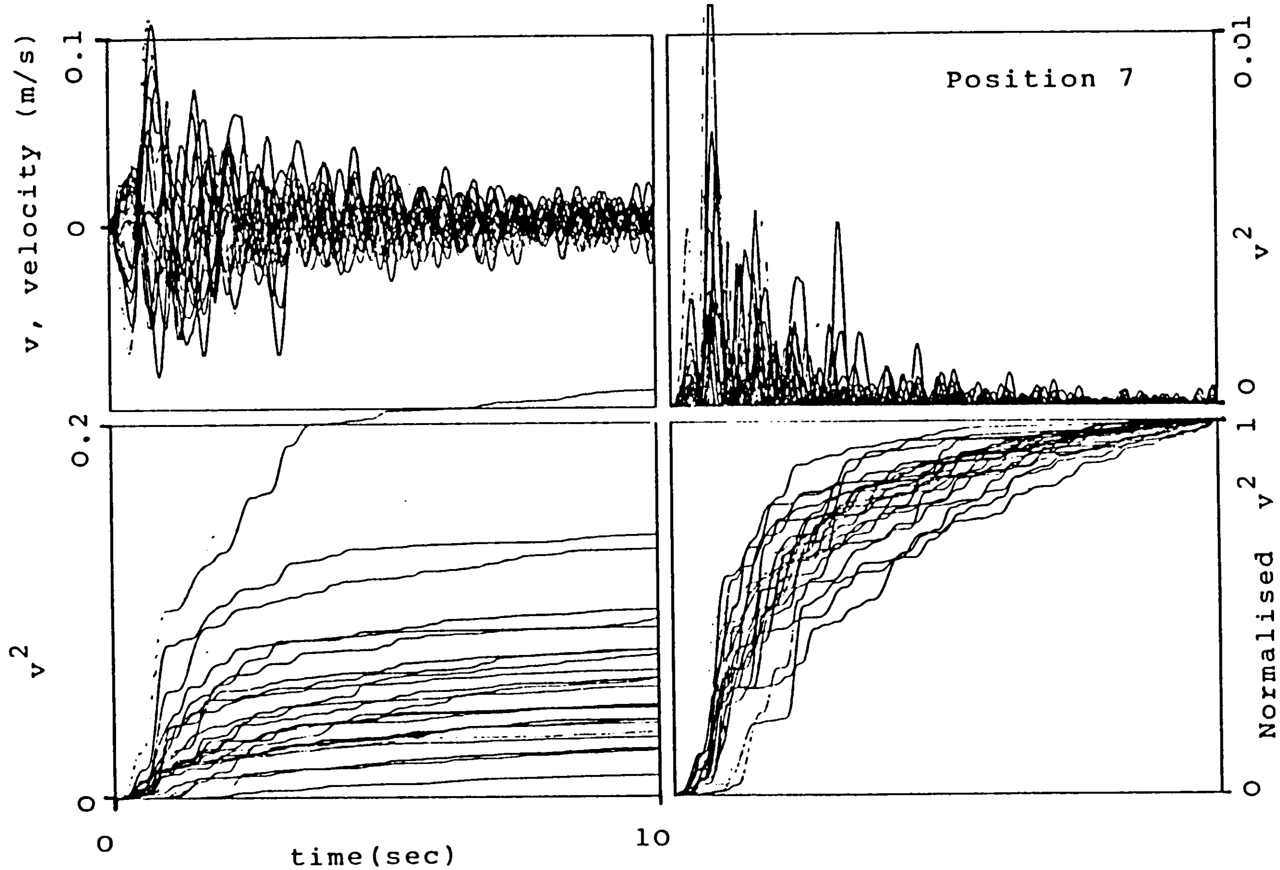

Fig. 7.8 A typical numerical model result.

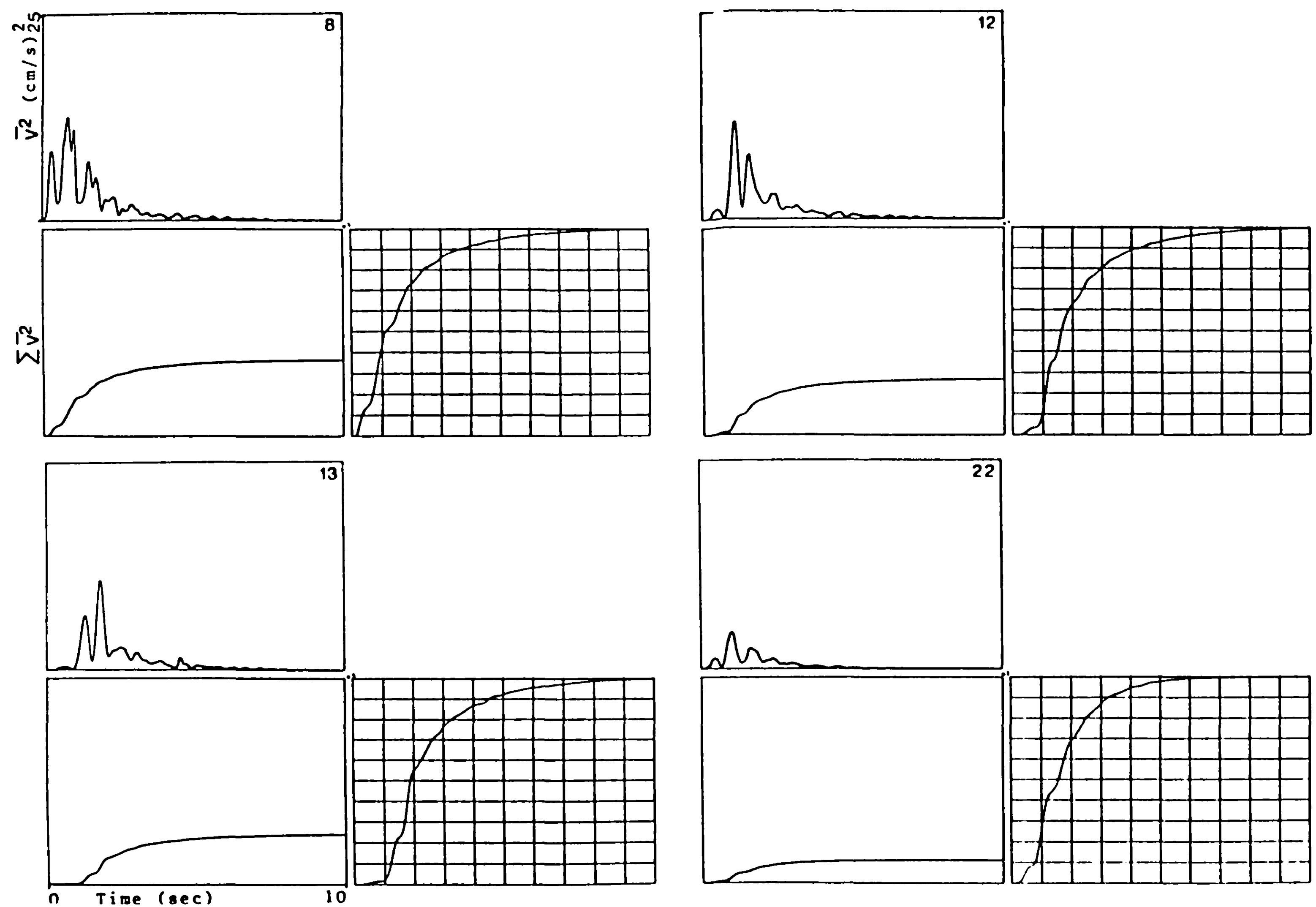

Fig. 7.9 Sample of plots obtained from the computational model.

formed soon after plunging. This is followed by a random oscillation which generally decays with time. These general characteristics are identical with the early predictions on the form of the breaker induced unorganised motion –similar to the seismogram records– as well as with the measured experimental velocity time histories. The quiescent part, identified in the latter records, is not shown in the numerical model results for obvious reasons.

Contrary to the experimental results, no regular motion is identified in the numerical model results. This discrepancy arises because the model does not account for resonant effects. The width of the area in which breaking takes place is considered infinite, all frequency components being affected in the same way.

The square of a time history has the effect of increasing the significance of the higher values and decreasing that of the small ones. The *spike* is quite clear in these plots, followed by a decaying motion. The trend in these plots becomes more apparent in the plot of v^2 against time.

The scatter in the predicted results is much larger than that in the measured ones. This might suggest that the model is conservative in predicting the random nature of the overturning process.

The similarity of the form of the individual predicted velocity time histories is shown in the plots of the normalised accumulation of energy curves, Σv^2. The effect of such plots is to *smooth* the record; the effect of the small numbers is reduced and the global trends are stressed.

Having derived the main characteristics of the *chaotic, unorganised, turbulent* (the term turbulent used in the broad sense as deviation from the ensemble average) breaker induced motion, as predicted by the numerical model, the temporal and spacial distribution of this motion may be described by considering the mean, or ensemble average, motion (fig. 7.9).

The plots of the normalised accumulation of kinetic energy with time show that in general about 70% of the energy is dissipated within two seconds after plunging. This value is in reasonable agreement with the laboratory measured results, regarding the energy dissipation offshorewards from the plunging point. The model, due to its nature, does not take secondary plungers into consideration and cannot therefore be compared with experimental results obtained shorewards from the plunging area.

	11.2	10.6	10.3	9.6	9.0	8.0
8.16	7.5	6.9	6.6	6.5	6.1	5.7
5.8	5.6	5.1		4.9	4.6	4.3
4.4		4.0		3.8	3.6	3.4
3.4		3.1		3.0	2.9	2.7

Table 7.1 Range in cm/s obtained from the numerical model

(Values correspond to locations shown in fig. 7.7)

The spacial distribution of the *range* of the unorganised motion, that is $v_{max}-v_{min}$, is illustrated in table 7.1. It is evident that the intensity of the motion decays much more rapidly in the vertical rather than the longitudinal direction. The range of the velocities is about halved when the depth increases from half the breaker height to $1^1/_2$ times the breaker height, and it is about a third of the first value at depths of about $2^1/_2$ times the breaker height. These values are also generally in reasonable agreement with the experimental results.

7.4.5 LIMITATIONS OF THE MICRO-MODEL

The proposed model describes the main features of the broken wave motion reasonably well. The physics behind the process of the broken wave motion generation are taken into consideration. Certain approximations are adopted however in order to produce an engineering model. The assumptions built into the model are hereby highlighted.

The penetration of the plunging jets is assumed to take place instantly, a local depression being formed. The shape of the depression is assumed to be the summation of a series of bell-shaped sinusoidal jets. This approximation is similar to Fourier's theorem in two-dimensional cases. The extension of the theorem to three-dimensional conditions is not supported by mathematical arguments; it is simply an engineering solution based on intuition. The random nature of the process however suggests that the error introduced from such an approximation is not significant.

The angle of impact of the plunging jet onto the receiving water mass is assumed to be vertical. As in the macro-model case, experimental observations suggest that a forward motion takes place in adition to the vertical one. The proposed model is close to reality when the breaker is steep. In other breaker types, the broken wave motion shorewards of the plunging point is stronger than the one offshorewards, whilst the model treats the motion as symmetrical about the plunging line.

A further assumption is that there are no non-linear interactions between the motion produced by the individual jets, the solution based on linear theory. Bearing in mind the small amplitude of the motion, this assumption is quite reasonable outside the immediate vicinity of plunging. Close to the plunging area the mathematical solution to the motion induced by a local disturbance of the water surface is not valid. The results from the proposed model are therefore applicable away from the plunging region.

These limitations highlight the complexity of the breaking/broken wave process whilst the assumptions built in the model simplify the process into a relatively easy numerical model.

7.4.6 DISCUSSION AND CONCLUSIONS ON MICRO-MODEL

The characteristics of the breaking induced motion may be summarised as follows:

a) There is a sudden increase of wave activity soon after plunging

b) The motion decays gradually after reaching its maximum intensity

c) The amplitude of the motion decays with depth

d) The motion, *a priori*, is a random wave one, which according to linear theory may be decomposed into the individual contributions which produced the motion. The motion therefore contains waves of all wavelenghts, the relative amplitude of each wavelength determined by the width of the jet, L. In general (appendix A) the wider the bell, L, the longer the predominant wavelength, L_{pred}, and in particular for sinusoidal shapes, L_{pred}=L.

The main features of the derived motion are in agreement with the experimental results.

One important result from the proposed model is that, two-dimensional breaking waves do generate three-dimensional waves covering a wide range of wave periods. If the breaking area is bounded by natural or man-made structures, the components of the wave motion that correspond to the natural modes of oscillation of the enclosed area are attenuated less than the other components. Eventually, only the components corresponding to the natural modes of oscillation of the bounded region will persist, in the form of standing waves, perpendicular to the incident wave direction. The experimental results as well as the visual observations show clearly the formation of a standing wave across the flume, whose period corresponds to one of the natural modes of oscillations of the bounded area.

Based on the same argument, breaking waves incident **normally** on a beach therefore present a **source** of longshore wave motion (it is the first time that such a proposition is made). The predominant period of this motion is not related directly to the period of the incident waves, but it is a function of the width of the plunging jet, the angle of impact of the plunger and the water depth. In bounded stretches of beach, a standing longshore wave, called **edge wave**, will result. Up to now, the generation of edge waves is described for **non breaking** wave conditions, in reflective systems (see section 2.5.2). The formation of **beach cusps** under such conditions is fairly well understood; they are the result of the interaction of the incident and edge waves. Regarding the formation of beach cusps under breaking wave conditions, there is a lack of a physical mechanism justifying the generation or presence of edge waves. The presented model opens new horizons in the understanding of this process, the detailed study of which however, is beyond the scope of this thesis.

7.5 SUMMARY

A conceptual physical/numerical model describing the *chaotic* broken wave motion has been presented. It is based on the observations that the plunging body of the overturning wave penetrates the forward face like a solid body. The resultant motion is considered from two different angles:

a) the macroscopic angle, in which the plunger is taken to be two-dimensional, and

b) the microscopic angle, in which the plunger is considered as the summation of a series of three-dimensional jets.

The new motion resulting from both treatments is in reasonable agreement with the experimental observations.

From the macroscopic point of view, a new secondary two-dimensional wave disturbance is generated at the plunging point. This motion may be described by the solution to the problem of the motion generated by a local disturbance on the water surface, the Cauchy- Poisson problem. In shallow water conditions a bore is formed by such a mechanism, propagating with the depth limited velocity. This mechanism provides a physical explanation to the bore simulation of the broken wave motion in the surf zone, a modelling based up to now on visual observations.

From the microscopic angle, the irregularities of the overturning wave face, amplified by surface tension effects are taken into consideration. The shape of the plunging jet is simulated as the result of the superposition of a series of bell–shaped sinusoidal jets. On impact with the forward face of the wave, the plunging face penetrates the receiving water body like a solid body. This penetration induces a surface wave motion which, using linear theory, is the summation of the motion generated by the individual jets that make up the plunging face. Superposition of these radial waves in the numerical model produces the temporal and spacial kinematics of the broken wave motion around a deep water steep plunging wave. The characteristics of this motion are in reasonable agreement with the experimental results. The characteristic *spike*, the heuristic prediction of which inspired this study, is quite evident. This is followed by an irregular motion, whose frequency components cover all wavelengths, as is evident from the mathematical solution used in deriving the motion.

The proposed conceptual model for the generation mechanism of the broken wave motion and the consequent computational model describing this motion open new horizons in the study of the breaking/broken wave problem. They show that the *chaotic, unorganised, or turbulent* broken wave motion does have some characteristic features which are related to the incident waves. Breaking waves present a source of secondary wave energy, derived from the incident wave energy. Part of this energy travels offshorewards, part shorewards and part alongshorewards. The proposition that breaking waves incident normally on a beach generate longshore wave motion introduces a new dimension in the study of longshore processes.

CHAPTER 8

AIR-ENTRAINMENT IN BROKEN WAVES

8.1 ABSTRACT

Air entrainment in broken waves is associated with the characteristics of the overturning face of the breaking wave. Surface tension produces segmentation of the overturning face. The plunging face may therefore be viewed as a series of three-dimensional jets. The identification of the similarity between the plunging jet of a breaking wave and that of a circular liquid jet permits the application of the knowledge on the latter process on to the former. The energy associated with air entrainment, which is derived from the wave energy, depends on the concentration and distribution of air entrainment. The application of suitable empirical formulae, derived for the plunging liquid jet problem, provides an estimate of the energy loss in breaking waves. This value, when applied to the case of regular breaking waves, gives an estimate of the proportion of the wave energy loss.

8.2 INTRODUCTION

The effect of surface tension on the overturning process of breaking waves is to segment the tip of the crest of the breaker (chapters 5 and 6). Jets are therefore formed on the plunging face of the wave. These jets, being in a state of free fall, are in turn affected by surface tension. They therefore tend to break up into stable shapes of equilibrium, namely spheres. On hitting the forward, undisturbed face of the wave, air is entrained into the receiving mass of water. These air pockets travel downwards with an initial speed equal to that of the water jets on impact. As they propagate their speed decreases and they also break up into spherical bubbles.

The depth of penetration of the air bubbles, as well as the distribution of air concentration have attracted a lot of interest in fields other than coastal engineering. In order to apply the characteristics of air entrainment associated with liquid jets ejected from a nozzle, a review of the state of the art on this topic is necessary. The state of knowledge on the process of plunging of liquid jets is first reviewed. The proposed model is then presented, and the results from this model are discussed.

8.3 LITERATURE REVIEW

A number of publications have dealt with the instability of liquid jets. This process is an undesirable feature of many industrial operations, such as the pouring of glass or metal. On the other hand, it is a desirable feature in mixing and reacting liquids and gases. Recently, the *ink-jet* printing method motivated scientists to investigate the details of the segmentation process of jets, as the understanding of the drop formation is crucial to the control of the ink printer.

Bogy (1979) presented a summary of the contributions to the solution of the problem of the segmentation of plunging liquid jets. The linear solutions to the problem of the segmentation of liquid cylinders, (Plateau (1864), Rayleigh (1878)) discussed in chapter 6, have been extended to consider disturbances of finite amplitude, viscosity and air friction. The wavelength of the fastest growing disturbance given by these higher order solutions is within 6% of the value predicted by linear theory.

"Air entrainment occurs when the inertial and gravity forces override the resisting forces due to viscosity and surface tension" (Kobus, 1984). The liquid segmentation and consequent air-entrainment are so sensitive to the initial conditions at the nozzle, that direct comparison between different studies and theoretical works cannot be made. A number of empirical formulae are available, but they are only applicable for the particular conditions under which the tests were carried out. A qualitative picture of the air-entrainment process may be derived from a review of the published results. For a quantitative description, a careful study is required as to determine what is most relevant from the available information and how it may be extrapolated for breaking waves.

Air entrainment by high velocity water jets was studied by Van de Sande (1972) for $We>10$ and $Re<5x10^5$. It was found that the theoretical analysis on liquid jet stability does not agree with the measurements. This was attributed to the assumption that the jet has an ideal sinusoidal shape, whereas experimental observations showed that such an assumption is an unrealistic simplification. " The shape is so irregular that a mathematical description of the shape seems impossible". In the same study, the physical mechanism of air-entrainment is proposed. The distinct processes proposed are:

a) Inside and at the rough surface of the jet, a core of air is captured and carried with the water.

b) At the periphery of the jet a laminar air boundary layer is developed.

c) The jet introduces a flow in the receiving liquid whose streamlines at the plunging point are directed parallel to the jet. A hole appears round the jet, caused not by the pressure of the air boundary layer, but by the flow of the liquid itself. This creates an underpressure which helps the entrainment of the captured air and the air boundary layer. In the case of obliquely impacting jets, the hole created by the jet gets larger. The underpressure increases and more air is entrained.

In a further study conducted by Van de Sande (1976), on low velocity jets, it was found that the correlation between air entrainment and jet characteristics is very poor. For example, the minimum velocity at which entrainment occurs is determined by local factors such as surface roughness and jet kinetic energy.

Similar studies were carried out by Ervine, McKeogh and Elsawy (1980), McKeogh and Ervine (1981), Kumagai and Endoh (1982). Some of the main conclusions reached by these studies may be summarised as follows:

a) Air entrainment cannot be described solely by Froude, Weber or Reynolds numbers.
b) For small heights of fall, rough jets entrain more air. For bigger heights of fall, the jet breaks up into discrete particles, loses momentum to the surrounding atmosphere and hence entrains less air.
c) For fully turbulent conditions, such as large heights of fall, the rate of air entrainment is dependent on the Froude number only (i.e. Gravity scaling law). For low flow rates and low heights of fall, surface tension prevents air entrainment.

Empirical formulae on air entrainment concentrations are presented in various publications. There is a significant degree of difference between each formula, in not only the form of the equation but in the selection of variables, as well. This apparent discrepancy does not undermine the accuracy or reliability of the studies. On the contrary, it highlights the complex nature of the entrainment process. The problem cannot yet be solved analytically or numerically. Experimentally, the geometrical shape of a plunging jet is so *chaotic* that it cannot be described, let alone quantified.

In conclusion, it may be said that the physical mechanism of air entrainment is fairly well understood. Gravity, surface tension and viscocity do play significant roles in the process. For great heights of fall, gravity is the predominant force; Froude scaling criteria may thus be employed under such conditions. In any particular application the choice of the empirical formula will depend on the special conditions under which the tests were carried out. In the case of plunging waves, the most suitable experimental results are the ones obtained by McKeogh and Ervine (1981). In this study, (fig. 8.1) the height of fall (0–6m), the jet velocity (0–10m/s), jet diameter (6, 9, 14, 25mm) and turbulence intensity of the jet were varied. Most of the other works were performed having in mind applications in chemical processes, whereas this study was carried out as a general fundamental study.

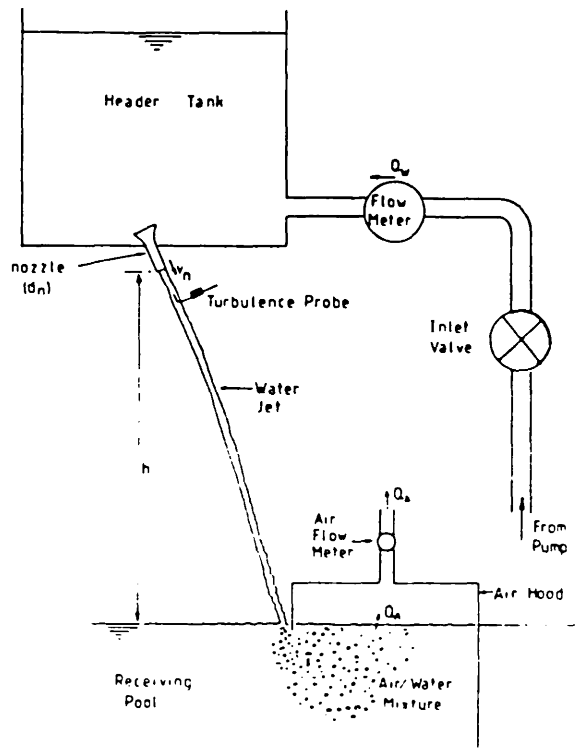

Fig. 8.1 Experimental set-up (McKeogh and Ervine, 1981)

8.4 DESCRIPTION OF PROPOSED MODEL

8.4.1 APPROACH

The approach followed in this model is based on the work of Fuhrboter (1970) (see section 2.5.1.7). In that study, uniform distribution of air bubbles was assumed. In the absence of any data, air concentration was left as a variable. The presented model incorporates the principles used by Fuhrboter, provides a physical mechanism of air entrainment and hence makes use of known properties of the process. The basic principles on which the model is based are discussed.

A certain amount of energy is required to entrain air in surface waves. This energy is derived from the wave energy and then dissipated in the form of microturbulence and wake motion as the bubbles rise to the surface. The energy dissipated by air entrainment is equal to the potential energy of the air, when the bubbles are at the greatest depth, where their kinetic energy is zero.

The concentration and distribution of air in the plunging area are first assumed. The energy associated with this entrainment is computed. Comparison between the energy dissipated due to air entrainment and the total energy of a regular wave, provides a direct estimate of the proportion of the wave energy loss when breaking takes place.

8.4.2 ENERGY STORED IN AIR BUBBLES

Consider a long column of pure water having width *dx* and unit depth (fig. 8.2a). Air is then entrained at depth *y* of the column (fig. 8.2b). The air concentration is then

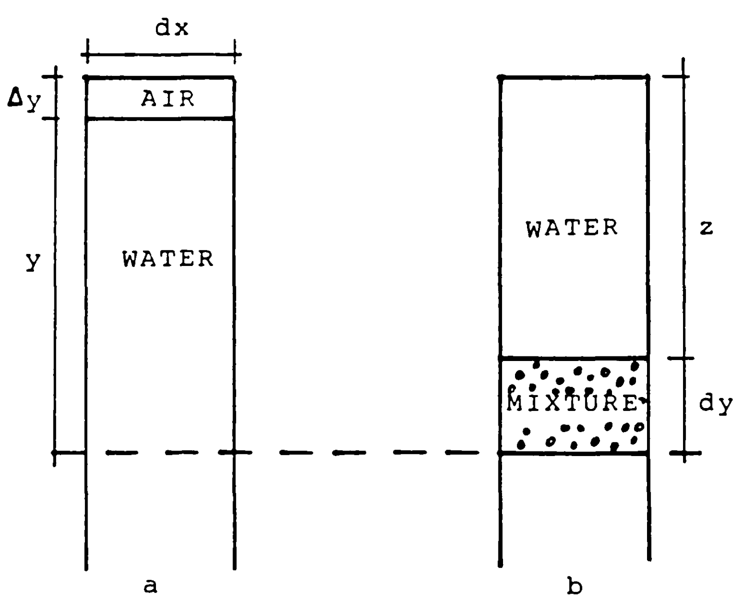

Fig. 8.2 Air-water column
a) No mixing
b) Air entrained to depth z, with concentration, c.

$$c = \frac{\Delta y}{dy} \qquad 8.1$$

The initial potential energy relative to the zero datum level, assuming the density of the air is negligible, is

$$E_1 = \frac{1}{2} \rho \, g \, dx \, y^2 \tag{8.2}$$

With air entrainment, the potential energy is equal to the sum of the energy due to the air-water mixture plus the energy of the water body.

$$E_2 = \rho \, g \, dy \, (1-c) \, dx \, dy/2 + \rho \, g \, z \, dx \, (dy+z/2) \tag{8.3}$$

where

$$z = y + \Delta y - dy \tag{8.4}$$

therefore

$$E_2 = \rho \, g \, dy \, (1-c) \, dx \, dy/2 + \rho \, g \, dx \, (y+\Delta y-dy)(dy+(y+\Delta y-dy)/2) \tag{8.5}$$

$$= \rho \, g \, dx/2 \, \{ \, y^2 + 2 \, y \, c \, dy + c(c-1) \, dy^2 \, \} \tag{8.6}$$

$$\Delta E = E_2 - E_1 = c \, \rho \, g \, dx \, dy \, \{ \, y + (c-1) \, dy/2 \, \} \tag{8.7}$$

The above equation (eqn 8.7) expresses the energy required to entrain air at depth y, the resulting air concentration being c.

8.4.3 AIR CONCENTRATION

The mechanism of air-entrainment in breaking waves is similar to that of air-entrainment from plunging liquid jets. The main differences between the two processes are:

a) In plunging jets, as reviewed in the literature, the process is a steady state one, whilst in the present case it is a transient process.
b) The width of the plunging liquid jets ejected from a nozzle is generally constant along the length of the jet, whilst in breaking waves the width varies, having the smallest size at the tip. An equivalent width is therefore used.

Bearing in mind the broad scatter of the results for the air-entrainment in liquid jets and the number of variables that one may use in predicting air concentration values, the equations derived from the experimental data by McKeogh and Ervine (1981) may be used to give an estimate of the energy dissipated by air bubbles in breaking waves.

Assuming the height of fall of the liquid plunging jet is equal to the breaker height, H_b, and that the width of the jet, for a typical breaker, is about one fifth of the breaker height (fig. 8.3), then

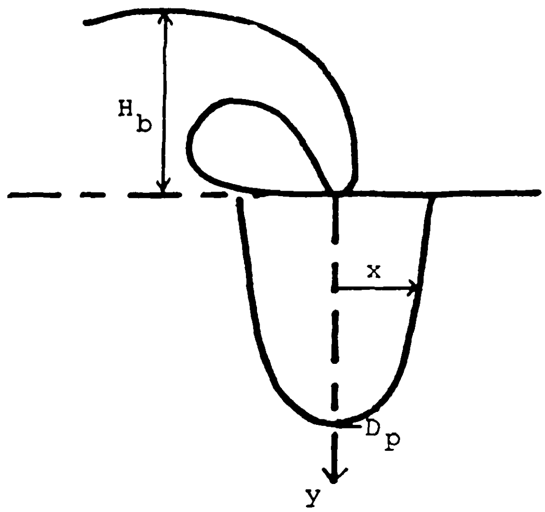

Fig. 8.3 Air entrainment region.

$$D_p = 4.2\ H_b^{0.7} \qquad \text{(in SI units)} \qquad 8.8$$

and
$$C_c = \frac{0.4}{1 + 3\ (y/D_p)^3} \qquad 8.9$$

$$C = C_c \frac{1}{1+5(x/x_b)^2+10(x/x_b)^3}\ , \quad x_b = D_p/4 \quad \text{for the upper half} \qquad 8.10$$

$$C = C_c\ (1 - x/x_b) \qquad x_b = D_p/10 \qquad \text{for the lower half} \qquad 8.11$$

where D_p is the depth of penetration,
x is the distance from the centre of the jet,
C is the air concentration,
C_c is the air concentration at the centre line.

8.4.3 NUMERICAL SCHEME - RESULTS

The static energy stored in the bubbles in an infinitesimal area, dx dy, as derived in equation 8.7 and neglecting the product dx.dy.dy/2 is

$$dE_{st} = \rho \; g \; dx \; dy \; c(x,y) \; y \qquad 8.12$$

$$E_{total} = \rho \; g \int_{x_b}^{-x_b} \int_0^{D_p} c(x,y) \; y \; dx \; dy \qquad 8.13$$

The potential energy stored in the air bubbles is computed using numerical integration (Simpson's rule) over a range of breaking wave heights. The results are shown on a graph of $E/2\rho g$ against breaker height, H (fig. 8.4).

As expected, the energy associated with air entrainment increases in a non-linear fashion with breaker height. A most useful quantity however, is the proportion of the wave energy, that is converted into potential energy, associated with air entrainment. Such an estimate is obtained by

a) considering the wave energy of a regular wave before breaking,
b) estimating the energy loss in air entrainment, as described above,
c) finding the proportion of b) to a).

The total wave energy of a regular wave, wavelength L and height H, using linear theory, is

$$E = \frac{1}{8} \rho \; g \; H^2 \; L \qquad 8.14$$

and therefore

$$\frac{E}{2\rho g} = \frac{1}{16} H^2 L \qquad 8.15$$

The variation of $E/2\rho g$ of regular waves, against H for various values of L is also plotted on figure 8.4. The proportion of the wave energy converted into potential energy and stored in the air bubbles may be directly derived, for any given wave height and wavelength by simply dividing the ordinates of the two curves, corresponding to the regular and the breaking wave heights, respectively. For a 2m wave with wavelength 14m, 1/4 of the wave energy is dissipated due to air entrainment. This value falls within the range of empirical values used in coastal studies.

For the same wave height, the steeper the breaker, that is the shorter the wavelength, the higher the proportion of energy dissipation. This result arises from the assumption that the energy associated with air entrainment depends only on the

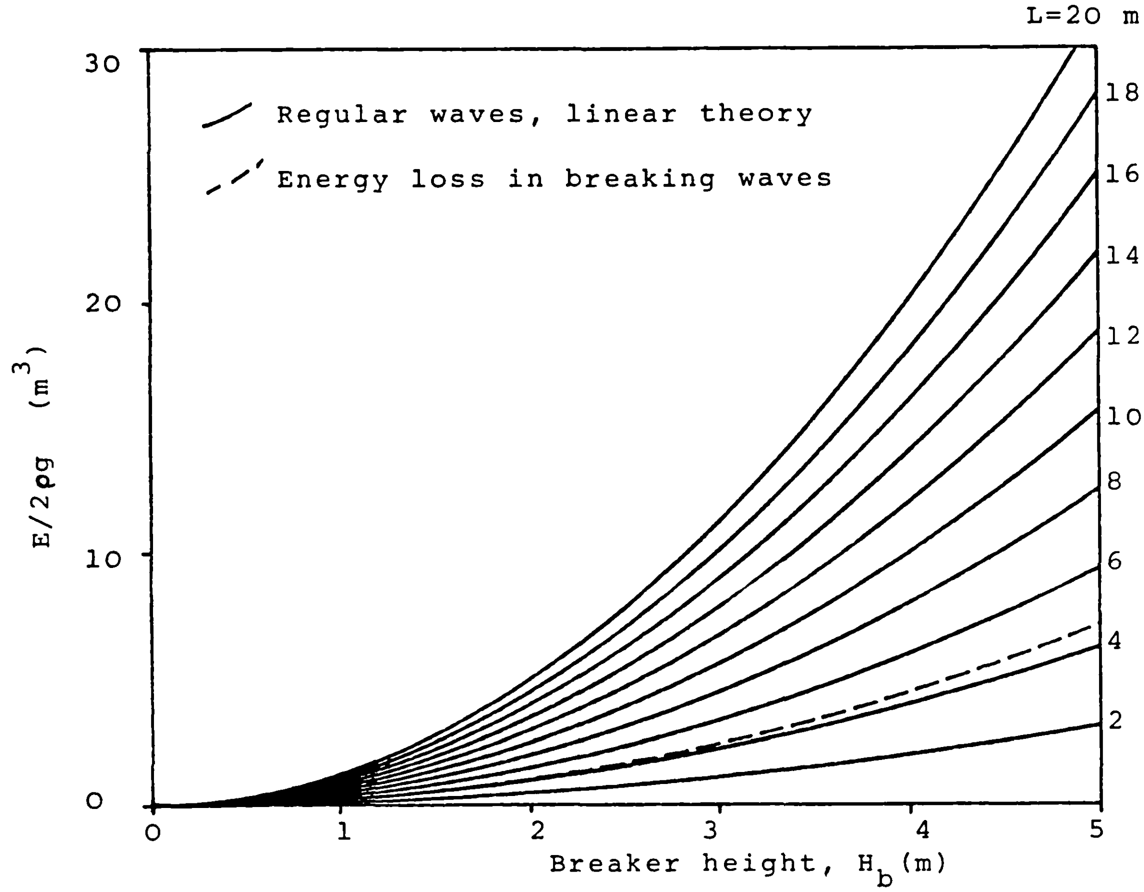

Fig. 8.4 Model results. E/2ρg against H for different L.

breaker height and that the jet hits the surface vertically. When the angle of incidence in inclined, secondary spash- jets are formed, which entrain in turn air. This process is not considered in the present model. Physical models have to be used instead. The advantage of mathematical models, however approximate they might be, is that they can assess the effects of scaling, as the physical mechanism is incorporated in them. In physical models geometric similarity is commonly satisfied, that is, model and prototype waves have the same steepness.

An alternative plot obtained from the numerical scheme is the variation of $E/2\rho g$ with H for various values of wave steepness H/L (fig. 8.5). The derived plot indicates that the energy dissipation due to air entrainment in fully dissintegrated jets does not follow Froude scaling law. **Smaller** waves lose **greater** proportion of energy than bigger ones, all having the same steepness. This may be explained by considering the physics behind the process of wave energy transformation. The kinetic energy of the plunging wave jet is partly converted into kinetic energy of the air bubbles. The bubbles penetrate the receiving water mass up to a depth at which their kinetic energy is all converted into potential energy. The depth of penetration, which is associated with the potential energy, does not follow geometric

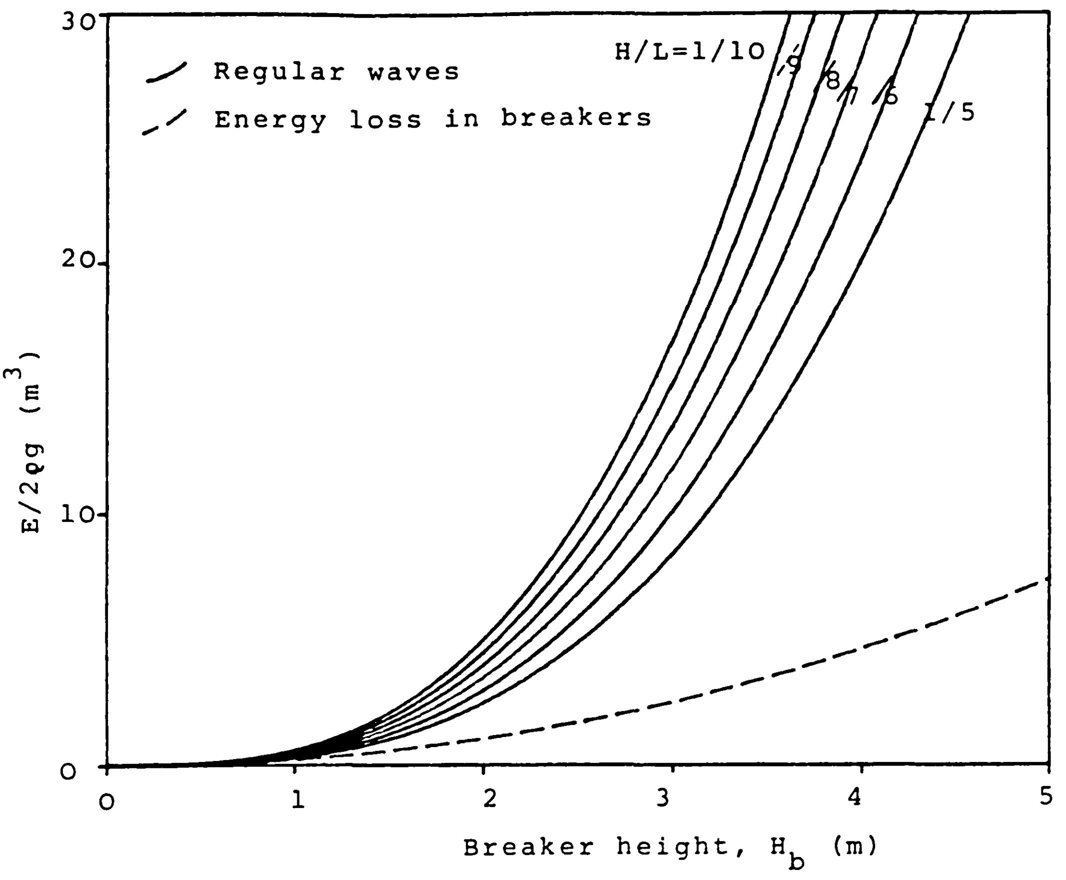

Fig. 8.5 Model results. $E/2\rho g$ against H for different breaker steepness, H/L.

similarity scaling laws, D_p=4.2$H_b^{0.7}$. Doubling the height of fall, does not produce doubling of the penetration depth; the depth increases 1.62 times instead of 2 times, hence less potential energy is stored in the bubbles and less proportion of the wave energy is lost due to air-entrainment.

8.4.5 DISCUSSION ON THE PROPOSED MODEL

The presented model aims primarily in establishing a **physical** mechanism for the process of air entrainment in breaking waves and secondly, in providing a first estimate of the energy associated with this process. In the absence of experimental data on the actual process, the empirically derived properties of the similar phenomenon of air entrainment due to plunging liquid jets ejected from a nozzle are employed. The similarity between the two processes is based on both visual observations and theoretical analysis of the segmentation of the overturning jet of a breaking wave into jets. The approximations and assumptions made in deriving the presented results impose certain limitations on the interpretation of the results.

Firstly, the horizontal velocity of the plunging jet is not considered. Although this factor might not have a considerable effect on the air concentration, it nevertheless affects the secondary jet-splash system; the more the secondary splashes, the more the energy loss.

Secondly, the angle of incidence of the plunging jet, which depends on the wave steepness is not considered, a factor which affects the air concentration.

Thirdly, the empirically derived formulae used in the presented model are not the ideal ones. A more relevant empirical study might have been the study of air entrainment due to the free fall of a sheet of water, like the experimental set-up illustrated in the video cassette, where the segmentation process was visualised.

The quantitative results of the model suggest that for a typical breaking wave with H/L=1/7, 20-30% of the wave energy is dissipated during breaking, for wave heights 2-3m. For fully dissintegrated jets, and the same wave steepness, the bigger the wave height, the less the proportion of energy dissipation due to air entrainment. In small waves, where little or no jet dissintegration occurs, the air entrainment is very little and hence the proportion of the energy loss will tend to zero.

Model tests with breaking waves cannot scale accurately the energy transfer process taking place during breaking. Knowledge however, of what the effects of scaling are, is of vital importance for the interpretation of the results. The presented approach throws some light on this problem and it also provides a tool for use in numerical models which require a means for changing the wave characteristics after wave breaking. Knowing the breaking wave height, an estimate of the energy loss due to air entrainment may now be easily obtained and the reduction in wave height, assuming the wave has not altered its form, may be calculated.

8.5 CONCLUSIONS

The physical mechanism of air entrainment in broken waves has been presented. The segmentation of the tip of the overturning face of breaking waves into jets enables the application of the knowledge on the characteristics of plunging liquid jets ejected from a nozzle, on the breaking wave problem.

A method for the estimation of the proportion of energy conversion from wave energy into potential energy in air bubbles entrained during plunging has also been presented. Although further work is required in obtaining relevant experimental results, general characteristics of scale effects were derived. Some estimates of the energy loss due to air entrainment were also obtained.

The problem of air entrainment in breaking/ broken waves and the associated dissipation of energy is far from a complete solution. The presented ideas advanced the initial ideas put forward by Fuhrboter by a step further, based on the identification of the formation of circular plunging liquid jets on the tip of an overturning wave. The combination of theory with experimetal results indicates the direction that is required to be followed in the understanding of the problem, "*for without theory practice is myopic, as without practice theory is uninformed*" (Cooper, 1988).

CHAPTER 9

SUMMARY - DISCUSSION

9.1 INTRODUCTION

Features of breaking/ broken waves have been studied experimentally and explained using novel ideas. The stages of this study are described and discussed in detail in each individual chapter. In this chapter, the main points and conclusions of the thesis are brought together.

In section 9.2 the contributions of this study on experimental aspects are summarised, and a brief summary of the obtained experimental data is presented in section 9.3.

The distinct stages of the breaking/ broken wave process identified in the thesis, and treated individually, are tied together into a continuous sequence of events (section 9.4). The problem of scale effects is then reviewed in the light of the proposed models (section 9.5).

The problem of the physics of breaking/ broken waves may be simulated to other processes. Such a process is described in section 9.6. A number of alternative processes were also considered in this study, but attempts to investigate them further proved fruitless. The philosophy that initiated the investigation of those processes and the stage reached, as well as recommendations for future work, are presented in section 9.7. Finally an epilogue concludes the thesis.

9.2 EXPERIMENTAL CONSIDERATIONS

Four main experimental problems were tackled:

a) The development of software so that the experimental process is accurately controlled. Programs were written by the author in low level language in order to achieve high operational speed on the one hand and save memory space on the other hand.

b) The Fiber Optics Laser Doppler Anemometer, FOLDA, posed great problems regarding the optimum conditions for its operation. The determination of the proper seeding material and the method of mixing it with the water proved a most frustrating and at the same time exciting task.

c) The absence of an analytical method for the generation of breaking waves in the laboratory initiated the search for such a solution. The answer was revealed unexpectedly when it was noticed that the rate of change of frequency of impulsively generated waves is the reverse of the rate of change of frequency of the wave maker generating deep water breaking waves, as proposed by Longuet-Higgins (1976). The time symmetric property of the laws of nature, coupled with the mathematical solution of the motion induced by a local concentration of energy, provided the answer to the problem of the generation of breaking waves in water of finite depth in the laboratory.

d) A technique used extensively in other fields of science, is image processing of video pictures. Computer software were written by the author and used on breaking waves. Computer enhanced pictures showed more clearly the segmentation process of overturning waves. The most remarkable application of this technique is in the measurement of velocities. The velocities at the wave boundary are firstly visualised and secondly, they are easily quantified. The achievement of the same effect with traditional methods would require much time and effort, whilst this tecnique is fast, simple and most of all, accurate and reliable.

9.3 EXPERIMENTAL DATA

Transverse velocity time histories were measured around two different breakers. In the absence of comparable experimental data, an early prediction was made. The philosophy behind this prediction is that, since wave breaking induces unorganised, chaotic, turbulent, three dimensional motion, a sudden increase of activity is initiated on wave plunging which decays with time and eventually comes to rest. The general form of this heuristic prediction proved to be correct. However, the Fourier components of this motion have periods far exceeding the "turbulent" range (generally less than 0.1 sec). Another unexpected observation is the presence of a standing wave across the flume. The physical justification of this motion posed a most interesting challenge.

A further experimental observation which initiated a lot of thinking is the presence of transverse features on the otherwise two-dimensional overturning wave crest. A link was suspected between the measured low frequency motion and the segmentation of the plunging jet.

9.4 THEORETICAL CONTRIBUTIONS

The wide range of aspects covered in the literature review proved invaluable in the development of the theoretical models. Classical ideas, ranging from the Cauchy-Poisson (1815) problem, to Plateau's (1864) surface tension works, to Lord Rayleigh (1898), Longuet-Higgins (1980) and Jansen (1986) have been employed in the thesis. These ideas have been used with the author's own ideas in the development of the following physical/ theoretical models.

a) The overturning face of the wave segments due to surface tension into an irregular shape. The transition from a smooth, horizontal cylindrical edge into a series of tongue-like plunging jets is described analytically by combining the two predominant forces, gravity and surface tension, into a single numerical model. The results from this model are used to quantify scale effects in breaking waves. The experimentally derived conclusion that, breaking waves of height less than 0.5m cannot be scaled up using gravity scaling laws, is derived for the first time analytically using the presented model.

b) The overturning jet penetrates the receiving water body like a solid body. Macroscopically, the irregularities of the plunging face are negligible compared to the overall shape of the jet. From this point of view, a two-dimensional wave disturbance is generated propagating both shorewards and offshorewards from the plunging point. This motion is modelled using the formulations of a local depression of the water surface. The general characteristics of the offshorewards travelling wave disturbance as recorded experimentally are in reasonable agreement with the theoretical predictions. This modelling, when applied to shallow water conditions predicts the formation of a bore travelling with the depth limited velocity $\sqrt{gh}$. This prediction is in line with the bore simulation used in the past for surf zone models.

c) Microscopically, the plunging face of the wave is considered as the summation of a series of bell-shaped sinusoidal jets. Each of these jets generates radial waves, the superposition of which produces the kinematics field associated with the plunging of the wave. A three-dimensional, unorganised motion is derived, the temporal and spacial distribution of which agrees reasonably well with the measured motion. This model shows that two-dimensional breaking waves incident normally on a beach present a source of longshore wave motion. The radial waves generated by each jet have a continuously increasing frequency. The resultant motion therefore, consists of a continuous wide range of frequency components. A standing wave will result when the transverse, or longshore broken wave motion is bounded in an area of discreet natural modes of oscillation. This new proposition may have potential applications in the understanding of physical processes taking place in the coastal region and are not yet fully understood.

d) Wave energy is converted, during the breaking/ broken wave process, into other forms of energy. A significant proportion of the wave energy is dissipated by air entraining the water mass. In the absence of data regarding air entrainment in breaking waves, the characteristics of the similar process of plunging liquid jets ejected from a nozzle are employed. The potential energy of the air concentration is obtained from first principles and design curves are hence derived predicting the proportion of wave energy dissipated in the form of air entrainment in breaking waves of different wavelengths and heights.

The distinct processes identified in the breaking/ broken wave process are described both physically and analytically. Emphasis is placed on the physical aspect, since the characteristics of these processes are universal and a sound understanding of their physics is vital in studying their particular application on breaking waves.

The proposed models of the different stages of the breaking/ broken wave process, namely,

a) segmentation,

b) induced broken surface wave motion, and

c) air entrainment

tie well together, from the physics point of view, as described above. Their link however, is not so strong when it comes to the quantitative description of the whole process. The main reason lies probably in the random nature of all three physical processes.

The segmentation of the tip of the overturning wave depends on the form of the initial disturbance across the crest. At present, the form of this disturbance cannot be experimentally described. The prediction of the shape and size of the disturbance remains a problem to be solved. In the case when the disturbance has *white noise* characteristics, the wavelength of the predominant sinusoid may be obtained.

The broken surface wave motion produced by the penetration of each individual jet has a predominant wavelength of the same order as the diameter of the jet. The three dimensional surface wave motion depends strongly on the nature of the plunging face. The description of this random mode of plunging is not yet possible. Under "controlled" experimental conditions the *microscopic* picture of the overturning stage varied considerably from wave to wave, although *macroscopically* they all appeared the same.

The splash following the initial plunging is much more sensitive to these microscopic characteristics. In many cases, like the ones tested in the laboratory, the splash may be higher than the incident wave and its effect on the broken wave motion is quite significant. These random factors do not undermine the validity of the arguments on which the model is based. On the contrary they highlight the complexity of the problem and support the use of random functions for the probabilistic prediction of the broken wave motion.

Regarding the problem of air entrainment in broken waves, the whole model is based on the argument that the overturning face of the wave is affected by surface tension in the same manner as liquid jets ejected from a nozzle. The quantitative predictions of this model do not depend on the numerical results of the segmentation or broken wave models. The empirically derived formulae used in this model take into account the physical process taking place during the free fall of the jets.

As a conclusion it may be said that the distinct processes modelled and presented in this thesis tie well together as far the physics is concerned. The random nature of all these processes, which is not described yet, does not allow quantitative linking of the individual models. More experimental work is required, both in the laboratory and the field, to verify the applicability of the proposed physical models and hence provide quantitative information for use as input data into the numerical models.

9.5 SCALE EFFECTS IN BREAKING/ BROKEN WAVES

It has been shown that the breaking/ broken wave process is affected by different factors during the individual stages into which the process is decomposed. Before reaching the breaking point (see fig. 2.1) the wave motion is predominantly governed by gravity. The Froude scaling law is therefore the appropriate similarity criterion.

During the free fall of the plunging jet, or overturning process, surface tension plays an important role. Surface tension effects are scaled using the Weber scaling law, which is different from the gravity scaling law. As surface tension affects strongly fluid bodies with high curvatures, or small radii of curvature, its *global* effects are minimal in big breakers, H_b>0.5m. This theoretical and experimental observation does not mean that surface tension has negligible effects in such big waves; it rather suggests that the characteristics of the incident wave do not affect the segmentation of the overturning wave. Model tests with breaking waves having H_b>0.5m take into account surface tension effects in the same manner as in full scale waves.

The induced broken wave motion is governed by gravity. However, the mechanism initiating this motion depends on surface tension. As a result, true representation of the three-dimensional broken wave field requires model wave heights greater than 0.5m. In the case however, where the two-dimensional shoreward broken wave motion is of interest, Froude scaling provides a good approximation.

During the 2-dimensional breaking/ broken wave process, wave energy is transformed mainly into:

a) turbulent kinetic energy,
b) 3-dimensional surface wave energy,
c) potential energy in air-entrainment,
d) seaward travelling wave disturbance,
e) sound.

Scaling of the energy transformation requires appropriate scaling of all the individual processes. The turbulent kinetic energy is modelled using Reynold's scaling law (viscosity /inertia scaling law). The broken wave motion depends not only on the initial motion initiated by the penetration of the plunging face of the wave, as modelled in the thesis, but also on the subsequent splashes. As shown by Peregrine (1981), the evolution of a splash depends also on the turbulent motion of the water body forming the splash. As a result, the overall broken wave motion is affected by gravity, surface tension and viscous forces. The potential energy associated with air entrainment cannot be satisfactorily scaled, at present, due to the lack of a complete theoretical model describing the process and the absence of suitable experimental results. The seaward travelling wave disturbance is a gravity effect whilst the sound produced at breaking is a function of the air entrainmnent.

Prediction of the energy dissipation in breaking waves is a most difficult problem. The inability of physical model tests to scale the above process enhances the need for the development of theoretical models.

9.6 SIMILAR PROCESSES

A simple physical process, equivalent to the breaking/ broken wave process is the free fall of jets, in the form of water emerging from a hose, when watering the garden say, or slow flows from a tap.

In both cases, the water initially has the form of a smooth cylindrical surface. Further away from the exit point, it is seen that the body has no longer a smooth cylindrical shape. It tends to form spherical droplets. At a certain distance a break–up point is observed, where the cylindrical surface turns into a sequence of isolated spheres.

If these drops hit a pond, or a bucket of water, it is observed that circular waves are emitted from the plunging point. Bubbles are also seen emerging from the initially undisturbed water, which burst on the surface. At the same time, a sound is heard. A splash is also formed which, depending on the jet velocity and the angle of impact, generates a series of jet–splash systems.

The physical laws governing this process are the same as that of the **segmentation** of the tip of the overturning wave, in which case the cylinder is horizontal, and the consequent **induced surface wave motion**, **turbulent motion due to fluid shearing**, **air entrainment**, **sound generation** and **splash formation**. This process takes place over such a short time that the transition from one stage to the other is not distinguishable by the naked eye.

The described simple physical process may be easily performed by the reader. Under steady state initial flow conditions, it will be observed that the resulting surface wave motion is not a steady state one. The induced kinematics field changes randomly with time, although the initial conditions of the cylinder are the same. This observation highlights the sensitivity of the whole process on the form of the initial disturbance on the cylindrical surface. This disturbance is very small and whatever precautions one may take, it cannot be eliminated.

9.7 ALTERNATIVE PROCESSES - SCOPE FOR FURTHER RESEARCH

The development of the above models used information scattered over a wide range of publications. In the course of this thesis many more reviews other than the ones presented were compiled in efforts to present new models associated with breaking waves. Some of them reached a dead end due to lack of theoretical support, some due to lack of facilities to cover missing data and some because it was found by others that a dead end lies ahead.

9.7.1 SOUND PRODUCED BY BREAKING WAVES

Many people say that they can recognise a breaking wave from its sound. They can tell whether it is big or small, plunging or spilling. The question that was attempted to tackle was: "if ordinary people can describe breaking waves from their sound, why scientists cannot". In a brief review of adjectives used in poetry and literature referring to breaking waves it was found that big waves are associated with *heavy*, low frequency sounds (*growl, thunder, roaring*), whilst small ones with *sweet*, high frequency sounds (*lullaby*).

Literature on this problem is not widely available. One of the reasons might be the importance of this topic for military purposes. The author collected underwater sound records associated with breaking waves, using an ordinary microphone. The records were then analysed at the British Library, National Sound Archive. Spectral analysis and sound intensity for different breakers were obtained. The presence of noise and the simplicity of the available equipment did not enable the derivation of useful information.

Research on the measurement of rainfall is concentrating on monitoring the underwater sound generated by raindrops striking the surface of a large body of water (Nystuen, 1986). The frequency of the sound produced by a single drop is inversely proportional to the radius of the drop, that is, big drops generate heavy sounds and small drops high frequency sounds.

This technique might be used in monitoring breaking waves in the sea. Interpretation of sound records, which are relatively cheap to obtain, might in the future describe the size and shape of breaking waves. For the time being, there are many practical problems for calibrating such a technique. Firstly, laboratory studies are hindered by the limited space usually available. Theoretical models apply in the far field, that is, distances bigger than the wavelength of sound. Laboratory studies are therefore not feasible. Secondly, in the field, breaking waves are usually associated with wind. Recording of sound under such conditions is distorted by the wind generated sound, filtering of which is not easy.

9.7.2 BEACH CUSPS

The formation and spacing of beach cusps (concave seaward cuspate patterns that tend to occur with a regular longshore spacing, plate 9.1), under breaking wave conditions incident normally on a uniformly sloping beach is a problem that remains unanswered. This phenomenon is explained quite well in the case of non-breaking waves on reflective systems, steep beaches (Battjes, 1988).

In the light of the proposed mechanism of transverse wave motion generation by two-dimensional breaking waves, the beach cusp problem may be approached from a new angle. Experimentally, it is proposed to investigate the transverse motion induced by regular waves breaking over the horizontal part of a composite slope. The proposed model predicts the formation of a standing wave across the channel. If the width of the channel is changed a different mode of harmonic oscillation will result. The predominant frequency of the breaker induced transverse wave motion may therefore be deduced. It is predicted that this frequency is related to the size of the breaker and not the period of the incident regular waves. This prediction is in agreement with laboratory and field data on beach cusps. The spacing of beach cusps associated with breaking waves is related to the breaker height (Komar, 1976), whilst for those associated with non breaking waves it is related to the incident wave period (Bowen and Huntley, 1984).

It is hoped that such an experiment will sometime be performed in a suitable wave channel and throw some light on this problem.

9.7.2.1 **Beach cusps and Plateau's rule**

The segmentation of the crest of an overturning wave was also proposed in the past as a possible explanation for the formation of beach cusps. Cloud (1966) mentioned that "*a breaking wave, of course, approximates a cylindrical form and, at the instant of collapse, it may shoot forward a regularly spaced array of jets that correspond to the segmentation of the cylindrical rim specified by Plateau's rule*". However, Cloud probably considered the cylindrical form to correspond to the one with **diameter the breaker height**, as he also stated that "*if this hypothesis were true, the average spacing of beach cusps would reflect the height of the waves that produced them.*"

Komar (1976) investigated Cloud's proposition. He considered the relationship between beach cusp spacing and breaker height, and rejected the hypothesis on the

Plate 9.1

Beach Cusps in Famagusta Bay, Cyprus

grounds of the discrepancy between the available data and the theoretical predictions. The physics behind Cloud's proposition were not discussed. It is also evident from the discussion that Komar had considered neither Plateau's experiments nor Worthington's hypothesis, on whose work Cloud based his argument.

In the light of the description of the segmentation process of the crest of an overturning wave (chapter 6), it is evident that Cloud misinterpreted Worthington's hypothesis and Komar failed to recognise this. In a personal communication with Cloud, the author pointed that Plateau's segmentation theory should apply to the liquid cylinder forming the edge of the breaker, and not to the hollow cylinder having as diameter the breaker height. Cloud's response was that he finds *no fault* with the author's interpretation and recommends the edge-wave literature for the explanation of the cusp formation.

The above publications misled the author at the initial stages of the work. It is the study of the original works of Plateau and Worthington that provided the stamina and courage to overcome the "obstacle" posed by Cloud's and Komar's publications and to propose an alternative mechanism that links the segmentation of the breaking wave to the beach cusp formation.

9.7.3 CROSS WAVES

An idea that was tested was whether the experimentally observed standing wave motion is cross wave motion. Cross waves are defined as, standing waves with crests at right angles to the primary wave direction. They generally have half the frequency of the primary wave (Garrett, 1970).

Cross waves derive their energy from the wave maker and not from the primary motion. The wave maker is about 30 metres away from the plunging area. The continuously varying frequency of the wave maker motion and the long distance separating the breaker region from the wave maker make the speculation of the cross wave generation an almost impossibility. The observed standing wave motion therefore results from the breaker and not the wave maker.

9.7.4 AIR-ENTRAINMENT IN OVERTURNING WAVES

Air entrainment in the coastal environment was treated in chapter 8. In the case of loading on structures by breaking waves, the modelling of air entrainment is of vital importance, since it affects significantly the intensity of the forces transmitted by the waves on to the structures. Structures arrest the momentum of the overturning waves. The force acting on the structures equals the rate of change of momentum of the wave, that is, the slower the process the less the magnitude of the force. The presence of air in the water- solid impact has the effect of prolonging the momentum change and reducing the force, acting thus as a "cushion".

The segmentation model proposes an increase of the surface area, thus enhancing the air entrainment in the overturning process. Further work is required on these lines in order, firstly to quantify this effect and secondly, to calibrate the model for use in wave loading studies.

9.8 EPILOGUE

The breaking/ broken wave problem has been presented in a new context. By concentrating on the physics behind the process analytical/ computational models have been derived which open new horizons in the understanding of this complex problem.

It is hoped that the contributions on the experimental techniques, generation of breaking waves, operation of the Fiber Optics Laser Doppler Anemometer, use of image processing will be found useful by researchers on this and similar fields.

The unique data collected revealed some exciting results. It is hoped that the methods introduced in the interpretation of this data will find support and be as successfully used in other hydraulics studies.

Studying breaking waves is a fascinating job. At this high-technology age, this classical problem presents a challenge to scientists, artists and above all engineers who face the task of fighting and/or working with them.

Our success lies in how well we **understand** breaking and broken waves. This study has put an extra *brick* on the *wall of the general knowledge* on the field on the one hand, whilst on the other hand it has identified an *empty bucket* in which it has put the *first drops*.

REFERENCES

REFERENCES

Basco D.R. (1985)
A qualitative description of wave breaking. ASCE, Journal of Waterway, port, coastal and ocean engineering, vol. 111, no. 2.

Battjes J.A. (1974)
Surf similarity. Proc. 14^{th} Int. Conf. on Coastal Eng., pp. 466-480.

Battjes J.A. and Sakai (1980)
Velocity field in a steady breaker. Proc. 17^{th} Int. Conf. on Coastal Eng., pp. 499-511.

Battjes J.A. (1988)
Surf-zone dynamics. Ann. Rev. Fluid Mech., vol. 20, pp. 257-293.

Bowen and Huntley (1984)
Waves, long waves and nearshore morphology, Marine Geology, vol. 60, pp. 1-13.

Bradshaw P. (1971)
An introduction to turbulence and its measurements. Pergamon press.

Bryant A.R. (1945)
Surface waves produced by underwater explosions. Comparison of the theory of W.G. Penney with experimental results from a 32-lb charge. As Penney (1945), pp. 701-706.

Bogy D.B. (1979)
Drop formation in a circular liquid jet. Ann. Rev. Fluid Mech., vol. 11, pp. 207-228

Burnside W. (1888)
On deep water waves resulting from a limited original disturbance. Proc. London Math. Soc., vol XX.

Charlesworth G. (1945)
Surface waves produced by firing underwater 32-lb charges of Polar Ammon Gelignite at various depths. As Penney (1945), pp. 695-700.

Cloud P.E. (1966)
Beach cusps: Responce to Plateau's Rule ? Science, vol. 154, pp. 890-891.

Cokelet E.D. (1977)
Breaking waves. Nature, vol 267, pp. 769-774.

Cokelet E.D. (1979)
Breaking waves - The plunging jet and interior flow field. Publ. in Mechanics of wave induced forces on cylinders, ed. Shaw.

Dalrymple R.A. (1976)
Wave-induced mass transport in water waves. ASCE, Journal of Waterways, Harbours Coastal Eng. Div. 102(WW2) pp. 255-264.

Dalton S. (1983)
Split Second. The World of High-speed Photography. Publ. J.M. Dent & sons Ltd, London.

Dombrowski N. and Frase R.P. (1954)
A photographic investigation into the disintegration of liquid sheets. Phil. Trans. Roy. Soc. Lon., ser A, vol. 247, pp. 101-130.

Dombrowski N. and Johns W.R. (1963)
The aerodynamic instability and disintegration of viscous liquid sheets. Chemical Eng. Science, vol. 188, pp. 203-214.

Easson W.J. and Greated C.A. (1984)
Breaking wave forces and velocity fields. Journal of Coastal Eng., Vol. 8, pp. 233-241.

Eckart C. (1948)
The approximate solution of one-dimensional wave equations. Review of modern physics, vol. 20, No.2, pp. 399-417.

Ervine D.A., McKeogh E.J. and Elsawy E.M. (1980)
Effect of turbulence intensity on the rate of air entrainment by plunging water jets. Proc. Inst. Civ. Eng., Part 2, 1980, vol. 69, pp. 425-445.

Flick, Guza and Inman (1981)
Elevation and velocity measurements of laboratory shoaling waves. Journal of Geophysical Research, vol. 86, pp. 4149-4160.

Fuhrboter A. (1970)
Air entrainment and energy dissipation in breakers. Proc. 12th Int. Conf. on Coastal Eng.

Fuhrboter A. (1986)
Model and prototype tests for wave impact and run-up on a uniform 1:4 slope. Coastal Eng., vol. 10, pp. 49-84.

Galvin J.G. (1968)
Breaker type classification on three laboratory beaches. Journal of Geophysical Research, vol. 73, no. 12, pp. 3651-3659.

Garrett C.J.R. (1970)
On cross-waves. J. Fluid. Mech., vol. 41, part 4, pp. 837-849.

Guza R.T. and Davis (1974)
Excitation of edge waves by waves incident on a beach. Journal of Geophysical Research, vol. 79, no. 9.

Guza R.T. and Inman (1975)
Edge waves and beach cusps. Journal of Geophysical Research, vol. 80, pp. 2997-3012.

Guza R.T. and Bowen A.J. (1976)
Finite amplitude edge waves. Journal of Marine Research, vol. 34, pp. 268-293.

Hattori and Aono (1985)
Experimental study on tirbulence. Structures under breaking waves. Proc. Coastal Eng. in Japan, vol. 28, pp. 97-116.

Hedges T.S. and Kirkgoz M.S. (1981)
An experimeantal study of the transformation zone of plunging breakers. Journal of Coastal eng., vol. 4, pp. 319-333.

Horikawa K. and Kuo C.T. (1966)
A study of wave transformation inside the surf zone. Proc. 10th Int. Conf. on Coatal Eng., pp. 217-233.

Jansen P.C.M. (1986)
Laboratory observations of the kinematics in the aerated region of breaking waves. Journal of coastal engineering, vol. 9, pp. 453–477.

Johnson J.W. and Bermel K.J. (1949)
Impulsive waves in shallow water as generated by falling weights. Trans. Amer. Geophysical Union, vol. 30, No. 2, pp. 223–230.

Joordan J.M. (1965)
Water waves generated by underwater explosions. Proc. specialty conf. on Coastal Eng., Santa Barbara, California, pp. 69–85.

Joordan J.M. (1966)
Model studies of impulsively-generated water waves. Proc. 10^{th} Int. Conf. on Coastal Eng., pp. 434–454.

Joordan J.M. (1972)
Impulsive waves: model and prototype correlations. Advances in Hydroscience, vol. 8, pp. 261–304.

Kelvin, Lord (1904)
On deep water two-dimensional waves produced by any given initiating disturbance. Philosorhical Magazine, 6^{th} ser., vol. 7, pp. 609–620.

Kirkgoz M.S. (1986)
Particle velocity prediction at the transformation point of plunging breakers. Journal of coastal engineering, vol. 10, pp. 139–147.

Kjeldsen S.P. and Myrhaug (1979)
Breaking waves in deep water and resulting wave forces. Proc. 11^{th} Annual Offshore Technology Conf., pp. 2515–2522.

Kjeldsen S.P. and Myrhaug (1980)
Wave-wave interactions, current-wave interactions and resulting extreme waves and breaking waves. Proc. 17^{th} Int. Conf. on Coastal Eng., pp. 2277–2303.

Kjeldsen S.P. (1982)
2- and 3-Dimensional deterministic freak waves. Proc. 18^{th} Int. Conf. on Coastal Eng., pp. 677–694.

Kjeldsen S.P. (1984)
The experimental verification of numerical models of plunging breakers. Proc. 19^{th} Int. Conf. on Coastal Eng., pp. 15–30.

Komar P.D. (1976)
Beach processes and sedimentation. Prentice-Hall.

Kranzer H.C. and Keller J.B. (1959)
Water waves produced by explosions. Journal of applied physics, vol. 30, No. 3, pp. 398–407.

Kumagai M. and Endogh K. (1982)
Effects of kinematic viscosity and surface tension on gas entrainment rate of an impinging liquid jet. Journal of Chem. Eng. Japan, vol. 15, no. 6, pp. 427–433.

Lamb H. (1904)
On deep water waves. Proc. London Mathematical Soc., Ser. 2, vol. II, pp. 371–401.

Lamb H. (1932)
Hydrodynamics. Cambridge Univ. Press, 6th edition.

Launder B.E. and Spaulding D.B. (1972)
Mathematical models of turbulence, Academic Press, London

Le Mehaute B. (1970)
Explosion generated water waves. 8th Symp. Naval Hydrodynamics, Pasadena, pp. 71–94.

Le Mehaute B. (1971)
Theory of explosion generated waves. Advances in Hydroscience, vol. 7, pp. 1–79.

Le Mehaute B., Wang S., Lu C.C. (1987)
Cavities, domes and spikes. Journal of Hydraulic Res. vol 25, pp. 583–602.

Longuet-Higgins M.S. (1953)
Mass transport in water waves. Phil. Trans. of the Royal Soc. of London, Ser. A, vol. 245, pp. 535–581.

Longuet-Higgins M.S. and Turner (1974)
An entraining plume model of a spilling breaker. Journal of Fluid Mech., vol. 63, part 1, pp. 1–20.

Longuet-Higgins M.S. and Cokelet E.D.(1976)
The deformation of steep surface waves on water. Proc. of the Royal Soc. of London, Series A, vol. 350, pp. 1–26.

Longuet-Higgins M.S.(1976)
Breaking waves in deep or shallow water. Proc. 10th conf. on Naval Hydrodynamics,

Longuet-Higgins M.S.(1976)
Recent developments in the study of breaking waves. Proc. 15th Int. conf. on Coastal Engineering, pp. 441–460.

Longuet-Higgins M.S. (1980)
On the formation of sharp corners at a free surface. Proc. of the Royal Soc. of London, Series A, vol. 371, pp. 453–478.

Lighthill J. (1978)
Waves in fluids. Cambridge Univ. Press.

Madsen P.A. and Svendsen I.A. (1983)
Turbulent bores and hydraulic jumps. Journal of Fluid Mech., vol. 129, pp. 1–25.

Mansard and Funke (1982)
A new approach to transient wave generation. Proc. 18th Int. Conf. on Coastal Eng., pp. 710–724.

Massey B.S. (1979)
Mechanics of fluids. 4th ed. Van Nonstrand Reinhold comp., London.

Mc Keogh E.J. and Ervine D.A. (1981)
Air entrainment rate and diffusion pattern of plunging liquid jets. Cham. Eng. Sci., vol. 36, pp. 1161–1172.

Miller R.L. (1976)
Role of vortices in surf zone prediction: sedimentation and wave forces. Publ. Beach and Nearshore Sedimentation, ed. R.A. Davis and R.L. Ethington, pp. 92–114.

Nadaoka K. and Kondoh T. (1982)
Laboratory measurements of velocity field structure in the surf zone by LDV. Proc. Coastal Eng. in Japan. vol. 25, pp. 125–145.

Nakagawa T. (1983)
On characteristics of the water particle velocity in a plunging breaker. Journal of Fluid Mech., vol. 126, pp. 251–268.

New, McIver and Peregrine (1985)
Computations of overturning waves. Journal of Fluid Mech., vol. 150, pp. 233–251.

Penney W.G. (1945)
Gravity waves produced by surface and underwater explosions. Publ. in Underwater explosions research, vol. 2, The Gas Globe, U.S. Office of Naval Res., Washington, 1950, pp. 679–693.

Peregrine D.H. and Svendsen I.A. (1978)
Spilling breaker, bores and hydraulic jumps. Proc. 16^{th} Int. Conf. on Coastal Eng., vol. 1, pp. 540–550.

Peregrine D.H. (1982)
Mechanics of breaking waves – A review of Euromech 102. Publ. in Mechanics of wave induced forces on cylinders, ed. Shaw, pp. 204–214.

Peregrine D.H. (1983)
Breaking waves on beaches. Annual Review of Fluid Mech., vol. 15, pp. 149–178.

Pidduck F.B. (1910)
On the propagation of a disturbance in a fluid under gravity. Proc. Royal Soc. London, vol. 83, ser. A, pp. 347–356.

Plateau J. (1863, 64, 65)
Experimental and theoretical researches on the figures of equilibrium of a liquid mass withdrawn from the action of gravity. Annual Report of the board of the Smithsonian Inst., 1863:207–285, 1864:285–369, 1865:411–435.

Prins J.E. (1957)
Water waves due to a local disturbance. Proc. 6^{th} Int. Conf. on Coastal Eng., pp. 147–162.

Prins J.E. (1958)
Characteristics of waves generated by a local disturbance. Trans. Amer. Geophysical Union, vol. 39, No. 5, pp. 865–874.

Rayleigh, Lord (1878)
On the instability of jets. Proc. London Math. Soc., pp. 4–13.

Rayleigh, Lord (1892)
On the instability of a cylinder of viscous liquid under capillary force. Phil. Mag. and Journal of Science, Ser. 5, vol. 34, No. 207, pp. 145–154.

Rayleigh, Lord (1909)
On the instantaneous propagation of a disturbance in a dispersive medium, exemplified by waves on water deep and shallow. Philosophical Magazine, vol. 18, Ser. 6, pp. 1–6.

Sakai T., Inada Y. and Sandanbata I. (1982)
Turbulence generated by wave breaking on a beach. Proc. 20^{th} Int. Conf. on Coastal Eng., pp. 3–21.

Sawaragi and Iwata (1974)
On the wave deformation after breaking. Proc. 14th Int. Conf. on Coastal Eng., pp. 481-499.

Secker and Warburg (1983)
The Invisible World-Sights beyond the limits of the naked eye. London.

Skladnev M.F. and Popov I.Y. (1969)
Studies of wave loads on concrete slope protections of earth dams. Symp. on Wave Action, Delft, paper no. 7.

Stive M.J.F. (1980)
Velocity and pressure field of spilling breakers. Proc. 17th Int. Conf. on Coastal Eng., pp. 547-566.

Stive M.J.F. (1984)
Energy dissipation in waves breaking on gentle slopes. Proc. 19th Int. Conf. on Coastal Eng., pp. 99-127.

Svendsen I.A., Madsen P.A. and Hansen J. (1978)
Wave characteristics in the surf zone. Proc. 16th Int. Conf. on Coastal Eng., vol.1, pp 520.

Svendsen I.A. and Madsen P.A. (1984)
A turbulent bore on a beach. Journal of Fluid Mech., vol. 148, pp. 73-96.

Svendsen I.A. (1986)
Analysis of surf zone turbulence. Inst. of Hydrodynamics and Hydraulic Eng., Techn. Univ. of Denmark, report no. 333.

Takeda I. and Sunamura T. (1983)
Formation and spacing of beach cusps. Coastal Eng. Japan, vol. 26, pp. 121-135.

Terazawa K. and Ri-Gakushi (1915)
On dep sea water waves caused by a local disturbance on or beneath the surface. Proc. Royal Soc. London, Ser. A, vol. 92, pp. 57-81.

Thomson J.J. and Newall H.F. (1885)
On the formation of vortex rings by drops falling into liquids and some allied phenomena. Proc. Royal Soc. London, vol. 39, pp. 417-436.

Thompson D.W. (1942)
Growth and form. Cambridge Univ. Press.

Unoki and Nakano (1953)
On the Cauchy-Poisson waves caused by the eruption of a submarine volcano. The oceanographic magazine, vol. 4, pp. 119-141, and vol. 5, pp. 1-13.

Van de Sande E. and Smith J.M. (1973)
Surface entrainment of air by high velocity water jets. Chem. Eng. Sci., vol. 28, pp. 1161-1168.

Van de Sande E. and Smith J.M. (1976)
Jet break-up and air entrainment by low velocity turbulent water jets. Chem. Eng. Sci., vol. 31, pp. 219-224.

Vinje T. and Brevig P. (1980)
Breaking waves on finite water depths. A numerical study. The Norwegian Inst. of Technology, Div. of Marine Hydrodynamics.

Wang H. , Sunamura T. and Hwang P.A. (1982)
Drift velocity at the wave breaking point. Journal of Coastal Eng., vol. 6, pp. 121-150.

Worthington M.A. (1879)
On the spontaneous segmentation of a liquid annulus. Proc. Royal Soc. London, vol. 30, pp. 49-61.

Worthington M.A. (1908)
A study of splashes. Longmans, Green and Co., London.

APPENDICES

APPENDIX A

LITERATURE REVIEW ON THE WAVES PRODUCED BY A LOCAL DISTURBANCE ON A WATER SURFACE

A.1 INTRODUCTION

The solution to the problem of the motion generated by a local disturbance on a water surface is found to have a number of applications in this thesis. The composition of a literature review on both the theoretical and experimental aspects of the problem is most essential for the successful use of this solution.

A.2 EVOLUTION OF THE THEORETICAL DEVELOPMENTS

The problem in question was first raised by the French Academy in 1816. Poisson and Cauchy presented their memoirs in which they independently derived a solution which for most purposes can be considered as practically complete.

Lamb (1904) summarised the essential results from the "clouds" of analysis in which Poisson and Cauchy were involved, and put the problem into a simple and easily intelligible shape.

Assuming linear theory and starting from the two-dimensional case, consider the origin being in the undisturbed surface and the y-axis vertically upwards. Bernoulli's equation then gives,

$$p = \rho \left[\frac{\partial \varphi}{\partial t} - gy \right] \qquad \text{A.1}$$

where p is the pressure, ρ the density and φ the potential function which satisfies the continuity equation,

$$\frac{\partial^2 \varphi}{\partial x^2} + \frac{\partial^2 \varphi}{\partial y^2} = 0 \qquad \text{A.2}$$

The elevation, η, of the disturbed surface, supposed free, is given by

$$\eta = \frac{1}{g} \left[\frac{\partial \varphi}{\partial t} \right]_{y=0} \qquad \text{A.3}$$

The kinematic condition is,

$$\frac{\partial \eta}{\partial t} = - \left[\frac{\partial \varphi}{\partial y} \right]_{y=0} \qquad \text{A.4}$$

The solution to this problem for the initial condition of an infinitesimal elevation is

$$\eta = \frac{1}{\pi x} \left\{ \frac{gt^2}{2x} - \frac{1}{3\cdot 5} \left[\frac{gt^2}{2x} \right]^3 + \frac{1}{3\cdot 5\cdot 7\cdot 9} \left[\frac{gt^2}{2x} \right] - \dots \right\} \qquad \text{A.5}$$

From equation A.5 it is evident that the crest, or trough, of the wave is associated with a definite value of $gt^2/2x$ and therefore that it travels over the surface with a **constant acceleration**. It appears that the region in the immediate neighbourhood of the origin may be regarded as a kind of source, emitting on each side an endless succession of waves of continually increasing amplitude and frequency. This persistent activity of the source is due to the assumed initial accumulation of a finite volume of elevated fluid on an infinitely narrow base, which implies an unlimited store of energy. In any practical case however, the initial elevation is distributed over a band of finite breadth. The disturbance at any point can be calculated by superimposing the disturbances produced by the infinitesimal elements that make up the original elevation.

At the initial stages, the various elements reinforce one another. But as time increases, the contributions from the different elements are not in phase any more. The result depends on the shape of the initial disturbance, but it is clear that the increase in amplitude ceases and ultimately a gradual dying out of the disturbance occurs.

Burnside (1888) approached the problem for deep water conditions from a different angle. According to Fourier's theorem, any shape can be expressed as the summation of a series of trigonometric functions. Consequently, the waves generated by a local elevation, constitute the summation of the waves produced by the individual components of the local elevation.

If the water surface is initially displaced and motionless, the surface profile being of the form

$$y_0 = A \cos(mx) \qquad \text{A.6}$$

then the surface elevation as a function of time and space is

$$y = A \cos(mx) \cos(\sqrt{mg}\, t) \qquad \text{A.7}$$

For an initial elevation of the form

$$y_0 = ca^2 /(a^2 + x^2) \qquad \text{A.8}$$

using Fourier's theorem

$$y = \sqrt{\pi}\,\frac{ca}{x}\left[\frac{gt^2}{4x}\right]^{1/2}\exp\left[-\frac{gt^2a}{4x^2}\right]\sin\left[\frac{gt^2}{4x}+\frac{\pi}{4}\right] \qquad \text{A.9}$$

A graphical illustration of the above solution (eqn A.9) is shown in figure A1.

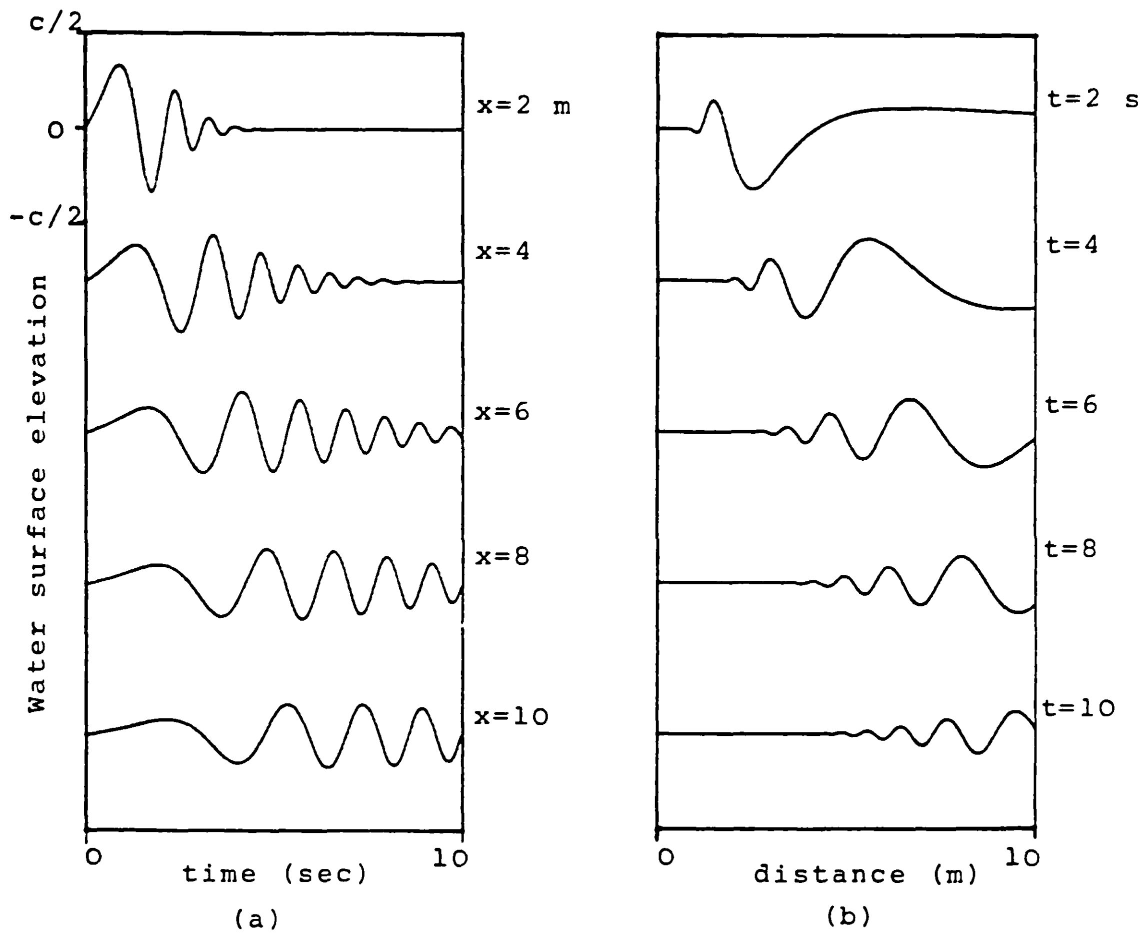

Fig. A1 Graphical illustration of eqn A.9 (a=0.5, c=1 m).
a) Time histories at x=2,4,6,8,10m
b) Surface profiles at t=2,4,6,8,10 sec.

The greatest amplitude at distance x is

$$\eta_{max} = \sqrt{\pi/2}\; c\,\sqrt{\frac{a}{ex}} \qquad \text{A.10}$$

and the amplitude has this value when

$$t = x\sqrt{\frac{2}{ga}} \qquad \text{A.11}$$

The predominant wavelength is therefore

$$L_{pred} = 4\pi a \qquad \text{A.12}$$

Similar expressions can be derived for different forms of initial disturbances. The conclusions from these solutions can be summarised as follows:

a) The greatest amplitude of displacement at any point is proportional to the magnitude of the initial disturbance and inversely proportional to the square root of the distance from the disturbed area.

b) The greatest disturbance is propagated with uniform velocity (eqn A.11).

c) The wavelength of the predominant motion is proportional to the width of the original disturbance (eqn A.12).

Lord Kelvin (1904) solved the Cauchy-Poisson problem in a simpler process. He used the stationary phase method. The result from this method is very similar to the Cauchy-Poisson solution but is obtained far quicker.

The introduction of finite depth was made by Lord Rayleigh (1909) who obtained the first term of a series expansion to the solution of the problem of an infinitesimal disturbance. Lord Rayleigh raised the attention to the fact of the instantaneous propagation of the disturbance which occurs irrespective of the depth being finite or infinite.

One year later, Pidduck(1910) derived the second term of the solution which involved heavy computational work.

Terazawa (1915) considered the motion at the centre, for some special cases of initial impulse and elevation in water of infinite depth, a point at which the previous solutions do not apply.

Interest in the problem was revived by Lord Penney (1945) who investigated the effects of underwater nuclear explosions. He studied the waves generated by a surface of revolution in deep water conditions. Starting with Lamb's solution for an infinitesimal elevation, the elevation at a particular point was computed as the summation of the waves produced by the infinitesimal areas which constitute the initial disturbance.

Eckart (1948) discussed the stationary method used in Lord Kelvin's approach and showed that this method is also the mathematical foundation for the

Hamilton–Jacobi theory. The waves produced from a centred disturbance were discussed from a general angle, verifying the conclusions derived from the earlier methods.

Unoki and Nakano (1953) considered the effects of frictional forces acting on the water particles. The frictional forces were assumed to be proportional to the velocity of the fluid particles. The components of these forces in the three directions x, y, z are $-2\mu u$, $-2\mu v$, $-2\mu w$ respectively and 2μ=5.5exp(−4)·1/sec. The consideration of the frictional effects introduces the additional term in the solution,

$$\eta_{friction} = \eta_{ideal} \cdot e^{-\mu t} \qquad \text{A.13}$$

For the case of an ideal fluid, μ=0, the derived expressions are in agreement with the corresponding expressions obtained by Lamb (1932).

Kranzer and Keller (1959) derived explicit formulae for the waves produced by an arbitrary axially symmetric initial disturbance in water of finite depth. The solution was derived according to the linear theory of surface waves. By application of the Hankel transform to the Laplace equation describing the flow and using Kelvin's stationary phase method, the surface elevation is given by,

$$\eta(r,t) \sim \frac{\eta_0 R}{r} B \cos 2\pi\left[\frac{t}{T} - \frac{r}{\lambda}\right] \qquad \text{for} \quad r \gg R \qquad \text{A.14}$$

where η_0 = initial elevation at the origin

R = effective radius of initial displacement such that

$$\left|\eta_0\right| R^2 = 2 \int_0^\infty \left|E(r)\right| r \, dr \qquad \text{A.15}$$

where $E(r)$ = initial elevation

$$B = \frac{1}{\eta_0 R h} E(\sigma/h) \left[\frac{\sigma \, \Phi(\sigma)}{-\Phi'(\sigma)}\right]^{1/2} \qquad \text{for } r < \sqrt{gh}\, t \qquad \text{A.16}$$

$$E(\sigma/h) = \int_0^\infty E(r) \, J_0(\sigma r/h) \, r \, dr \qquad \text{A.17}$$

where J_0 is the Bessel function of zero order and h the water depth,

and $$\Phi(\sigma) = \frac{1}{2}\left[\frac{\tanh\sigma}{\sigma}\right]^{1/2} + \frac{1}{2(\cosh\sigma)^{3/2}}\left[\frac{\sigma}{\sinh\sigma}\right]^{1/2} - \frac{r}{\sqrt{gh}\, t} \qquad \text{A.18}$$

Corresponding expressions were also obtained for the two-dimensional problem as well as for the case of an initial impulse.

State of the art reviews on this problem were presented by Le Mehaute (1970, 1971) and Jordaan (1972). Research work over the 1960's concentrated mainly on experimental verification of the theory and the effects of the waves generated by a local disturbance when approaching natural and man made structures.

The above mentioned solutions apply in the far field, that is, at distances much larger than the width of the initial disturbance. Le Mehaute et Al (1987) derived a linear solution which applies at and near the origin. It was found that the solutions are not oscillatory at the origin. The vertical projection of water at the origin was explained theoretically by a discontinuity in the initial conditions.

A.3 COMPARISON BETWEEN THE DIFFERENT SOLUTIONS

The case of a rectangular elevation in deep water was considered by Burnside (1888) and Unoki et al. (1953). Both solutions, although derived from different methods give the same result:

$$y = \frac{4c}{\sqrt{\pi}} \left[\frac{x}{gt^2}\right]^{1/2} \sin \frac{gt^2a}{4x^2} \sin \left[\frac{gt^2}{4x} + \frac{\pi}{4} \right] \qquad \text{A.19}$$

The same result is also obtained using Kranzer's method.

Burnside (1888) considered the case of a local elevation described by

$$y = c \, \frac{a^2}{a^2+x^2} \qquad \text{A.20}$$

The solution to this problem was found to be

$$y = \sqrt{\pi} \, \frac{ca}{x} \left[\frac{gt^2}{4x} \right]^{1/2} \exp\left[- \frac{gt^2a}{4x^2} \right] \sin\left[\frac{gt^2}{4x} + \frac{\pi}{4} \right] \qquad \text{A.21}$$

The solution to the same problem using Kranzer's method is

$$y = \frac{2}{\sqrt{\pi}} \frac{ca}{x} \left[\frac{gt^2}{4x} \right]^{1/2} \int \frac{a}{a^2+x^2} \cos(x\sigma/h) \, dx \quad \sin \left[\frac{gt^2}{4x} + \frac{\pi}{4} \right] \qquad \text{A.22}$$

Comparison between the two solutions using numerical integration over a finite length indicated an agreement within 10%.

All solutions are based on the same fundamental laws of motion, but they employ different mathematical treatment in obtaining the result. All methods are good approximations. The choice on the use of the most appropriate method depends on the given conditions and the computational facilities available. Undoubtedly, Kranzer's method gives the most complete solution but, as shown above, it is not always the most convenient to use.

A.4 PROPERTIES OF THE WAVES GENERATED BY A DISTURBANCE

The dispersive nature of the waves produced by a local disturbance was one of the earliest properties discovered. Even before any physical or mathematical treatment was attempted, the ever decreasing length of the waves and the succession of waves produced, has been known to philosophers and poets in classical times.

The rate of change of the angular frequency is constant in deep water conditions and is independent of the nature and characteristics of the original disturbance. However, as the depth decreases the waves are retarded and their wavelength and period are less than in deep water. The waves produced by the same initial elevation in two different water depths are illustrated in figure A2.

The amplitude of the waves varies with time and space and this variation depends on the form of the initial disturbance. The characteristics of the waves when the amplitude is maximum are the predominant ones. The predominant wavelength is independent of the distance from the disturbance; it is solely a function of the shape of the disturbance. The wider the disturbance, the longer the predominant waves are. Due to the complexity of the solution the determination of the predominant characteristics cannot, in general, be obtained analytically. For the parabolical elevation studied by Burnside, the predominant wavelength is $4\pi a$.

The predominant characteristics change with depth. The shallower the water depth, the less the range of periods and wavelengths, hence, the more the energy transferred to the long periods and wavelengths. The first waves in the wave train are therefore the predominant ones. The predominant wavelengths and periods in shallow water are hence longer than in deep water.

The amplitudes of individual waves are modulated into groups of successively smaller amplitude by the slowly varying Bessel function (eqns A.14–18). The number of waves in a given group increases with time or distance travelled. Also the length of a group increases linearly with time and distance.

An interesting feature is the formation of the first wave. In deep water

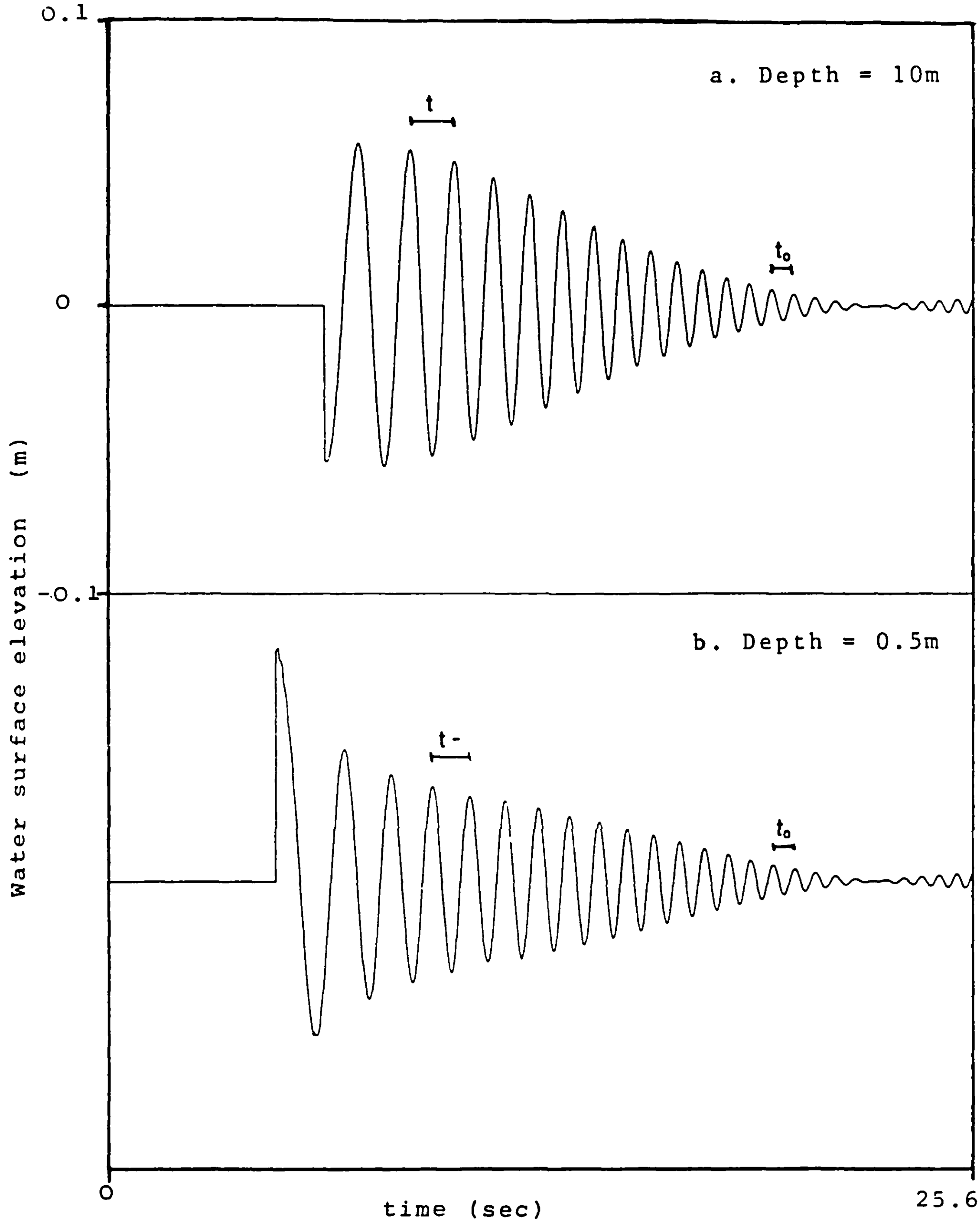

Fig. A2 Elevation time histories produced by a 2-D elevation (eqn A.20) with a=0.35, c=0.4, x=10 in water depth a)10 and b)0.5 (all units in m) conditions the elevation rises gradually from zero. However, as the depth decreases the arrival of the first wave is delayed and a bigger mass of water travels with the depth limited velocity. This sudden discontinuity, known as a bore, has different characteristics from the following waves. Its duration varies with the water depth and the distance from the disturbance.

It must be born in mind that, all the analytical methods assume linear wave theory; that is, the amplitude of the waves is linearly related to the height of the initial disturbance. However, it is known that steeper waves travel faster and a change in the wave characteristics is expected with increasing size of disturbance. As there is a limiting steepness a wave can have, it is very likely that waves produced by a high initial elevation might break.

A.5 EXPERIMENTAL VERIFICATION

Experimental results on the waves produced by a local disturbance are generally found in reports about the effects of underwater explosions.

Charlesworth (1945) monitored the amplitude of surface waves produced by a 32-lb charge detonated at various depths in a gravel pit with 4.5m of water. The experimental results were compared by Bryant (1945) with the theoretical expressions derived by Penney (1945). The agreement was found excellent up to the arrival of the second crest.

Johnson (1949) performed a series of experiments on waves generated by dropping steel discs into a body of still water. The aim of these experiments was to obtain information on the characteristics ot the impulsively generated waves resulting from an atomic explosion. The experiments were performed in a basin so that the waves were three-dimensional. By monitoring the wave height at different points it was found that the wave height at a particular point increases as the potential energy increases, until a certain value of potential energy is reached, beyond which little increase in wave height occurs. This indicates that the higher energy content of the weight, the greater the percentage of energy going into the splash. Comparing the energy loss in the splash produced by two discs with the same potential energy but different mass, it was observed that the light disc, moving with higher speed, loses more energy in the splash than the heavy disc with smaller speed.

Analysis of the wavelength showed that it varies directly as the distance from the disc. It was empirically shown to be somehow a function of the diameter of the object, the depth of the water and the height of fall.

Unoki and Nakano (1953) studied the formation of the waves produced by the eruption of a volcano and recorded on Hachijo Island, Japan, in September 1952. From descriptions by people who witnessed the events, the water surface at the time of the eruption was still. Suddenly, it heaved up to a water dome with dimensions of about 5m high and 200m wide. The wave records were compared with theoretical predictions for cylindrical local elevations and impulses acting over an area with radius 2.2km. Comparison between the field measurements and theory showed a considerable agreement regarding the variation of period and wave height with time.

Prins (1957, 1958) investigated the waves produced by a rectangular elevation or depression in a long narrow tank with 35cm of water depth (fig. A3). The results from these experiments can be summarised as follows:

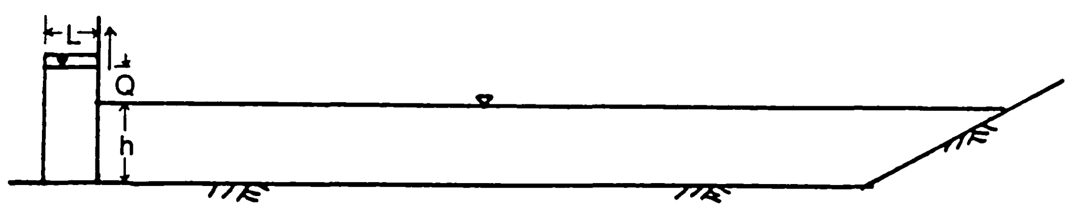

Fig. A3 Experimental set-up showing the box with the sliding wall creating the initial elevation or depression.

a) With increasing Q/h and L/h, where the symbols are defined in fig. A3, the leading wave tends to the solitary wave form and finally reaches the stage where its shape closely approximates the Boussinesq wave form.
b) The height of the wave is dependent on Q. For deep water the elevation is proportional to Q. As soom as a bore occurs, the height is reduced.
c) The height of the wave does not affect the phase velocity.
d) The phase periods agree with the theory.
e) The amplitude envelope is well expressed by theory.
f) There is no difference between the waves resulting from an initial elevation and those from a depression.
g) The amplitude of the waves is smaller than the theoretical predictions using Kranzer's method.

Prins (1957) mentions in his discussion that "... *this study may give an* *indication of the characteristics of the waves of shorter period originated from a breaking wave."*

The waves produced by a nuclear explosion at Bikini, Marshall Islands and recorded at four distant islands were studied by Van Dorn (1961). Comparison of the results with the theory of Kranzer (1959) shows that the theory predicts the observed arrival times with an error of less than 1%. The theory also predicts adequately the rate of amplitude decay with distance, after allowing for corrections due to back scattering from the islands and depth variations along the bed.

The waves generated by the sudden withdrawal of a paraboloid plunger, 4.2m in diameter, in a wave basin 28.5m by 27.9m and 0.9m deep with 0.75m of water depth, were studied by Joordan (1965, 1966). It was found that:

a) The period of the dominant waves is relatively insensitive to the influence of the depth. It is also insensitive to the distance of travel and remains a constant throughout the wave dispersion. This dominant period is solely a function of the wave generating disturbance.

b) The simulated impulsively-generated waves in the laboratory were about 0.6 times the height predicted by the expression of Kranzer and Keller (1959) for the same paraboloid dimensions.

c) The behaviour of periodicities and group envelopes as well as the attenuation of the wave maximum obtained experimentally agree substantially with the analytical theory of Kranzer and Keller (1959).

A.6 DISCUSSION

The evolution of the solutions to the problem of waves produced by an original disturbance on the surface spans over the last two centuries (table A.1).

The problem, first raised by the French Academy with a view of advancing the science, was revived after the second world war in order that the effects of nuclear explosions could be assessed. The different solutions agree with each other, irrespective of the mathematical approach, and the experimental results verify them reasonably well.

The application of these theories remained within the mathematical and physical circles. The solutions to the problem of the waves produced by a local disturbance on the water surface are used in this thesis in:

YEAR	NAME	DEPTH	SHAPE	DIR.	COMMENTS
1827	Cauchy-Poisson	Infinite	Infinitesimal	2-D	
1888	Burnside	Infinite	Any shape	2-D	Fourier theory
1904	Lamb	Infinite	Infinitesimal	3-D	As Cauchy
1904	Kelvin	Infinite	Infinitesimal	2-D	Stationary phase
1909	Rayleigh	Finite	Infinitesimal	2-D	First term
1910	Pidduck	Finite	Infinitesimal	2-D	Second term
1925	Terazawa	Infinite	Given shape	3-D	Near disturbance
1945	Penney	Infinite	Dome	3-D	As Lamb
1948	Eckart	Finite	Arbitrary	2-D	New method
1953	Unoki et Al	Infinite	Given shape	3-D	Friction effects
1959	Kranzer	Finite	Any shape	2/3	Complete solution
1987	Le Mehaute	Finite	Any shape	3-D	Near origin

TABLE A.1 Evolution of the solutions to the problem of the waves generated by an original disturbance on the surface

a) generation of breaking waves in the laboratory,

b) description of the 2-d surface wave motion induced by wave plunging,

c) modelling the 3-d, irregular surface wave motion induced by the plunging of a series of jets, formed on the crest of an overtyurning wave.

APPENDIX B

IMAGE PROCESSING

B.1 BASIC PRINCIPLES

The image of an object, when viewed through a video camera, is projected on to a sensor. This sensor consists of photo capacitive cells that convert light focused by the lens into measurable electrical charges. The amount of charge in each cell, called **pixel**, varies according to the intensity of the light received by each cell. In the sensor, the charge that is stored by each cell is picked up once per frame by a scanning process which takes the charge from each cell. The video signal consists therefore of a sequence of varying amounts of charge corresponding to each pixel scanned.

A conventional video recorder captures 25 frames per second. The Kodak Ektapro 1000 high speed video system has a scanning cycle of 60 frames per second for an image array of 192 rows with 240 pixels per row. A frame rate of 1000 frames per second is achieved by scanning 16 rows of pixels simultaneously.

When a computer receives a video signal, the analog information is converted into digital form. A number is assigned to each pixel depending on the amount of charge. In black and white pictures, black has no voltage whilst white has the saturation value. On 8-bit analog to digital (A/D) convertors, black is stored as zero and white as 255.

A powerful facility is the Look Up Tables (LUT). In its simplest form an LUT may be considered as an array of 256 cells, numbered from 0 to 255. The value of each pixel (0 to 255) routes the signal to the cell with the same address. The value corresponding to that pixel is then changed to the value stored in that LUT cell. If the contents of the LUT cells are the same as their addresses, then the image remains unchanged. If however, the contents of the same cells vary from 255 to 0, instead of 0 to 255, a negative or inverted image is displayed.

Plate *A1* shows 256 cells (16×16) with grey level values ranging from 0 to 255 from top to bottom and left to right (top left hand corner = 0 - black, bottom right = 255 - white). If these are considered as LUT cells, then plate *A2* produces the negative image. Plate *A3* is a linear contrast LUT that performs the operation : all values less than 50 become 0; all values greater than 200 become 255 and the values between are linearly stretched to cover the range 0 to 255.

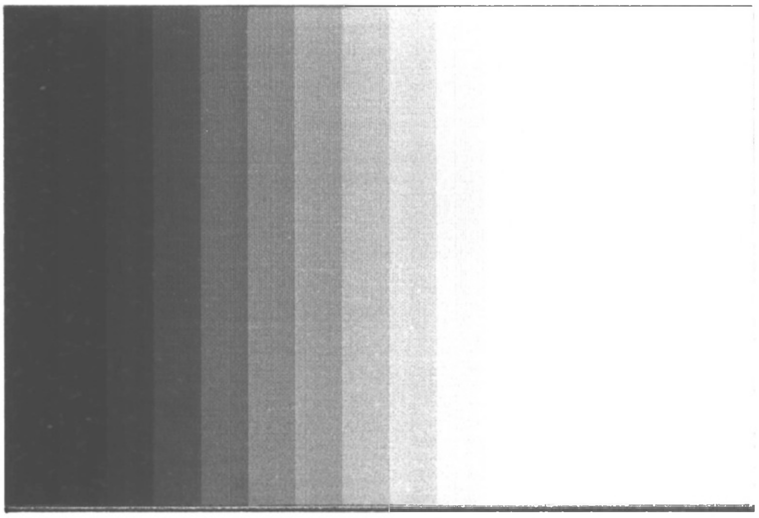

PLATE A1 LUT BOXES WHOSE CONTENTS ARE THE SAME AS THE ADDRESSES.

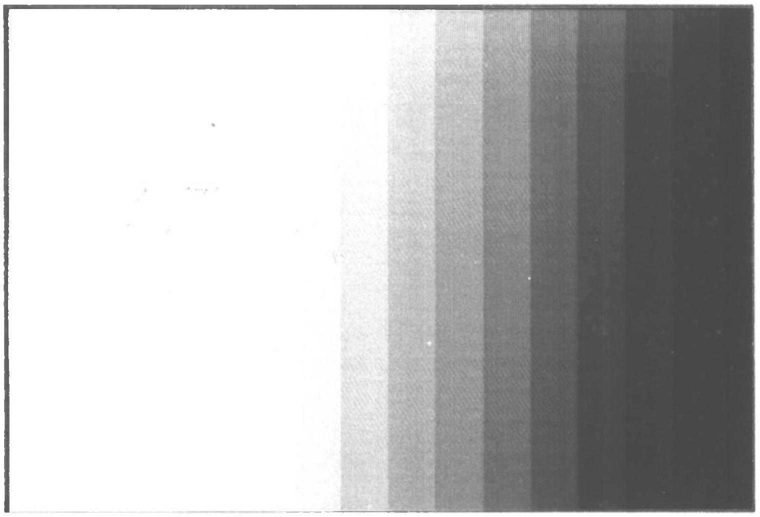

PLATE A2 LUT PRODUCING THE NEGATIVE IMAGE.

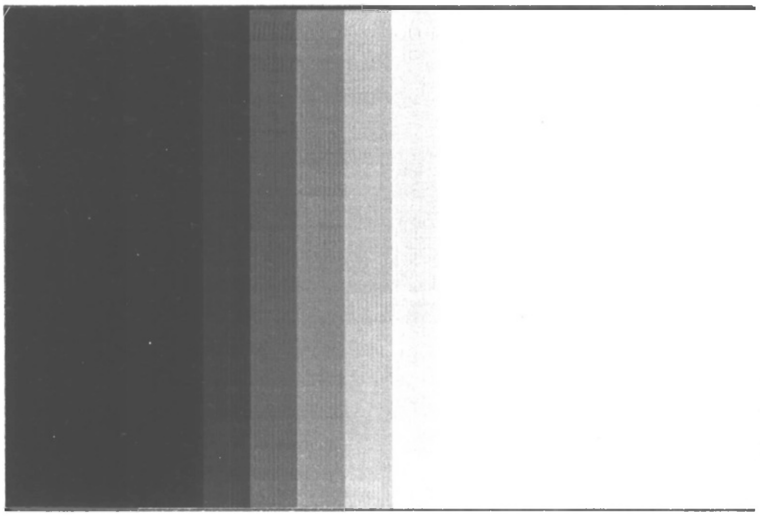

PLATE A3 LUT PRODUCING A LINEAR CONTRAST TRANSFORMATION.

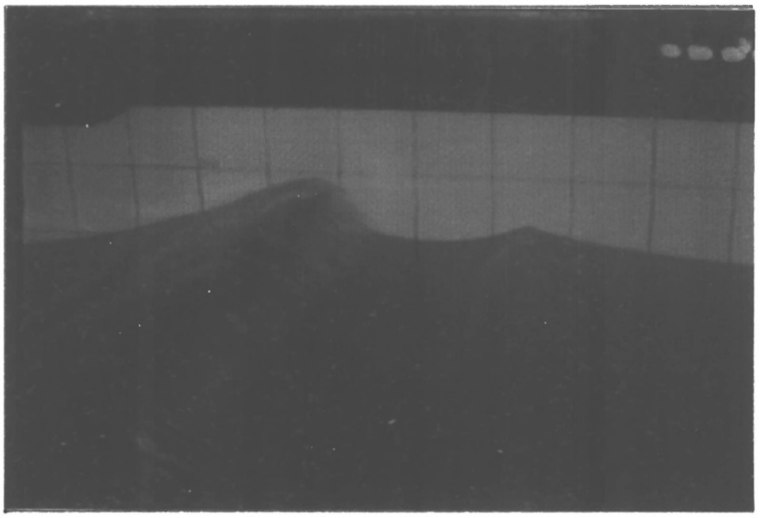

PLATE A4 ORIGINAL IMAGE.

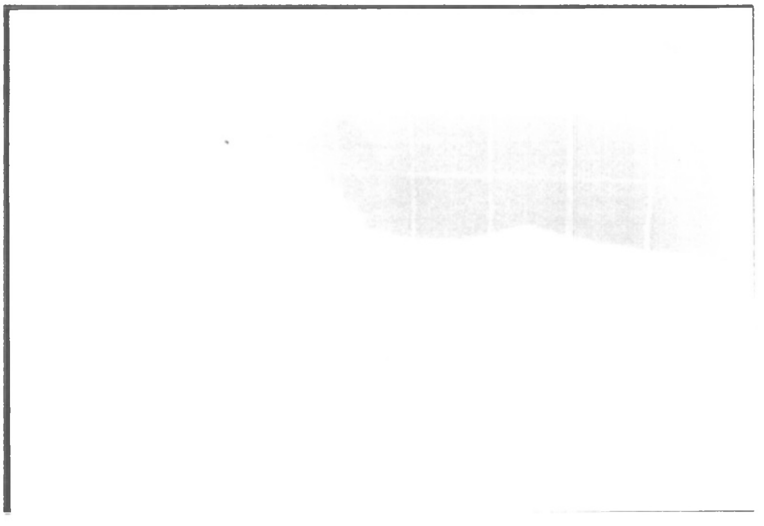

PLATE A5 NEGATIVE IMAGE.

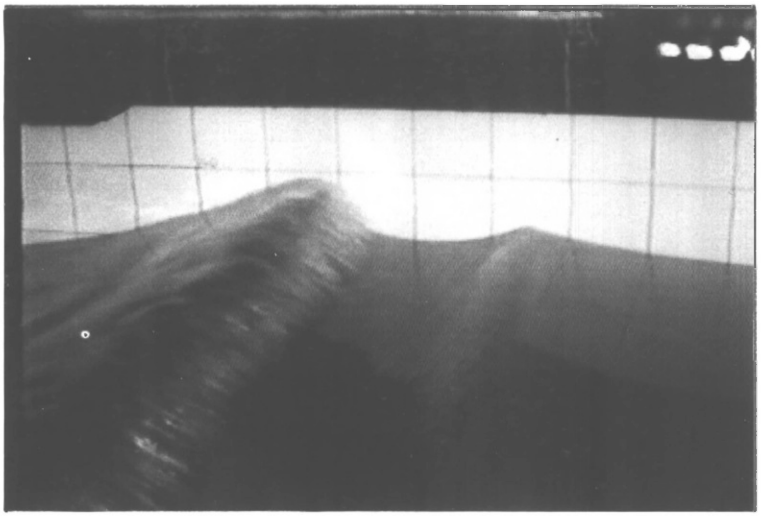

PLATE A6 CONTRAST ENHANCED IMAGE.

An illustration of the use of LUTs is shown on plates A4–6.

B.2 IMAGE PROCESSING SOFTWARE

The software, developed by the author, uses both FORTRAN and C–language routines. The C–language routines are lower level ones. The main program is in FORTRAN language and communication with the frame grabber board is performed through the C–language routines.

The main program makes use of two two–dimensional arrays of 512×512 pixels each. The first one stores the original frame and the second one the processed frame. All operations are performed on the original array (*ipixel*) and stored on the other array (*newp*). Two unprocessed pictures may also be stored in software. They may be **added**, **subtracted** or **superimposed**, that is, displaying the odd lines from one frame and the even lines from the other frame.

Image processing may be performed on only a part of the frame, called **window**, whose location and dimensions are selected by the user. The basic operations that may be performed from the menu–styled program are the following.

Linear Contrast

For any given image, only a finite range of grey levels is available. The difference between the maximum and minimum values is called the *contrast range*. A simple but useful operation is the linear expansion of the values within the contrast range over the available range. This transformation is diagrammatically shown in figure A4 and described by

$$g = \begin{cases} 0 & \text{for } g < g_{min} \\ 255 & \text{for } g > g_{max} \\ \dfrac{g - g_{min}}{g_{max} - g_{min}} & \text{for } g_{min} \leq g \leq g_{max} \end{cases}$$

where g is the pixel value and g_{min}, g_{max} define the contrast range.

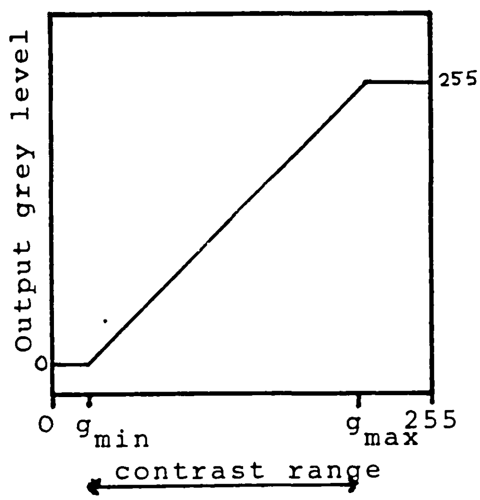

Fig. A4 Linear contrast

Histogram Equalisation

This is a non-linear contrast enhancement transformation which tends to enhance low-contrast information. The histogram of the image grey level values is first computed (fig. A5). The distribution curve is then obtained by adding up the histogram values. The normalised distribution curve is then directly used for the transformation (fig. A6).

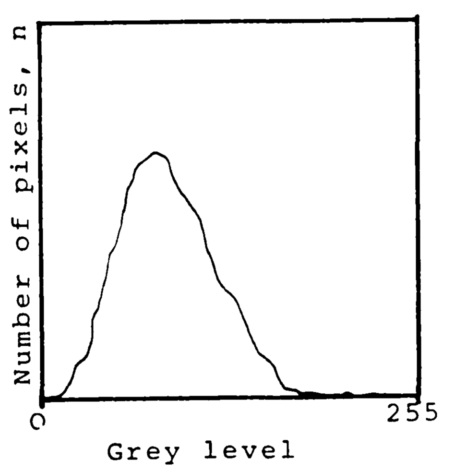

Fig. A5 Grey level histogram of original image

In both the linear contrast and the histogram equalisation image enhancement, the user has the option of defining the limits over which the transformation takes place. Namely, in linear contrast, the minimum and maximum values derived from the computer may be suppressed and new values entered by the user. The distribution curve in the histogram equalisation transformation may be displayed on

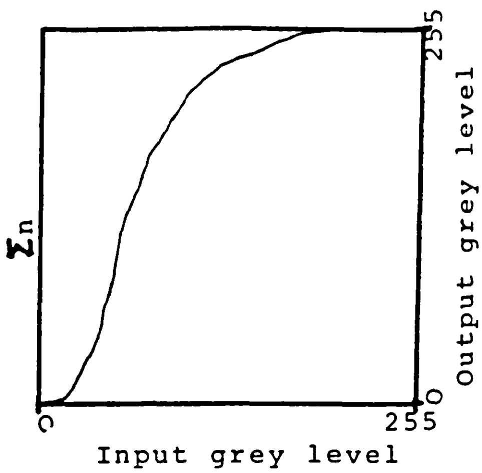

Fig. A6 Grey level distribution curve

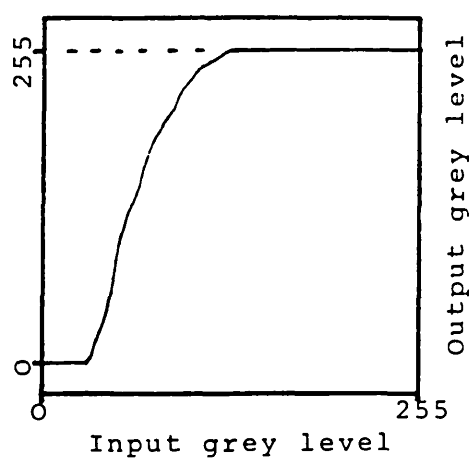

Fig. A7 Cut-off of the two ends

the top right hand corner of the image. This curve has usually an "s"-shape (plate A7). The two ends of the curve may be removed by introducing cut-off values as shown in figure A7. (Plate A7).

Both contrast and histogram equalisation tranformations may be performed either through the LUTs or by changing the *newp* array. The operation through the LUTs is much faster. As the computer allows the use of 16 sets of LUTs the transformation may be stored for use at a later stage. A **menu of contrasts** allows the user to select any one of the 16 LUTs. LUT number 1 is reserved for the original image, i.e. its contents are 0 to 255 and LUT 2 is reserved for the **negative** image, i.e. its contents vary from 255 to 0. These LUTs are initiated by the routine **initial**.

Filtering

Noise smoothing, low-pass filtering

Noise is a relative term. Extreme values are usually considered as noise. A technique which *smooths* an image replaces each pixel with a weighted average of the neighbouring values in the time and/or space domain. In digital image processing smoothing is generally performed in the space domain (plate A8). A *point-spread* function for a linear smoothing operation is

$$\begin{bmatrix} 1/9 & 1/9 & 1/9 \\ 1/9 & 1/9 & 1/9 \\ 1/9 & 1/9 & 1/9 \end{bmatrix}$$

A non-linear operation which detects extreme variations and replaces them by a local average is the following : if the difference between a pixel and the average of its neighbouring pixels is greater than a threshold, then replace the pixel by that average, otherwise leave it as it is.

Edge enhancement, high pass filtering

Edge enhancement, sharpening or crispening techniques are used to increase visibility of low contrast edges and usually lead to increased perception of detail. Edge enhancement may be obtained through high-pass filtering. A point-spread function for such an operation is

$$\begin{bmatrix} -1/8 & -1/8 & -1/8 \\ -1/8 & 1 & -1/8 \\ -1/8 & -1/8 & -1/8 \end{bmatrix}$$

The derivatives of the image may also be used for edge enhancement. Such transformation is the Prewitt Operator described by

$$\begin{bmatrix} A & B & C \\ H & \text{Pixel} & D \\ G & F & E \end{bmatrix} \qquad \begin{aligned} \text{Pixel} &= \sqrt{x^2 + y^2} \\ x &= C-A + D-H + E-G \\ y &= A-G + B-F + C-E \end{aligned}$$

A simple form of high pass filtering in the space domain is the subtraction of successive images. This is achieved by storing successive images in the two arrays, *ipixel and newp*, and then subtracting the corresponding pixel values. (Plate A9).

Grey level extraction

In this subroutine the grey levels along a specified straight line of the original image are obtained and displayed along a horizontal straight line of the same length on the top right hand corner.

Zoom, grab, snap

These are routines that do not interfere with the stored images (*ipixel* and *newp*). *Grab* initiates a continuous acquisition of frames and *snap* "freezes" the picture, the equivalent of "pause" in conventional video recorders. *Zoom* magnifies the **top left** hand corner of the image by factors 1,2 or 3 (plates A10-13).

Load

For any operation to be effective, the current image in the frame grabber board must be loaded on to the arrays *ipixel* and *newp*. *Newp* contains the original image superimposed by the processed image in the window, if any. If a new window is chosen, the *newp* array must be reloaded with the original image, *ipixel*.

Window on top left hand corner

Since the zoom operator applies only on the top left hand corner, magnifying a particular part of the image may be done by shifting the window to the top left corner and then calling the zoom routine. (Plate A10).

Mouse

A simple "mouse" simulation routine enables the user to move a white spot around the image. The user can specify the *jog*, the step size of moving about, and then direct the bright spot with the keys 'u', 'h', 'j', 'n' for up, left, right, down respectively. The coordinates of the spot and its grey level may be displayed on request. This facility is extremely useful in defining the window or the line along which the pixel values are displayed.

Circle

An interesting part of the picture may be pointed out by enclosing it in a "circle", a shape which usually appears as an *ellipse*. The reason for this apparent discrepancy lies in the way the different display monitors work. The computer considers the image as a square one, (512x512 square pixels). Display monitors are not usually square, although some of them have adjustable display dimensions. The shape of the computer generated circle will therefore depend on the aspect ratio between the width and height of the screen. The user may bring back the ellipse into a circle by defining the aspect ratio of the display unit. The same principle also applies for the video copy processor, the facility that prints the image onto paper. This instrument receives an analog signal (video signal) and at the press of a button (*print*) it **snaps** a picture. The picture is then reproduced on to paper of size 100x66 mm. (Plates A1-13).

Save and load on computer hard disc

Interesting frames may be stored on the computer hard disc for analysis at a later stage. The huge size of the arrays, 512x512x2 bytes, requires half megabyte memory for each frame. This limits the number of images that may be stored at any one instant. However, the fact that the grey values range only between 0 and 255 implies that about half of the space occupied by each pixel value (2 bytes, -32767 to +32767) is not exploited. Writing two pixel values in one number implies that the range of that number is 0 to 65535, which is greater than the range of a two-byte number (65534). An "engineering" compromise is employed. If two successive pixel values are equal to 255(bright) then set one of them to 254. This approximation enables the amount of stored images to be doubled whilst very little information is modified.

Black backround

A particular part of an image may be emphasised by erasing the rest of the picture. This is achieved by setting the pixels outside the window equal to 0 (black). The routines which involve plotting, such as histogram equalisation graph, usually require the operation of the black backround routine, so that the displayed information is clearly seen.

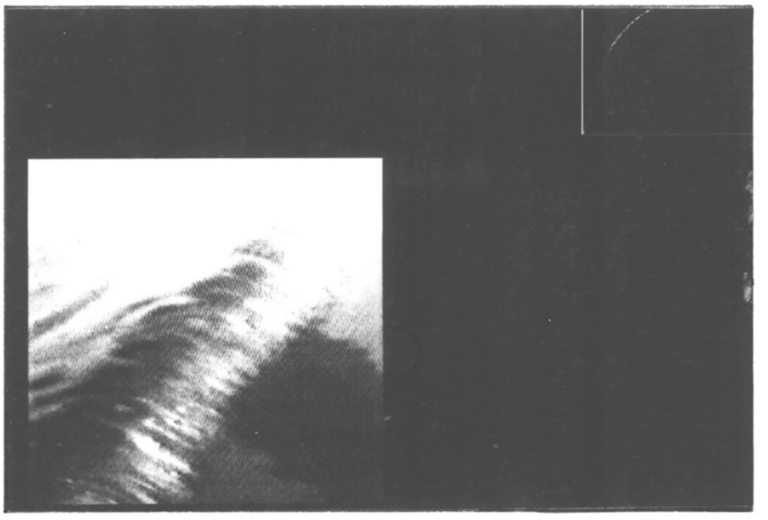

PLATE A7 HISTOGRAM EQUALISATION.

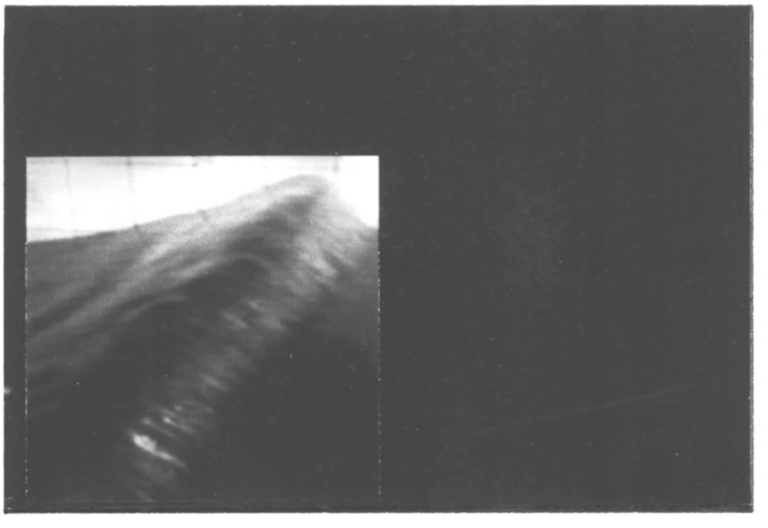

PLATE A8 LOW PASS FILTERING.

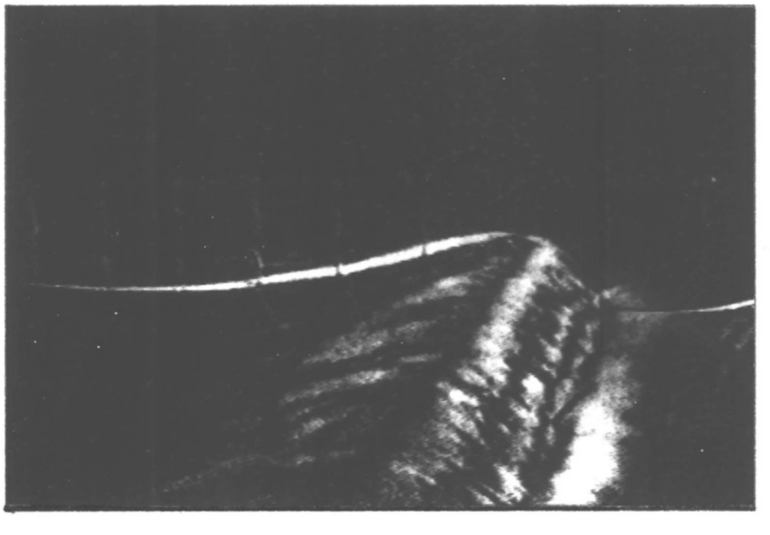

PLATE A9 IMAGE SUBTRACTION - HIGH PASS FILTERING.

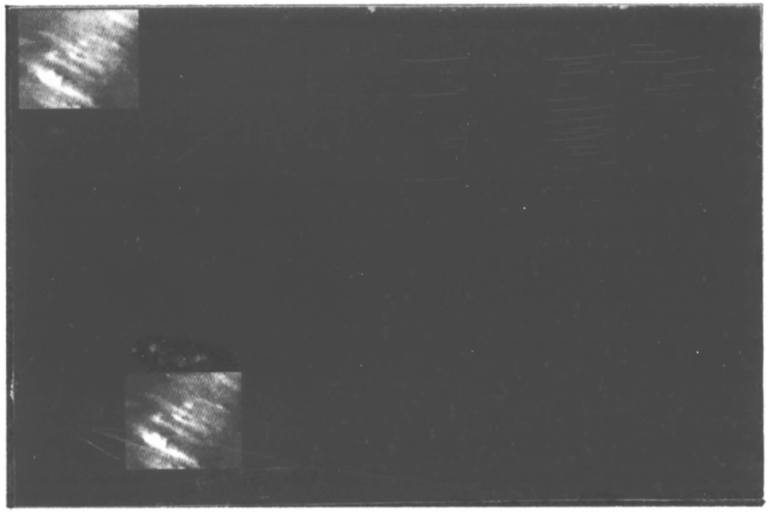

PLATE A10 WINDOW SHIFTED TO TOP LEFT HAND CORNER.

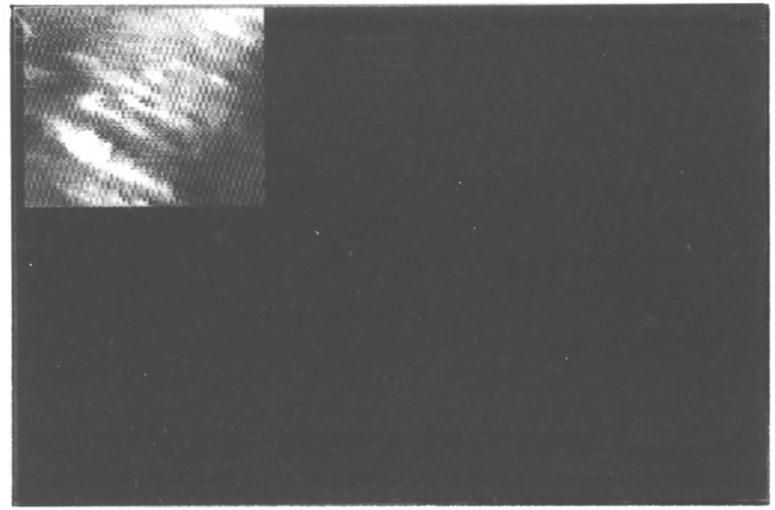

PLATE A11 ZOOM FACTOR = 1.

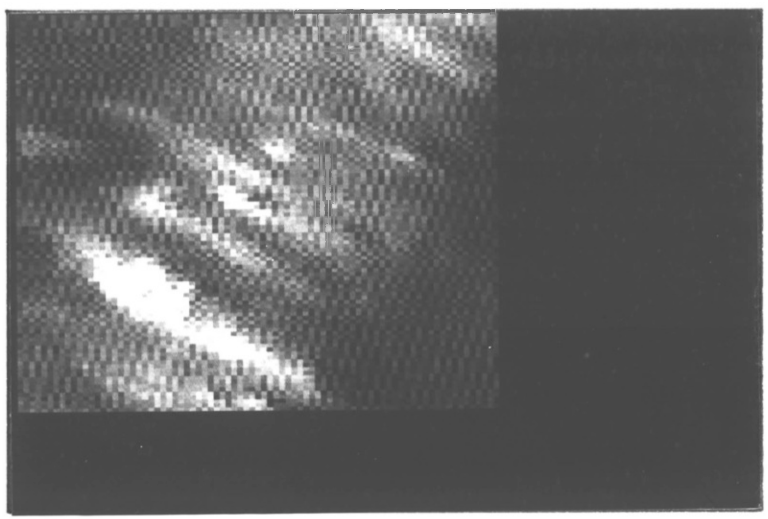

PLATE A12 ZOOM FACTOR = 2.

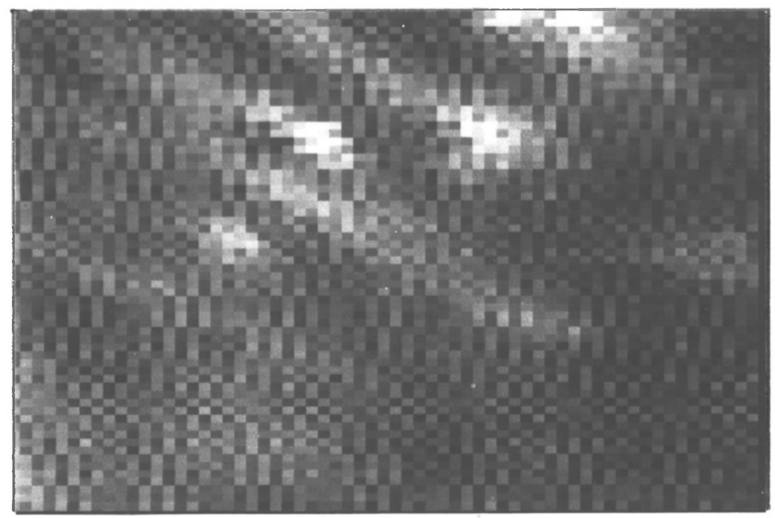

PLATE A13 ZOOM FACTOR = 3.